

**MODULATION OF CHEMICAL REACTIVITY USING
PHOTORESPONSIVE DITHIENYLETHENES**

by

Heeramatee (Hema) Devi Samachetty
B.Sc. (Hons.), University of Mauritius, 1999

THESIS SUBMITTED IN PARTIAL FULFILLMENT OF
THE REQUIREMENTS FOR THE DEGREE OF

DOCTOR OF PHILOSOPHY

In the
Department of Chemistry

© Heeramatee (Hema) Devi Samachetty 2007

SIMON FRASER UNIVERSITY

Summer 2007

All rights reserved. This work may not be
reproduced in whole or in part, by photocopy
or other means, without permission of the author.

APPROVAL

Name: Heeramatee(Hema) Devi Samachetty

Degree: Doctor of Philosophy

Title of Thesis: Modulation Of Chemical Reactivity Using Photoresponsive Dithienylethenes

Examining Committee: Dr. G.R. Agnes
Chair
Professor, Department of Chemistry

Dr. N.R. Branda
Senior Supervisor
Professor, Department of Chemistry

Dr. P.D. Wilson
Supervisor
Associate Professor, Department of Chemistry

Dr. C.J. Walsby
Supervisor
Assistant Professor, Department of Chemistry

Dr. E. Plettner
Internal Examiner
Associate Professor, Department of Chemistry

Dr. R.H. Mitchell
External Examiner
Professor, Department of Chemistry
University of Victoria

Date Defended/Approved: June 29, 2007



SIMON FRASER UNIVERSITY
LIBRARY

Declaration of Partial Copyright Licence

The author, whose copyright is declared on the title page of this work, has granted to Simon Fraser University the right to lend this thesis, project or extended essay to users of the Simon Fraser University Library, and to make partial or single copies only for such users or in response to a request from the library of any other university, or other educational institution, on its own behalf or for one of its users.

The author has further granted permission to Simon Fraser University to keep or make a digital copy for use in its circulating collection (currently available to the public at the "Institutional Repository" link of the SFU Library website <www.lib.sfu.ca> at: <<http://ir.lib.sfu.ca/handle/1892/112>>) and, without changing the content, to translate the thesis/project or extended essays, if technically possible, to any medium or format for the purpose of preservation of the digital work.

The author has further agreed that permission for multiple copying of this work for scholarly purposes may be granted by either the author or the Dean of Graduate Studies.

It is understood that copying or publication of this work for financial gain shall not be allowed without the author's written permission.

Permission for public performance, or limited permission for private scholarly use, of any multimedia materials forming part of this work, may have been granted by the author. This information may be found on the separately catalogued multimedia material and in the signed Partial Copyright Licence.

While licensing SFU to permit the above uses, the author retains copyright in the thesis, project or extended essays, including the right to change the work for subsequent purposes, including editing and publishing the work in whole or in part, and licensing other parties, as the author may desire.

The original Partial Copyright Licence attesting to these terms, and signed by this author, may be found in the original bound copy of this work, retained in the Simon Fraser University Archive.

Simon Fraser University Library
Burnaby, BC, Canada

ABSTRACT

The development of molecular systems that show reversible changes in their structures and functions is an active area of research as it has potential applications in molecular devices. One of the most promising photoresponsive frameworks is found in the 1,2-dithienylethenes (DTEs) because they can be toggled between two thermally stable and structurally unique forms when irradiated with the appropriate wavelengths of light and provide a practical means to regulate the chemical and physical properties of molecular devices. However, there are only a few examples that take advantage of these reversible structural and electronic differences between the two forms of DTE derivatives to influence chemical reactivity.

The DTE backbone is well-suited to modulate chemical reactivity since the electronic differences between the ring-open and the ring-closed isomers can be used as the “on” and “off” functions to start and stop reactions using light as the external stimulus and has potential applications in the design of light-activated reagents, catalysts, and biochemical reagents. The research presented in this thesis focuses on integrating photoswitching and nucleophilicity using a pyridine-functionalized DTE to demonstrate the concept of photomodulating reactivity and catalysis.

The first approach uses axial coordination to a metalloporphyrin as a probe to assess the differences in Lewis basicity between the two DTEs. The results show that the ring-open isomer is more effective as a ligand than the ring-closed form. This difference in coordination ability indicates that the pyridine is less Lewis basic in the ring-closed form of the DTE system.

The second approach consists of evaluating this concept in chemical synthesis using *pseudo*-first-order kinetics to probe the differences in the apparent rates of alkylation between the two DTE isomers. The results show that the ring-open form reacts faster than the ring-closed form indicating that the pyridine is less nucleophilic in the ring-closed form of the DTE system.

The application of the DTE system as a potential nucleophilic catalyst is also investigated and the results show that the ring-open isomer gives a higher yield of product than the ring-closed isomer indicating that the ring-open isomer is acting as the more efficient catalyst for the reaction.

Keywords: photoresponsive frameworks, dithienylethenes, nucleophilicity

To my husband, Corbin, and my parents, Dewan and Chitra

ACKNOWLEDGEMENTS

My senior supervisor, Dr. Neil Branda, is thanked for his advice, guidance, and support over the course of my doctoral studies. The training I received during my time as a member of his research group has helped me develop better research, teaching, and writing skills.

The other members of my supervisory committee, Dr. Peter Wilson and Dr. Charles Walsby, are thanked for their suggestions and advice.

Dr. Bettina Wüstenberg is thanked for the preparation of the dicyanoethylene-thienylethene used for the preliminary studies discussed in the *Future Work* section of *Chapter 2*. Dr. Andrew Lewis and Mr. Colin Zhang are thanked for their invaluable advice and assistance with the NMR experiments discussed in *Chapter 3*. Nippon Zeon Corporation is thanked for providing octafluorocyclopentene.

My past and present lab colleagues are thanked for their friendship and helpful discussions over the years.

My parents, Dewan and Chitra, my sisters, Simla and Karmila, and their families are thanked for being so supportive throughout my studies. My husband, Corbin, is thanked for his understanding and unwavering support, especially during the last few months of writing.

TABLE OF CONTENTS

Approval	ii
Abstract	iii
Dedication	v
Acknowledgements	vi
Table of Contents	vii
List of Equations	xi
List of Figures	xiii
List of Schemes	xviii
List of Tables	xix
List of Abbreviations	xx
1 Introduction to the Photoresponsive Dithienylethene (DTE)	
Architecture	1
1.1 Molecular Devices and Molecular Switching	1
1.2 Photochromism.....	2
1.3 The Dithienylethenes	2
1.3.1 Photochemical Ring-Closing Reaction	3
1.3.2 Photostationary State.....	5
1.3.3 Photochemical Cycling.....	5
1.3.4 Functionalization of DTEs.....	6
1.4 Differences Between the Ring-Open and the Ring-Closed Isomers of DTEs	7
1.4.1 Geometric Differences (Through-Space Communication).....	8
1.4.2 Electronic Differences (Through-Bond Communication).....	9
1.5 Control of Reactivity	10
1.5.1 Steric and Electronic Effects on Chemical Reactivity	11
1.6 Integration of Photoswitching and Chemical Reactivity	11
1.6.1 Use of Steric Changes to Modulate Reactivity	12
1.6.2 Use of Electronic Changes to Control Reactivity	13
1.7 Control of Nucleophilicity using Photoresponsive DTEs.....	15
1.8 Summary	17
1.9 Preview of Thesis	17

2	Photomodulation of Coordination Chemistry in a Photoresponsive DTE System	20
2.1	Integration of DTEs and Nucleophilicity.....	20
2.2	Introduction to Axial Binding to Metalloporphyrins Containing Ruthenium.....	22
2.3	¹ H NMR Spectroscopy as a Diagnostic Tool to Probe Axial Coordination	25
2.3.1	Chemical Exchange.....	25
2.3.2	Ring-Current Effects in Metalloporphyrins.....	27
2.3.3	Monitoring the Photochemical Interconversion by NMR Spectroscopy.....	28
2.3.4	Needs and Considerations for Solvent Selection.....	29
2.4	IR Spectroscopy as a Diagnostic Tool to Study Axial Coordination	30
2.4.1	Importance of the Carbon Monoxide Ligand	30
2.5	Project Design	32
2.6	Results and Discussion	34
2.6.1	Synthesis of the RuTTP(CO)(EtOH)	34
2.6.2	Synthesis of the Model Compounds	35
2.6.3	Axial Coordination of the Model Compounds to Ruthenium Porphyrin	36
2.6.4	Assessment of the Difference in Coordination Behaviour Between the Pyridylthiophene Control 2.3 and the Monomethylated Bipyridinium Control 2.4	39
2.6.5	Synthesis of the Monobenzylated DTEs 2.1 and 2.2	43
2.6.6	UV-Vis Absorption Spectra, Photochemical Cycling, and ¹ H NMR Spectra of the Monoalkylated DTE 2.1	47
2.6.7	Axial Coordination of Ring-Open and Ring-Closed DTE's 2.1 and 2.2	50
2.6.8	Assessment of the Difference in Coordination Behaviour Between the Two Isomers (2.1 and 2.2) of the Monobenzylated DTE	53
2.6.9	Reasons for the Low Selectivity	59
2.6.10	Assessment of the Difference in Coordination Behaviour Between the Two Isomers (2.1 and 2.2) of the Monobenzylated DTE in the Presence of the Lewis Basic Pyridylthiophene 2.3	59
2.6.11	Assessment of the Electronic Differences Between the Two Isomers (2.1 and 2.2) of the Monobenzylated DTE by IR Spectroscopy.....	67
2.7	Conclusions	74
2.8	Future Work	74
2.9	Experimental	77

3	Modulation of Chemical Reactivity using Photoresponsive DTEs.....	98
3.1	Introduction to Light-Induced Switching of Reaction Rates	98
3.1.1	Choice of Test Reaction	98
3.2	Technique of Flooding.....	100
3.3	¹ H NMR Spectroscopy as a Diagnostic Tool.....	102
3.4	Results and Discussion	103
3.4.1	Photochemical Synthesis of the Monobenzylated DTE 3.1	103
3.4.2	UV-Vis Absorption Spectra, Photochemical Cycling, and ¹ H NMR Spectra of the Monobenzylated DTE 3.1	104
3.4.3	Synthesis of the Dibenzylated DTE 3.1	107
3.4.4	UV-Vis Absorption Spectra, Photochemical Cycling, and ¹ H NMR Spectra of the Dibenzylated DTE 3.3	107
3.4.5	Choice of Reaction Conditions	111
3.4.6	Reactivity of the Ring-Open Form of the Monocationic DTE 3.1	115
3.4.7	Reactivity of the Ring-Closed Form of the Monocationic DTE 3.2	118
3.4.8	Phototuning the Alkylation Reaction of the Monobenzylated DTE <i>In Situ</i> ..	123
3.5	Reactivity of the Ring-Open and the Ring-Closed <i>Bis</i> (pyridine).....	128
3.5.1	Consecutive First-Order Reactions	129
3.6	Results and Discussion	132
3.6.1	Choice of Reaction Conditions	132
3.6.2	Reactivity of the Ring-Open Form of the <i>Bis</i> (pyridine) 3.5	132
3.6.3	Reactivity of the Ring-Closed Isomer of the <i>Bis</i> (pyridine) 3.6	139
3.7	Conclusions	147
3.8	Future Work	149
3.9	Experimental	150
4	Photomodulation of Catalysis using DTEs.....	166
4.1	Introduction to Photoregulation of Catalysis	166
4.2	Choice of Reaction	167
4.3	Results and Discussion	169
4.3.1	Assessment of the Effect of the Ring-Open (4.1) and the Ring-Closed (4.2) Isomers of the Monoalkylated DTE on the Reaction of the Aldehyde 4.3 and the Acetylenyl Derivative 4.4	170
4.4	Conclusion.....	177
4.5	Future Work	177

4.6	Experimental	178
5	Conclusions	186
6	Appendix	189
6.1	Supplementary ¹ H NMR Spectra.....	189
6.1.1	Selective NOE Experiments for <i>Chapter 2</i>	189
6.1.2	Selective NOE experiments for <i>Chapter 3</i>	192
6.1.3	Axial Coordination Experiments for <i>Chapter 2</i>	194
6.1.4	<i>Pseudo</i> -First-Order Experiments for <i>Chapter 3</i>	201
6.1.5	Consecutive <i>Pseudo</i> -First-Order Experiments for <i>Chapter 3</i>	207
6.2	Supplementary <i>T</i> ₁ Relaxation Measurements for <i>Chapter 3</i>	213
6.3	Supplementary <i>Pseudo</i> -First-Order Plots for <i>Chapter 3</i>	218
6.4	Supplementary IR Studies for <i>Chapter 2</i>	221
7	References	225

LIST OF EQUATIONS

Equation 1.3.1. Photoisomerization reaction of the DTE architecture.....	3
Equation 1.3.2. Equation used to calculate photostationary state.....	5
Equation 1.4.1. Reversible photocyclization of a DTE.....	9
Equation 1.7.1. Controlling nucleophilicity using a photoresponsive DTE.....	16
Equation 2.1.1. The free pyridine ring ‘A’ of the monocationic DTEs 2.1 and 2.2 displays differing nucleophilicity	21
Equation 2.2.1. General reaction between a pyridine and RuTTP(CO)(EtOH)	24
Equation 2.3.1. ¹ H NMR spectroscopy as a tool to monitor the photochemical interconversion	29
Equation 3.2.1. Rate law for a system that follows second-order kinetics.....	100
Equation 3.2.2. Simplified rate equation in the presence of a very large excess of reagent ‘B’	101
Equation 3.2.3. Equation showing the exponential decrease in the concentration of ‘A’ with time under <i>pseudo</i> -first-order conditions.....	101
Equation 3.2.4. Linear equation relating the natural log of the concentration of ‘A’ with time.....	101
Equation 3.4.1. Photochemical synthesis of the monobenzylated 3.1	103
Equation 3.4.2. Synthesis of the dibenzylated <i>bis</i> (pyridinium) <i>bis</i> (hexafluorophosphate) 3.3	107
Equation 3.4.3. Equation relating the mole fraction of the monobenzylated <i>bis</i> (pyridinium) 3.1 to the peak integrals ‘a’, ‘b’ and ‘p’.....	113
Equation 3.4.4. Equation relating the mole fraction of the dibenzylated <i>bis</i> (pyridinium) 3.3 to the peak integrals ‘a’, ‘b’ and ‘p’.....	113
Equation 3.4.5. Equation relating the mole fraction of the monobenzylated <i>bis</i> (pyridinium) 3.2 to the peak integrals ‘a’, ‘b’ and ‘p’.....	120
Equation 3.4.6. Equation relating the mole fraction of the dibenzylated <i>bis</i> (pyridinium) 3.4 to the peak integrals ‘a’, ‘b’ and ‘p’.....	120
Equation 3.4.7. The structural flexibility of the ring-open isomer 3.1 allows the pendant pyridine and the positively charged pyridinium moiety to converge towards each other	123
Equation 3.5.1. Rate expression for the change in the concentration of ‘A’ with time	130
Equation 3.5.2. Rate expression for the change in the concentration of ‘I’ with time.....	130
Equation 3.5.3. Rate expressions for the change in the concentration of ‘P’ with time ...	130
Equation 3.5.4. Integrated rate expression for the exponential decrease in the concentration of ‘A’ with time	130

Equation 3.5.5.	Integrated rate expression showing that the concentration of 'I' with time is the difference of two exponentials	131
Equation 3.5.6.	Integrated rate expression for the increase in the concentration of 'P' with time.....	131
Equation 3.6.1.	Relating the mole fraction of the <i>bis</i> (pyridine) 3.5 to the peak integrals 'a', 'b' and 'c'.....	135
Equation 3.6.2.	Relating the mole fraction of the monobenzylated <i>bis</i> (pyridinium) 3.1 to the peak integrals 'a', 'b' and 'c'.....	135
Equation 3.6.3.	Relating the mole fraction the dibenzylated <i>bis</i> (pyridinium) 3.3 to the peak integrals 'a', 'b' and 'c'.....	135
Equation 3.6.4.	Integrated rate expressions for the exponential decrease in the concentration of the <i>bis</i> (pyridine) 3.5 with time	137
Equation 3.6.5.	Integrated rate expression showing that the concentration of the generated monobenzylated DTE 3.1 with time.....	137
Equation 3.6.6.	Integrated rate expression for the concentration of the dibenzylated DTE 3.3 with time.....	138
Equation 3.6.7.	Relating the mole fraction of <i>bis</i> (pyridine) 3.6 to the peak integrals 'a', 'b', 'c' and 'd'.....	142
Equation 3.6.8.	Relating the mole fraction of the monocation 3.2 to the peak integrals 'a', 'b', 'c' and 'd'.....	142
Equation 3.6.9.	Relating the mole fraction of the dibenzylated <i>bis</i> (pyridinium) 3.4 to the peak integrals 'a', 'b', 'c' and 'd'.....	142
Equation 3.6.10.	Integrated rate expressions for the exponential decrease in the concentration of the <i>bis</i> (pyridine) 3.6 with time	144
Equation 3.6.11.	Integrated rate expression showing that the concentration of the generated monobenzylated DTE 3.2 with time.....	144
Equation 3.6.12.	Integrated rate expression for the concentration of the dibenzylated DTE 3.4 with time.....	144
Equation 3.9.1.	Equation relating the intensity I of a peak to the relaxation time T_1	156
Equation 4.2.1.	Pyridine-catalyzed addition of aldehyde 4.3 to DMAD 4.4	168

LIST OF FIGURES

Figure 1.3.1.	Structure of a generalized DTE chromophore showing the sites ('A', 'B', 'C', and 'D') that are the easiest to decorate	7
Figure 1.6.1.	Photoresponsive bis(oxazoline) DTE ligand used to reversibly bind copper	13
Figure 1.6.2.	Photoresponsive DTEs 1.2 and 1.3 used to photomodulate pK _a	14
Figure 1.6.3.	Modified DTE system with an electron-donating substituent at the internal position of the thiophene ring bearing the phenol group	14
Figure 2.2.1.	Generalized structure of a Ru(II) carbonyl porphyrin with a vacant axial coordination site that can readily be accessed by Lewis bases	23
Figure 2.2.2.	Difference in coordination behaviour between the ring-open isomer 2.1 and the ring-closed isomer 2.2	25
Figure 2.3.1.	Variations in the nature of the observable NMR signals for a hypothetical system	26
Figure 2.4.1.	The σ -bond of CO between the ruthenium metal $d(z^2)$ or $d(x^2-y^2)$ orbitals in ruthenium(carbonyl)porphyrins.....	31
Figure 2.4.2.	The π -bond formed by backbonding of the electron density on the ruthenium centre [$d(xy)$, $d(xz)$, or $d(yz)$] into the empty π^* orbital on the CO.....	31
Figure 2.5.1.	Model compounds 2.3 and 2.4 for the ring-open (2.1) and the ring-closed (2.2) isomers	33
Figure 2.6.1.	Difference in binding strength between the pyridylthiophene 2.3 and the monomethylated bipyridinium 2.4	39
Figure 2.6.2.	Assessment of the effect of the pyridylthiophene 2.3 on a solution of the porphyrin complex 2.4RuP by ¹ H NMR spectroscopy	42
Figure 2.6.3.	UV-Vis absorption spectra and photochemical cycling of the monobenzylated DTE 2.1	47
Figure 2.6.4.	¹ H NMR spectroscopy as a tool to monitor the photocyclization reaction of the ring-open isomer 2.1	49
Figure 2.6.5.	Assessment of the effect of the ruthenium porphyrin on an equimolar mixture of the ring-open (2.1) and the ring-closed (2.2) isomers of the monobenzylated DTE by ¹ H NMR spectroscopy	58
Figure 2.6.6.	Molecular model representation of the ring-closed form of the monobenzylated DTE 2.2	59
Figure 2.6.7.	Assessment of the effect of the pyridylthiophene 2.3 on a mixture of the free and bound ring-open and ring-closed monobenzylated DTEs by ¹ H NMR spectroscopy	63

Figure 2.6.8.	Assessment of the effect of the ring-opening and the ring-closing reaction on the distribution of free (2.3) and bound (2.3RuP) pyridylthiophene by ¹ H NMR spectroscopy.....	66
Figure 2.6.9.	IR spectroscopy as a tool to assess the electronic variations between the porphyrin complexes of the model compounds (2.3 and 2.4) and the two DTE isomers (2.1 and 2.2)	68
Figure 2.8.1.	Generalized structure of a DTE system where the pyridine is electronically communicated to (1) an electron-donating group (EDG) located at the internal position of the thiophene in the ring-open isomer and (2) an electron-withdrawing group (EWG) in the ring-closed form.....	76
Figure 3.4.1.	(a) Changes in the UV-Vis absorption spectra of a CH ₃ CN solution of the ring-open form 3.1 of the monobenzylated <i>bis</i> (pyridinium)	105
Figure 3.4.2.	Selected ¹ H NMR spectra of the ring-open isomer 3.1 (a) before irradiation and (b) after irradiation with 365 nm light for 10 min.....	106
Figure 3.4.3.	(a) Changes in the UV-Vis absorption spectra of the ring-open form 3.3 of the dibenzylated <i>bis</i> (pyridinium) upon irradiation with 365 nm light.....	108
Figure 3.4.4.	Selected ¹ H NMR spectra of the ring-open isomer 3.3 (a) before irradiation and (b) after irradiation with 365 nm light for 10 min.....	109
Figure 3.4.5	Representative example showing the use of ¹ H NMR spectroscopy to monitor the progress of the reaction of the ring-open isomer 3.1	112
Figure 3.4.6.	Representative example of the plot of the natural log of the concentration of the monocationic DTE 3.1 against time	116
Figure 3.4.7.	Representative example showing the use of ¹ H NMR spectroscopy to monitor the progress of the reaction of the ring-closed isomer 3.2	119
Figure 3.4.8.	Representative example of the plot of the natural log of the concentration of the monocationic DTE 3.2 against time	121
Figure 3.4.9.	Graph showing the <i>in situ</i> photoregulation of the rate of reaction of a solution of the ring-open isomer 3.1	126
Figure 3.5.1.	Reaction of the ring-closed (3.6) and ring-open (3.5) isomers of the <i>bis</i> (pyridine) with 4-bromobenzyl bromide.....	129
Figure 3.6.1.	Partial ¹ H NMR spectra showing the aromatic region of a solution of the ring-closed isomer 3.5 in CD ₃ CN.....	134
Figure 3.6.2.	Plots of the concentration of the <i>bis</i> (pyridine) 3.5 , the monocation 3.1 , and the dication 3.3 against time.....	136
Figure 3.6.3.	Partial ¹ H NMR spectra showing the aromatic region of a solution of the ring-closed isomer 3.6 in CD ₃ CN.....	141
Figure 3.6.4.	Plots of the concentration of the <i>bis</i> (pyridine) 3.6 , the monocation 3.2 , and the dication 3.4 against time.....	143

Figure 3.9.1.	The inversion-recovery pulse sequence	155
Figure 4.1.1.	The more nucleophilic ring-open isomer 4.1 can be expected to act as a better catalyst than its ring-closed counterpart 4.2	167
Figure 4.3.1.	Partial ¹ H NMR spectra showing the peaks corresponding to the starting 3-nitrobenzaldehyde 4.3 (a) before, (b) after the reaction with DMAD 4.4 and the ring-open isomer 4.1 under condition A, and (c) after the reaction with DMAD 4.4 and the ring-open isomer 4.1 under condition B for 2 days.....	171
Figure 4.3.2.	Partial ¹ H NMR spectra showing the peaks corresponding to the starting 3-nitrobenzaldehyde 4.3 (a) before, (b) after the reaction with DMAD 4.4 and the ring-closed isomer 4.2 under condition A, and (c) after the reaction with DMAD 4.4 and the ring-closed isomer 4.2 under condition B for 2 days.....	172
Figure 4.3.3.	The pyridylthiophene 4.6 , which is a close representative of the ring-open isomer 4.1 , is expected to be more effective as a catalyst than the monomethylated bipyridinium 4.7 , which is a close analogue of the ring-closed isomer 4.2	173
Figure 4.3.4.	Partial ¹ H NMR spectra showing the peaks corresponding to the starting 3-nitrobenzaldehyde 4.3 (a) before, (b) after the reaction with DMAD 4.4 and the pyridylthiophene 4.6 under condition A, and (c) after the reaction with DMAD 4.4 and the pyridylthiophene 4.6 under condition B for 2 days.....	174
Figure 4.3.5.	Partial ¹ H NMR spectra showing the peaks corresponding to the starting 3-nitrobenzaldehyde 4.3 (a) before, (b) after the reaction with DMAD 4.4 and the monomethylated bipyridinium 4.7 under condition A, and (c) after the reaction with DMAD 4.4 and the monomethylated bipyridinium 4.7 under condition B for 2 days.....	175
Figure 4.5.1.	(a) Ring-open and ring-closed isomers of the non-fluorinated version of the monobenzylated DTE.....	178
Figure 6.1.1.	Partial ¹ H NMR spectra of the 1-D NOE experiments on the monomethylated bipyridinium 2.4	189
Figure 6.1.2.	Partial ¹ H NMR spectra of the 1-D NOE experiments on the ring-open isomer 2.1	190
Figure 6.1.3.	Partial ¹ H NMR spectra of the 1-D NOE experiments on the ring-closed isomer 2.2	191
Figure 6.1.4.	Partial ¹ H NMR spectra of the 1-D NOE experiments on the ring-open isomer 3.1	192
Figure 6.1.5.	Partial ¹ H NMR spectra of the 1-D NOE experiments on the ring-open isomer 3.1	193
Figure 6.1.6.	¹ H NMR spectra showing the peaks corresponding to (a) the pyridylthiophene 2.3 and (b) the monomethylated bipyridinium 2.4	194

Figure 6.1.7.	^1H NMR spectra showing the peaks corresponding to the complex 2.4RuP	195
Figure 6.1.8.	^1H NMR spectra showing the redistribution of free (2.3 and 2.4) and bound (2.3RuP and 2.4RuP) ligands.....	196
Figure 6.1.9.	^1H NMR spectra showing the peaks corresponding to an equimolar mixture of the ring-open isomer 2.1 and the ring-closed isomer 2.2	197
Figure 6.1.10.	^1H NMR spectra when 0.93 molar equiv of RuTTP(CO)(EtOH) is added to an equimolar mixture of the ring-open isomer 2.1 and the ring-closed isomer 2.2	198
Figure 6.1.11.	^1H NMR spectra when pyridylthiophene 2.3 is added to a mixture of the ring-open isomer 2.1 , the ring-closed isomer 2.2 and the RuTTP(CO).....	199
Figure 6.1.12.	^1H NMR spectra when the mixture of the ring-open isomer 2.1 , the ring-closed isomer 2.2 , the RuTTP(CO), and the pyridylthiophene 2.3 is irradiated with 365 nm light for 10 min.....	200
Figure 6.1.13.	^1H NMR spectra showing the peaks corresponding to a solution of the ring-open isomer 3.1 in CD_3CN before the addition of an excess of 4-bromobenzyl bromide.....	201
Figure 6.1.14.	^1H NMR spectra showing the progress of the reaction of a solution of the ring-open isomer 3.1 in CD_3CN with an excess of 4-bromobenzyl bromide after 5 h.....	202
Figure 6.1.15.	^1H NMR spectra showing the progress of the reaction of a solution of the ring-open isomer 3.1 in CD_3CN with an excess of 4-bromobenzyl bromide after 20 h.....	203
Figure 6.1.16.	^1H NMR spectra showing the peaks corresponding to a solution of the ring-closed isomer 3.2 in CD_3CN before adding an excess of the 4-bromobenzyl bromide.....	204
Figure 6.1.17.	^1H NMR spectra showing the progress of the reaction of a solution of the ring-closed isomer 3.2 in CD_3CN with an excess of 4-bromobenzyl bromide after 5 h.....	205
Figure 6.1.18.	^1H NMR spectra showing the progress of the reaction of a solution of the ring-closed isomer 3.2 in CD_3CN with an excess of 4-bromobenzyl bromide after 20 h.....	206
Figure 6.1.19.	^1H NMR spectra showing the peaks corresponding to a solution of the ring-open isomer 3.5 in CD_3CN before adding an excess of 4-bromobenzyl bromide.....	207
Figure 6.1.20.	^1H NMR spectra showing the progress of the reaction of a solution of the ring-open isomer 3.5 in CD_3CN with an excess of 4-bromobenzyl bromide after 5 h.....	208

Figure 6.1.21.	¹ H NMR spectra showing the progress of the reaction of a solution of the ring-open isomer 3.5 in CD ₃ CN with an excess of 4-bromobenzyl bromide after 10 h.....	209
Figure 6.1.22.	¹ H NMR spectra showing the peaks corresponding to a solution of the ring-closed isomer 3.6 in CD ₃ CN before the addition of an excess of the 4-bromobenzyl bromide.....	210
Figure 6.1.23.	¹ H NMR spectra showing the progress of the reaction of a solution of the ring-closed isomer 3.6 in CD ₃ CN with an excess of 4-bromobenzyl bromide after 8 h.....	211
Figure 6.1.24.	¹ H NMR spectra showing the progress of the reaction of a solution of the ring-closed isomer 3.6 in CD ₃ CN with an excess of 4-bromobenzyl bromide after 16 h.....	212
Figure 6.2.1.	Relaxation measurements (T ₁) for the ring-open (3.5) and the ring-closed (3.6) isomers of the <i>bis</i> (pyridine).....	213
Figure 6.2.2.	T ₁ relaxation measurements for the ring-open isomer (3.1) of the monobenzylated DTE.....	214
Figure 6.2.3.	T ₁ relaxation measurements for the ring-closed isomer (3.2) of the monobenzylated DTE.....	215
Figure 6.2.4.	T ₁ relaxation measurements for the ring-open isomer (3.3) of the dibenzylated DTE.....	216
Figure 6.2.5.	T ₁ relaxation measurements for the ring-closed isomer (3.4) of the dibenzylated DTE.....	217
Figure 6.3.1.	Plots of the natural log of the concentration of the ring-open isomer 3.1 against time	218
Figure 6.3.2.	Plots of the natural log of the concentration of the ring-open isomer 3.1 against time	219
Figure 6.3.3.	Plots of the natural log of the concentration of the ring-closed 3.2 against time.....	220
Figure 6.4.1.	Selected IR spectra showing the CO stretching frequencies when RuTTP(CO) is axially coordinated to (a) the pyridylthiophene 2.3 , (b) the monomethylated bipyridinium 2.4 , (c) the ring-open isomer 2.1 , and (d) the ring-closed isomer 2.2	221
Figure 6.4.2.	Selected IR spectra of the porphyrin-DTE complex 2.1RuP	222
Figure 6.4.3.	Selected IR spectra of the porphyrin-DTE complex 2.2RuP	223
Figure 6.4.4.	Selected IR spectra of the porphyrin-DTE complex 2.1RuP	224

LIST OF SCHEMES

Scheme 1.3.1. The <i>parallel</i> and <i>anti-parallel</i> conformations of the DTE	4
Scheme 1.4.1. Reversible photocyclization of a DTE	8
Scheme 2.6.1. Synthesis of porphyrin RuTTP(CO)(EtOH).....	34
Scheme 2.6.2. Synthesis of model compounds 2.3 and 2.4	36
Scheme 2.6.3. Effect of the more Lewis basic pyridylthiophene control 2.3 on a solution of the monomethylated bipyridinium-porphyrin complex 2.4RuP	41
Scheme 2.6.4. Synthesis of the monobenzylated DTE 2.2	44
Scheme 2.6.5. Difference in binding strength between the ring-open (2.1) and the ring-closed (2.2) isomers of the monobenzylated DTE	54
Scheme 2.6.6. Comparison of the coordination ability of the ring-open (2.1) and the ring-closed (2.2) isomers of the monobenzylated DTE	56
Scheme 2.6.7. Effect of the more Lewis basic pyridylthiophene control 2.3 on a mixture of the free and bound ring-open and ring-closed monobenzylated DTEs.....	61
Scheme 2.6.8. Use of the pyridylthiophene 2.3 to gauge the effect of the ring-opening and the ring-closing reaction on the coordination behaviour of the monobenzylated DTE.....	65
Scheme 2.6.9. The <i>parallel</i> and <i>anti-parallel</i> conformations of the ring-open DTE-porphyrin complex 2.1RuP	71
Scheme 2.8.1. Difference in binding strength between the ring-open (2.11) and the ring-closed (2.12) isomers of the DCTE.....	75
Scheme 3.1.1. Differences in reactivity between the monobenzylated DTEs 3.1 and 3.2	99
Scheme 3.4.1. Ring-opening and ring-closing reaction steps used to photoregulate reactivity <i>in situ</i>	124
Scheme 3.5.1. General example of a reaction showing two consecutive first-order reaction steps.....	129
Scheme 3.6.1. Consecutive <i>pseudo</i> -first-order sequence for the ring-open isomer 3.5	133
Scheme 3.6.2. Consecutive <i>pseudo</i> -first-order sequence for the ring-closed isomer 3.6 ...	140
Scheme 4.2.1. Mechanism for the pyridine catalyzed reaction of aldehydes with DMAD	169

LIST OF TABLES

Table 2.6.1.	Selected ^1H NMR data showing the free and bound forms of the pyridylthiophene 2.3	37
Table 2.6.2.	Selected ^1H NMR data showing the free and bound forms of the monomethylated bipyridinium 2.4	38
Table 2.6.3.	Selected ^1H NMR data showing the free and bound forms of the ring-open isomer 2.1	51
Table 2.6.4.	Selected ^1H NMR data showing the free and bound forms of the ring-closed isomer 2.2	52
Table 2.6.5.	List of CO stretching frequencies.....	70
Table 2.6.6.	Observed changes in the CO stretching frequencies on the photochemical interconversion of the DTE–porphyrin hybrids (2.1RuP and 2.2RuP)	73
Table 3.4.1.	Calculated apparent <i>pseudo</i> -first-order rate constants for the reaction of three independent solutions of the ring-open isomer 3.1 with an excess of 4-bromobenzyl bromide.....	114
Table 3.4.2.	List of apparent <i>pseudo</i> -first-order rate constants for the reaction of three samples of the ring-open isomer 3.1 with an excess of 4-bromobenzyl bromide.....	117
Table 3.4.3.	List of apparent <i>pseudo</i> -first-order rate constants for the reaction of three samples of the ring-closed isomer 3.2 with an excess of 4-bromobenzyl bromide.....	122
Table 3.4.4.	The observed in situ changes in the apparent <i>pseudo</i> -first-order rate constants at 22°C by alternating irradiation at 365 nm and > 490 nm over 3-hour intervals.....	127
Table 3.6.1.	Apparent <i>pseudo</i> -first-order rate constant for the reaction of <i>bis</i> (pyridine) 3.5 with an excess of bromobenzyl bromide	138
Table 3.6.2.	Apparent <i>pseudo</i> -first-order rate constant for the reaction of the monobenzylated DTE 3.1 with an excess of 4-bromobenzyl bromide	139
Table 3.6.3.	Apparent <i>pseudo</i> -first-order rate constant for the reaction of the <i>bis</i> (pyridine) 3.6 with an excess of 4-bromobenzyl bromide.....	145
Table 3.6.4.	Apparent <i>pseudo</i> -first-order rate constant for the reaction of the monobenzylated DTE 3.2 with an excess of 4-bromobenzyl bromide	146
Table 3.6.5.	Average apparent <i>pseudo</i> -first-order rate constants for the reaction of the ring-open and the ring-closed isomers of the <i>bis</i> (pyridine) and the monobenzylated DTE with an excess of 4-bromobenzyl bromide	147
Table 4.3.1.	Results of the reaction of 3-nitrobenzaldehyde 4.3 with DMAD 4.4 in the presence of isomers 4.1 and 4.2 and model compounds 4.6 and 4.7	176

LIST OF ABBREVIATIONS

°C	degrees Celsius
1-D NOE	one dimensional nuclear Overhauser effect
anal.	elemental analysis
aq	aqueous
Ar	aromatic group
b _L	bound ligand
br	broad (NMR)
¹³ C NMR	carbon nuclear magnetic resonance spectroscopy
calcd	calculated (elemental analysis)
CI	chemical ionization (mass spectrometry)
cm ⁻¹	wave number (IR spectroscopy)
CO	carbon monoxide
COSY	¹ H- ¹ H correlation spectroscopy (NMR)
d	doublet (NMR)
δ	chemical shift (NMR)
DCM	dichloromethane
DCTE	dicyanoethylene-thienylethene
dd	doublet of doublets
DMAD	dimethylacetylene dicarboxylate
DMAP	<i>N,N</i> -dimethyl-4-aminopyridine
DME	1,2-dimethoxyethane
DN	donor number
DTE	dithienylethene
EDG	electron donating group

ϵ	molar absorptivity
equiv	equivalent(s)
Et ₂ O	diethyl ether
EtOAc	ethyl acetate
EtOH	ethanol
EWG	electron withdrawing group
f _L	free ligand
FT-IR	Fourier-transform infrared spectroscopy
h	hour(s)
¹ H NMR	proton nuclear magnetic resonance
Hz	Hertz (cycles per second)
IR	infrared
<i>J</i>	coupling constant (NMR)
<i>k'</i>	<i>pseudo</i> -first-order rate constant
K _a	acid dissociation constant
KBr	potassium bromide disc (IR spectroscopy)
<i>k_{off}</i>	decomplexation rate
<i>k_{on}</i>	complexation rate
lit	literature (value)
λ	wavelength
LRMS	low resolution mass spectrometry
m	multiplet (NMR)
M	molarity
M ⁺	molecular ion (mass spectrometry)
MALDI-TOF	matrix assisted laser desorption ionization – time of flight

MeOH	methanol
mg	milligram(s)
MHz	megahertz
min	minute(s)
mL	millilitres
mM	millimolar
mmHg	millimeters of mercury
mmol	millimole(s)
mmol	micromolar
molar equiv	molar equivalent
Mp	melting point
<i>m/z</i>	mass to charge ratio
nm	nanometers
NMR	nuclear magnetic resonance
pH	acidity scale
pK _a	-log of K _a
ppm	parts per million
PSS	photostationary state
RuP	ruthenium porphyrin
s	singlet (NMR)
sec	second(s)
σ	sigma bond
T ₁	relaxation time (NMR)
THF	tetrahydrofuran
TLC	thin layer chromatography

TPP	5,10,15,20-tetraphenylporphyrin
TTP	5,10,15,20-tetratolylporphyrin
UV	ultraviolet (light)
Vis	visible (light)
W	Watt(s)

1 INTRODUCTION TO THE PHOTORESPONSIVE DITHIENYLETHENE (DTE) ARCHITECTURE

The research presented in this chapter is reproduced in part with permission “*Pure and Applied Chemistry*, copyright 2006, IUPAC” from: Samachetty, H. D. and Branda, N. R. “Integrating Molecular Switching and Chemical Reactivity Using Photoresponsive Hexatrienes” *Pure Appl. Chem.* **2006**, *78*, 2351-2359.

1.1 Molecular Devices and Molecular Switching

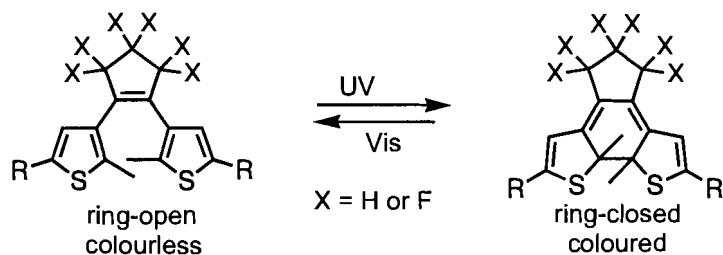
A molecular device is composed of molecules that are designed to perform a specific function. The human body can be considered as a collection of such molecular devices that are responsible for (1) enabling motion, (2) controlling the thought and sensory processes, and (3) repairing damage.¹ The practical operation of artificial molecular-scale devices relies heavily on the presence of programmable elements within the molecular systems that allows the functions and properties of the molecules to be regulated on demand. Molecular systems that can be reversibly transformed between two distinct isomers having unique structural and electronic properties when subjected to an external stimulus, have the potential to significantly influence the development of numerous materials science technologies and structural biology.² This potential is based on the fact that the dramatic changes in their structural and electronic characteristics can be used as switching elements in molecular-scale devices.

1.2 Photochromism

The use of light as an external trigger for a reaction is appealing since the wavelength of modern lasers are tuneable and monochromatic such that they can be used in a controllable fashion and under conditions that are mild enough to minimize danger to sensitive biomaterials. Molecular systems that are capable of reversibly interconverting between two isomers having unique absorption spectra when stimulated by light are termed photochromic.^{3,4} The property changes that occur between the two isomers are not only responsible for the dramatic changes in colour but can also result in changes in (1) optical properties such as luminescence,⁵⁻⁹ refractive index,¹⁰⁻¹² and optical rotation,¹³⁻¹⁸ (2) magnetic interactions,¹⁹ (3) electronic conductance,²⁰⁻²³ and (4) redox properties²⁴⁻³⁰ The photomodulation of these properties has potential applications in optoelectronic technologies such as waveguides and optical information storage systems.

1.3 The Dithienylethenes

There are many classes of organic photochromic compounds and some of the common examples include azobenzenes, spiropyrans, dihydropyrans, fulgides, spirooxazines and dithienylethenes. However, most of these photoresponsive compounds cannot be used as switching elements in devices in a practical setting because they are limited by one or more of the following factors: (1) the thermal reversibility of the photochromic reaction at the temperature of operation of the device, (2) the formation of photochemical side-products over repetitive photoisomerization cycles, and (3) the synthetic difficulties involved in preparing functionalized versions that do not interfere with the photochromic behaviour of the device.^{2,3}

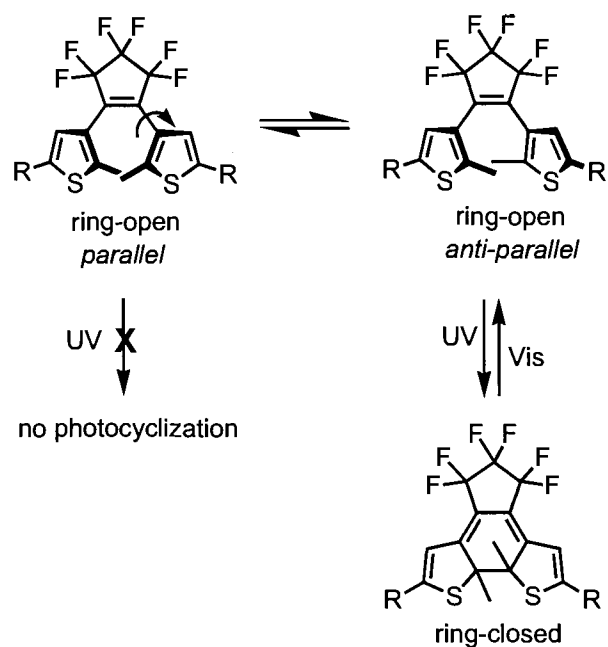


Equation 1.3.1. Photoisomerization reaction of the DTE architecture between the colourless ring-open form and the coloured ring-closed form induced by different wavelengths of light.

One of the most promising photoresponsive frameworks is found in the 1,2-dithienylethenes (DTEs) because they satisfy numerous physical and chemical properties required for practical use in functional materials and devices. DTE derivatives all contain a hexatriene backbone that results in the interconversion between colourless ring-open isomers and coloured ring-closed isomers by alternate irradiation with UV and visible light, respectively (Equation 1.3.1). These derivatives show remarkable photofatigue resistance (more than 10,000 ring-opening/ring-closing cycles reported for some DTEs) and thermal stability (some DTEs have been shown to remain in their ring-closed forms for more than 3 months at 80°C).³¹⁻³³ The research presented in this thesis focuses on the use of DTEs as photoresponsive systems and in the following sections a more detailed discussion of the photochromism of DTEs is provided.

1.3.1 Photochemical Ring-Closing Reaction

The ring-open form of the DTE can exist in two conformations, namely the *parallel* conformation with the two thiophene rings in mirror symmetry and the *anti-parallel* conformation where the molecule has a C_2 axis of symmetry. The two DTE conformers are illustrated in Scheme 1.3.1.



Scheme 1.3.1. The *parallel* and *anti-parallel* conformations of the DTE.

The photoisomerization event involves the $4n+2$ Woodward and Hoffmann-allowed, conrotatory, ring-closing reaction of the photoexcited *anti-parallel* conformation.^{32,34} This conformational requirement has been extensively studied by Irie and coworkers and they have shown that locking the DTE backbone in the parallel conformation inhibits photochromism, while derivatives that favour the *anti-parallel* conformation tend to have higher quantum yields.³⁵⁻³⁷ Although the ring-closing reaction of the *parallel* conformation via a disrotatory process is thermally allowed from the ground state, it is not observed due to the large activation barrier created by the steric hindrance of the central methyl groups.³⁸

1.3.2 Photostationary State

The term photostationary state (PSS) is used to evaluate the photochromic performance of DTE systems. The PSS describes the percentage of ring-open molecules that undergo the photocyclization event at a particular wavelength as shown in Equation 1.3.2.^{31-33,39,40}

$$\text{PSS} = \frac{\text{\# of molecules that isomerized}}{\text{total\# of molecules}} \times 100\%$$

Equation 1.3.2. Equation used to calculate photostationary state.

Some DTEs have been shown to exhibit very pronounced photochromic properties resulting in virtually total conversion to the ring-closed form (PSS \approx 100%).²⁹ DTE systems that can be fully converted to their ring-closed forms are of great importance since they provide a handle for complete “on-off” type of switching function. The term PSS will be used throughout this thesis to refer to the ring-closing (ring-opening) reaction of the ring-open (ring-closed) isomer by irradiation with the appropriate wavelengths of light until no further change is observed either by UV-Vis or ¹H NMR spectroscopy for the solution studies or IR spectroscopy for the solid-state studies (KBr matrix) presented in *Chapter 2*.

1.3.3 Photochemical Cycling

In order to use DTE-based systems as switching elements that allow the properties and functions of a device to be turned “on” and “off” on demand, they must be capable of interconverting between their ring-open and ring-closed forms without forming photochemical side-products or degrading. Compounds that can undergo numerous ring-

closing/ring-opening cycles, without significant photodegradation, are termed photofatigue resistant. One appealing feature of DTEs is their impressive degree of fatigue resistance and examples of such systems that can be cycled up to 10,000 times with minimal observable degradation (< 10%) have been reported.³³ As an alternative to testing the fatigue resistance over hundreds of cycles, which requires an automated cycling system, our research group has resorted to manual cycling experiments where alternate irradiation with UV and visible light are carried out, while monitoring the absorption spectra over a few cycles. In this thesis, the photofatigue resistance of DTE systems will be tested over ten ring-closing/ring-opening cycles.

1.3.4 Functionalization of DTEs

One appealing quality of DTEs is that a variety of functional groups can be incorporated into the system using a wide range of synthetic techniques without compromising the photochromic behaviour of the DTE. This synthetic modification is conveniently achieved through simple functional group transformations on a preassembled DTE scaffold or by functionalizing the thiophene rings prior to assembling the DTE architecture. The most common positions for the introduction of functional groups are at the C5-positions (terminal positions labelled 'A' and 'B' in Figure 1.3.1) of the two thiophene rings. Sites 'A' and 'B' are the ones that most dramatically affect the optical properties of the ring-closed form due to the creation of the extended π -conjugated pathway. In this thesis, these positions will be referred to as the "external" positions. Other sites that can be synthetically tailored are the C2-positions (labelled 'C' and 'D' in Figure 1.3.1) of the thiophene heterocycles (which are the carbon atoms that undergo a change in hybridization from sp^2 to sp^3 upon the photocyclization event).

Changing the ‘C’ and ‘D’ positions from alkyl groups to aryl groups alters the electrochromic behaviour of the backbone. The work of Branda and Peters^{26,27} has shown that when ‘C’ and ‘D’ are alkyl groups, the derivatives undergo oxidative ring-closing and when ‘C’ and ‘D’ are aryl groups, the derivatives undergo oxidative ring-opening. These positions will be referred to as the “internal” positions in this thesis. Thus, such synthetic modifications introduce the element of control over the properties of DTE systems and add to the appeal of DTEs as photoresponsive functional materials.

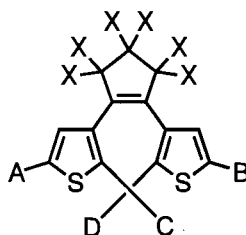


Figure 1.3.1. Structure of a generalized DTE chromophore showing the sites (‘A’, ‘B’, ‘C’, and ‘D’) that are the easiest to decorate.

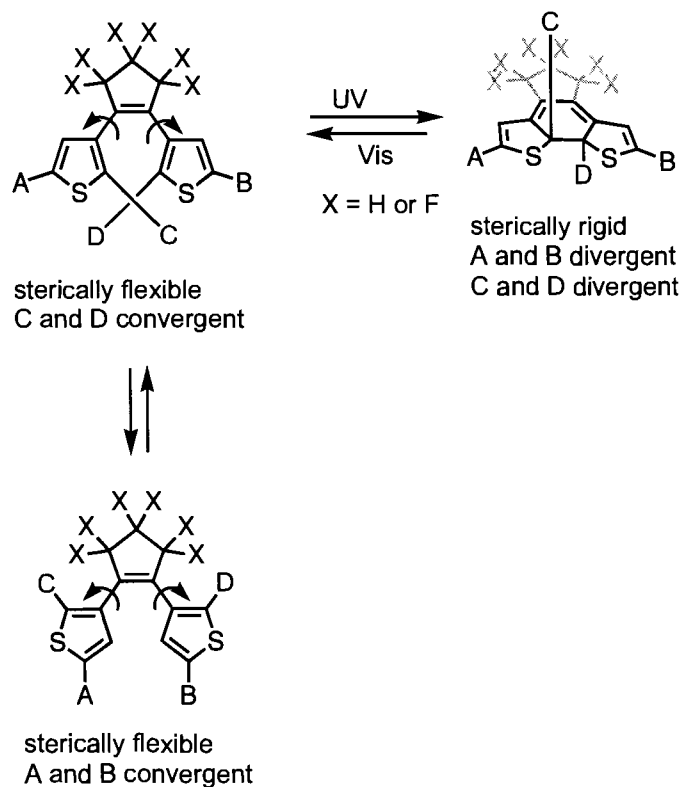
1.4 Differences Between the Ring-Open and the Ring-Closed Isomers of DTEs

As already mentioned, photoresponsive DTEs can be toggled between two thermally stable forms when irradiated with the appropriate wavelengths of light and provide a practical means of regulating the chemical and physical properties of molecular devices. The appealing feature of the DTE backbone is that the two interconverting isomers exhibit dramatic geometric and electronic differences. Most research groups focus on the electronic differences between the two isomers and the resulting variations in properties such as optics, magnetism, conductance and redox potentials, all of which have potential applications in optoelectronic technologies. In this thesis, the main emphasis is on the through-space and the through-bond communication between the

functional groups that are pendant on the DTE backbone that arises due to the geometric and the electronic differences between the two DTE isomers.

1.4.1 Geometric Differences (Through-Space Communication)

In the ring-open isomer, there is relatively free rotation around the two carbon-carbon bonds joining the thiophene heterocycles to the central cyclopentene ring, as shown in Scheme 1.4.1. This structural flexibility allows (1) the interconversion between the *parallel* and the *anti-parallel* conformations previously mentioned in *Section 1.3.1*, (2) the functional groups 'A' and 'B' occupying the external positions of the thiophene heterocycles to converge towards each other, and (3) the functional groups 'C' and 'D' located at the internal positions of the thiophene rings to converge towards each other.

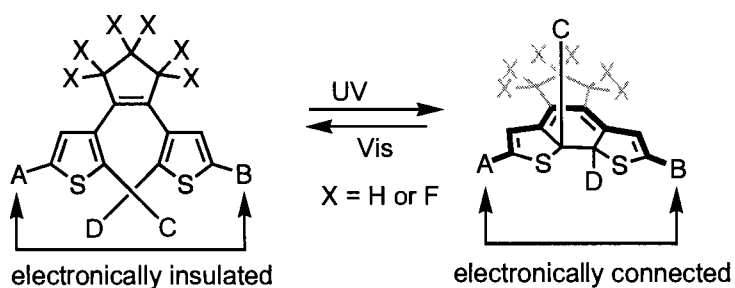


Scheme 1.4.1. Reversible photocyclization of a DTE. The free rotation in the ring-open isomer results in a flexible and convergent state while the opposite is true for the ring-closed isomer.

The ring-closing event generates a rigid structure, due to the creation of the fused tricyclic structure, and forces groups ‘A’ and ‘B’ to diverge away from each other. Similar structural constraints apply for groups ‘C’ and ‘D’. This convergence and divergence provides a means to create and destroy molecular recognition sites and surfaces capable of binding and release and can be very useful for regulating host-guest chemistry and coordination chemistry.

1.4.2 Electronic Differences (Through-Bond Communication)

In the ring-open isomer, the two π -systems are localized within each of the two thiophene rings and the pendant groups ‘A’ and ‘B’ are cross-conjugated through the DTE backbone. Also, the two thiophene rings are not coplanar such that the groups ‘A’ and ‘B’ are electronically insulated from each other and should be electronically independent. Upon photochemical ring-closure, the π -system is extended creating a linear π -conjugated pathway through the entire DTE backbone as illustrated in bold in Equation 1.4.1.



Equation 1.4.1. Reversible photocyclization of a DTE. In the ring-closed form, the two π -systems are localized within each of the two thiophene rings and the pendant groups ‘A’ and ‘B’ are cross-conjugated through the DTE backbone groups such that ‘A’ and ‘B’ are electronically insulated from each other. The photochemical ring-closure creates a linear π -conjugated pathway through the entire DTE backbone such that the ends of the conjugated pathway are in electronic communication and allows the groups ‘A’ and ‘B’ to sense the electronic nature of each other.

The cyclization event creates a state where the ends of the conjugated pathway are in electronic communication and allows the groups 'A' and 'B' to sense the electronic nature of each other. In principle, any type of property that is dependent on electronic communication between the groups located at the external positions 'A' and 'B' can be photoregulated between its "on" and "off" states. In fact, this through-bond communication between the two pendant groups 'A' and 'B' has been used to regulate optics, magnetism, electrical conductance, and redox potentials, as previously mentioned. However, the goal of this thesis is to take advantage of the changes in the extent of through-bond communication between the ring-open and the ring-closed states to regulate reactivity.

1.5 Control of Reactivity

The development of molecular systems that show reversible changes in their structures and functions is an active area of research, as it has potential applications in molecular devices. However, there are only a few examples that take advantage of these reversible changes to influence chemical reactivity.⁴¹⁻⁴³ Controlling the outcome of a chemical reaction is a fundamental goal of chemical research. The practical reasons for seeking such control include: (1) improving the efficiency of reactions and suppressing unwanted side reactions, (2) creating new reagents that can react faster, (3) generating increasingly complex molecular structures quickly, efficiently, and in large quantities for use in drug research, and (4) synthesizing small building blocks encoded with the necessary information to self-assemble into more complex supramolecular structures that can mimic biological systems.

1.5.1 Steric and Electronic Effects on Chemical Reactivity

The reactivity of a compound is influenced by the steric and electronic environment around the functional groups located at the reaction site of the compound. This influence can be strong enough to start or stop the reaction or to alter the reaction pathway. The two major factors influencing the outcome or the extent of a reaction are steric effects⁴⁴ and electronic effects.^{45,46}

Influencing chemical reactivity using steric effects involves taking advantage of one of the following: (1) the shape and the accessibility of the reaction site,^{47,48} (2) a change in hybridization of the carbon at the reactive site occurring during the course of the reaction leading to the creation or the relief of strain,⁴⁹⁻⁵¹ and (3) conformational effects^{52,53} that allow or prevent the compound from adopting the proper orientation for the reaction to take place.

The control of chemical reactivity using electronic effects can be achieved by either varying the extent of polarization⁵⁴⁻⁵⁶ or the extent of delocalization⁵⁷ of the electron-density at the reaction site. Such variations in electronic effects are the basis of polar reactions involving nucleophiles (electron-rich species) and electrophiles (electron-poor species).

1.6 Integration of Photoswitching and Chemical Reactivity

The incorporation of light-responsive compounds into molecular systems leads to the possibility of turning a reaction “on” or “off” using light as an external stimulus and opens the door to the design of photoactive reagents. This has the potential to advance synthetic methods, catalysis and the controlled delivery of biochemical reagents.

Catalysis-based chemical synthesis accounts for about 60% of the current chemical products and about 90% of the chemical processes.⁵⁸ Also, the controlled-delivery of biochemical reagents *in vitro* or *in vivo* to induce a response in cells for biochemical and biophysical experiments is of keen interest. Many important site-selective drug delivery strategies require the reagent to be in its inactive form before reaching the targeted cells or tissues and rely on the “prodrug” design.^{59,60} A prodrug is a drug, which is initially in an inactive (or significantly less active) form and is converted into the active compound by processes such as metabolism, hydrolysis or using an external trigger.^{61,62} Introducing photoswitching elements in such systems can provide a handle to start or stop the formation of the biochemical reagent at a targeted site using light.

The DTE backbone is well suited to modulate chemical reactivity because the geometric or electronic differences between the ring-open and the ring-closed isomers described previously can potentially be used as the “on” and “off” functions to start and stop reactions using light.

1.6.1 Use of Steric Changes to Modulate Reactivity

Branda and coworkers⁴¹ recently used the differences in geometry between the ring-open and the ring-closed isomers of the *bis*(oxazoline) **1.1** (shown in Figure 1.6.1) to regulate reactivity. In this example, they took advantage of the light-induced ring-opening and ring-closing reactions to create and distort a chelation site between the chiral oxazoline moieties located at the internal positions of the thiophene rings to regulate the binding of a copper(I) ion. They then showed that this copper complex can be used as a catalyst to photomodulate the stereochemical outcome of a cyclopropanation reaction.

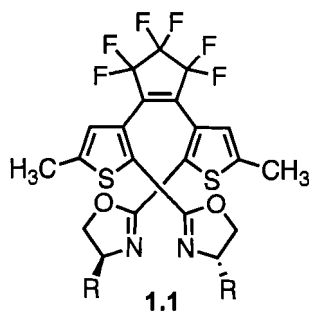


Figure 1.6.1. Photoresponsive *bis*(oxazoline) DTE ligand used to reversibly bind copper.

They successfully demonstrated that the changes in geometry and binding are significant, as proven by the fact that the ring-closed form (when isolated) shows insignificant stereoselectivity. However, the performance of this system is limited by the very low PSS making it hard to access the completely ring-closed form (“off” state of the switch) *in situ*.

1.6.2 Use of Electronic Changes to Control Reactivity

Lehn and coworkers⁴² described an example where the electronic communication between a phenol and an electron-withdrawing pyridinium group located across the backbone of DTE **1.2** (shown in Figure 1.6.2) can be photochemically created or disrupted to modulate the acidity of the phenolic OH. Their approach is based on the assumption that stabilization of the negative charge of the conjugate base of the phenol by the electron-withdrawing moiety may be possible in the ring-closed form owing to the creation of the linear π -conjugation across the DTE backbone, resulting in the enhanced acidity of the system. Although their initial system is limited by the decomposition of the ring-closed form of the DTE **1.2**, they demonstrated that the dissociation constant of the DTE **1.3** (formed as a side-product upon deprotonation of the phenol moiety of the ring-

closed form of **1.2** with a saturated solution of methanolic potassium hydroxide) can be successfully enhanced (by a factor of 16) upon ring-cyclization.

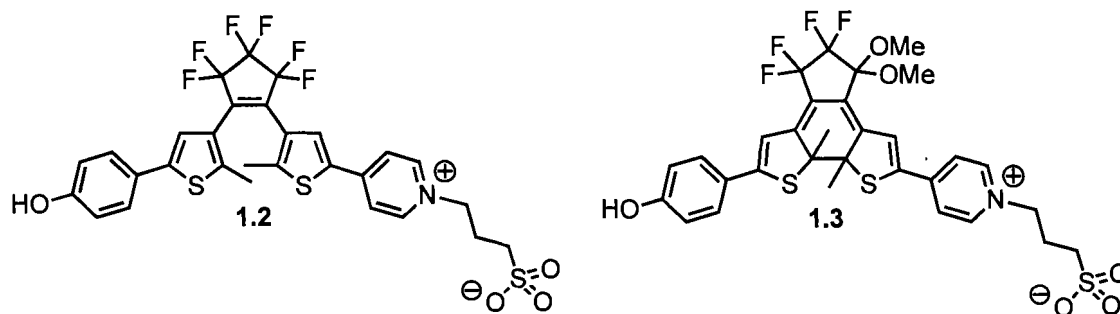


Figure 1.6.2. Photoresponsive DTEs **1.2** and **1.3** used to photomodulate pK_a . The phenolic OH of the DTEs **1.2** and **1.3** have different pK_a values due to the changes in electronic communication between the two sides of the photoresponsive backbone.

A more recent example,⁴³ uses a modified version of compound **1.2** in which an electron-donating 4-methoxyphenyl group is introduced at the internal position of the thiophene bearing the phenol group (shown in Figure 1.6.3) with the view of creating a more pronounced difference in pK_a values between the ring-open and the ring-closed isomers. In this system, the ring-open form is electronically connected to the electron-donating 4-methoxyphenyl group while the ring-closed form is insulated.

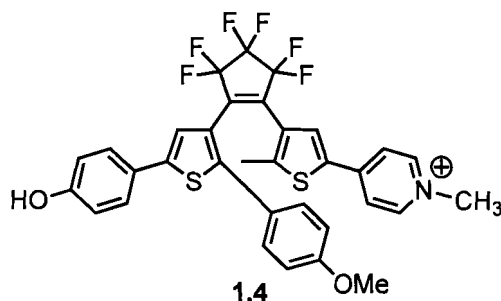


Figure 1.6.3. Modified DTE system with an electron-donating substituent at the internal position of the thiophene ring bearing the phenol group.

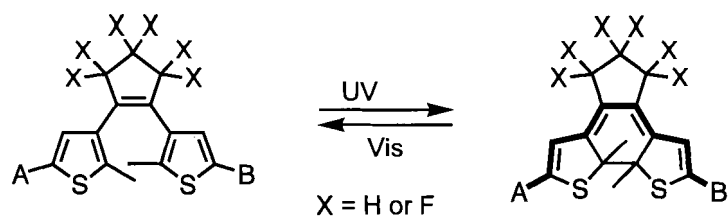
However, the use of this system is limited by the fact that under high pH conditions (pH values greater than the pK_a of the phenolic form of DTE **1.4**) the photocyclization reaction of the phenolate form of DTE **1.4** does not occur.

1.7 Control of Nucleophilicity using Photoresponsive DTEs

The examples discussed in the previous section show that it is possible to photoregulate the pK_a of a compound using light. My research goals were to apply similar principles to regulate nucleophilicity with light as an external stimulus. Nucleophilicity is the term used to define the ability of an atom to donate its electron density to the antibonding orbital of a reactant and is thus heavily dependent on the availability of electron density on the atom. The possibility to photomodulate nucleophilic strength has potential applications in the design of light-activated reagents and catalysts. In fact, aside from the use of Brønsted acids and bases, one popular approach to accelerating a chemical reaction is nucleophilic catalysis. Nucleophilic catalysis is used in the acylation, phosphorylation, and sulphonylation of alcohols, amines and thiols as well as in the hydrolysis of esters and related reactions and has widespread applications in organic chemistry, polymer chemistry, agricultural and pharmaceutical industries and biochemistry.⁶³⁻⁶⁵ Nature makes use of the variations in nucleophilic strength in various enzyme active sites to efficiently catalyze acylation and hydrolytic reactions.⁶⁶

Since the ring-opening and ring-closing reaction of DTEs influence the potential polarization of electrons through the DTE backbone, the goal of the work described in this thesis is to investigate whether the changes in electronics between the two DTE

isomers can be used to photomodulate nucleophilicity because of the potential control it provides as previously mentioned.



Equation 1.7.1. Controlling nucleophilicity using a photoresponsive DTE. The nucleophilicity of the functional group ‘A’ can be photomodulated due to the changes in electronic communication between the two sides of the conjugated backbone in the ring-open and the ring-closed DTE isomers when ‘B’ is either an electron-donating or an electron-withdrawing group.

For instance, the lack of coplanarity and linear π -conjugation in the ring-open isomer electronically insulates the two thiophene rings from each other and a nucleophilic functional group ‘A’ will not sense the effect of the functional group ‘B’, located at the external position of the second thiophene ring. The photocyclization event allows a linear π -conjugation pathway along the DTE backbone where there is electronic communication between ‘A’ and ‘B’ (shown in bold in Equation 1.7.1) and it is reasonable to expect that, depending on the nature of the functional group ‘B’ (electron-donating or electron-withdrawing), the nucleophilicity of ‘A’ can be enhanced or lowered. One classic example where the electronic effects of the functional group plays a major role in the nucleophilicity of a pyridine is N,N-dimethyl-4-aminopyridine (DMAP), which is one of the most efficient and widely used nucleophilic catalysts.^{64,67}

1.8 Summary

The goal of the work presented in this thesis is to relate photoswitching and chemical reactivity in photoresponsive systems because it has potential applications in the design of light-activated reagents and catalysts as already described. In this introductory chapter, the few literature precedents for molecular systems that take advantage of the geometric and electronic differences between the ring-open and ring-closed DTE isomers to modulate chemical reactivity have been presented. These examples outline how the structural and electronic properties of DTEs can be fine-tuned by rationally, and easily, “decorating” both the external C5 and the internal C2 positions of the thiophene rings which adds to the versatility and appeal of DTE derivatives as switching elements.

1.9 Preview of Thesis

Photoresponsive DTE systems have the potential to advance synthetic methods and catalysis. These applications require systems that show measurable differences in chemical reactivity. It is well documented that the nucleophilicity and Lewis basicity of a nitrogen-containing compound is very sensitive to its electronic environment. Consequently, it is possible to control the extent of the changes in nucleophilicity and Lewis basicity by fine-tuning the electronic framework of the groups attached to the nitrogen-containing compound. The research presented in this thesis focuses on integrating photoswitching and nucleophilicity using a pyridine-functionalized DTE to demonstrate the concept of photomodulating reactivity and catalysis and is a starting

point for the development of better devices that can have potential impact in structural biology and materials science applications.

In *Chapter 2*, the synthesis and photochromic properties of a photoresponsive pyridine-functionalized monobenzylated DTE derivative are described. Axial coordination to a metalloporphyrin was used as a probe to demonstrate that the differences in the extent of π -conjugation between the two DTE isomers affect the Lewis basicity of the free nitrogen atom. One key feature about this study is that it made use of the very simple and yet diagnostic ^1H NMR spectroscopic technique to indicate that the ring-open isomer is approximately 1.3 times more effective as a ligand than its ring-closed form.

In the first part of *Chapter 3*, the apparent rates of alkylation of the free pyridines of the ring-open and ring-closed isomers of the monobenzylated DTE are investigated as an alternative probe to demonstrate that the presence of the electron-withdrawing pyridinium group affects the nucleophilic character of the pendant pyridine moiety. The results indicate that the ring-open form of the monobenzylated DTE reacts approximately 3 times faster than its ring-closed counterpart. In the second part of *Chapter 3*, consecutive *pseudo*-first-order kinetics was used to probe the differences in reactivity between the ring-open and the ring-closed isomers of the *bis*(pyridine) (precursor used in the synthesis of the monobenzylated DTE) and the monobenzylated DTE to better understand the through-bond and the through-space effects of having (1) two pyridines and (2) a pyridine and an electron-deficient pyridinium at the external positions of the DTE backbone.

In *Chapter 4*, the attempts to use the DTE system as a nucleophilic catalyst are discussed. The results show the concept of phototuning reactivity with the ring-open isomer acting as the more efficient catalyst than its ring-closed counterpart.

This thesis concludes with a brief discussion of the results of this research and identifies potential problems that need to be addressed before DTE systems can be used to control reactivity and catalysis in a more practical setting.

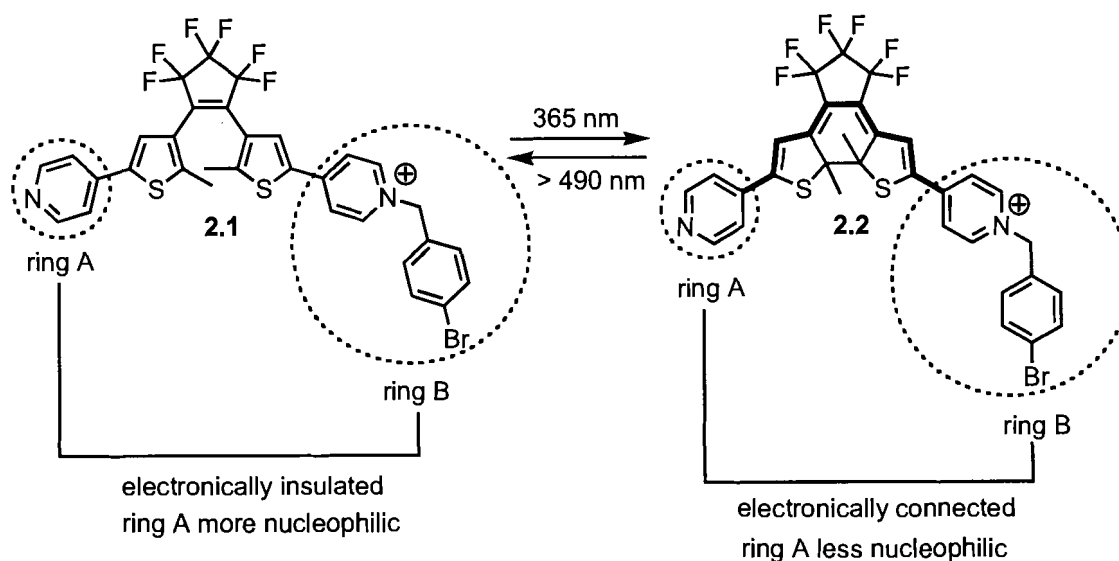
2 Photomodulation of Coordination Chemistry in a Photoresponsive DTE System

The research presented in this chapter is reproduced in part with permission “*Chemical Communications*, copyright 2005, The Royal Society of Chemistry” from: Samachetty, H. D. and Branda, N. R. “Photomodulation of Lewis basicity in a pyridine-functionalized 1,2-dithienylcyclopentene” *Chem. Commun.* **2005**, 2840-2842.

2.1 Integration of DTEs and Nucleophilicity

Controlling the outcome of a chemical reaction is a fundamental goal of chemical research and processing, and the practical reasons for seeking such control range from suppressing unwanted side products to synthesizing new structures and new materials that can mimic biological systems. As discussed in *Chapter 1*, the DTE backbone is well-suited to modulate chemical reactivity since the electronic differences between the ring-open and the ring-closed isomers can be used as the “on” and “off” functions to start and stop reactions using light. DTEs have the potential to act as the switching elements in photoactive reagents, catalysts, and biochemical reagents. The few reports that take advantage of the changes in electronic communication between the two DTE isomers were presented in the introductory chapter. The research discussed in this chapter takes advantage of the fact that the ring-opening and the ring-closing reaction of DTEs influences the potential polarization of electrons through the DTE backbone to photomodulate the nucleophilicity of an appropriately functionalized DTE derivative. Nucleophilicity was chosen as the target concept because it is a fundamental kinetic property that plays an important role in many chemical reactions.⁶⁸ Given that Lehn and coworkers⁴² used a DTE system to modulate pKa, a fundamental thermodynamic

property, my hypothesis was that the photoregulation of nucleophilicity in DTE systems should also be possible. The approach discussed in this chapter takes advantage of the fact that the nucleophilic character of a nitrogen-containing compound is dependent on the electronic influence of the groups attached to it.⁶⁹⁻⁷¹ The concept is illustrated in Equation 2.1.1, which shows the system that incorporates a nucleophilic pyridine (labelled as ring 'A' in Equation 2.1.1) and an electron-withdrawing pyridinium (labelled as ring 'B' in Equation 2.1.1) into the DTE backbone.



Equation 2.1.1. The free pyridine ring 'A' of the monocationic DTEs **2.1** and **2.2** displays differing nucleophilicity. The difference in nucleophilicity is due to the changes in electronic communication between the two sides of the DTE backbone.

The idea here is to use the pyridine group as a test nucleophile. In the case of the ring-open isomer **2.1**, the thiophene heterocycles are electronically independent such that the free pyridine (ring 'A') is insulated from the electron-deficient pyridinium (ring 'B'). The photocyclization event allows electronic communication along the DTE backbone (shown in bold in Equation 2.1.1) and it is reasonable to expect that the pyridine 'A' will sense the electron-withdrawing character of the pyridinium 'B', through an inductive

polarization effect, resulting in a lowering of the nucleophilicity. Since it is an inductive effect, it can be expected that the change in nucleophilic character between the two DTE isomers will be small. Prior to evaluating this concept in chemical synthesis, axial coordination to a metalloporphyrin is a useful probe to determine whether there is a measurable difference in reactivity between the ring-open isomer **2.1** and its ring-closed counterpart **2.2**.

2.2 Introduction to Axial Binding to Metalloporphyrins Containing Ruthenium

Porphyrins and metalloporphyrins play a key role in many biological processes such as photosynthesis, oxygen transport and storage, electron transport and oxygen activation and utilization.^{72,73} Attempts to model these properties and to elucidate the fundamental aspects of reactivity and mechanism have led to an active area of research involving synthetic metalloporphyrins. The synthetic versatility and rich photochemical and redox properties of metalloporphyrins also make them particularly interesting in the field of supramolecular chemistry,^{74,75} where they are used as building blocks for the construction of artificial systems with special built-in properties. One strategy in the design of multicomponent supramolecular assemblies involves axial coordination to ruthenium(II) carbonyl porphyrins.⁷⁶⁻⁷⁸ It is well-established that Ru(II) complexes generally adopt an octahedral geometry such that the presence of the Ru(II) in carbonyl porphyrins introduces a sixth coordination site (axial position), shown in Figure 2.2.1, that can readily be accessed by Lewis bases such as pyridines and pyridine-containing compounds.

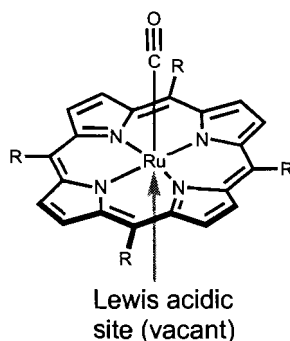
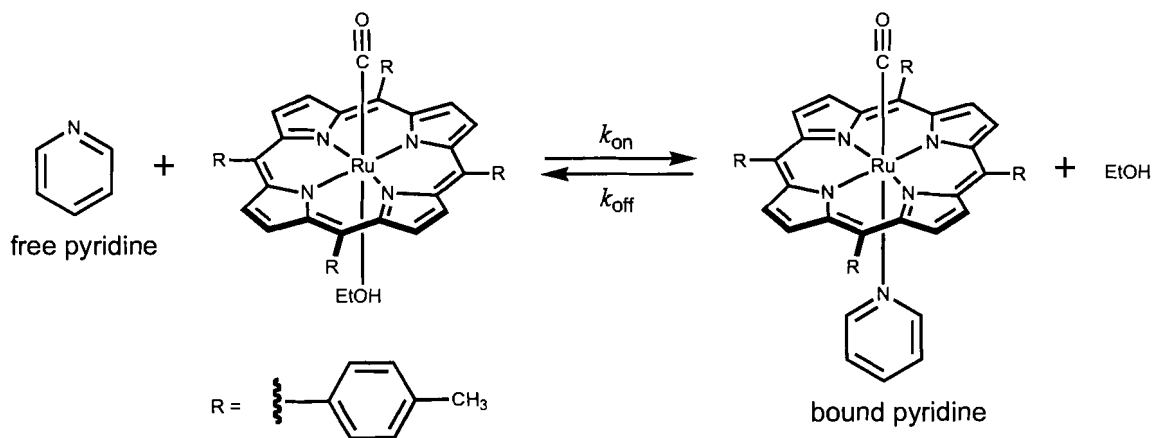


Figure 2.2.1. Generalized structure of a Ru(II) carbonyl porphyrin with a vacant axial coordination site that can readily be accessed by Lewis bases.

Previous members of our research group have taken advantage of this strategy, using the ethanol adduct of the already known 5,10,15,20-tetratolylruthenium(II) carbonyl porphyrin [RuTTP(CO)(EtOH)]⁷⁹ as the metalloporphyrin reagent, to (1) show the unprecedented self-assembly of both linear and three-dimensional multicomponent porphyrin arrays constructed around transition metal complexes,^{80,81} (2) self-assemble rotaxane stoppers,⁸² and (3) achieve non-destructive readout in a DTE–porphyrin hybrid.⁹ It is well-known that the EtOH ligand of the metalloporphyrin reagent RuTTP(CO)(EtOH) is easily displaced by stronger Lewis bases such as pyridines as shown by the Equation 2.2.1. The pyridine is not permanently bound to the porphyrin and the bond between the pyridine and the porphyrin is kinetically labile. Previous work on the axial coordination of pyridines to ruthenium porphyrins have shown that the rate constant for the complexation reaction (k_{on}) is fast ($\sim 10^6\text{--}10^7 \text{ M}^{-1}\text{sec}^{-1}$) while the rate constant for the reverse step (k_{off}) is slow ($\sim 10^{-1} \text{ sec}^{-1}$).⁸³ The term “free” refers to the uncoordinated pyridine while the term “bound” refers to the pyridine in the pyridine–porphyrin adduct. This terminology will be referred to regularly throughout this chapter when monitoring the axial coordination event.



Equation 2.2.1. General reaction between a pyridine and RuTTP(CO)(EtOH). The stronger Lewis basic pyridine easily displaces the labile EtOH ligand to form the pyridine–porphyrin adduct. The term “free” is used to denote the pyridine when it is not axially coordinated to the metalloporphyrin while the term “bound” is used to denote the pyridine when it is axially coordinated to the metalloporphyrin.

The work presented in this chapter uses the fact that axial coordination involves a Lewis acid–Lewis base interaction to probe the difference in Lewis basicity between the ring-open isomer **2.1** and the ring-closed isomer **2.2**. The idea behind this approach is that the more Lewis basic the pyridine ligand, the stronger the binding strength between the ruthenium metal and the nitrogen of the pyridine (Ru–N bond) and the more stable the resulting porphyrin complex. For instance, the Ru–N bond can be expected to be stronger in the case of the more Lewis basic ring-open isomer **2.1** compared to the ring-closed isomer **2.2** such that it is reasonable to expect that the porphyrin–DTE complex of the ring-open isomer **2.1** will be more stable than that of the ring-closed form **2.2** (Figure 2.2.2).

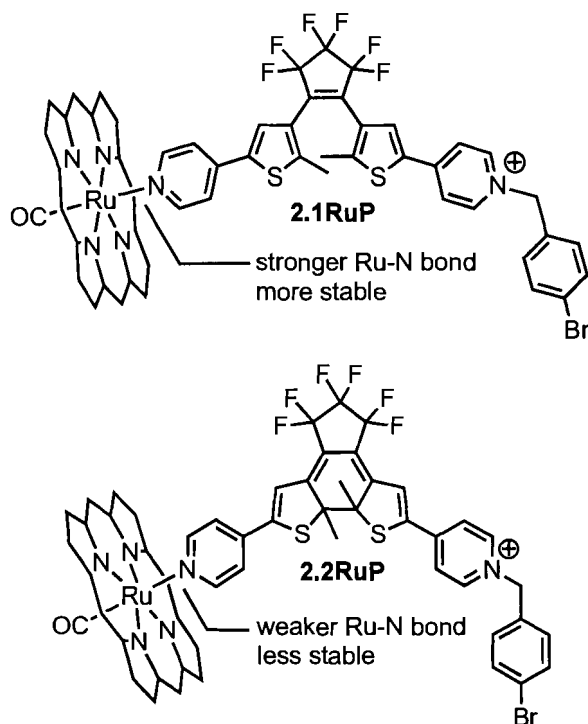


Figure 2.2.2. Difference in coordination behaviour between the ring-open isomer **2.1** and the ring-closed isomer **2.2**. The more Lewis basic ring-open isomer **2.1** can be expected to form the more stable porphyrin–DTE complex than the ring-closed isomer **2.2**. The *p*-tolyl groups at the meso positions and the double bonds of the porphyrin have been omitted here for simplicity.

One convenient aspect of using axial coordination to a ruthenium porphyrin as a probe is that the differences between the ring-open isomer and the ring-closed isomer can be assessed by ^1H NMR spectroscopy and IR spectroscopy. The reasons for this are discussed in more details in *Sections 2.3* and *2.4*.

2.3 ^1H NMR Spectroscopy as a Diagnostic Tool to Probe Axial Coordination

2.3.1 Chemical Exchange

The signals observed by NMR spectroscopy can vary if the monitored nucleus can “partition” between two magnetically non-equivalent sites and common examples include protons or carbon atoms involved in *cis-trans* isomerization, rotation about the carbon-

nitrogen bond in amides, proton exchange between solvent and solute, and complex formation. In the NMR context, the nucleus is said to undergo *chemical exchange* between the sites.⁸⁴ For instance, for a hypothetical system consisting of a free ligand f_L and a bound ligand b_L , the nature of the observed signal will depend on the complexation rate (k_{on}) and the decomplexation rate (k_{off}).

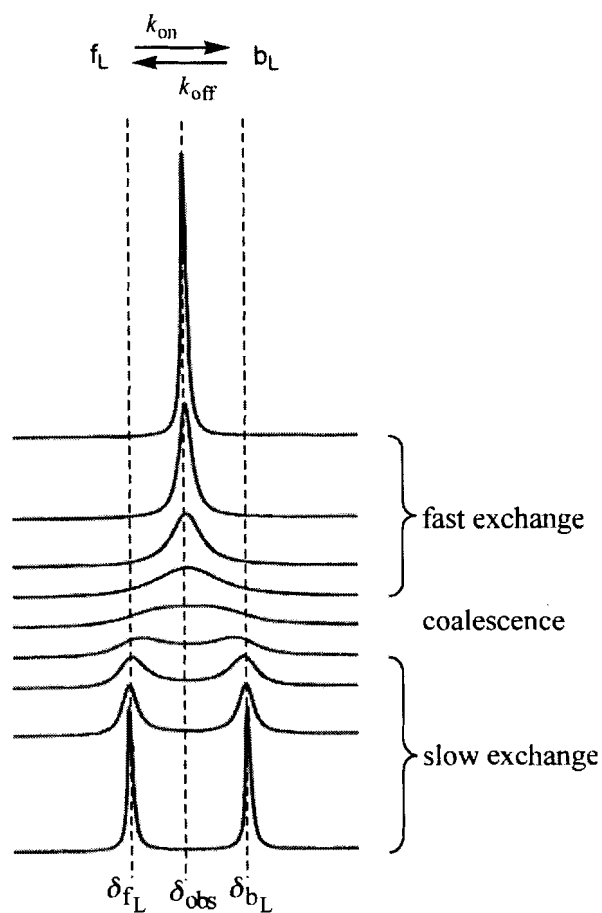


Figure 2.3.1. Variations in the nature of the observable NMR signals for a hypothetical system. The signals correspond to a system exhibiting slow chemical exchange, coalescence, and fast chemical exchange between its free and bound states. Adapted from reference 84.

The three classifications used are (1) slow exchange, (2) coalescence, and (3) fast exchange and are illustrated in Figure 2.3.1 where δ_{f_L} corresponds to the chemical shift

of the free state and δ_{bL} refers to the chemical shift of the bound state while δ_{obs} refers to the observed chemical shift corresponding to the average of the free and bound states.

It is well established that the N-Ru binding process of pyridine-containing compounds to ruthenium porphyrins is slow on the NMR time scale.^{79,85-87} Consequently the ^1H NMR spectrum has two signals, one corresponding to the free compound and one corresponding to the bound compound such that the integration of the area under each peak gives the amount of each state.

It can thus be expected that the axial coordination of the pyridine-containing DTE ligand to RuTTP(CO) will give sharp, unchanging peaks for the statistical mixture of free and bound ligand, assuming the chemical shifts are unique for each compound. This provides an elegant means to instantly measure the relative ratios of all compounds in a single NMR experiment and the coordination behaviour of the ring-open isomer **2.1** and the ring-closed isomer **2.2** can be assessed.

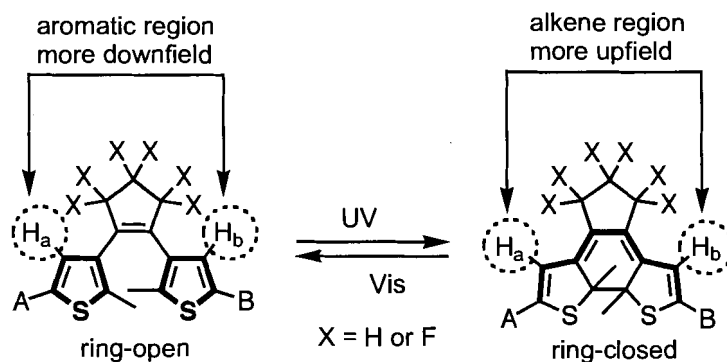
2.3.2 Ring-Current Effects in Metalloporphyrins

The ^1H NMR spectra of metalloporphyrins and their complexes show some striking chemical shifts. The shifts are attributable to the circulating π -electrons about a closed conjugated path in the porphyrin ring that lead to the anisotropic ring effect.⁸⁸ As a result, the ^1H chemical shifts in porphyrins are very dependent on the distance and the orientation of the protons with respect to the delocalization pathway of the π -electrons of the porphyrin ring. Protons above or inside the porphyrin ring are in the shielding region and are shifted more upfield, whereas protons in the plane of the macrocycle but at the periphery are in the deshielding region and appear more downfield in the NMR spectrum.

This distance and orientation dependence with respect to the shielding cone of the porphyrin makes ^1H NMR spectroscopy a useful diagnostic tool for monitoring the axial coordination of the pyridine-containing DTE isomers **2.1** and **2.2** to the ruthenium porphyrin. Indeed, the protons immediately adjacent to the pyridine nitrogen that is axially coordinated to the ruthenium porphyrin are expected to move the furthest upfield upon complexation. These protons typically move by as much as 7.5 ppm upfield upon complexation to $\text{RuTTP}(\text{CO})$.⁸¹

2.3.3 Monitoring the Photochemical Interconversion by NMR Spectroscopy

^1H NMR spectroscopy is also very useful for monitoring the progress of the photochemical interconversion (ring-opening and ring-closing) processes. Previous work on DTEs has shown that the resonances of the methine protons on the thiophene rings generally show an upfield shift upon the photocyclization process.²⁹ This can be ascribed to the loss of aromaticity of the heterocycles when the ring-closing reaction takes place. In the ring-open form, the methine protons are attached to an aromatic thiophene ring (shown in bold in the structure to the left in Equation 2.3.1) such that they appear more downfield (in the aromatic region) in the ^1H NMR spectrum than in the ring-closed form, where these protons are attached to a conjugated polyene (shown in bold in the structure to the right in Equation 2.3.1) and thus appear more upfield (in the alkene region). Furthermore, the extent of ring-cyclization can be obtained by measuring the relative integrals of the areas under the peaks for the corresponding pairs of signals for the two isomers. The signals for the thiophene protons will be referred to regularly throughout this chapter and in the rest of this thesis when monitoring the ring-opening and the ring-closing reactions unless otherwise specified.



Equation 2.3.1. ^1H NMR spectroscopy as a tool to monitor the photochemical interconversion. The structure of the ring-open and the ring-closed forms of a generalized DTE backbone showing the protons that experience the upfield change in their chemical shifts due to the loss of the aromaticity of the thiophene rings upon the photocyclization event.

2.3.4 Needs and Considerations for Solvent Selection

Solvent selection plays a crucial role when studying axial coordination to metalloporphyrins and two key considerations are (1) solvent effects and (2) solubility. Producing reliable results requires a good understanding of what properties of the solvent can affect the stability of the generated metalloporphyrin complex. Since axial coordination involves a donor-acceptor-type of interaction, solvents that have the ability to donate electron density can compete for the metal centre of the metalloporphyrin. One measure of the solvent's ability to interfere with such interactions is the solvent's donor number (DN) as reported by Gutmann,⁸⁹ which he obtained by comparing the enthalpies of reaction of various solvents with antimony(V) chloride. Solvents with lower DN values are expected to provide less competition for the metalloporphyrin. Kadish and Chang⁹⁰ used a different approach by comparing the magnitude of the formation constant for the adduct between a tetraphenylporphyrin $\text{Ru}(\text{TPP})(\text{CO})$ and various solvents. These studies indicated that pyridine was a better competitor for the sixth coordination site than acetone and nitromethane.

It can thus be expected that axial coordination of the pyridine-containing DTE ligand to ruthenium porphyrin will not be affected by the use of acetone or non-competing solvents like dichloromethane.

It is also important to ensure that the ruthenium porphyrin, the ligand and the resulting coordination complex are soluble in the chosen solvent. Ruthenium porphyrins are very soluble in chloroform, dichloromethane, benzene, and toluene and the solubility of coordination complex usually increases in those solvents. The solubility of all the species becomes very relevant when the relative ratios of free and bound ligand have to be assessed by spectroscopic techniques.

2.4 IR Spectroscopy as a Diagnostic Tool to Study Axial Coordination

2.4.1 Importance of the Carbon Monoxide Ligand

The presence of the carbon monoxide ligand (CO) on the ruthenium porphyrin provides a handle to assess the changes in electron density around the metal centre using IR spectroscopy. This spectroscopic technique is convenient in this case because the CO stretching frequency is in an uncluttered region of the IR spectrum.

There are two components to the bonding of CO to a metal: (1) σ -bonding and (2) π -backbonding.⁹¹ The first component involves the interaction between the highest occupied molecular orbital of the CO ligand (which has predominantly C character) and a vacant $d(z^2)$ or $d(x^2-y^2)$ orbital on the ruthenium(II) centre forming a σ -bond as shown in Figure 2.4.1. This interaction leads to an increase in electron density on the ruthenium ion.

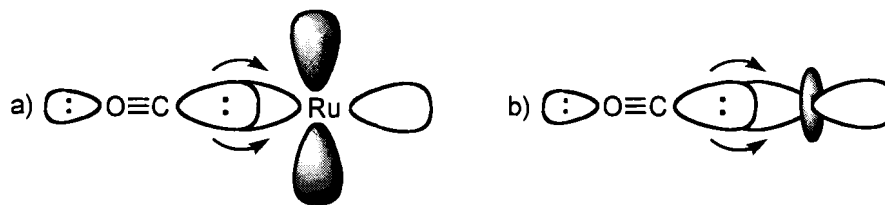


Figure 2.4.1. The σ -bond of CO between the ruthenium metal $d(z^2)$ or $d(x^2-y^2)$ orbitals in ruthenium(carbonyl)porphyrins. The arrows represent the direction of electron delocalization.

The second component involves π -backbonding from a filled metal $d(xz)$ or $d(yz)$ orbital into the empty π^* orbital on the CO ligand as illustrated in Figure 2.4.2.

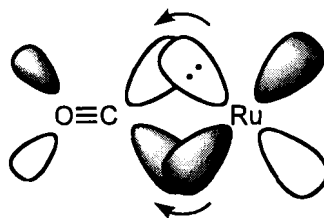


Figure 2.4.2. The π -bond formed by backbonding of the electron density on the ruthenium centre ($d(xy)$, $d(xz)$, or $d(yz)$) into the empty π^* orbital on the CO.

The two components of this bonding are synergistic: the more σ donation by the carbonyl (or other sigma-donors on the ruthenium centre), the stronger the π -backbonding interaction.⁹² This occupation of the π^* orbital on the CO does lead to a decreased bond order in the carbon monoxide molecule itself. In other words, as the π -backdonation becomes stronger, the CO bond order decreases compared to that of the free ligand and the two consequences are (1) a lengthening of the C-O bond and (2) a decrease in the carbonyl stretching frequency in the IR spectrum.

It is well established that the changes in the CO stretching frequencies of Ru(CO)porphyrins are intimately linked to the type of ligand occupying the sixth coordination site^{79,87,93} such that any changes in the electronic effects of the ligand *trans*

to the CO ligand are reflected in the observed CO stretching frequencies.⁹⁴ Thus, it seems reasonable to assume that the same technique can be used to demonstrate the electronic variations between the ring-open isomer **2.1** and the ring-closed isomer **2.2** of the pyridine-containing DTE monocation.

2.5 Project Design

The approach used in this thesis can be first illustrated by using two model compounds that were chosen to mimic the electronic properties of the ring-open isomer **2.1** and the ring-closed isomer **2.2**. In this way, the coordination behaviour of the model compounds with RuTTP(CO)(EtOH) can be carried out as a preliminary test to: (1) verify whether the labile EtOH ligand can be displaced by each of the two pyridyl ligands and (2) determine whether there is an observable difference in their ability to coordinate to the ruthenium porphyrin. Such information about the coordination behaviour of the two model compounds will help assess the differences in the coordination behaviour of the two isomers of the monobenzylated DTE since they can be expected to show similar trends.

3-Bromo-2-methyl-5-pyridylthiophene **2.3** is expected to be a close representative of the ring-open isomer **2.1**, where the pyridine is electronically insulated from the positively charged pyridinium group (top two structures in Figure 2.5.1). 1-Methyl-4,4'-bipyridinium **2.4**, where the pyridine is directly linked to the electron-withdrawing pyridinium group, is expected to be a close analogue for the ring-closed isomer **2.2**, where the pyridine is electronically connected to the electron-deficient pyridinium group through the DTE backbone (bottom two structures in Figure 2.5.1). Both the pyridylthiophene **2.3** and the ring-open isomer **2.1** are expected to act as better ligands for

the ruthenium porphyrin than the monomethylated bipyridinium **2.4** and the ring-closed isomer **2.2**.

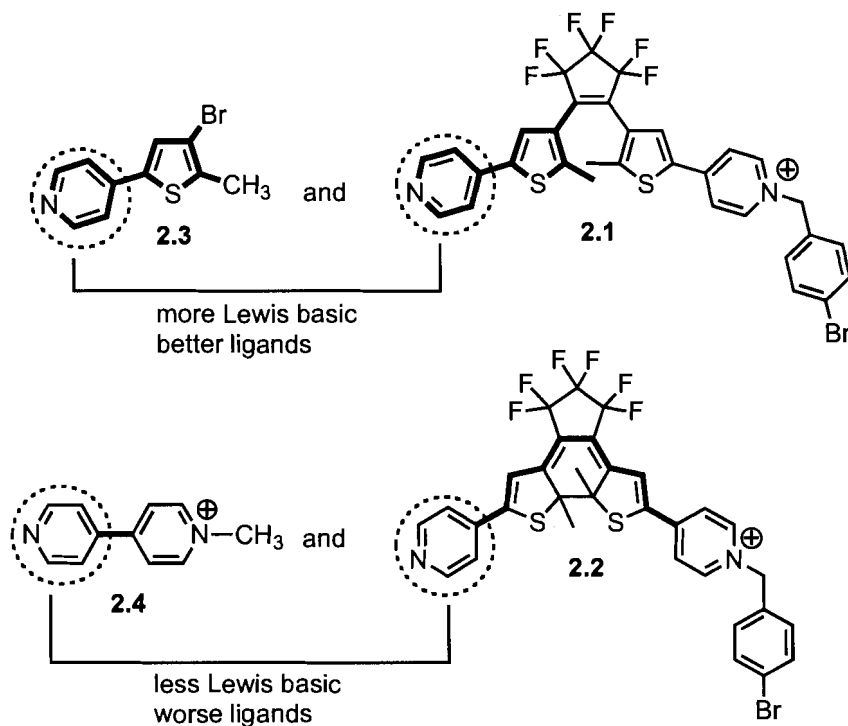
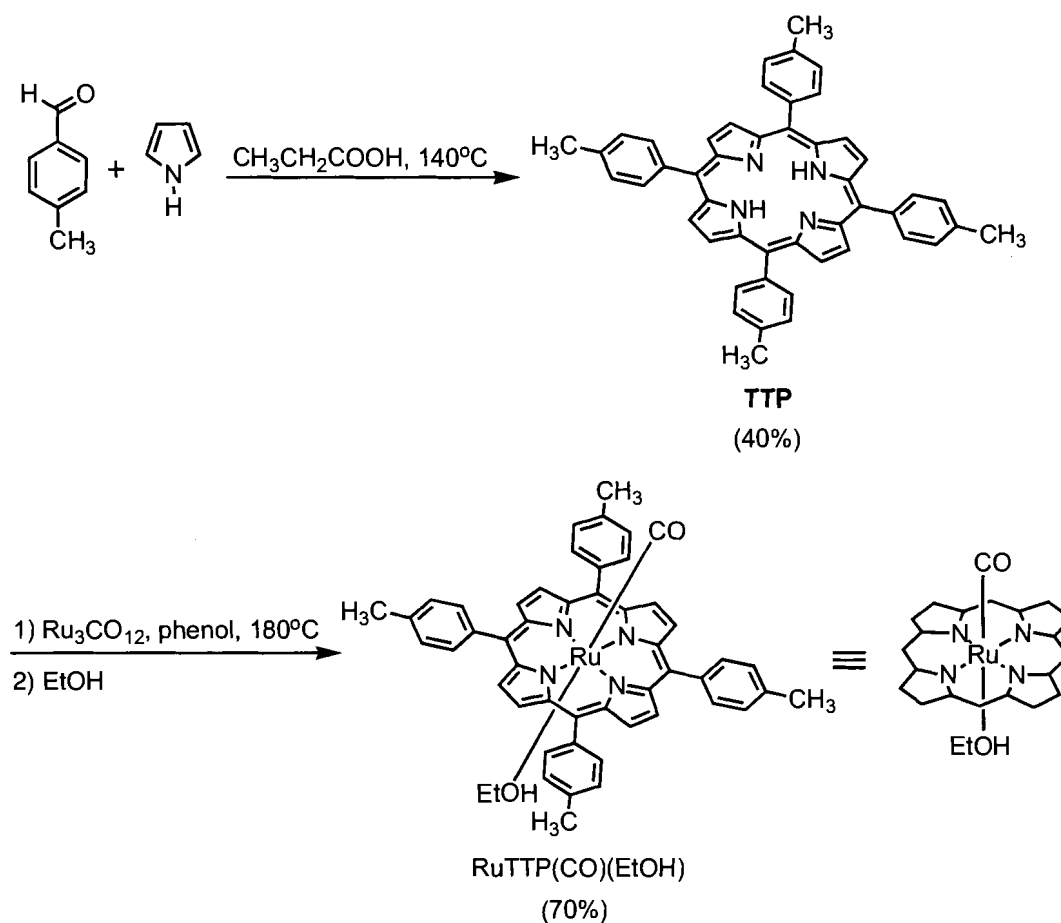


Figure 2.5.1. Model compounds **2.3** and **2.4** for the ring-open (**2.1**) and the ring-closed (**2.2**) isomers.

2.6 Results and Discussion

2.6.1 Synthesis of the RuTTP(CO)(EtOH)

The metalloporphyrin reagent RuTTP(CO)(EtOH) needed for the coordination studies was prepared in two steps following the same literature procedure used by a previous member of our research group, as shown in Scheme 2.6.1.⁹⁵



Scheme 2.6.1. Synthesis of porphyrin RuTTP(CO)(EtOH).

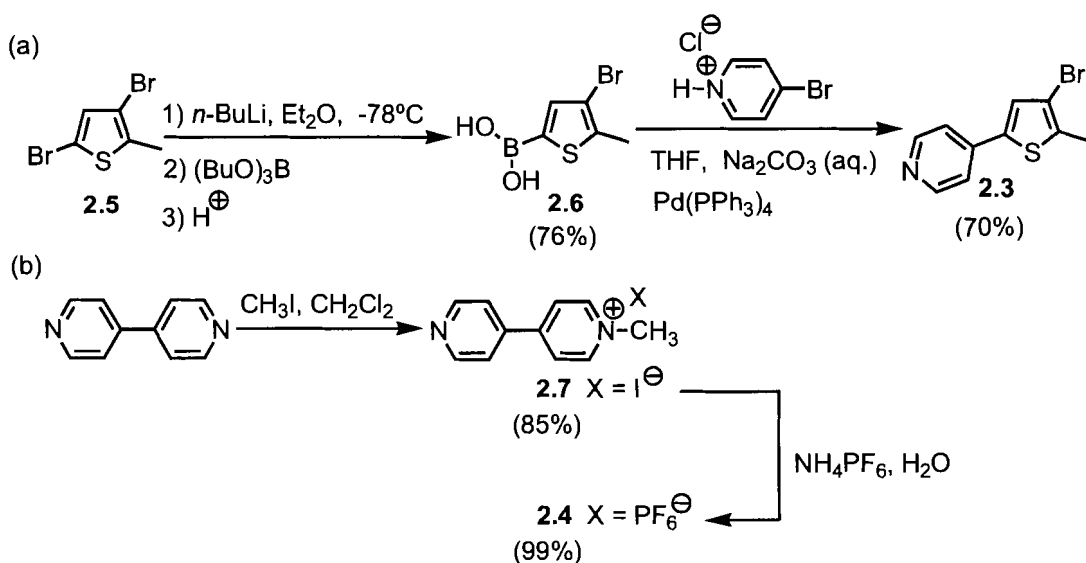
The first step of the reaction involved heating a mixture of pyrrole and *p*-tolualdehyde in propionic acid at 140°C to generate the *meso*-substituted porphyrin **TTP**. The desired ruthenium porphyrin was prepared by heating three molar equivalents of

$\text{Ru}_3\text{CO}_{12}$ with one molar equivalent of **TTP** in phenol at 180°C and was isolated as the ethanol adduct $\text{RuTTP}(\text{CO})(\text{EtOH})$ after work-up and chromatographic purification. Throughout this thesis, the porphyrin $\text{RuTTP}(\text{CO})(\text{EtOH})$ is represented as the simplified structure shown at the bottom right of Scheme 2.6.1 where the *p*-tolyl groups at the meso positions and the double bonds are omitted for simplicity.

2.6.2 Synthesis of the Model Compounds

3-Bromo-2-methyl-5-pyridylthiophene **2.3** was prepared in two steps according to the procedure previously described by Lehn and coworkers as shown in part (a) of Scheme 2.6.2.²⁹ The thiopheneboronic acid **2.6** was prepared by a lithium-halogen exchange reaction on the known 3,5-dibromo-2-methylthiophene **2.5**⁹⁶ followed by treatment with tri-*n*-butylborate and acidic work-up. The key pyridylthiophene **2.3** was then obtained by a palladium-catalyzed Suzuki coupling reaction of the boronic acid **2.6** and 4-bromopyridinium hydrochloride in aqueous base.

The synthesis of 1-methyl-4,4'-bipyridinium iodide **2.7** was easily achieved by the alkylation reaction of the commercially available 4,4'-bipyridine using iodomethane following literature procedure⁹⁷ as shown in part (b) of Scheme 2.6.2. However, with the iodide as the counter anion, the monomethylated bipyridinium **2.7** was found to be insoluble in both CH_2Cl_2 and acetone. As already mentioned, the choice of solvent is important when studying axial coordination to metalloporphyrins and an ion exchange to the more organic soluble hexafluorophosphate salt was carried out. The exchange process was done by dissolving the iodide salt **2.7** in the minimum amount of water followed by the gradual addition of solid ammonium hexafluorophosphate leading to the precipitation of the monomethylated bipyridinium as its hexafluorophosphate salt **2.4**.



Scheme 2.6.2. Synthesis of model compounds **2.3** and **2.4**. (a) Synthesis of pyridylthiophene **2.3** as a model compound for the ring-open isomer **2.1**; (b) synthesis of monomethylated bipyridinium **2.4** as a close analogue for the ring-closed form **2.2**.

2.6.3 Axial Coordination of the Model Compounds to Ruthenium Porphyrin

In order to verify whether the EtOH ligand coordinated to the ruthenium centre of the porphyrin in RuTTP(CO)(EtOH) can be displaced by the pyridylthiophene **2.3** and the monomethylated bipyridinium **2.4**, the coordination behaviour of each of the model compounds was investigated independently.

The porphyrin complex **2.3RuP** was prepared in an NMR tube by adding small portions of a weighed amount of the Ru(TTP)(CO)(EtOH) to a solution (5.3×10^{-2} M) of the pyridylthiophene **2.3** in CD_2Cl_2 until complete disappearance of the peaks corresponding to the free ligand was observed by ^1H NMR spectroscopy. The chemical shift values of the protons corresponding to the free and bound (δ_{free} and δ_{bound} , respectively) forms of the pyridylthiophene **2.3** are listed in Table 2.6.1.

Table 2.6.1. Selected ^1H NMR data (400 MHz, CD_2Cl_2) showing the respective chemical shift values of the protons corresponding to the free and bound ($\delta_{(\text{free})}$ and $\delta_{(\text{bound})}$, respectively) forms of the pyridylthiophene **2.3** upon axial coordination of a solution (5.3×10^{-2} M) of the pyridylthiophene **2.3** in CD_2Cl_2 to $\text{RuTTP}(\text{CO})$.

Proton	$\delta_{(\text{free})}$	$\delta_{(\text{bound})}$	$\Delta\delta$
H^{a}	8.56	1.47	-7.09
H^{b}	7.38	5.31-5.33*	-(2.05-2.07)*
H^{c}	7.34	6.40	-0.94
H^{d}	2.44	2.06	-0.38

*The peak H^{b} in the porphyrin complex **2.3RuP** is reported as a range because it partially overlaps with the solvent peak.

The same procedure was repeated for the formation of the coordination complex **2.4RuP** starting from a solution (4.3×10^{-2} M) of the monomethylated bipyridinium **2.4** in CD_3COCD_3 . In this case, CD_3COCD_3 was used owing to the poor solubility of the pyridyl ligand **2.4** in CD_2Cl_2 . The chemical shift values for the protons corresponding to the free and bound ($\delta_{(\text{free})}$ and $\delta_{(\text{bound})}$, respectively) forms of the monomethylated bipyridinium **2.4** are listed in Table 2.6.2. The signals corresponding to the free monomethylated bipyridinium **2.4** were assigned using ^1H - ^1H COSY and selective 1-D NOE experiments prior to the axial coordination experiment.

Table 2.6.2. Selected ^1H NMR data (400 MHz, CD_3COCD_3) showing the chemical shift values of the protons corresponding to the free and bound ($\delta_{(\text{free})}$ and $\delta_{(\text{bound})}$ respectively) forms of the monomethylated bipyridinium **2.4** upon axial coordination of a solution (4.3×10^{-2} M) of the pyridyl ligand **2.4** in CD_3COCD_3 to $\text{RuTTP}(\text{CO})$.

Proton	$\delta_{(\text{free})}$	$\delta_{(\text{bound})}$	$\Delta\delta$
H^{a}	9.27	8.79	-0.48
H^{b}	8.87	1.79	-7.08
H^{c}	8.68	7.63-7.65*	-(1.03-1.05)*
H^{d}	7.99	6.07	-1.92
H^{e}	4.70	4.37	-0.33

*The peak H^{c} in the porphyrin complex **2.4RuP** is reported as a range because it partially overlaps with one of the peaks corresponding to the bound porphyrin.

The formation of both complexes was accompanied by significant upfield shifts in the ^1H NMR spectra for all hydrogen atoms as expected for protons lying within the shielding cone of the porphyrin. The protons immediately adjacent to the pyridine nitrogen that is axially coordinated to the metalloporphyrin were the most dramatically affected and were seen to move the furthest upfield (by ~ 7.1 ppm in both cases) upon complexation, as anticipated. Furthermore, removal of the solvent under reduced pressure afforded the pyridylthiophene–porphyrin complex **2.3RuP** and the monomethylated bipyridinium–porphyrin complex **2.4RuP** as burgundy solids. Both complexes were characterized by means of ^1H and ^{13}C NMR, FT-IR, UV-Vis spectroscopy, mass

spectrometry and elemental analysis and the results were consistent with the structures shown in Tables 2.6.1 and 2.6.2.

2.6.4 Assessment of the Difference in Coordination Behaviour Between the Pyridylthiophene Control 2.3 and the Monomethylated Bipyridinium Control 2.4

The results from the previous section have shown that the pyridyl moieties in control molecules 2.3 and 2.4 can quantitatively displace the labile EtOH ligand of the ruthenium porphyrin RuTTP(CO)(EtOH) to form their respective adducts **2.3RuP** and **2.4RuP**. The next step was to compare the coordination ability of the pyridylthiophene control 2.3 to that of the monomethylated bipyridinium control 2.4.

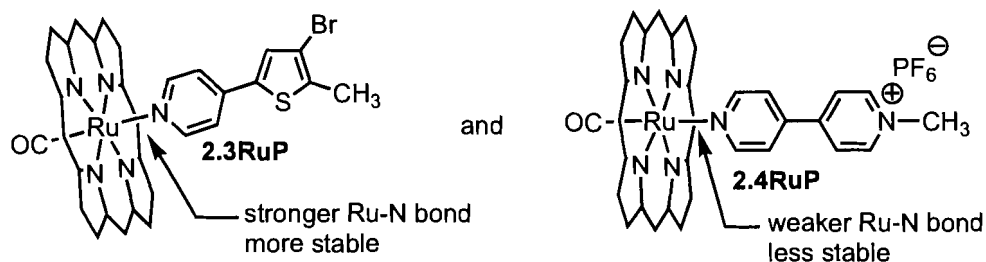
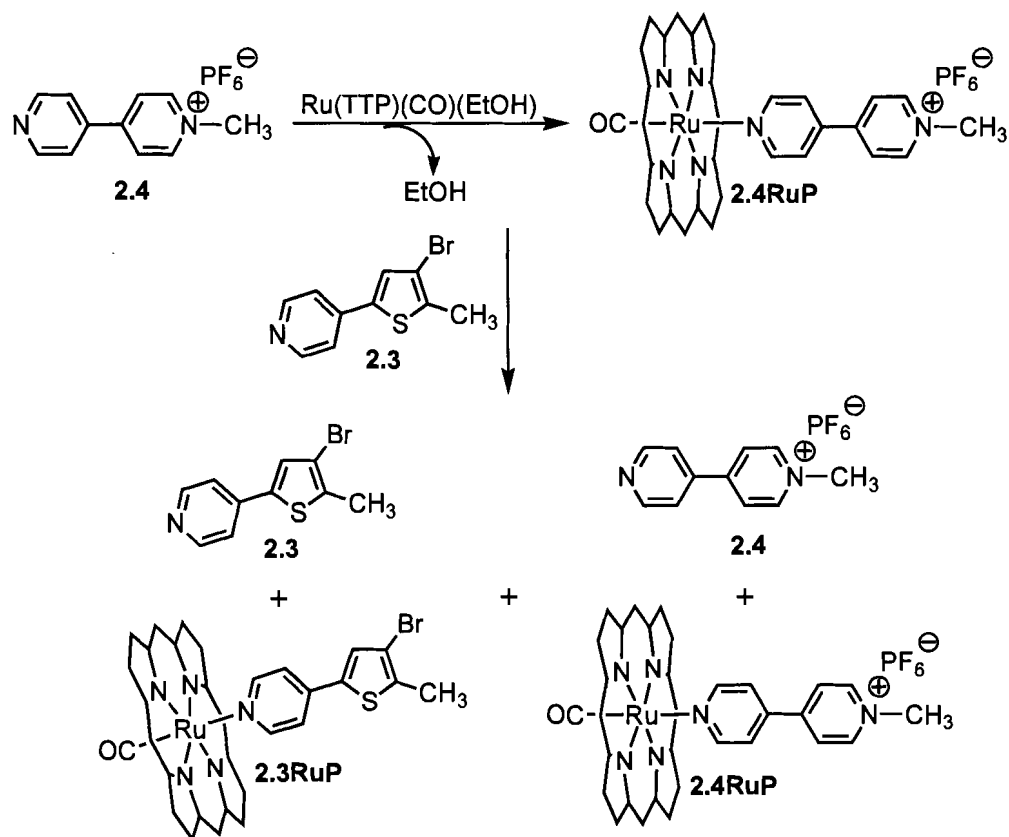


Figure 2.6.1. Difference in binding strength between the pyridylthiophene 2.3 and the monomethylated bipyridinium 2.4. The more Lewis basic pyridylthiophene 2.3 can be expected to form the more stable porphyrin–DTE complex than the monomethylated bipyridinium 2.4.

The binding strength (Ru–N bond) between the ruthenium porphyrin and the pyridine ligand can be expected to be stronger and hence more stable in the case of the more Lewis basic pyridylthiophene 2.3 than in the case of the monomethylated bipyridinium 2.4 (Figure 2.6.1). Consequently, the pyridylthiophene 2.3 is expected to be a better ligand for axial coordination to the ruthenium porphyrin than the monomethylated bipyridinium 2.4.

One approach to demonstrate this difference in coordination behaviour is to add one molar equivalent of the pyridylthiophene control **2.3** to a solution containing the complex **2.4RuP**. In the absence of any free RuTTP(CO)(EtOH), the pyridylthiophene **2.3** will act as a competing ligand for the porphyrin site of the monomethylated bipyridinium–porphyrin complex **2.4RuP** and, assuming it is the better Lewis base, will displace some of the ligand **2.4** to form the pyridylthiophene–porphyrin adduct **2.3RuP**. This will lead to a redistribution of the complexes **2.3RuP** and **2.4RuP** and the free ligands (**2.3** and **2.4**), where the more stable complex is expected to predominate. It is thus reasonable to expect that the more Lewis basic pyridylthiophene **2.3** will displace more of the monomethylated bipyridinium **2.4** from its porphyrin complex **2.4 RuP** such that there will be more of the pyridylthiophene–porphyrin adduct **2.3RuP** than the monomethylated bipyridinium–porphyrin complex **2.4RuP**.

To demonstrate this concept, the porphyrin adduct **2.4 RuTTP(CO)** was prepared by adding the metalloporphyrin to a solution (5.3×10^{-3} M) of the monomethylated bipyridinium **2.4** in CD₃COCD₃ following the same procedure used in *Section 2.6.3*. The competing pyridylthiophene **2.3** (as shown in Scheme 2.6.3) was added in small portions until 1 molar equiv was observed by measuring the relative integrals of the areas under the peaks corresponding to the free (**2.3** and **2.4**) and bound (**2.3RuP** and **2.4RuP**) ligands using ¹H NMR spectroscopy. The result of this experiment is the redistribution of the bound and free ligands as illustrated by the ¹H NMR spectra in Figure 2.6.2.



Scheme 2.6.3. Effect of the more Lewis basic pyridylthiophene control **2.3** on a solution of the monomethylated bipyridinium-porphyrin complex **2.4RuP**. It can be expected that the former will displace some of the monomethylated bipyridinium **2.4** from the porphyrin complex **2.4RuP** leading to a redistribution of free (**2.3** and **2.4**) and bound (**2.3RuP** and **2.4RuP**) ligands.

The monomethylated bipyridinium **2.4** has a three-proton singlet at 4.70 ppm (peak 'f_e') corresponding to the methyl group of the compound and axial coordination to the ruthenium porphyrin leads to an upfield shift to 4.37 ppm (peak 'b_e') in the resulting complex **2.4RuP** (Figure 2.6.2). The methyl group on the pyridylthiophene ligand **2.3** shows a three-proton singlet at 2.45 ppm (peak 'f_j') but formation of the porphyrin complex **2.3RuP** leads to an upfield shift to 2.09 ppm (peak 'b_j'), which partially overlaps with the residual solvent peak (CD₃COCD₃), and prevents the direct comparison of the relative integrals corresponding to 'f_j' and 'b_j'.

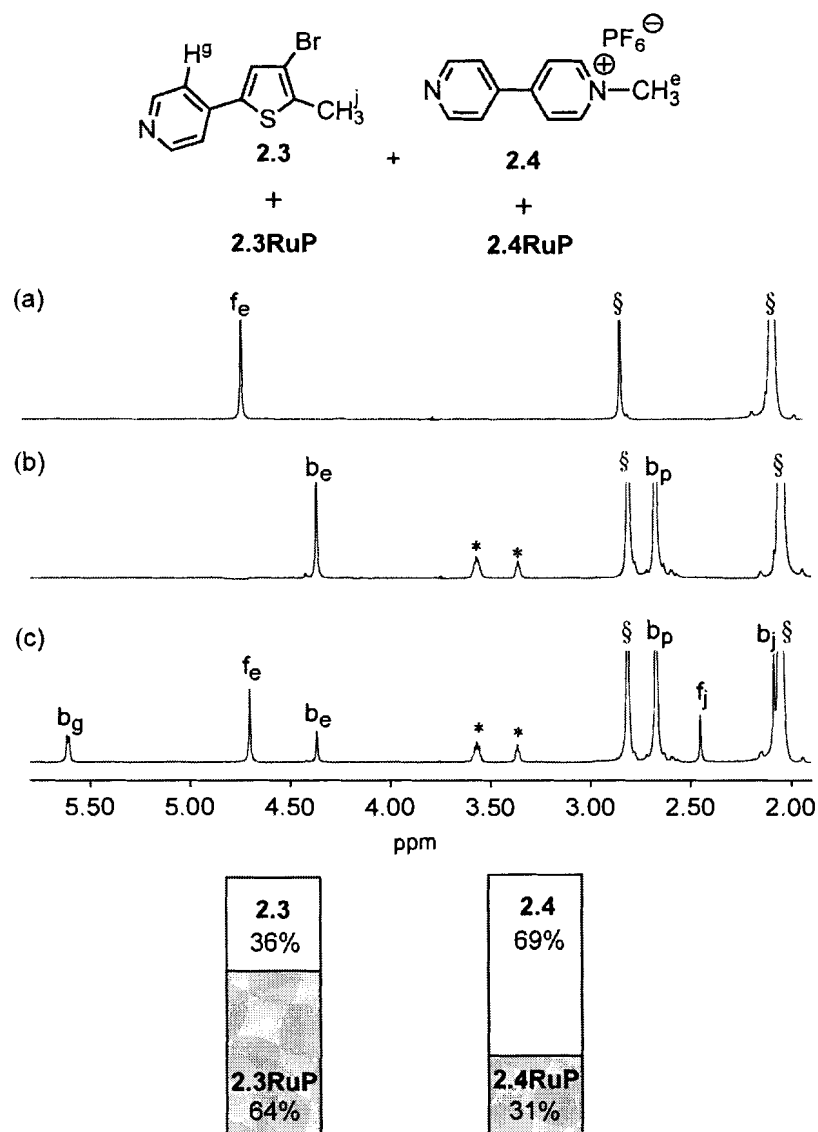
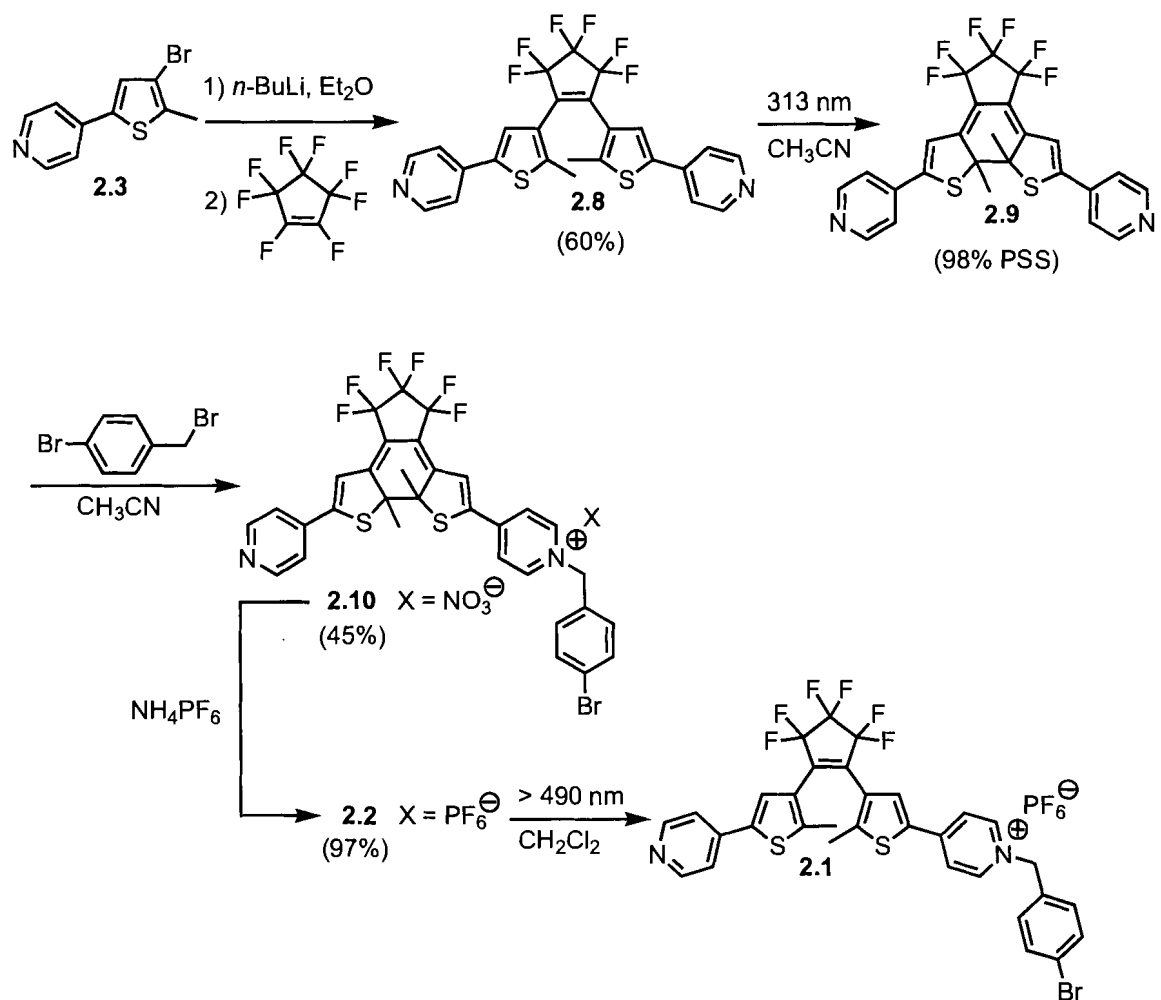


Figure 2.6.2. Assessment of the effect of the pyridylthiophene **2.3** on a solution of the porphyrin complex **2.4RuP** by ^1H NMR spectroscopy. Partial ^1H NMR (600 MHz, CD_3COCD_3) spectra (a) of the free monomethylated bipyridinium **2.4**, (b) after adding 1 molar equiv of the metalloporphyrin $\text{RuTTP}(\text{CO})(\text{EtOH})$ to generate the monomethylated bipyridinium–porphyrin complex **2.4RuP** and (c) after the addition of 1 molar equiv of the stronger Lewis basic pyridylthiophene **2.3** leading to the displacement of the weaker Lewis basic monomethylated bipyridinium from the porphyrin complex **2.4RuP**. The result of this experiment is the redistribution of free (**2.3** and **2.4**) and bound (**2.3RuP** and **2.4RuP**) ligands as shown by the bar charts. The letter ‘f’ denotes signals for the free ligands and ‘b’ denotes signals for the bound ligands. The (§) denotes signals corresponding to the residual solvent peak (2.05 ppm) and the dissolved water peak (2.75 ppm). The (*) denotes signals corresponding to the EtOH (3.57 and 3.39 ppm) displaced upon axial coordination of the pyridyl ligand **2.4** to $\text{RuTTP}(\text{CO})$. The subscript ‘p’ denotes the signal for the porphyrin (2.67 ppm). The relative amounts of the free (**2.3** and **2.4**) and bound (**2.3RuP** and **2.4RuP**) are shown by the bar charts and these values were obtained from the relative integrals of the areas under the peaks corresponding to ‘f_e’, ‘b_e’, ‘f_j’ and ‘b_j’. These values indicate that the pyridylthiophene **2.3** is the more effective ligand.

An alternate peak of interest for the bound pyridylthiophene **2.3** is the two-proton doublet at 5.61 ppm (peak 'b_g'), which can be attributed to the β-protons of the pyridine in **2.3RuP**. It is possible to determine which of the two pyridyl ligands forms the more stable complex upon axial coordination to RuTTP(CO)(EtOH) by comparing the relative ratios of the peak integrals for the bound to free ligands by measuring the areas under the peaks corresponding to 'f_e', 'b_e', 'f_j' and 'b_g'. The relative amounts of each are shown by the bar charts in Figure 2.6.2. The results indicate that there was about two times more of the pyridylthiophene **2.3** axially coordinated to the ruthenium porphyrin than the monomethylated bipyridinium **2.4** and support the concept that the pyridylthiophene **2.3** is the more effective ligand. The difference in coordination behaviour between the two model compounds **2.3** and **2.4** acts as an incentive to continue the project and test the axial coordination of the ring-open isomer **2.1** and the ring-closed isomer **2.2**.

2.6.5 Synthesis of the Monobenzylated DTEs 2.1 and 2.2

The key monobenzylated DTE **2.2** was prepared in four steps, as shown in Scheme 2.6.4, starting from the known pyridylthiophene **2.3**, which was prepared according to the procedure described by Lehn and coworkers²⁹ as already discussed in *Section 2.6.2*.



Scheme 2.6.4. Synthesis of the monobenzylated DTE **2.2** as its hexafluorophosphate salt in four steps starting from the pyridylthiophene precursor **2.3**.

The synthesis began with a lithium-halogen exchange reaction of the pyridylthiophene **2.3** with *n*-butyllithium and quenching with octafluorocyclopentene to give the *bis*(pyridine) DTE **2.8** following literature procedure.²⁹ It must be pointed out here that direct treatment of the ring-open *bis*(pyridine) **2.8** with one molar equivalent of 4-bromobenzyl bromide gives a high yield of the undesired dibenzylated DTE as a side-product and it is found that optimal yields of the monobenzylated DTE can be achieved by performing the alkylation reaction on the ring-closed *bis*(pyridine) **2.9** as shown in

Scheme 2.6.4. This observation already suggests that the ring-open isomer has two similar thiophenes while the ring-closed isomer has two communicating thiophenes and will be discussed in more detail in *Chapter 3*. The second step entailed generating the ring-closed form **2.9** of the *bis*(pyridine). This was done by irradiating a solution (5.8×10^{-3} M) of the *bis*(pyridine) **2.8** in anhydrous CH₃CN with a hand-held TLC lamp as a source of 313 nm-light (or 365 nm-light for other DTE systems) and monitoring aliquots of the sample by ¹H NMR spectroscopy until no further change was observed. These two wavelengths of light (313 and 365 nm) will be referred to regularly throughout this chapter and in the rest of this thesis when carrying out the ring-closing reactions. The progress of the photocyclization event was assessed by monitoring the methine peaks of the thiophene rings (7.63 ppm for the ring-open isomer **2.8** as opposed to 7.02 ppm for the ring-closed form **2.9**) as discussed earlier in *Section 2.3.3* until a solution containing 98% of the ring-closed isomer **2.9** was observed at the PSS. Without attempting to isolate the pure ring-closed isomer **2.9**, the solution was treated with 1 molar equiv of 4-bromobenzyl bromide. Chromatographic purification (silica gel) allowed any unreacted ring-closed *bis*(pyridine) **2.9** to be recovered by eluting with CH₃CN. Changing the solvent system to a mixture of CH₃CN-H₂O-saturated KNO₃ (100:10:0.01) afforded the ring-closed form of the monobenzylated *bis*(pyridinium) as its nitrate salt **2.10**, which was subsequently used for the kinetic studies in *Chapter 3*. A five-fold increase in the amount of saturated KNO₃ in the solvent system allowed the ‘side product’ (dibenzylated DTE) to be eluted off the column and the photochromic properties of its hexafluorophosphate salt will be discussed in more detail in *Chapter 3*. The next step involved the exchange of the nitrate counter anions in the monobenzylated DTE **2.10** for

the more organic soluble hexafluorophosphate anions. The ion-exchange was carried out by dissolving the nitrate salt **2.10** in the minimum amount of EtOH followed by the addition of a saturated solution of NH_4PF_6 leading to the precipitation of the monobenzylated DTE as its hexafluorophosphate salt **2.2**. The ring-opening reaction of the latter was achieved by irradiating a solution (3.3×10^{-3} M) of the monobenzylated *bis*(pyridinium) **2.2** in CH_2Cl_2 with a broad band visible light source fitted with a 490 nm cut off filter to eliminate higher energy light until the greenish blue solution turned colourless and monitoring aliquots of the sample by ^1H NMR spectroscopy until no further change was observed. The light of wavelength greater than 490 nm will be used regularly throughout this chapter and in the rest of this thesis when carrying out ring-opening reactions. The progress of the ring-opening reaction was assessed by monitoring the methine peaks of the thiophene rings (7.13 and 6.89 ppm for the ring-closed isomer **2.2** as opposed to 7.87 and 7.48 ppm for the ring-open **2.1**) as discussed earlier in *Section 2.3.3* until complete disappearance of the peaks corresponding to the ring-closed isomer **2.2** was observed at the PSS. The ring-open isomer **2.1** was collected after evaporation of the solvent without any purification.

Both the nitrate salt (**2.10**) and the hexafluorophosphate salt (**2.1**) of the monobenzylated DTE were characterized by means of ^1H and ^{13}C NMR, FT-IR, UV-Vis spectroscopy, mass spectrometry, and elemental analysis. The results were consistent with the structures shown in Scheme 2.6.4.

2.6.6 UV-Vis Absorption Spectra, Photochemical Cycling, and ^1H NMR Spectra of the Monoalkylated DTE 2.1

The photochemical interconversion between the ring-open (**2.1**) and the ring-closed (**2.2**) isomers of the monoalkylated DTE resulted in a colour change and subsequent differences in the UV-Vis absorption profiles of the two isomers, as illustrated in part (a) of Figure 2.6.3.

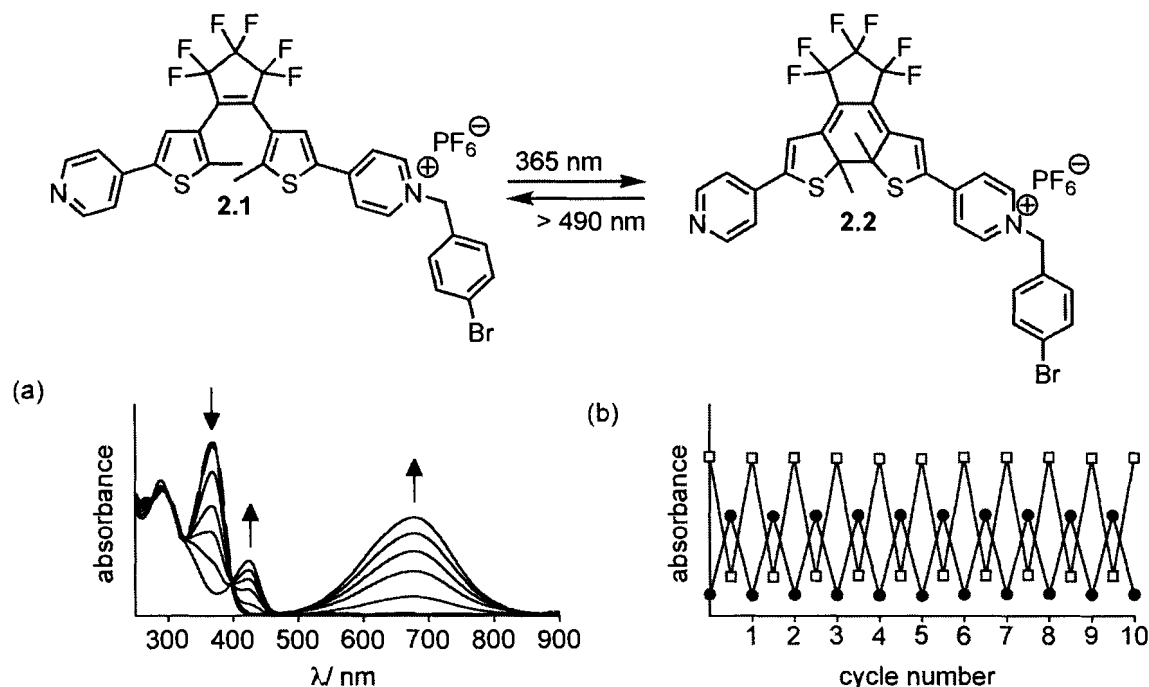


Figure 2.6.3. UV-Vis absorption spectra and photochemical cycling of the monobenzylated DTE **2.1**. (a) Changes in the UV-Vis absorption spectra of a CH_2Cl_2 solution ($2.5 \times 10^{-5} \text{ M}$) of the ring-open isomer **2.1** upon irradiation with 365 nm light until no further increase in the absorption band at 679 nm was observed at the PSS. Total irradiation periods are 0, 5, 10, 15, 20 and 30 sec. The dashed trace (---) shown in bold corresponds to the spectrum after irradiation of the solution of the ring-closed isomer **2.2** at the PSS with light of wavelengths greater than 490 nm for 5 min regenerating the original UV-Vis trace corresponding to the ring-open isomer **2.1**. (b) Photochemical cycling of a CH_2Cl_2 solution ($2.5 \times 10^{-5} \text{ M}$) of the monoalkylated DTE between its ring-open form **2.1** and its ring-closed form **2.2**. The figure shows the changes in the absorptions at 370 nm (open squares) and 679 nm (black circles) during alternate irradiation at 365 nm for 30 s and light of wavelengths greater than 490 nm for 5 min.

The UV-Vis absorption study of a CH_2Cl_2 solution ($2.5 \times 10^{-5} \text{ M}$) of the ring-open form **2.1** showed the appearance of an absorption band in the visible region of the spectrum (679 nm) corresponding to the coloured ring-closed form **2.2** when irradiated

with 365 nm light for 5 sec. The solution was irradiated with 365 nm light until no further increase in the absorption band at 679 nm was observed at the PSS. Subsequent exposure of the solution to visible light (light of wavelengths greater than 490 nm) was accompanied by the complete disappearance of the absorption band in the visible region of the spectrum (679 nm) and the regeneration of the original UV-Vis absorption trace corresponding to the ring-open isomer **2.1** as shown by the dashed trace shown in bold in part (a) of Figure 2.6.3. Furthermore, alternate irradiation with 365 nm light and wavelengths greater than 490 nm showed no apparent signs of photodegradation after 10 cycles as shown in part (b) of Figure 2.6.3.

The photochemical interconversion between the ring-open (**2.1**) and the ring-closed (**2.2**) isomers of the monoalkylated DTE was also analyzed using ^1H NMR spectroscopy. The signals in the ^1H NMR spectra of the ring-open isomer **2.1** and the ring-closed isomer **2.2** (shown in Figure 2.6.4) were assigned using ^1H - ^1H COSY and selective 1-D NOE experiments. The ring-closing event was carried out by irradiating a CD_2Cl_2 solution (2.0×10^{-3} M) of the ring-open isomer **2.1** with 365 nm light in a quartz NMR tube and the following observations were made: (1) the ring-closing reaction was accompanied by the appearance of a new set of signals corresponding to the ring-closed isomer **2.2** while the peaks corresponding to the ring-open form **2.1** gradually decreased in intensity and after 10 min, the peaks corresponding to the ring-open isomer **2.1** were no longer observed; (2) the solution of the generated ring-closed isomer **2.2** showed no apparent signs of degradation even after prolonged irradiation with 365 nm light over a 2-hour-period; (3) the irradiation of the solution containing the ring-closed isomer **2.2** with light of wavelengths greater than 490 nm resulted in the complete regeneration of the

peaks corresponding to the ring-open isomer **2.1** without the formation of the photostable side-products that are occasionally observed for DTE compounds lacking substituents at the C-4 position of the thiophene rings.^{98,99}

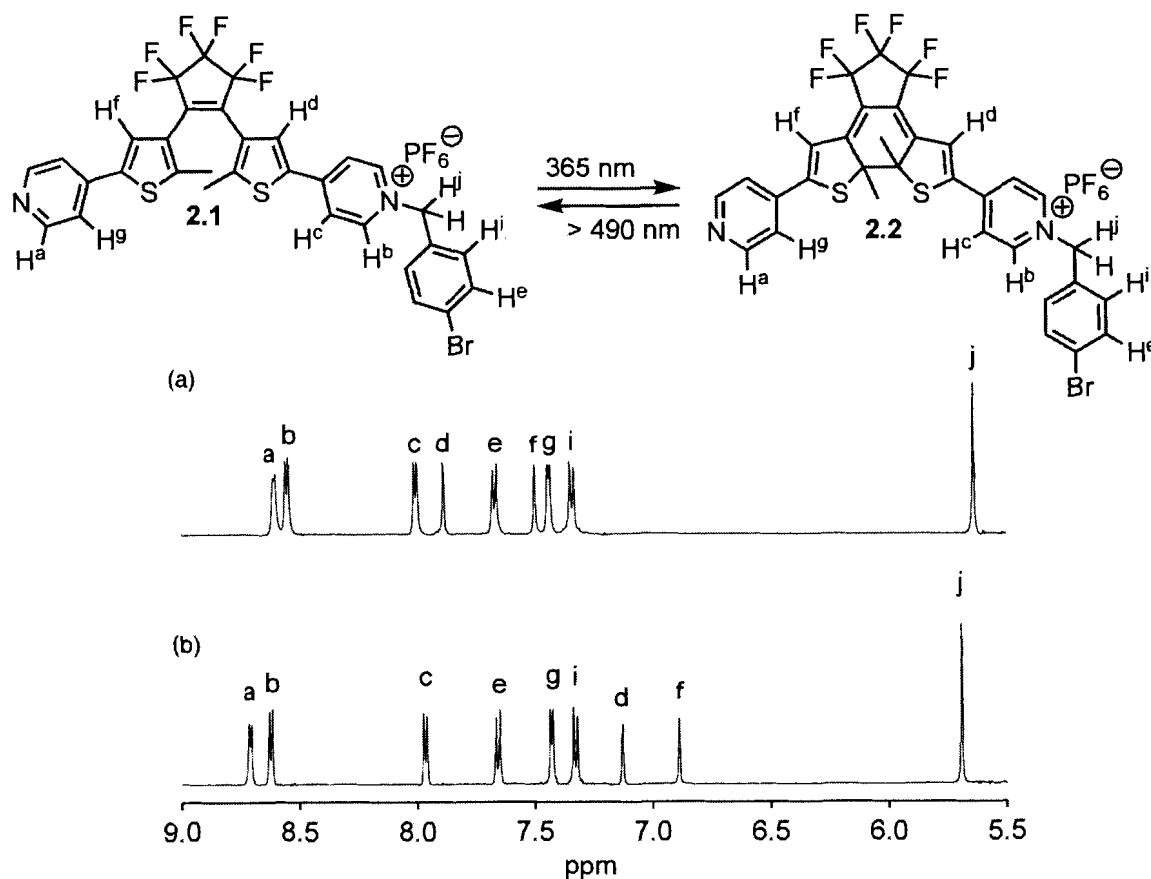


Figure 2.6.4. ^1H NMR spectroscopy as a tool to monitor the photocyclization reaction of the ring-open isomer **2.1**. Selected ^1H NMR spectra (500 MHz) of a CD_2Cl_2 solution (2.0×10^{-3} M) of the ring-open isomer **2.1** (a) before irradiation and (b) after irradiation with 365 nm light for 10 min to produce the ring-closed isomer **2.2** at the PSS. The PSS was obtained by irradiating the solution of the ring-open isomer **2.1** with 365 nm light until the peaks corresponding to the ring-open form **2.1** were no longer observed.

The UV-Vis and ^1H NMR studies show that the monobenzylated *bis*(pyridinium) exhibits excellent photochromic properties and that the photochemical interconversion between the ring-open (**2.1**) and the ring-closed (**2.2**) isomers can easily be carried out with high PSSs. The next step consisted of investigating the coordination behaviour of each isomer towards the metalloporphyrin $\text{RuTTP}(\text{CO})(\text{EtOH})$.

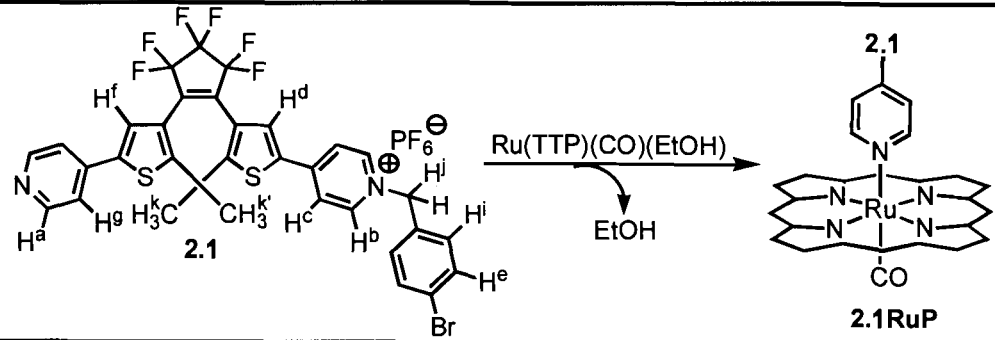
2.6.7 Axial Coordination of Ring-Open and Ring-Closed DTE's 2.1 and 2.2

Although the previous studies in this thesis have shown that the controls, pyridylthiophene **2.3** and monomethylated bipyridinium **2.4**, can displace the labile EtOH occupying the sixth coordination site of the ruthenium porphyrin, there is still a need to verify whether both the ring-open isomer **2.1** and the ring-closed isomer **2.2** of the monobenzylated DTE can also axially coordinate to the ruthenium porphyrin.

The porphyrin complex **2.1RuP** was prepared in an NMR tube by adding small portions of a weighed amount of the RuTTP(CO)(EtOH) to a known volume (0.6 mL) of a stock solution (9.0×10^{-3} M) of the ring-open isomer **2.1** in CD₂Cl₂ until complete disappearance of the peaks corresponding to the free monoalkylated DTE **2.1** was observed by ¹H NMR spectroscopy.

The same volume (0.6 mL) of the stock solution (9.0×10^{-3} M) of the ring-open isomer **2.1** in CD₂Cl₂ was transferred into a quartz NMR tube and the sample was irradiated with 365 nm light until complete disappearance of the peaks corresponding to the ring-open isomer **2.1** was observed at the PSS as already discussed in *Section 2.6.6*. The generated ring-closed isomer **2.2** was treated with RuTTP(CO)(EtOH) using the same procedure used for the ring-open isomer **2.1**.

Table 2.6.3. Selected ^1H NMR data (600 MHz, CD_2Cl_2) showing the respective chemical shift values of the protons corresponding to the free and bound ($\delta_{(\text{free})}$ and $\delta_{(\text{bound})}$, respectively) forms of the ring-open isomer **2.1** upon axial coordination of a solution (9.0×10^{-3} M) of the ring-open DTE **2.1** in CD_2Cl_2 to $\text{RuTTP}(\text{CO})(\text{EtOH})$.



Proton	$\delta_{(\text{free})}$	$\delta_{(\text{bound})}$	$\Delta\delta$
H ^a	8.58	1.47	-7.11
H ^b	8.53	8.44	-0.09
H ^c	7.98	7.83	-0.16
H ^d	7.87	7.64	-0.23
H ^e	7.65	7.61	-0.04
H ^f	7.48	6.56	-0.92
H ^g	7.42	5.36	-2.06
H ⁱ	7.32	7.26	-0.06
H ^j	5.62	5.56	-0.06
H ^k	2.10	1.63	-0.47
H ^{k'}	2.01	1.62	-0.39

Table 2.6.4. Selected ^1H NMR data (600 MHz, CD_2Cl_2) showing the respective chemical shift values of the protons corresponding to the free and bound ($\delta_{(\text{free})}$ and $\delta_{(\text{bound})}$, respectively) forms of the ring-closed isomer **2.2** upon axial coordination of a solution (9.0×10^{-3} M) of the ring-closed DTE **2.2** in CD_2Cl_2 to $\text{RuTTP}(\text{CO})(\text{EtOH})$.

Proton	$\delta_{(\text{free})}$	$\delta_{(\text{bound})}$	$\Delta\delta$
H^{a}	8.71	1.55	-7.16
H^{b}	8.62	8.53	-0.09
H^{c}	7.97	7.81	-0.16
H^{d}	7.13	6.92	-0.21
H^{e}	7.66	7.61	-0.05
H^{f}	6.89	5.89	-1.00
H^{g}	7.43	5.35	-2.08
H^{i}	7.33	7.26	-0.07
H^{j}	5.69	5.62	-0.07
H^{k}	2.26	1.82	-0.44
$\text{H}^{\text{k}'}$	2.25	1.77	-0.48

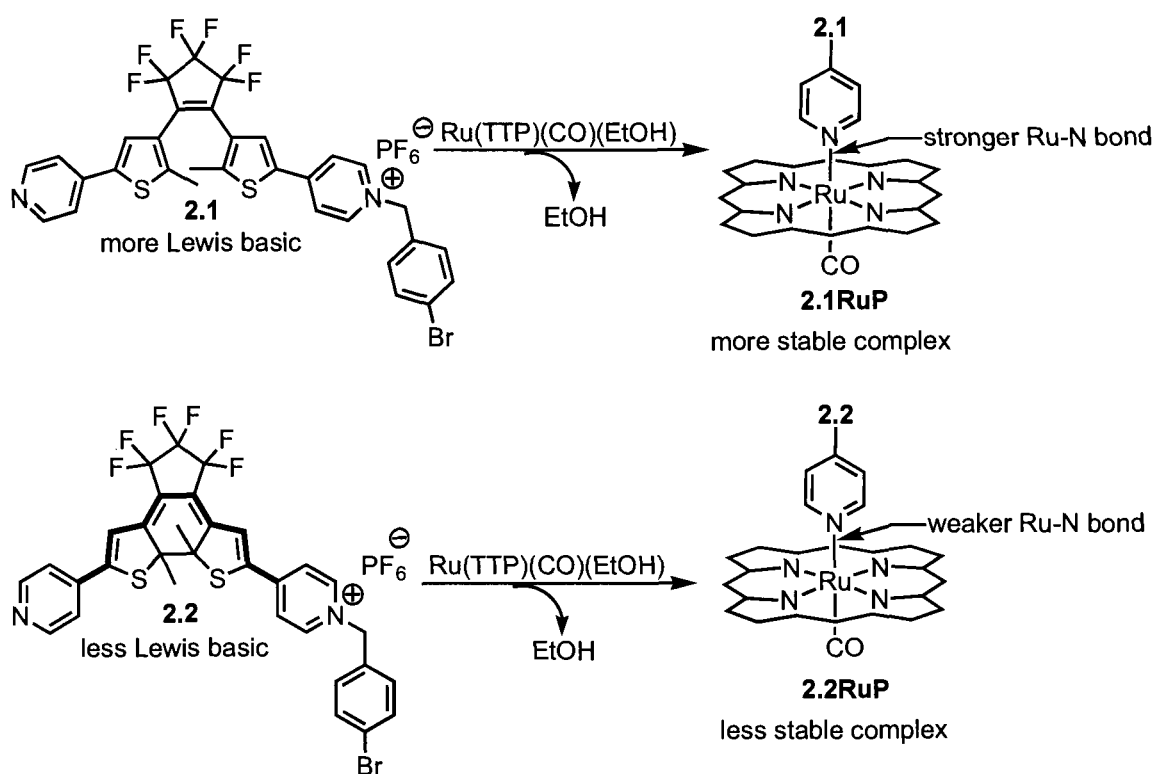
The results were similar to those observed for the model compounds **2.3RuP** and **2.4RuP**: (1) the formation of both complexes was accompanied by the significant upfield shifts observed in the ^1H NMR spectra for all hydrogen atoms within the porphyrin's anisotropic ring current and (2) the protons immediately adjacent to the pyridine nitrogen that is axially coordinated to the metalloporphyrin were the most dramatically affected and were seen to move the furthest upfield upon complexation as listed in Tables 2.6.3 and 2.6.4, respectively. The removal of the solvent under reduced pressure afforded the ring-open DTE–porphyrin complex **2.1RuP** as a burgundy solid and the ring-closed DTE–porphyrin complex **2.2RuP** as a dark greenish brown solid. Both complexes were characterized by means of ^1H and ^{13}C NMR, FT-IR, UV-Vis spectroscopy, mass spectrometry, and elemental analysis. The results were consistent with the structures shown in Tables 2.6.3 and 2.6.4.

2.6.8 Assessment of the Difference in Coordination Behaviour Between the Two Isomers (2.1 and 2.2) of the Monobenzylated DTE

The study in *Section 2.6.4* has shown that the pyridylthiophene **2.3**, which is a close analogue of the ring-open isomer **2.1**, is a better ligand for the ruthenium porphyrin than the monomethylated bipyridinium **2.4**, which is a close representative of the ring-closed isomer **2.2**. It can thus be expected that the coordination behaviour of the ring-open isomer **2.1** and the ring-closed isomer **2.2** will show a similar trend to that for the model compounds.

The lack of electronic communication between the two cross-conjugated thiophenes in the ring-open isomer **2.1** insulates the pyridine from the positively charged pyridinium group (Scheme 2.6.5) such that it can be expected to be more Lewis basic and

to form the more stable complex with the ruthenium porphyrin (i.e. forming a stronger Ru–N bond). In the ring-closed isomer **2.2** the thiophenes are electronically connected through the linearly conjugated DTE backbone (shown in bold in the bottom left structure in Scheme 2.6.5) and the Lewis basicity of the pyridine is lowered owing to the electron-withdrawing effect of the pyridinium group. Consequently, the complex formed with the ruthenium porphyrin is expected to be less stable (i.e. the formation of a weaker Ru–N bond).



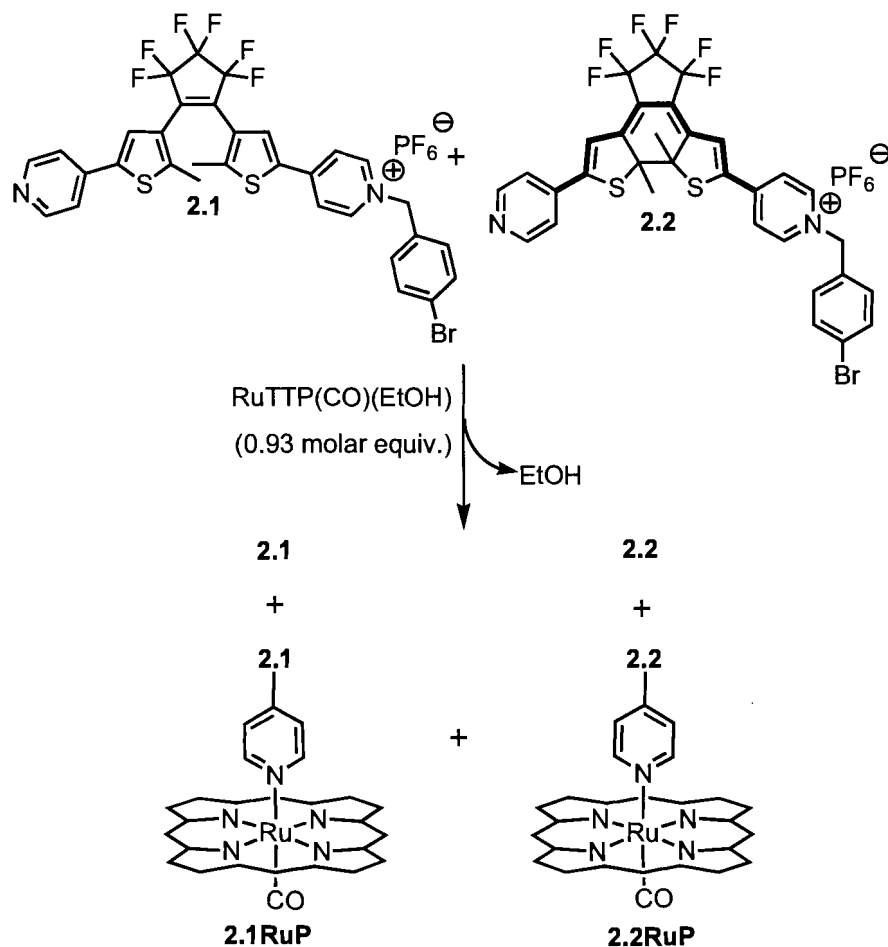
Scheme 2.6.5. Difference in binding strength between the ring-open (**2.1**) and the ring-closed (**2.2**) isomers of the monobenzylated DTE. The more Lewis basic ring-open isomer **2.1** can be expected to form the more stable DTE–porphyrin complex than its ring-closed counterpart owing to the stronger Ru–N bond.

One approach for gaining further insight into the magnitude of the difference in the coordination behaviour between the two isomers of the monoalkylated DTE involves comparing the coordination of a 1:1 mixture of the ring-open isomer **2.1** and the ring-

closed isomer **2.2** with less than one molar equiv of the RuTTP(CO)(EtOH). This approach takes advantage of the fact that both the ring-open isomer **2.1** and the ring-closed isomer **2.2** can coordinate to the ruthenium porphyrin and are in the same solution. However, by limiting the amount of the RuTTP(CO)(EtOH) to less than one molar equiv, the pyridyl ligands **2.1** and **2.2** are forced to compete for the sixth coordination site of the porphyrin such that the more stable complex will be the more predominant complex. Thus, it is reasonable to expect that more of the more Lewis basic ring-open isomer **2.1** will coordinate to the porphyrin than the ring-closed isomer **2.2**.

To verify the difference in coordination behaviour between the ring-open (**2.1**) and the ring-closed (**2.2**) isomers, a solution (1.1×10^{-3} M) of the ring-open isomer of the monobenzylated DTE **2.1** in CD₂Cl₂ was irradiated with 365 nm light until an equimolar mixture of the ring-open isomer **2.1** and the ring-closed isomer **2.2** was generated, as monitored by measuring the relative integrals of areas under the peaks corresponding to the methine peaks of the thiophene rings (7.87 and 7.48 ppm for the ring-open **2.1** isomer as opposed to 7.13 and 6.89 ppm for the ring-closed isomer **2.2**) as discussed in *Section 2.3.3*. Treatment of this equimolar mixture (shown in Scheme 2.6.6) with less than one molar equivalent of RuTTP(CO)(EtOH) was achieved by adding small portions of a weighed amount of the ruthenium porphyrin to the NMR sample and measuring the relative integrals of the peaks corresponding to the total free ligands (ring-open form **2.1** and ring-closed form **2.2**) and the total bound ligands (**2.1RuP** and **2.2RuP**) by ¹H NMR spectroscopy. Since the main requirement of this experiment was to ensure that the two pyridyl ligands **2.1** and **2.2** compete for the porphyrin site, the addition of the ruthenium porphyrin was stopped when measurement of the integral values indicated that 0.93

molar equiv of the metalloporphyrin was present compared to each of the ligands (i.e. the ring-open isomer **2.1**, the ring-closed isomer **2.2** and the metalloporphyrin RuTTP(CO)(EtOH) were present in the ratio 1:1:0.93).



Scheme 2.6.6. Comparison of the coordination ability of the ring-open (**2.1**) and the ring-closed (**2.2**) isomers of the monobenzylated DTE. The addition of less than 1 molar equiv (0.93 molar equiv) of RuTTP(CO)(EtOH) to an equimolar mixture of both isomers generates a 1:1:0.93 mixture so that both isomers compete for the sixth coordination site of the metalloporphyrin. This addition is expected to lead to a different distribution of free (**2.1** and **2.2**) and bound (**2.1RuP** and **2.2RuP**) ligands due to the difference in binding strength arising from the difference in Lewis basicity between the ring-open isomer **2.1** and the ring-closed isomer **2.2**.

The methyl region of the spectrum is very helpful since it allows the ratios of bound (porphyrin-DTE complex **2.1RuP** and porphyrin-DTE complex **2.2RuP**) to free

(ring-open form **2.1** and ring-closed form **2.2**) ligand to be calculated by measuring their respective integrals. As shown in Figure 2.6.5, the ring-open isomer **2.1** has two three-proton singlets at 2.02 ppm (peak 'f_{k_o'}) and 2.10 ppm (peak 'f_{k_o'}'), which can be attributed to the methyl peaks of the thiophene rings linked to the pyridine group and the pyridinium group, respectively. Axial coordination to the ruthenium porphyrin showed the characteristic upfield shift in the peaks to 1.62 ppm (peak 'b_{k_o'}) and 1.63 ppm (peak 'b_{k_o'}'). The two three-proton singlets associated with the methyl groups of the thiophene rings linked to the pyridine ring (peak 'f_{k_c'}) and the pyridinium ring (peak 'f_{k_c'}) in the ring-closed isomer **2.2** almost overlap with each other and appear at 2.25 and 2.26 ppm, respectively. Similar upfield shift in the signals to 1.77 ppm (peak 'b_{k_c'}) and 1.82 ppm (peak 'b_{k_c'}) were observed upon axial coordination to the porphyrin.

It is possible to determine which of the two isomers of the monoalkylated DTE forms the more stable complex with the metalloporphyrin using the integral values corresponding to the bound ('b_{k_o'}, 'b_{k_o'}, 'b_{k_c'} and 'b_{k_c'}) and free ('f_{k_o'}, 'f_{k_o'}, 'f_{k_c'} and 'f_{k_c'}) methyl peaks as shown in Figure 2.6.5. Thus, by comparing the relative ratios of the peak integrals for the bound to free DTE ligands, which were measured to be 52:48 in the case of **2.1RuP:2.1** and 42:58 in the case of **2.2RuP:2.2**, as shown by the bar charts in Figure 2.6.5, it was established that there was about 1.3 times more of the ring-open isomer axially coordinated to the ruthenium porphyrin than the ring-closed counterpart. This implies that the ring-open isomer **2.1** acts as a better ligand for the porphyrin than the ring-closed form **2.2**, albeit to a small extent. The low selectivity is discussed in more detail in the next section.

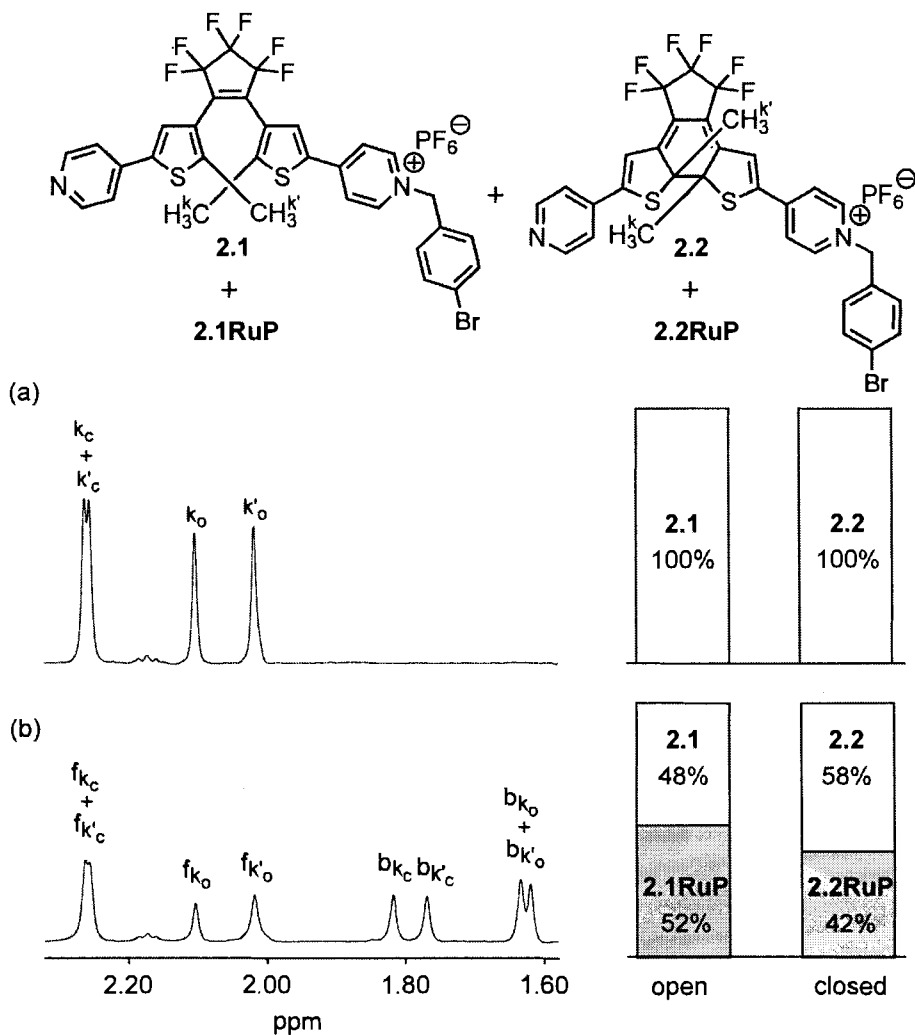


Figure 2.6.5. Assessment of the effect of the ruthenium porphyrin on an equimolar mixture of the ring-open (**2.1**) and the ring-closed (**2.2**) isomers of the monobenzylated DTE by ^1H NMR spectroscopy. Partial ^1H NMR (600 MHz, CD_2Cl_2) spectra showing the peaks corresponding to the CH_3 protons (a) before and (b) after 0.93 molar equiv of $\text{RuTTP}(\text{CO})(\text{EtOH})$ is added to the 1:1 mixture of the ring-open isomer **2.1** and the ring-closed isomer **2.2** giving rise to a 1:1:0.93 mixture of ring-open isomer **2.1**:ring-closed isomer **2.2**: $\text{RuTTP}(\text{CO})$ where 'f' denotes signals for the free ligands and 'b' denotes signals for the bound ligands while the subscript 'o' represents peaks corresponding to the ring-open form and the subscript 'c' refers to peaks corresponding to the ring-closed form. The relative amounts of the free (**2.1** and **2.2**) and bound (**2.1RuP** and **2.2RuP**) are shown by the bar charts and indicate that the more Lewis basic ring-open isomer is a better ligand for the ruthenium porphyrin than its ring-closed isomer **2.2** with approximately 1.3 times more of the ring-open isomer **2.1** axially coordinated to the ruthenium porphyrin than the ring-closed counterpart **2.2**.

2.6.9 Reasons for the Low Selectivity

The disappointingly low selectivity can be attributed to the fact that the free pyridine ring may not be completely coplanar with the conjugated backbone in the ring-closed isomer owing to the free rotation about the single bond. This implies that the Lewis base will not feel the full effect of the electron-withdrawing pyridinium moiety at the other end of the delocalized π -electron system. Molecular modelling calculations support the suggestion that the free pyridine ring is twisted 20-30° out of coplanarity from the π -conjugated backbone in the ring-closed isomer **2.2**, as illustrated in Figure 2.6.6.

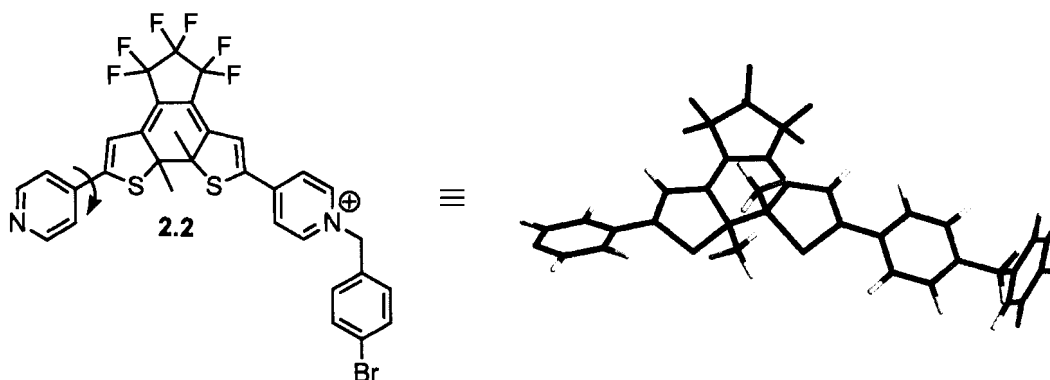
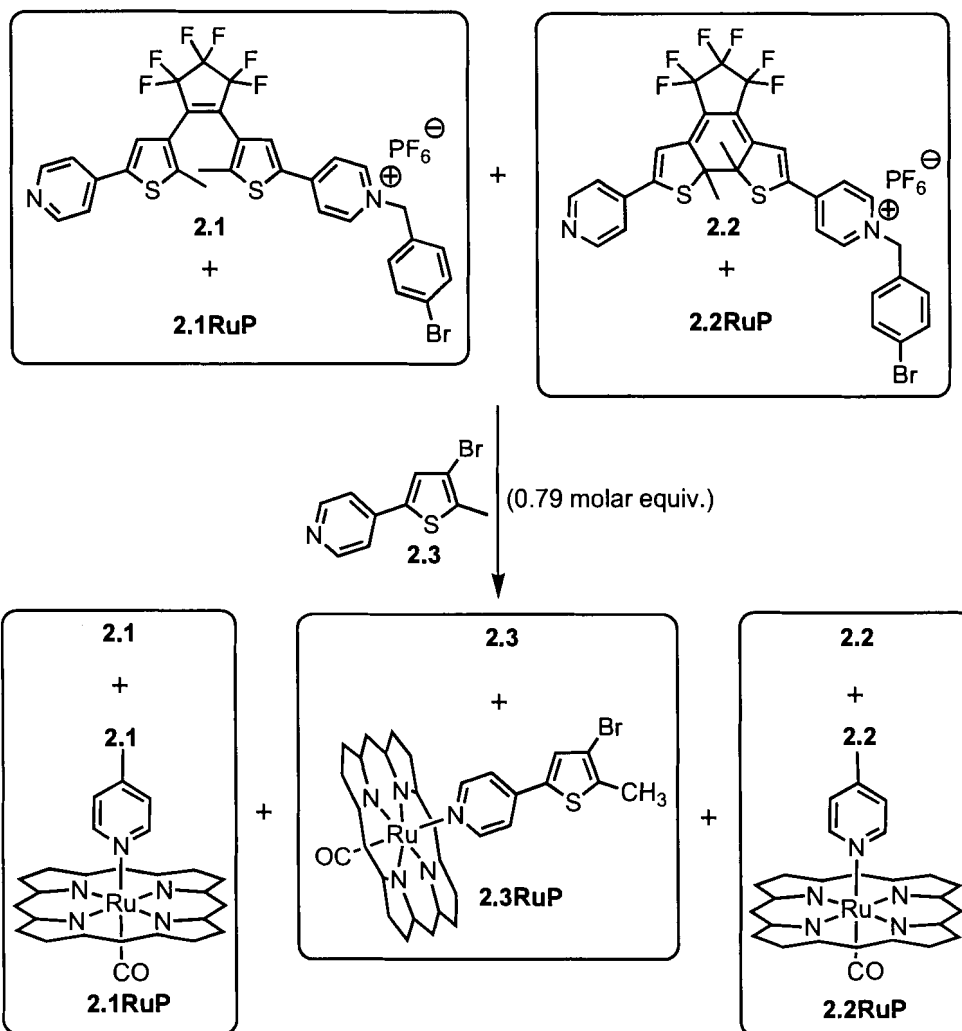


Figure 2.6.6. Molecular model representation of the ring-closed form of the monobenzylated DTE **2.2**. Molecular model calculations support the suggestion that the free pyridine is twisted out of coplanarity from the DTE backbone in the ring-closed form **2.2**. Equilibrium geometries at the ground state are determined by AM1 calculations using SpartanTM '02 for Macintosh.

2.6.10 Assessment of the Difference in Coordination Behaviour Between the Two Isomers (2.1 and 2.2) of the Monobenzylated DTE in the Presence of the Lewis Basic Pyridylthiophene 2.3

The small magnitude in the difference in coordination behaviour between the ring-open isomer **2.1** and the ring-closed isomer **2.2** prompted the execution of a different experiment in an attempt to provide additional support to the initial results obtained in

Section 2.6.8. One approach involves the addition of another pyridine-containing ligand that is expected to be more Lewis basic than the ring-closed form **2.2** of the DTE ligand to the mixture of free (**2.1** and **2.2**) and bound (**2.1RuP** and **2.2RuP**) DTEs generated in the previous NMR experiment. The idea behind this study is to provide a competing pyridine ligand for the sixth coordination site of the ruthenium porphyrin leading to the displacement of some of the ring-closed isomer **2.2** from its less stable porphyrin complex **2.2RuP** in favour of the more stable pyridyl additive–porphyrin adduct. The addition of less than one molar equivalent of the competing ligand compared to each of the DTE isomers (**2.1** and **2.2**) ensures that the latter does not completely displace all of the ring-open isomer **2.1** and the ring-closed isomer **2.2** from their respective complexes (in the event that it is more Lewis basic than both isomers). In this way, the competing ligand acts as a convenient reference to gauge the effect of the ring-opening and the ring-closing reaction on the coordination behaviour of the monoalkylated DTE by simply monitoring the change in the ratio of bound to free pyridyl additive after irradiating the NMR mixture with light of wavelengths greater than 490 nm to generate the fully ring-open state and after exposure of the mixture to 365 nm light to generate the fully ring-closed state. It can be expected that this ratio will increase on going from the fully ring-open to the fully ring-closed mixture.



Scheme 2.6.7. Effect of the more Lewis basic pyridylthiophene control **2.3** on a mixture of the free and bound ring-open and ring-closed monobenzylated DTEs. The addition of less than 1 molar equiv (0.79 molar equiv) of the competing Lewis basic pyridylthiophene **2.3** to the mixture of free (**2.1** and **2.2**) and bound (**2.1RuP** and **2.2RuP**) DTEs generated in the previous NMR experiment to form a mixture consisting of the ring-open isomer **2.1**, the ring-closed isomer **2.2**, the metalloporphyrin, and the pyridylthiophene **2.3** (1:1:0.93:0.79) leads to a redistribution of free (**2.1**, **2.2** and **2.3**) and bound (**2.1RuP**, **2.2RuP** and **2.3RuP**) ligands.

The pyridylthiophene **2.3** has been used as a close analogue of the ring-open DTE **2.1** in the previous sections of this chapter and it seems reasonable to expect that it will be more Lewis basic than the ring-closed DTE isomer **2.2** such that it is a suitable candidate to take on the role of the competing ligand. To demonstrate this point, less than one molar equivalent of the pyridylthiophene **2.3** compared to each of the DTE ligands (**2.1** and **2.2**) was added in small portions to the mixture of free (**2.1** and **2.2**) and bound (**2.1RuP** and **2.2RuP**) DTEs generated in the previous NMR experiment, as shown in Scheme 2.6.7, leading to a mixture (1:1:0.93:0.79) consisting of the ring-open isomer **2.1**, the ring-closed isomer **2.2**, the ruthenium porphyrin and the pyridylthiophene **2.3**, respectively. The subsequent redistribution of ligands and complexes was monitored by ^1H NMR spectroscopy.

The methyl region of the spectrum, as shown in Figure 2.6.7, indicates that the addition of the competing pyridylthiophene ligand **2.3** was accompanied by the appearance of a three-proton singlet at 2.45 ppm (peak 'f_q'), which is attributable to the methyl group of the free pyridylthiophene **2.3** as well as another peak further upfield at 2.09 ppm corresponding to the methyl group of the porphyrin complex **2.3RuP** and which partially overlaps with the three-proton singlet (peak 'f_{k_o}') of the methyl group on the ring-open isomer **2.1**. The appearance of peaks corresponding to both the free pyridylthiophene **2.3** and the bound ligand **2.3RuP** indicates that the pyridylthiophene **2.3** does provide a competing pyridine ligand for the ruthenium porphyrin.

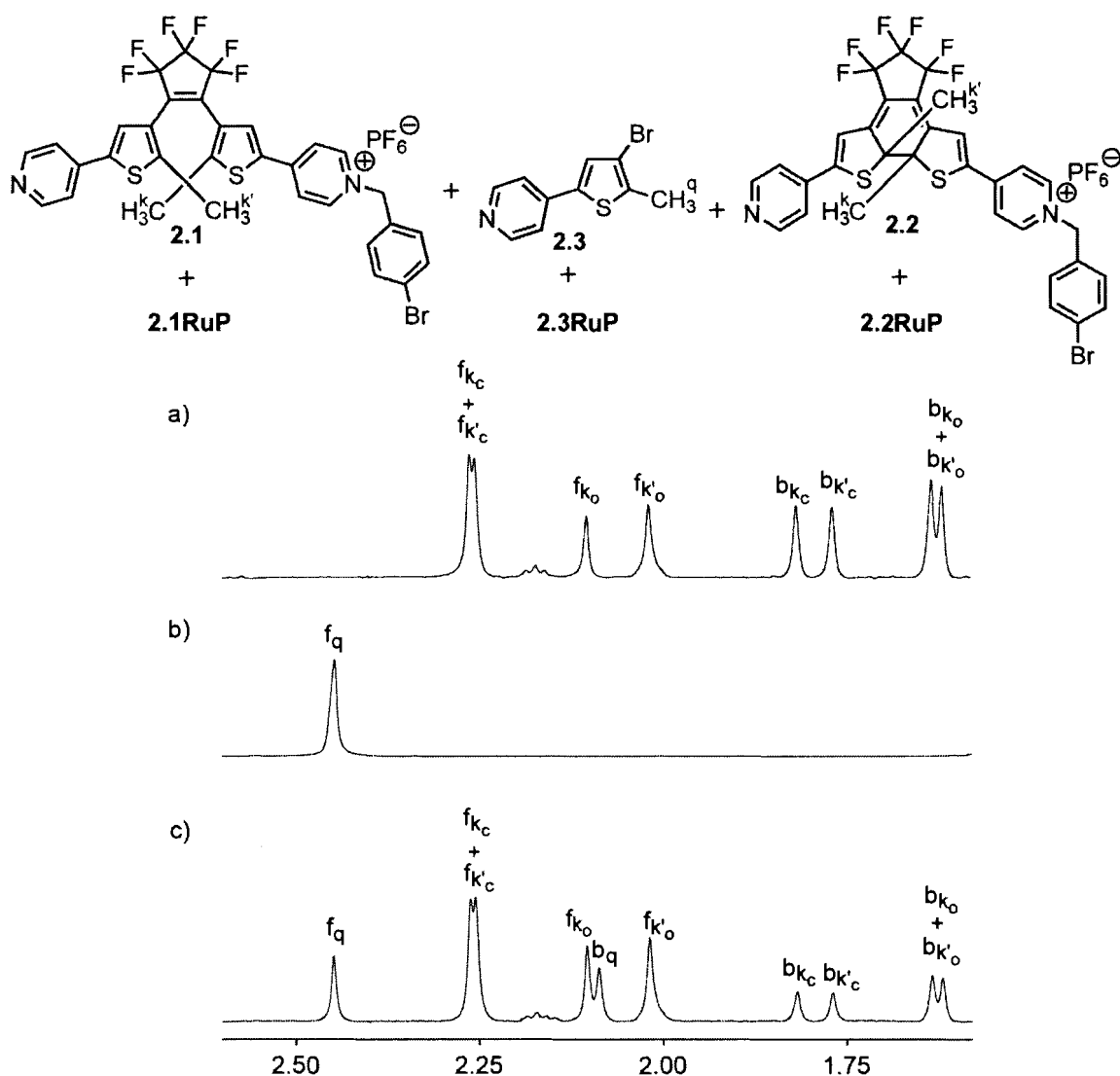
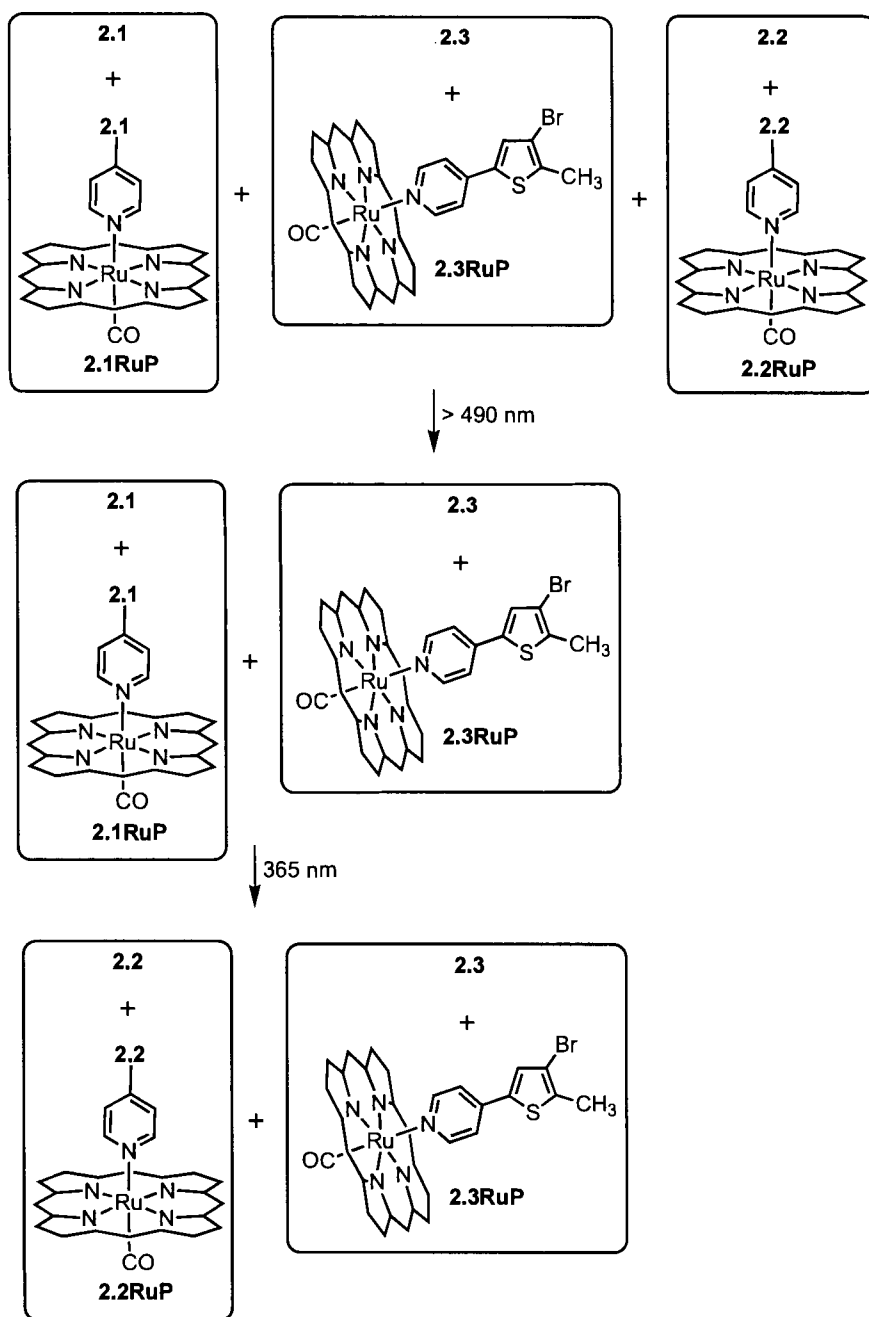


Figure 2.6.7. Assessment of the effect of the pyridylthiophene **2.3** on a mixture of the free and bound ring-open and ring-closed monobenzylated DTEs by ^1H NMR spectroscopy. Partial ^1H NMR (600 MHz, CD_2Cl_2) spectra showing the peaks corresponding to the CH_3 protons (a) of the free (**2.1** and **2.2**) and bound (**2.1RuP** and **2.2RuP**) ligands in the mixture (1:1:0.93) consisting of the ring-open isomer **2.1**, the ring-closed isomer **2.2**, and the RuTTP(CO), (b) of the free pyridylthiophene **2.3** and (c) when 0.79 molar equiv of the competing Lewis basic pyridylthiophene **2.3** was added to the mixture shown in (a) giving rise to a mixture (1:1:0.93:0.79) consisting of the ring-open isomer **2.1**, the ring-closed isomer **2.2**, the RuTTP(CO), and the ligand **2.3** leading to a redistribution of free (**2.1**, **2.2**, and **2.3**) and bound (**2.1RuP**, **2.2RuP**, and **2.3RuP**) ligands. The 'f' denotes free and the 'b' denotes bound and the subscript 'o' represents peaks corresponding to the ring-open form and the subscript 'c' denotes peaks corresponding to the ring-closed form.

The next step consisted of assessing the effect of the ring-opening and the ring-closing reactions on the distribution of free (**2.3**) and bound (**2.3RuP**) pyridylthiophene, as shown in Scheme 2.6.8. The ring-opening reaction was achieved by irradiating the mixture of free (**2.1**, **2.2**, and **2.3**) and bound (**2.1RuP**, **2.2RuP** and **2.3RuP**) species with light of wavelengths greater than 490 nm and monitoring the methyl peaks corresponding to the free (**2.1** and **2.2**) and bound (**2.1RuP** and **2.2RuP**) DTEs (2.10, 2.01, 1.63, and 1.62 ppm for the ring-open isomer **2.1** and 2.26, 2.2.5, 1.82 and 1.77 ppm for the ring-closed isomer **2.2**) until the peaks corresponding to the free and bound forms of the ring-closed isomer **2.2** were no longer observed by ¹H NMR spectroscopy, as shown in part (b) of Figure 2.6.8. Furthermore, the effect of the ring-opening reaction on the distribution of free (**2.3**) and bound (**2.3RuP**) pyridylthiophene was obtained by measuring the relative integrals of the areas under the peaks for the corresponding pairs of signals. The relative amounts of each are shown by the bar chart in part (b) of Figure 2.6.8.

The ring-closing reaction was achieved by irradiating the mixture of free (**2.1** and **2.3**) and bound (**2.1RuP** and **2.3RuP**) species, generated in the previous step and shown in Scheme 2.6.8, with 365 nm light and monitoring the methyl peaks corresponding to the free (**2.1** and **2.2**) and bound (**2.1RuP** and **2.2RuP**) DTE isomers until the peaks corresponding to the free and bound forms of the ring-open isomer **2.1** were no longer observed by ¹H NMR spectroscopy, as shown in part (c) of Figure 2.6.8.



Scheme 2.6.8. Use of the pyridylthiophene **2.3** to gauge the effect of the ring-opening and the ring-closing reaction on the coordination behaviour of the monobenzylated DTE. Irradiation of the mixture consisting of the ring-open isomer **2.1**, the ring-closed isomer **2.2**, the metalloporphyrin, and the pyridylthiophene **2.3** (1:1:0.93:0.79) with light of wavelengths greater than 490 nm leads to the complete ring-opening of both the free (**2.2**) and the bound (**2.2RuP**) forms of the ring-closed DTE. Exposure of the resulting NMR sample with 365 nm light leads to the complete ring-closing of both the free (**2.1**) and the bound (**2.1RuP**) forms of the ring-open DTE. The ring-opening and the ring-closing reactions can be expected to affect the distribution of free (**2.3**) and bound (**2.3RuP**) pyridylthiophene.

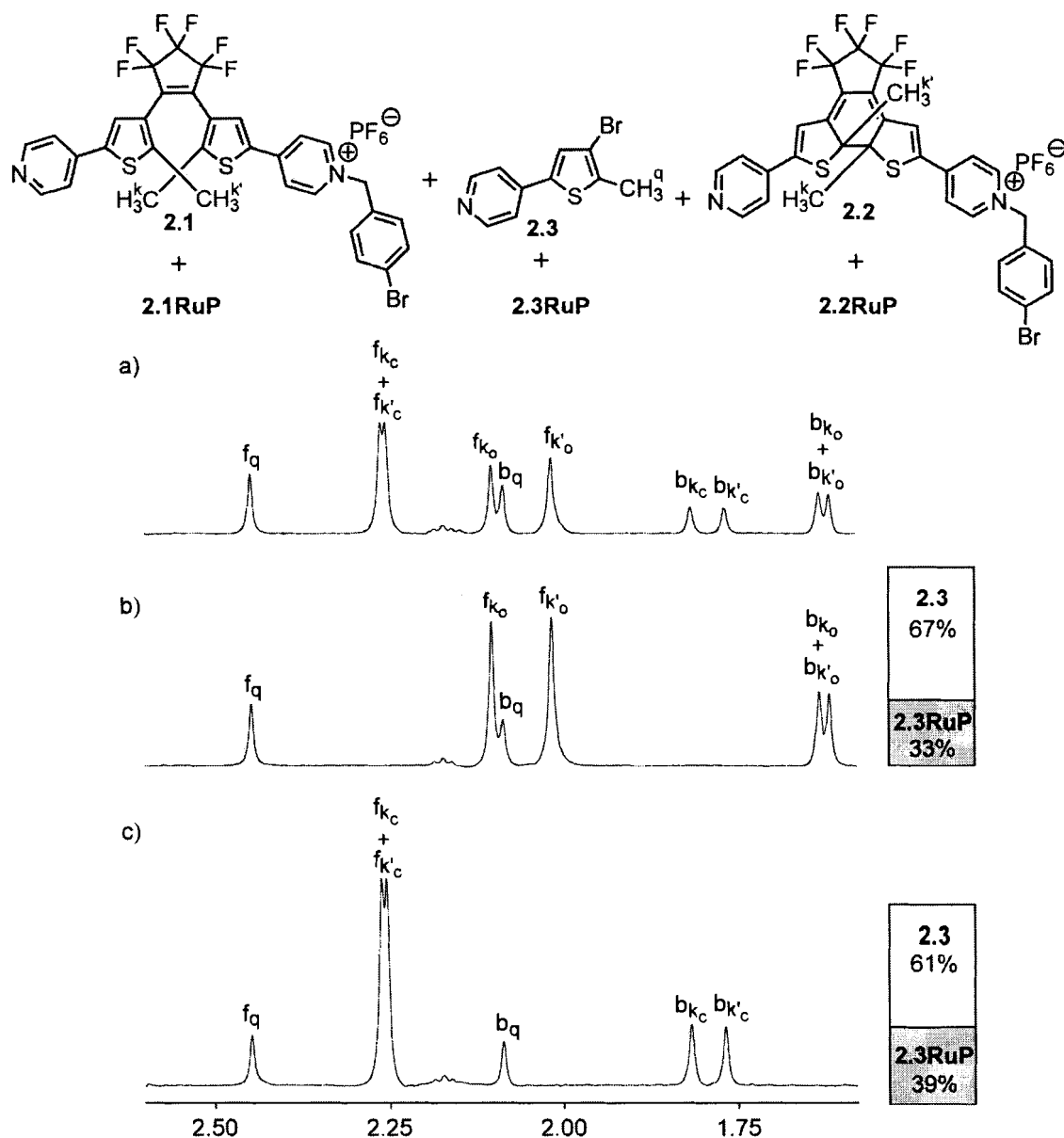


Figure 2.6.8. Assessment of the effect of the ring-opening and the ring-closing reaction on the distribution of free (**2.3**) and bound (**2.3RuP**) pyridylthiophene by ^1H NMR spectroscopy. Partial ^1H NMR (600 MHz, CD_2Cl_2) spectra showing the peaks corresponding to the CH_3 protons of the mixture of free ligands (ring-open isomer **2.1**, ring-closed isomer **2.2**, and pyridylthiophene **2.3**) and their respective porphyrin complexes (**2.1RuP**, **2.2RuP**, and **2.3RuP**) (a) before and (b) after irradiation with light of wavelengths greater than 490 nm for 20 min until the peaks corresponding to the free (**2.2**) and the bound (**2.2RuP**) forms of the ring-closed DTE were no longer observed. The partial spectrum (c) was obtained by irradiating the mixture of free (**2.1** and **2.3**) and bound (**2.1RuP** and **2.3RuP**) species, generated in the previous step (b), with 365 nm light for 10 min until the peaks corresponding to the free (**2.1**) and bound (**2.1RuP**) forms of the ring-open DTE were no longer observed. The letter ‘f’ denotes free and ‘b’ denotes bound and the subscript ‘o’ represents peaks corresponding to the ring-open form. The relative amounts of the free (**2.3**) and bound (**2.3RuP**) pyridylthiophene are shown by the bar charts and indicate that the amount of axially coordinated pyridylthiophene **2.3RuP** increases on going from the fully ring-open system to the fully ring-closed system.

Furthermore, the effect of the ring-closing reaction on the distribution of free (**2.3**) and bound (**2.3RuP**) pyridylthiophene was obtained by measuring the relative integrals of the areas under the peaks for the corresponding pairs of signals. The relative amounts of each are shown by the bar chart in part (c) of Figure 2.6.8. The values observed are consistent with the predicted trend where the amount of axially coordinated pyridylthiophene **2.3RuP** increases on going from the fully ring-open system to the fully ring-closed system. In fact, there was slightly less than 1.2 times more of the pyridylthiophene **2.3** axially coordinated to the ruthenium porphyrin when the system was in its fully ring-closed state as opposed to its fully ring-open state. This change, albeit small, indicates that the ring-open isomer **2.1** is the more effective ligand for RuTTP(CO)(EtOH) than its ring-closed form **2.2** and supports the results obtained in *Section 2.6.8*.

2.6.11 Assessment of the Electronic Differences Between the Two Isomers (2.1** and **2.2**) of the Monobenzylated DTE by IR Spectroscopy**

As described in *Section 2.4* of this thesis, it is well documented that the CO stretching frequencies of Ru(CO) porphyrins are intimately linked to the type of ligand occupying the sixth coordination site.^{79,87,93} The fact that these CO stretching frequencies lie in an uncluttered region of the IR spectrum makes IR spectroscopy a convenient tool to assess the electronic variations between: (1) the pyridylthiophene **2.3** and the monomethylated bipyridinium **2.4** control compounds and (2) the two isomers of the monobenzylated DTE (**2.1** and **2.2**).

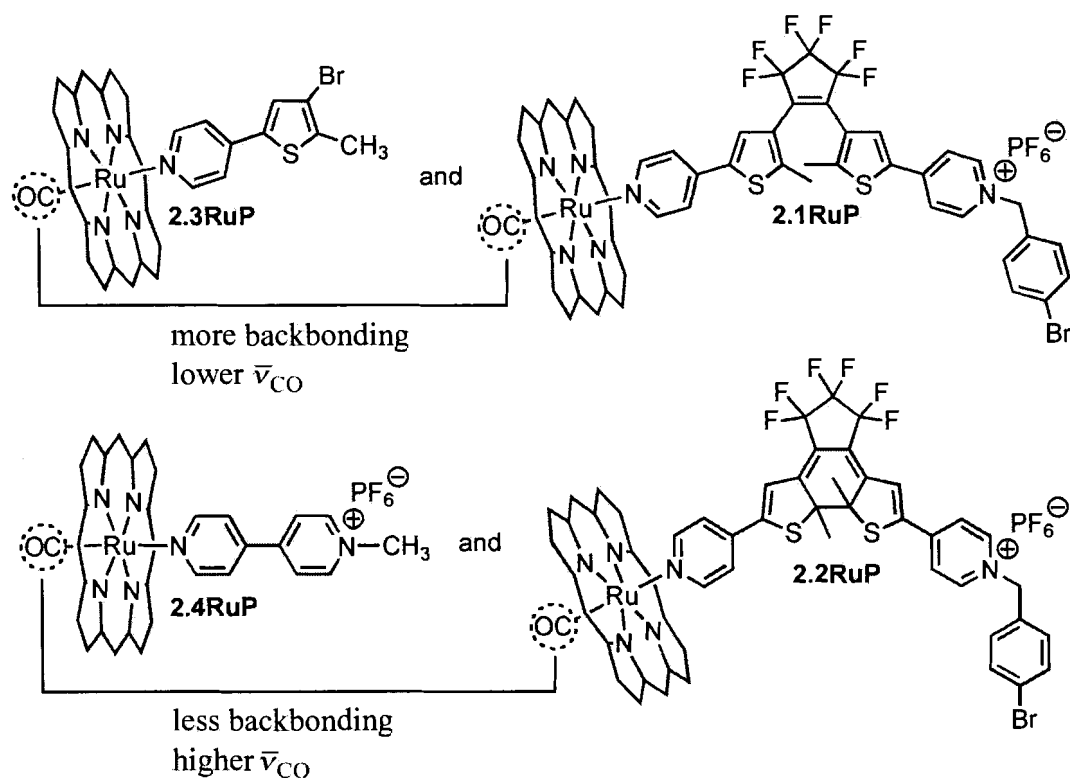


Figure 2.6.9. IR spectroscopy as a tool to assess the electronic variations between the porphyrin complexes of the model compounds (**2.3** and **2.4**) and the two DTE isomers (**2.1** and **2.2**). The pyridylthiophene–porphyrin complex **2.3RuP** and the ring-open DTE–porphyrin adduct **2.1RuP** will lead to an increase in the electron density around the ruthenium centre resulting in more π backbonding ($\text{Ru} \rightarrow \text{CO}$) and lower CO stretching frequencies than in the case of the monomethylated bipyridinium–porphyrin adduct **2.4RuP** and the ring-closed DTE–porphyrin complex **2.2RuP**.

The studies described in *Sections 2.6.4* and *2.6.8* have shown that the pyridylthiophene **2.3** is a close analogue for the ring-open isomer **2.1** while the monomethylated bipyridinium **2.4** is a close representative for the ring-closed isomer **2.2**. In fact, both the pyridyl ligands **2.3** and **2.1** have been shown to act as better ligands for the ruthenium porphyrin than the pyridyl ligands **2.4** and **2.2**. Thus, it can be expected that the stronger Ru–N bond in both the pyridylthiophene–porphyrin complex **2.3RuP** and the ring-open DTE–porphyrin adduct **2.1RuP** will lead to an increase in the electron density around the ruthenium centre resulting in more $\text{Ru} \rightarrow \text{CO}$ π backbonding than in the case of the monomethylated bipyridinium–porphyrin adduct **2.4RuP** and the ring-

closed DTE–porphyrin complex **2.2RuP**. Consequently, it seems reasonable to expect that the CO stretching frequency will be greater when the sixth coordination site of the ruthenium porphyrin is occupied by the ring-closed isomer **2.2** or its model compound **2.4** than when occupied by the ring-open isomer **2.1** or its model compound **2.3** (Figure 2.6.9). In order to assess the electronic influence of the model compounds (**2.3** and **2.4**) and the monobenzylated *bis*(pyridine) (**2.1** and **2.2**) on the CO stretching frequency, the metalloporphyrin reagent RuTTP(CO)(EtOH) and the coordination compounds formed when the ruthenium porphyrin is axially coordinated to the pyridylthiophene **2.3**, the ring-open isomer **2.1**, the monomethylated bipyridinium **2.4** and the ring-closed isomer **2.2** were cast in KBr pellets and analyzed independently by IR spectroscopy and the CO stretching frequencies ($\bar{\nu}_{\text{CO}}$) are listed in Table 2.6.5.

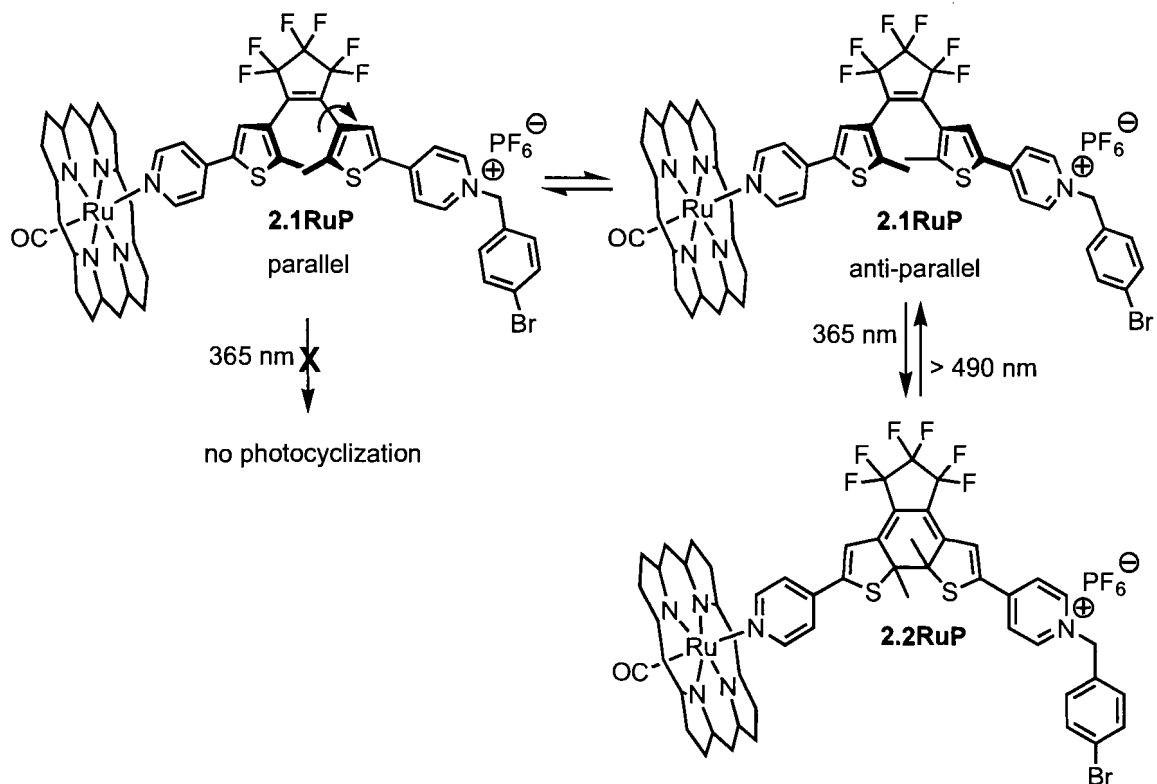
The IR spectrum for the pyridylthiophene–porphyrin hybrid **2.3RuP** shows that there was an increase in the CO stretching frequency to 1951 cm^{-1} compared to the frequency observed (1946 cm^{-1}) for RuTTP(CO)(EtOH). This is indicative of a decrease in the Ru \rightarrow CO backbonding brought about by the introduction of the pyridyl moiety and is consistent with the trend observed in the literature for the axial coordination of pyridyl moieties to other ruthenium porphyrin complexes.⁷⁹ Changing the ligand to the ring-open monobenzylated DTE to form the DTE–porphyrin adduct **2.1RuP** showed similar CO stretching frequency (1949 cm^{-1}) to its model compound **2.3RuP**, as predicted. The complex generated upon axial coordination of the monomethylated bipyridinium **2.4** to the ruthenium porphyrin had a CO stretching frequency of 1956 cm^{-1} indicative of a more pronounced decrease in the Ru \rightarrow CO backbonding than in the case of the pyridylthiophene complex **2.3RuP**. The ring-closed DTE–porphyrin complex

2.2RuP also showed an increase in its CO stretching frequency (1956 cm^{-1}) compared to the ring-open DTE–porphyrin hybrid **2.1RuP**. This decrease in Ru \rightarrow CO backbonding can be ascribed to the lower electron density on the ruthenium centre when the sixth coordination site is occupied by the ring-closed form **2.2** of the DTE or its model compound **2.4** and is suggestive of a weaker Ru–N bond in both cases as predicted. These values indicate that the ring-closed form **2.2** of the monoalkylated DTE and its model compound **2.4** are weaker ligands than the ring-open form **2.1** of the DTE and its model compound **2.3** and support the results obtained in the NMR experiments discussed in this chapter.

Table 2.6.5. List of CO stretching frequencies. The values correspond to the ruthenium porphyrin RuTTP(CO)(EtOH) and the coordination compounds formed when the porphyrin was axially coordinated to the pyridylthiophene **2.3**, the ring-open isomer **2.1**, the monomethylated bipyridinium **2.4** and the ring-closed isomer **2.2** and cast in KBr pellets.

KBr pellet ^a	$\bar{\nu}_{\text{CO}}\text{ (cm}^{-1}\text{)}$
RuTTP(CO)(EtOH)	1946
2.3RuP	1951
2.1RuP	1949
2.4RuP	1956
2.2RuP	1954

^a Each pellet was prepared by mixing anhydrous KBr and the respective porphyrin coordination complex (approximate ratio of 100:1 by weight of the KBr to the coordination complex) and using 100 mg of the resulting mixture to cast the pellet.



Scheme 2.6.9. The *parallel* and *anti-parallel* conformations of the ring-open DTE-porphyrin complex **2.1RuP**. The KBr matrix is not flexible enough to accommodate the conformational requirements of the photoisomerization reaction and renders the mixture partially inactive.

Further investigation of the photochromic properties of the monoalkylated DTE-porphyrin hybrid in the solid matrix revealed that the KBr pellet of the ring-open DTE-porphyrin complex **2.1RuP** required more than 2 hours of irradiation with 365 nm light for the CO stretching frequency to increase to 1952 cm^{-1} . This result showed that only about 50% conversion to the ring-closed form had occurred in the solid matrix in contrast to the solution studies where irradiation of a CD_2Cl_2 solution ($1.1 \times 10^{-3} \text{ M}$) of the complex **2.1RuP** with 365 nm light showed a new set of signals corresponding to the completely ring-closed complex **2.2RuP** after only 10 min. This marked decrease in the photosensitivity of the DTE moiety in the solid-state can be ascribed to the environmental constraints imposed on the ring-open form by the solid KBr matrix. As discussed in the

introductory chapter, it is well documented that two equal energy conformers of DTE derivatives coexist: (1) the parallel conformation with the two thiophene rings in mirror symmetry and (2) the anti-parallel conformation where the two thiophene rings have a C_2 axis of symmetry and that only one of them is free to undergo the ring-closing reaction as shown in Scheme 2.6.9.^{31-33,37}

The close packing in the solid KBr pellet likely prevents the free rotation and does not allow conformational interconversion between the photoinactive *parallel* and the photoactive *anti-parallel* conformer. This renders the mixture partially inactive. Similar environmental constraints on DTE derivatives have been described.^{100,101} To overcome this limitation, a similar approach to the work previously described by Uchida and coworkers¹⁰⁰ was adopted where the IR studies were carried out starting from the pellet prepared from the fully-ring-closed isomer **2.2RuP**. Exposure of this pellet having a stretching frequency of 1954 cm^{-1} to light of wavelengths greater than 490 nm for 1 h resulted in the shifting of the stretching frequency to 1949 cm^{-1} corresponding to the CO stretch of the fully-ring-open complex **2.1RuP**. Complete photocyclization to the ring-closed complex **2.2RuP** was achieved upon re-irradiation of the above pellet with 365 nm light sending the CO stretch back to 1954 cm^{-1} after 90 min. The CO stretching frequencies are reported in Table 2.6.6. These results indicate that the photochromic behaviour of the ring-open (**2.1RuP**) and the ring-closed (**2.2RuP**) monobenzylated DTE-porphyrin can be retained in the solid matrix by casting the pellet using the fully-ring-closed **2.2RuP**, which predisposes the latter to favour the productive *anti-parallel* conformation and allows the ring-opening and the ring-closing reactions to take place.

Table 2.6.6. Observed changes in the CO stretching frequencies when the photochemical interconversion of the DTE–porphyrin hybrids (**2.1RuP** and **2.2RuP**) were investigated in the solid KBr matrix.

KBr pellet	$\bar{\nu}_{\text{CO}}$ (cm ⁻¹)
2.1RuP ^a	1949
2.1RuP $\xrightarrow{365 \text{ nm}}$ 2.2* RuP ^b	1952
2.2RuP ^c	1954
2.2RuP $\xrightarrow{> 490 \text{ nm}}$ 2.1* RuP ^d	1949
2.1* RuP $\xrightarrow{365 \text{ nm}}$ 2.2* RuP ^e	1954

^a Coordination compound formed when the ruthenium porphyrin was axially coordinated to the ring-open isomer **2.1** and cast in a KBr pellet. ^b Irradiation of the KBr pellet of the ring-open DTE-porphyrin complex **2.1RuP** to 365 nm light for more than 2 h generated about 50% of the ring-closed DTE–porphyrin complex **2.2*RuP** *in situ*. ^c Complex formed when the ruthenium porphyrin was axially coordinated to the ring-closed isomer **2.2** and cast in a KBr pellet. ^d Exposure of the KBr pellet of the ring-closed DTE-porphyrin complex **2.2RuP** to light of wavelengths greater than 490 nm for 1 h led to the fully ring-open DTE–porphyrin adduct **2.1*RuP** *in situ*. ^e Re-irradiation of the fully ring-open DTE–porphyrin adduct **2.1*RuP** generated above with 365 nm light led to the fully ring-closed DTE–porphyrin adduct **2.2*RuP** *in situ* after 90 min.

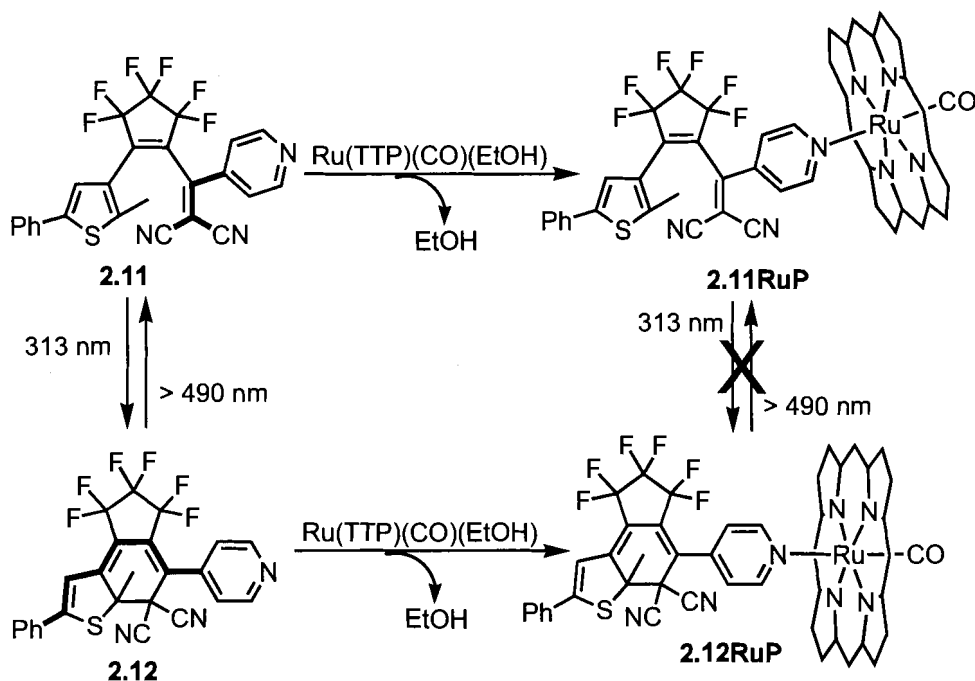
2.7 Conclusions

The goal of this project was to show the concept of photomodulation of nucleophilicity by incorporating a nucleophilic pyridine and an electron-deficient pyridinium into the DTE backbone. This was achieved using coordination chemistry as a probe by examining the stability of axially substituted ruthenium porphyrin complexes prepared from both the ring-open and the ring-closed isomers of the DTE system. The results show that the ring-open isomer **2.1** is more effective as a ligand than its ring-closed counterpart. This difference in coordination ability, albeit small, can be attributed to a decrease in the Lewis basicity of the nitrogen of the pyridine owing to the electronic communication between the free pyridine and the electron-withdrawing pyridinium group in the ring-closed isomer **2.2**. This result acts as an incentive to evaluate the concept of photomodulating nucleophilicity in chemical synthesis and to determine the extent to which this small difference in electronics between the two DTE isomers can influence the outcome of a chemical reaction. This research will be presented in *Chapter 3*.

2.8 Future Work

Although the presented research introduces and shows the success of the concept of photomodulation of Lewis basicity, the small magnitude of the change between the two DTE isomers of the chosen system shows that further synthetic modifications are required before it can be used in a practical setting. Since the concept takes advantage of the fact that the Lewis basic character of a pyridine is dependent on the electronic influence of the groups attached to it, one factor that can be addressed involves improving the electronic communication between the pyridine and the electron-

withdrawing group (or can also be an electron-donating group) in one isomer compared to the other.



Scheme 2.8.1. Difference in binding strength between the ring-open (**2.11**) and the ring-closed (**2.12**) isomers of the DCTE. The more Lewis basic ring-closed isomer **2.12** acts as a better ligand for the metalloporphyrin than its ring-open isomer **2.11** but the introduction of the metalloporphyrin shuts down the photochromic behaviour of the DCTE-porphyrin hybrid.

One approach that may improve the electronic communication and consequently the magnitude of the change between the two isomers involves re-designing the DTE system so that the pyridine is directly connected to either an electron-withdrawing (EWG) or an electron-donating group (EDG) instead of being electronically connected through the DTE backbone. The dicyanoethylene-thienylethene (DCTE) architecture **2.11**, which was synthesized by a former member of the group¹⁰², represents a good model of a DTE system where the pyridine can sense the electronic pull of the electron-withdrawing dicyanoethylene group through the linear π -conjugated pathway as illustrated in bold in Scheme 2.8.1. The photocyclization event generates the ring-closed

isomer **2.12**, where the pyridine is insulated from the dicyanoethylene group. The break in the linear π -conjugated pathway is due to the change in hybridization of the carbon involved in the formation of the new C–C bond from sp^2 to sp^3 . Thus, it can be expected that the ring-closed isomer **2.12** will act as a stronger coordinating ligand.

Preliminary ^1H NMR studies indicate that when less than one molar equiv of $\text{Ru}(\text{TTP})(\text{CO})(\text{EtOH})$ is added to a 1:1 mixture of **2.11** and **2.12**, the ring-closed form **2.12** acts as a stronger ligand for the ruthenium porphyrin. However, incorporation of the metalloporphyrin in the system has a detrimental effect on the photochemistry of the pyridine ligand and, once either coordination complex is formed, it no longer retains its photoresponsive behaviour. Similar effects have been observed in the past with other complexes.¹⁰³ This example shows that even though the electronic properties of DTE isomers can be easily fine-tuned, it is critical that the group chosen to impart the desired electronic effect does not inhibit the photoswitching behaviour.

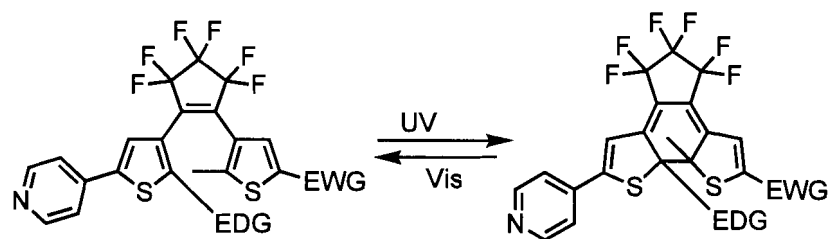


Figure 2.8.1. Generalized structure of a DTE system where the pyridine is electronically communicated to (1) an electron-donating group (EDG) located at the internal position of the thiophene in the ring-open isomer and (2) an electron-withdrawing group (EWG) in the ring-closed form.

Another approach involves the introduction of an EDG at the internal position of the thiophene bearing the pyridine group and an EWG at the external position of the other thiophene so as to create system where the pyridine is electronically communicated to (1) the EDG in the ring-open isomer and (2) the EWG in the ring-closed isomer as shown in

Figure 2.8.1. Recently, Irie and coworkers⁴³ used this strategy to modify the system previously described by Lehn and coworkers⁴² in an attempt to create a more pronounced difference in the acidity of a phenolic OH between the two DTE isomers.

2.9 Experimental

Materials. All solvents for synthesis were dried and degassed by passing them through steel columns containing activated alumina under nitrogen using a solvent purification system (MBraun). All other solvents were used as received. Solvents for NMR analysis (Cambridge Isotope Laboratories) were used as supplied. Column chromatography was performed using neutral alumina (activity II-III) for the purification of the ruthenium porphyrin RuTTP(CO)(EtOH) and 1,2-*bis*(2'-methyl-5'-(pyrid-4''-yl)thien-3'-yl)perfluorocyclopentene **2.8** while the other compounds were purified using silica gel 60 (230-400 mesh) from Silicycle Inc. All other reagents and starting materials were purchased from Aldrich with the exception of Pd(PPh₃)₄ and Ru₃(CO)₃, which were purchased from Strem. Compounds 5,10,15,20-tetratolylporphyrin TTP,¹⁰⁴ 3,5-dibromo-2-methylthiophene **2.5**,⁹⁶ and 3-bromo-2-methyl-5-thiopheneboronic **2.6**²⁹ were prepared according literature procedures and their syntheses are not be reported, herein.

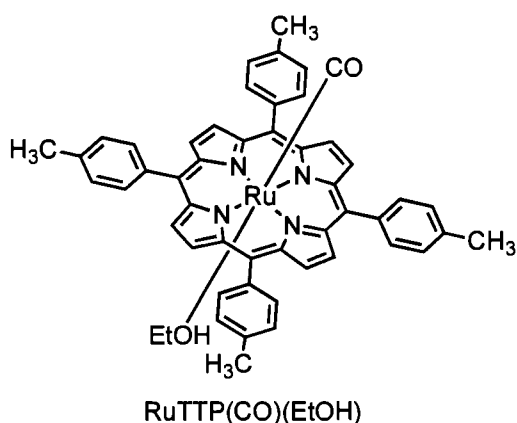
Techniques. Melting points (Mp) were measured on a Gallenkamp capillary melting point apparatus. ¹H and ¹³C NMR characterizations were performed on a Varian Mercury 400 instrument working at 400.1 MHz for ¹H NMR and 100.6 MHz for ¹³C NMR or a Varian Inova 500 instrument working at 499.8 MHz for ¹H NMR and 125.7 MHz for ¹³C NMR or a Bruker AMX 600 instrument working at 600.1 MHz for ¹H NMR and 150.5

MHz for ^{13}C NMR or a Bruker TCI 600 instrument working at 600.3 MHz for ^1H NMR and 150.5 MHz for ^{13}C NMR. The ^{13}C NMR spectra are ^1H -decoupled but ^{19}F -coupled. Assignments were confirmed using ^1H - ^1H COSY and selective 1-D NOE experiments when necessary. Chemical shifts (δ) are reported in parts per million relative to tetramethylsilane using the residual solvent peak as an internal reference. Coupling constants (J) are reported in Hertz. Indistinguishable peaks are denoted with asterisks (*). FT-IR measurements were performed using a Nicolet Nexus 670 instrument. FT-IR measurements of the CO stretching frequencies of the porphyrin complexes **2.1RuP**, **2.2RuP**, **2.3RuP** and **2.4RuP** cast as KBr pellets were performed at a resolution of 1 cm^{-1} in the spectral region $2200\text{-}1800\text{ cm}^{-1}$. UV-Vis measurements were performed using a Varian Cary 300 Bio spectrophotometer. Low resolution mass spectrometry (LRMS) measurements were performed using an HP5985 mass spectrometer with isobutane as the chemical ionization source or a matrix assisted laser desorption/ionization source (MALDI) using a PerSeptive Biosystems Voyager-DE instrument and the MALDI-TOF mass spectra were obtained using 2,5-hydroxybenzoic acid as the matrix. Microanalyses (Anal.) were performed on a Carlo Erba Model 1106 CHN analyzer.

KBr pellets. All the pellets used for the FT-IR measurements were prepared by mixing the KBr reagent and the coordination complex in the approximate ratio of 100:1 by weight of KBr reagent to coordination complex and the same amount of the homogeneous mixture (100 mg) was used to cast the pellet.

Photochemistry. Standard hand-held lamps used for visualizing TLC plates (Spectroline E-series, $470 \mu\text{W cm}^{-2}$) were used to carry out the ring-closing reactions. A 313 nm light source was used for the *bis*(pyridine) **2.8** and a 365 nm light source was used for the monobenzylated DTE **2.1** and its porphyrin complex **2.1RuP**. The same light source was used to carry out the ring-closing reaction of the DTE–porphyrin complex **2.1RuP** cast in a KBr pellet. The ring-opening reactions of the monobenzylated DTE **2.2** and its porphyrin adduct **2.2RuP** (both in solution and when cast in a KBr pellet) were carried out using the light of a 150 W tungsten source that was passed through a 490 nm cut-off filter to eliminate higher energy light.

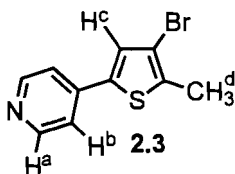
Calculations. The equilibrium geometry at the ground state for the ring-closed isomer was determined using semi-empirical AM1 and PM3 calculations using Spartan '02 for Macintosh from Wavefunction Inc.



Synthesis of ruthenium carbonyl metalloporphyrin complex Ru(TTP)(CO)(EtOH).⁹⁵

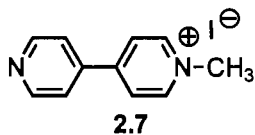
The known *meso*-tetratolylporphyrin TTP¹⁰⁴ (502 mg, 0.748 mmol) and Ru₃(CO)₁₂ (751 mg, 1.17 mmol) were treated with phenol (2.00 g, 21.3 mmol) and the reaction mixture

was heated under reflux for 45 min. The source of heat was removed and the reaction mixture was slowly allowed to cool to room temperature after which, EtOH (1 mL) was added. The crude product was precipitated by the addition of cold H₂O (2 mL), collected by vacuum filtration and washed with cold H₂O (3 × 2 mL). The resultant dark brown solid was purified by flash chromatography (neutral alumina: activity II-III, eluting first with CH₂Cl₂ and finally with a mixture of EtOH:CH₂Cl₂ = 5:95) and recrystallization from EtOH afforded Ru(TTP)(CO)(EtOH) (461 mg, 70%) as a red solid. Mp: >240 °C. ¹H NMR (CD₂Cl₂, 400 MHz): δ 8.72 (s, 8H), 8.09 (d, 4H, *J* = 7.2 Hz), 7.75 (d, 4H, *J* = 7.2 Hz), 7.56 (d, 4H, *J* = 7.2 Hz), 7.54 (d, 4H, *J* = 7.2 Hz), 2.69 (s, 12H). ¹³C NMR (CD₂Cl₂, 100 MHz): δ 182.0, 144.5, 139.8, 137.6, 134.6, 134.3, 132.0, 127.8, 127.6, 122.3, 21.6. UV/Vis (CH₂Cl₂): λ_{max}/ nm (log ε/M⁻¹cm⁻¹) 240 (4.49), 305 (4.31), 410 (5.38), 530 (4.31), 563 (3.33). FT-IR (KBr-cast): 3022, 2929, 2060, 2020, 2000, 1945, 1601, 1528, 1514, 1431, 1343, 1300, 1178, 1076, 1009, 797, 716 cm⁻¹.



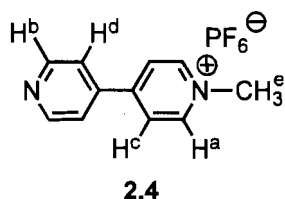
Synthesis of 3-bromo-2-methyl-5-(4'-pyridyl)thiophene 2.3.²⁹ A mixture of THF (50 mL) and saturated aqueous Na₂CO₃ solution (50 mL, 2M) was deoxygenated by bubbling N₂ through the solution for 45 min, treated with 4-bromopyridine hydrochloride (2.81 g, 14.4 mmol) and N₂ was bubbled through the solution for an additional 5 min. 3-Bromo-2-methyl-5-thiopheneboronic acid **2.6**²⁹ (2.90 g, 13.1 mmol) and Pd(PPh₃)₄ (35 mg, 0.030 mmol) were immediately added and the reaction was heated at reflux for 20 h under an

N₂ atmosphere. The heat source was removed and the reaction was allowed to slowly cool to room temperature after which the aqueous layer was removed and extracted with CHCl₃ (3 × 50 mL). The combined organic layers were washed with brine (200 mL), dried over anhydrous Na₂SO₄, filtered and concentrated to dryness *in vacuo*. The crude product was purified using a short column (silica, hexanes/EtOAc = 6:1 containing 1% of NEt₃) yielding an off-white solid. Recrystallization from EtOAc afforded the pyridylthiophene **2.3** (2.35 g, 70%) as colourless crystals. Mp: 80–82 °C (lit. 83 °C). ¹H NMR (CD₂Cl₂, 400 MHz): δ 8.56 (H^a, d, 2H, *J* = 5.6 Hz), 7.38 (H^b, d, 2H, *J* = 5.6 Hz); 7.34 (H^c, s, 1H), 2.44 (H^d, s, 3H). ¹³C NMR (CD₂Cl₂, 100 MHz): δ 150.7, 140.3, 138.1, 136.8, 128.0, 119.3, 110.6, 15.1. FT-IR (KBr-cast): 3056, 3027, 2910, 1598, 1494, 1412, 1324, 1222, 1159, 1008, 988, 862, 812, 760, 718 cm⁻¹. LRMS (CI isobutane): *m/z* 254, 256 [M+H]⁺.

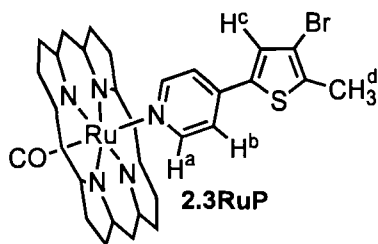


Synthesis of 1-methyl-4,4'-bipyridinium iodide 2.7.⁹⁷ 4,4'-Bipyridine (1.80 g, 11.0 mmol) was dissolved in anhydrous CH₂Cl₂ (10 mL) and iodomethane (0.80 mL, 14 mmol) was quickly added using a syringe. The solution was heated under reflux with constant stirring for 2 h under an N₂ atmosphere. The heating mantle was removed and the mixture was slowly allowed to cool to ambient temperature. The resultant yellow precipitate was filtered and thoroughly washed with EtOAc. The crude product was recrystallized from MeOH to give compound **2.7** (2.79 g, 85%) as yellow crystals. Mp: >

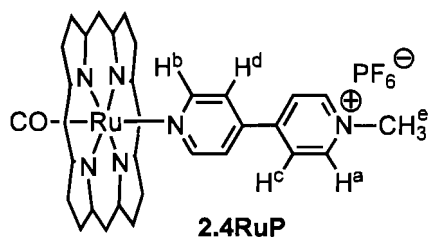
250 °C (lit. > 248 °C). ^1H NMR (DMSO- d_6 , 400 MHz): δ 9.14 (d, 2H, $J = 6.6$ Hz), 8.87 (d, 2H, $J = 6.0$ Hz), 8.62 (d, 2H, $J = 6.6$ Hz), 8.04 (d, 2H, $J = 6.0$ Hz), 4.38 (s, 3H). ^{13}C NMR (DMSO- d_6 , 100 MHz): δ 153.0, 151.0, 146.3, 141.2, 125.8, 122.3, 47.5. LRMS (CI isobutane): m/z 171 $[\text{M-I}]^+$.



Synthesis of 1-methyl-4,4'-bipyridinium hexafluorophosphate 2.4. The 1-methyl-4,4'-bipyridinium iodide **2.7** (1.54 g, 5.17 mmol) was dissolved in water (1 mL) and solid ammonium hexafluorophosphate was slowly added whereupon a pale yellow precipitate was observed. More of the ammonium salt was added until no further precipitate was generated. The solid was collected by vacuum filtration and washed with copious amounts of cold water yielding the hexafluorophosphate salt of the monomethylated bipyridinium **2.4** (1.61 g, 99%) as a very pale yellow solid. Mp: 209–211 °C. ^1H NMR (CD_3COCD_3 , 400 MHz): δ 9.21 (H^a , d, 2H, $J = 6.0$ Hz), 8.87 (H^b , d, 2H, $J = 5.6$ Hz), 8.65 (H^c , d, 2H, $J = 6.0$ Hz), 7.99 (H^d , d, 2H, $J = 5.6$ Hz), 4.67 (H^e , s, 3H). ^{13}C NMR (CD_3COCD_3 , 100 MHz): δ 154.0, 151.5, 146.5, 141.5, 125.8, 122.0, 48.2. FT-IR (KBr-cast) 3144, 3046, 1654, 1601, 1553, 1528, 1489, 1414, 1329, 1227, 1197, 1071, 838, 716 cm^{-1} . LRMS (MALDI, 2,5-hydroxybenzoic acid): m/z 171 $[\text{M-PF}_6]^+$. Anal. Calcd for $\text{C}_{11}\text{H}_{11}\text{N}_2\text{PF}_6$: C, 41.79; H, 3.51; N, 8.86. Found: C, 41.61; H, 3.57; N, 8.63.



Synthesis of the pyridylthiophene–porphyrin coordination complex 2.3RuP. The pyridylthiophene **2.3** (9 mg, 0.04 mmol) was dissolved in CD_2Cl_2 (0.7 mL) and transferred into a NMR tube. The metalloporphyrin $\text{RuTTP}(\text{CO})(\text{EtOH})$ (31 mg, 0.037 mmol) was slowly added using a spatula until the formation of a 1:1 complex was observed by ^1H NMR spectroscopy. The solvent was removed under reduced pressure yielding complex **2.3RuP** (38 mg, 99%) as a burgundy solid. Mp: >250 °C. (* denotes peaks that overlap) ^1H NMR (CD_2Cl_2 , 400 MHz): δ 8.66 (s, 8H), 8.11 (d, 4H, $J = 7.2$ Hz), 7.96 (d, 4H, $J = 7.2$ Hz), 7.56 (d, 4H, $J = 7.2$ Hz), 7.51 (d, 4H, $J = 7.2$ Hz), 6.40 (H^c , s, 1H), 5.33-5.31* (H^b , m, 2H), 2.68 (s, 12H), 2.06 (H^d , s, 3H), 1.47 (H^a , d, 2H, $J = 6.4$ Hz). ^{13}C NMR (CD_2Cl_2 , 100 MHz): δ 180.5, 144.3, 143.9, 139.8, 138.8, 137.7, 137.3, 135.6, 134.4, 134.2, 131.9, 128.2, 127.5, 127.3, 121.9, 117.0, 110.5, 21.4, 14.8. UV/Vis (CH_2Cl_2): λ_{max} / nm ($\log \epsilon/\text{M}^{-1}\text{cm}^{-1}$) 246 (4.17), 314 (4.17), 414 (4.99), 533 (3.87), 570 (3.37). FT-IR (KBr-cast) 3022, 2925, 2861, 2059, 2024, 1951, 1606, 1533, 1494, 1445, 1382, 1348, 1295, 1217, 1183, 1105, 1066, 1012, 789, 711 cm^{-1} . LRMS (MALDI-TOF): m/z 254, 256 $[(\text{M}+\text{H})-\text{RuTTP}(\text{CO})]^+$. Anal. Calcd for $\text{C}_{59}\text{H}_{44}\text{N}_5\text{ORuSBr}$: C, 67.36; H, 4.22; N, 6.66. Found: C, 66.99; H, 4.15; N, 6.40.

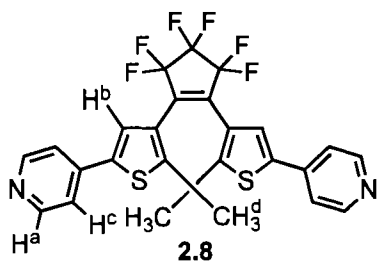


Synthesis of the monomethylated bipyridinium–porphyrin coordination complex

2.4RuP. A solution of the monomethylated bipyridinium **2.4** (11 mg, 0.034 mmol) in CD_3COCD_3 (0.8 mL) was transferred into an NMR tube. The metalloporphyrin $\text{RuTTP}(\text{CO})(\text{EtOH})$ (29 mg, 0.034 mmol) was added in small portions using a spatula until the formation of a 1:1 complex was observed by ^1H NMR spectroscopy. The dark solution was concentrated to dryness *in vacuo* giving of the product **2.4RuP** (37 mg, 98%) as a dark red solid. Mp: >250 °C. (* denotes peaks that overlap) ^1H NMR (CD_3COCD_3 , 400 MHz): δ 8.79 (H^a , d, 2H, $J = 6.4$ Hz), 8.68 (s, 8H), 8.12 (d, 4H, $J = 7.2$ Hz), 7.95 (d, 4H, $J = 7.2$ Hz), 7.65-7.63* (H^c , m, 6H), 7.55 (d, 4H, $J = 7.2$ Hz), 6.07 (H^d , d, 2H, $J = 6.4$ Hz), 4.37 (H^e , s, 3H), 2.67 (s, 12H), 1.79 (H^a , d, 2H, $J = 6.4$ Hz). ^{13}C NMR (CD_3COCD_3 , 100 MHz): δ 145.9, 145.3, 143.9, 139.9, 139.6, 137.3, 134.2, 134.1, 132.0, 127.6, 127.3, 125.1, 121.9, 120.3, 48.1, 21.0. UV/Vis (CH_2Cl_2): λ_{max} / nm ($\log \epsilon/\text{M}^{-1}\text{cm}^{-1}$) 248 (4.62), 305 (4.35), 413 (5.45), 533 (4.30), 568 (3.60). FT-IR (KBr-cast): 3124, 3022, 2925, 1956, 1635, 1606, 1528, 1499, 1441, 1412, 1343, 1304, 1217, 1188, 1100, 1071, 1008, 842, 798, 725 cm^{-1} . LRMS (MALDI-TOF) : m/z 171 $[\text{M-RuTTP}(\text{CO}), \text{PF}_6]^+$. Anal. Calcd for $\text{C}_{60}\text{H}_{47}\text{N}_6\text{ORuPF}_6$: C, 64.69; H, 4.25; N, 7.54. Found: C, 64.85; H, 4.34; N, 7.41.

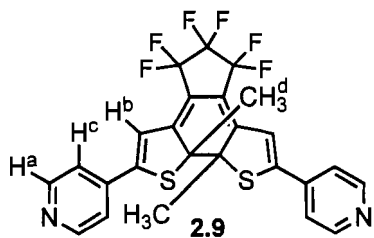
Comparing the coordination ability of the pyridylthiophene 2.3 and the monomethylated bipyridinium 2.4 to the ruthenium porphyrin RuTTP(CO)(EtOH).

A solution (5.3×10^{-3} M) of the monomethylated bipyridinium **2.4** (1.2 mg, 0.004 mmol) in CD₃COCD₃ (0.70 mL) was transferred into an NMR tube. Part of an approximately weighed amount of the metalloporphyrin RuTTP(CO)(EtOH) (4 mg) was added in small portions using a spatula until the complete disappearance of peaks corresponding to the free pyridyl ligand **2.4** was observed by ¹H NMR spectroscopy indicative of the formation of a 1:1 complex. Part of an approximately weighed amount of the competing pyridylthiophene **2.3** (2 mg) was then added in small portions until one molar equivalent was observed by measuring the relative integrals of the signals corresponding to the free (**2.3** and **2.4**) and bound (**2.3RuP** and **2.4RuP**) ligands by ¹H NMR spectroscopy. The difference in the coordination behaviour between the two pyridyl ligands was assessed by comparing the relative ratios of the peak integrals for the bound to free ligands, which were measured to be 0.64:0.36 for **2.3RuP:2.3** and 0.31:0.69 in the case of **2.4RuTTP:2.4**. The ¹H NMR spectra for this study are shown in the appendix.

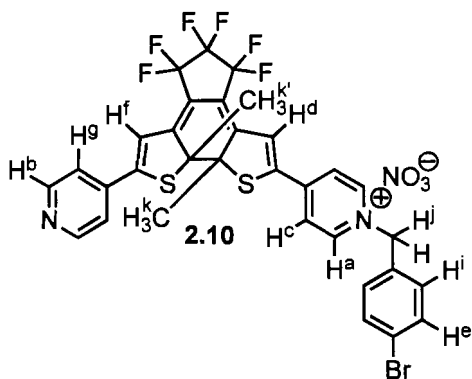


Synthesis of 1,2-bis(2'-methyl-5'-(pyridin-4''-yl)thien-3'-yl)perfluorocyclopentene 2.8.²⁹

A solution of 3-bromo-2-methyl-5-pyridylthiophene **2.3** (199 mg, 0.787 mmol) in anhydrous THF (30 mL) was cooled to $-78\text{ }^{\circ}\text{C}$ using a dry ice/acetone bath and *n*-BuLi (0.32 mL, 2.5 M in hexanes, 0.79 mmol) was slowly added dropwise under an N_2 atmosphere. The resulting deep red solution was then treated with perfluorocyclopentene (53 μL , 0.40 mmol) through a cooled gas tight syringe whereby the solution turned green. The cooling bath was removed and the solution was allowed to slowly warm up to ambient temperature and quenched with a saturated solution of NH_4Cl (30 mL). The aqueous layer was removed and extracted with CH_2Cl_2 ($3 \times 30\text{ mL}$) and the combined organics were washed with a saturated solution of NaHCO_3 (100 mL), dried over anhydrous Na_2SO_4 , filtered and the solvent was removed on the flash evaporator. The crude brown product was purified by flash chromatography (neutral alumina: activity II-III, hexanes/EtOAc = 2:1). Recrystallization of the resultant green solid from EtOAc afforded the *bis*(pyridine) **2.8** (123 mg, 60%) as a white powder. Mp: $179\text{--}181\text{ }^{\circ}\text{C}$ (lit. $181\text{ }^{\circ}\text{C}$). ^1H NMR (CD_2Cl_2 , 400 MHz): δ 8.58 (H^{a} , d, 4H, $J = 6.0\text{ Hz}$), 7.50 (H^{b} , s, 2H); 7.42 (H^{c} , d, 4H, $J = 6.0\text{ Hz}$), 2.01 (H^{d} , s, 6H). ^{13}C NMR (CD_2Cl_2 , 100 MHz): δ 150.4, 143.4, 140.0, 139.3, 126.1, 124.6, 119.4, 14.5 (8 of 11 carbons found). FT-IR (KBr-cast): 3070, 3032, 2964, 2856, 1630, 1596, 1552, 1504, 1441, 1413, 1339, 1274, 1222, 1193, 1116, 1056, 989, 964, 896, 815, 740, 691 cm^{-1} . LRMS (CI isobutane): m/z 523 $[\text{M}+\text{H}]^+$.

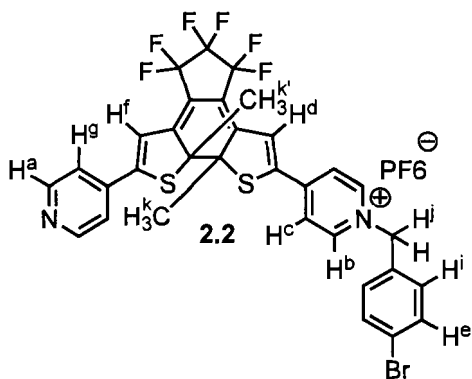


Photochemical synthesis of the ring-closed isomer (2.9) of the *bis*(pyridine). A solution of the ring-open isomer (2.8) of the *bis*(pyridine) (61 mg, 0.12 mmol) was dissolved in CH₃CN (20 mL) and the solution was irradiated with 313 nm light. Aliquots (2 mL) of the reaction mixture were removed via a pipette at regular intervals, concentrated to dryness *in vacuo*, and redissolved in CD₃CN and monitored by ¹H NMR spectroscopy until a solution containing 98% of the ring-closed form 2.9 was obtained at the PSS. No attempts to isolate the pure ring-closed were made and the remaining 2% was assigned to the ring-open form 2.8. ¹H NMR (CD₃CN, 400 MHz): δ 8.67 (H^a, d, 4.H, *J* = 6.0 Hz), 7.52 (H^c, d, 4.H, *J* = 6.0 Hz), 7.02 (H^b, s, 2H), 2.21 (H^d, s, 6H).

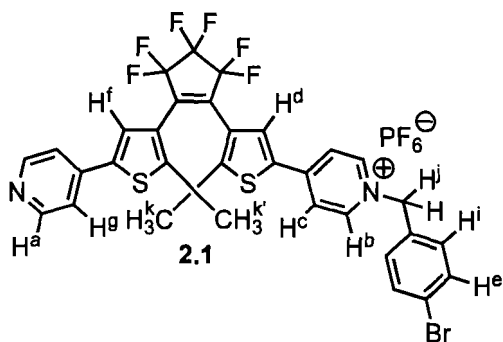


Synthesis of the nitrate salt of the ring-closed isomer (2.10) of 1-[5'-(pyrid-4''-yl)-2'-methylthien-3'-yl]-2-{2'''-methyl-5'''-[N-(4''''-bromobenzyl-pyrid)-4''''-yl]thien-3'''-yl}perfluorocyclopentene. The ring-open isomer (2.8) of the *bis*(pyridine) (61 mg, 0.12

mmol) was dissolved in anhydrous CH₃CN (20 mL) and the solution was irradiated with 313 nm light. Aliquots (2 mL) of the reaction mixture were removed via a pipette at regular intervals, concentrated to dryness *in vacuo*, and redissolved in CD₃CN and monitored by ¹H NMR spectroscopy until a solution containing 98% of the ring-closed form **2.9** was obtained at the PSS. The resultant dark blue solution was treated with 4-bromobenzyl bromide (29 mg, 0.12 mmol) and left to stir at room temperature for 7 days under an N₂ atmosphere. The solvent was evaporated to dryness *in vacuo* and purification by flash chromatography (silica, CH₃CN to remove any unreacted **2.9** followed by a mixture of CH₃CN: H₂O: a saturated solution of KNO₃ = 100: 1: 0.01) gave the nitrate salt of the ring-closed monobenzylated DTE **2.10** (39 mg, 45%) as a dark blue solid. Mp: 138–140 °C. ¹H NMR (CD₃CN, 500 MHz): δ 8.72 (H^a, d, 2H, *J* = 6.5 Hz), 8.70 (H^b, d, 2H, *J* = 6.0 Hz), 8.05 (H^c, d, 2H, *J* = 6.5 Hz), 7.65 (H^e, d, 2H, *J* = 8.5 Hz), 7.54 (H^g, d, 2H, *J* = 6.0 Hz), 7.39 (Hⁱ, d, 2H, *J* = 8.5 Hz), 7.30 (H^d, s, 1H), 7.06 (H^f, s, 1H), 5.74 (H^j, s, 2H), 2.24 (H^k, s, 3H), 2.23 (H^{k'}, s, 3H). ¹³C NMR (CD₃OD, 125 MHz): δ 160.3, 154.5, 151.7, 151.3, 149.5, 149.3, 146.1, 141.5, 133.9, 133.7, 132.2, 126.3, 125.3, 124.5, 122.4, 118.8, 70.0, 67.8, 64.5, 25.8, 25.5 (21 of 26 carbons found). UV/Vis (CH₃CN): λ_{max}/ nm (log ε/M⁻¹cm⁻¹) 649 (4.12). FT-IR (KBr-cast): 3124, 2930, 2866, 1635, 1596, 1561, 1504, 1474, 1384, 1341, 1276, 1217, 1197, 1129, 1091, 1054, 979, 933, 844, 818, 748 cm⁻¹. LRMS (MALDI-TOF): *m/z* 691, 693 [M-NO₃]⁺. Anal. Calcd for C₃₂H₂₂S₂F₆N₃BrO₃: C, 50.94; H, 2.94; N, 5.57. Found: C, 50.62; H, 3.15; N, 5.30.

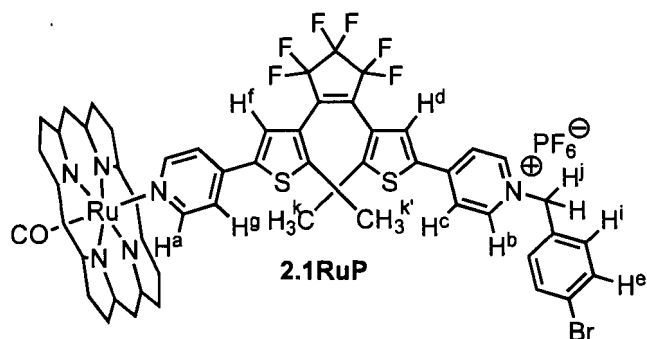


Synthesis of the hexafluorophosphate salt of the ring-closed isomer (2.2) of 1-[5'-(pyrid-4''-yl)-2'-methylthien-3'-yl]-2-{2'''-methyl-5'''-[N-(4''''-bromobenzyl)-pyrid-4''''-yl]thien-3'''-yl}perfluorocyclopentene. The ring-closed isomer (2.10) of the monobenzylated DTE nitrate (39 mg, 5.2 μmol) was dissolved in the minimum amount of EtOH (~2 mL) followed by the addition of a saturated solution of NH_4PF_6 whereupon a dark bluish precipitate was observed. More of the saturated solution of NH_4PF_6 was added until no further precipitate was generated. The solid was collected by vacuum filtration and washed with copious amounts of cold water yielding the hexafluorophosphate salt of the ring-closed monobenzylated DTE **2.2** (42 mg, 97%) as a dark blue solid. ^1H NMR (CD_2Cl_2 , 500 MHz): δ 8.71 (H^a , d, 2H, $J = 6.0$ Hz), 8.62 (H^b , d, 2H, $J = 6.5$ Hz), 7.97 (H^c , d, 2H, $J = 6.5$ Hz), 7.66 (H^e , d, 2H, $J = 8.5$ Hz), 7.43 (H^g , d, 2H, $J = 6.0$ Hz), 7.33 (H^i , d, 2H, $J = 8.5$ Hz), 7.13 (H^d , s, 1H), 6.89 (H^f , s, 1H), 5.69 (H^j , s, 2H), 2.26 (H^k , s, 3H), 2.25 ($\text{H}^{k'}$, s, 3H). UV/Vis (CH_2Cl_2): λ_{max} / nm ($\log \epsilon/M^{-1}\text{cm}^{-1}$) 679 (4.17).



Photochemical synthesis of the hexafluorophosphate salt of the ring-open isomer (2.1) of 1-[5'-(pyrid-4''-yl)-2'-methylthien-3'-yl]-2-{2'''-methyl-5'''-[N-(4''''-bromobenzyl)-pyrid-4''''-yl]thien-3'''-yl}perfluorocyclopentene. The ring-closed isomer (2.2) of the monobenzylated DTE hexafluorophosphate (42 mg, 0.050 mmol) was dissolved in anhydrous CH_2Cl_2 (15 mL) and the solution was irradiated with light of wavelengths greater than 490 nm until the dark greenish blue solution turned colourless. Aliquots (2 mL) of the reaction mixture were removed via a pipette, concentrated to dryness *in vacuo*, and redissolved in CD_2Cl_2 and monitored by ^1H NMR spectroscopy until complete disappearance of the peaks corresponding to the ring-closed isomer 2.2 (methine peaks of the thiophene rings at 7.89 and 7.13 ppm) was observed at the PSS. The solvent was evaporated to dryness yielding the ring-open monobenzylated DTE 2.1 (40 mg, 98%) as an off-white solid. Mp: 121–123 °C. ^1H NMR (CD_2Cl_2 , 500 MHz): δ 8.58 (H^{a} , d, 2H, $J = 6.0$ Hz), 8.53 (H^{b} , d, 2H, $J = 7.0$ Hz), 7.98 (H^{c} , d, 2H, $J = 7.0$ Hz), 7.87 (H^{d} , s, 1H), 7.65 (H^{e} , d, 2H, $J = 8.0$ Hz), 7.48 (H^{f} , s, 1H), 7.42 (H^{g} , d, 2H, $J = 7.0$ Hz), 7.32 (H^{h} , d, 2H, $J = 8.0$ Hz), 5.62 (H^{i} , s, 2H), 2.10 (H^{k} , s, 3H), 2.01 ($\text{H}^{\text{k}'}$, s, 3H). ^{13}C NMR (CD_2Cl_2 , 150 MHz): δ 152.0, 150.1, 149.6, 145.4, 144.4, 141.5, 140.0, 135.1, 133.7, 132.0, 131.5, 131.4, 131.3, 128.6, 126.2, 125.8, 125.4, 123.4, 120.4, 64.2, 15.8, 15.3 (22 of 26 carbons found). UV/Vis (CH_2Cl_2): λ_{max} / nm ($\log \epsilon/\text{M}^{-1}\text{cm}^{-1}$) 370 (4.41).

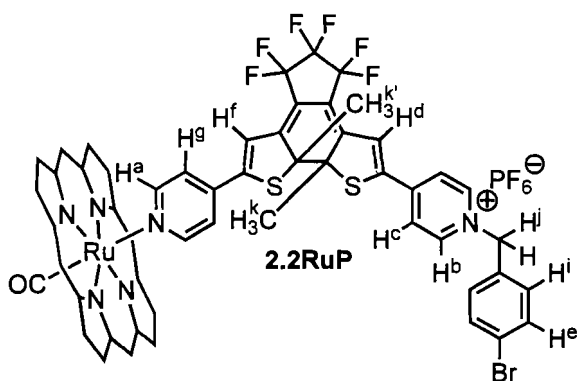
FT-IR (KBr-cast): 3071, 3034, 2965, 2866, 1637, 1597, 1551, 1512, 1491, 1473, 1442, 1412, 1339, 1275, 1223, 1196, 1143, 1117, 1056, 1014, 990, 964, 844, 793, 740 cm^{-1} .
 LRMS (MALDI-TOF): m/z 691, 693 $[\text{M-PF}_6]^+$. Anal. Calcd for $\text{C}_{32}\text{H}_{22}\text{S}_2\text{F}_{12}\text{N}_2\text{BrP}$: C, 45.89; H, 2.65; N, 3.34. Found: C, 46.24; H, 2.88; N, 3.05.



Synthesis of the ring-open monobenzylated DTE-porphyrin coordination complex

2.1RuP. A stock solution (9.0 mM) of the hexafluorophosphate salt of the monobenzylated DTE **2.1** (19 mg, 22 μmol) in CD_2Cl_2 (2.5 mL) was prepared and a known volume of that solution (0.6 mL) was transferred into an NMR tube. The metalloporphyrin $\text{RuTTP}(\text{CO})(\text{EtOH})$ (~ 5 mg) was added in small portions using a spatula until the formation of a 1:1 complex was observed by ^1H NMR spectroscopy. The solvent was removed under reduced pressure yielding complex **2.1RuP** (9 mg, 99%) as a dark burgundy solid. Mp: > 245 $^\circ\text{C}$. ^1H NMR (CD_2Cl_2 , 500 MHz): δ 8.65 (s, 8H), 8.44 (H^b , d, 2H, $J = 7.0$ Hz), 8.10 (d, 4H, $J = 7.5$ Hz), 7.94 (d, 4H, $J = 7.5$ Hz), 7.83 (H^c , d, 2H, $J = 7.0$ Hz), 7.64 (H^d , s, 1H), 7.61 (H^e , d, 2H, $J = 8.0$ Hz), 7.56 (d, 4H, $J = 7.5$ Hz), 7.51 (d, 4H, $J = 7.5$ Hz), 7.26 (H^i , d, 2H, $J = 8.0$ Hz), 6.56 (H^f , s, 1H), 5.56 (H^j , s, 2H), 5.36 (H^g , d, 2H, $J = 6.5$ Hz), 2.68 (s, 12H), 1.63 (H^k , s, 3H), 1.62 ($\text{H}^{k'}$, s, 3H), 1.47 (H^a , d, 2H, $J = 6.5$ Hz). ^{13}C NMR (CD_2Cl_2 , 150 MHz): δ 151.7, 149.4, 145.3, 144.7, 144.6,

144.3, 144.1, 138.8, 138.01*, 137.97*, 135.0, 133.7, 132.2, 131.5, 131.43*, 131.38*, 131.3, 131.2, 128.2, 127.9, 127.6, 125.7, 125.4, 125.1, 123.5, 123.2, 123.0, 117.9, 64.2, 21.6, 15.4, 15.0 (32 of 37 carbons found). UV/Vis (CH₂Cl₂): λ_{max} / nm (log $\epsilon/M^{-1} \text{cm}^{-1}$) 305 (3.40), 413 (4.10), 534 (2.99), 568 (2.47). FT-IR (KBr-cast) 2956, 2924, 2853, 1949, 1635, 1561, 1509, 1461, 1445, 1382, 1348, 1295, 1217, 1183, 1105, 1091, 1009, 847, 711 cm^{-1} . LRMS (MALDI-TOF): m/z 691, 693 [M-RuTTP(CO)-PF₆]⁺. Anal. Calcd for C₈₁H₅₈N₆ORuS₂BrF₁₂P: C, 59.49; H, 3.57; N, 5.14. Found: C, 59.20; H, 3.39; N, 5.26.



Synthesis of the ring-closed monobenzylated DTE-porphyrin coordination complex

2.2RuP. Another portion (0.6 mL) of the stock solution (9.0 mM) of the hexafluorophosphate salt of the monobenzylated DTE **2.1** (19 mg, 22 μmol) in CD₂Cl₂ (2.5 mL), was transferred into a quartz NMR tube. The solution was irradiated with 365 nm light until complete ring-cyclization to the ring-closed DTE **2.2** was observed at the PSS as monitored by ¹H NMR spectroscopy. The metalloporphyrin RuTTP(CO)(EtOH) (~5 mg) was added in small portions using a spatula until the formation of a 1:1 complex was observed by ¹H NMR spectroscopy. The solvent was removed under reduced pressure yielding of complex **2.2RuP** (9 mg, 99%) as a dark greenish brown solid. Mp: >

245 °C. ^1H NMR (CD_2Cl_2 , 500 MHz): δ 8.65 (s, 8H), 8.53 (H^b , d, 2H, $J = 7.0$ Hz), 8.10 (d, 4H, $J = 7.0$ Hz), 7.93 (d, 4H, $J = 7.0$ Hz), 7.81 (H^c , d, 2H, $J = 7.0$ Hz), 7.61 (H^e , d, 2H, $J = 8.5$ Hz), 7.56 (d, 4H, $J = 7.0$ Hz), 7.51 (d, 4H, $J = 7.0$ Hz), 7.26 (H^i , d, 2H, $J = 8.5$ Hz), 6.92 (H^d , s, 1H), 5.89 (H^f , s, 1H), 5.62 (H^j , s, 2H), 5.35 (H^g , d, 2H, $J = 6.5$ Hz), 2.68 (s, 12H), 1.82 (H^k , s, 3H), 1.77 ($\text{H}^{k'}$, s, 3H), 1.55 (H^a , d, 2H, $J = 6.5$ Hz). ^{13}C NMR (CD_2Cl_2 , 150 MHz): δ 157.8, 153.1, 149.2, 149.1, 147.1, 145.1, 144.3, 143.5, 139.4, 137.9, 137.8, 135.4, 133.7, 132.3, 131.5, 130.9, 127.9, 127.6, 125.6, 125.2, 123.8, 119.0, 117.6, 67.3, 66.9, 64.8, 25.4, 25.2, 21.7 (27 of 37 carbons found). UV/Vis (CH_2Cl_2): λ_{max} /nm ($\log \epsilon / \text{M}^{-1} \text{cm}^{-1}$) 295 (3.38), 413 (4.13), 533 (3.05), 568 (2.73), 687 (2.92). FT-IR (KBr-cast) 3025, 2925, 2861, 1954, 1634, 1533, 1474, 1455, 1348, 1320, 1295, 1217, 1183, 1133, 1066, 1090, 1073, 1054, 1009, 845, 797, 719 cm^{-1} . LRMS (MALDI-TOF): m/z 691, 693 $[\text{M-RuTTP}(\text{CO})\text{-PF}_6]^+$. Anal. Calcd for $\text{C}_{81}\text{H}_{58}\text{N}_6\text{ORuS}_2\text{BrF}_{12}\text{P}$: C, 59.49; H, 3.57; N, 5.14. Found: C, 59.09; H, 3.27; N, 5.47.

Comparing the coordination ability of the ring-open (2.1) and the ring-closed (2.2) isomers of the monobenzylated DTE to the ruthenium porphyrin RuTTP(CO)(EtOH). A stock solution (1.1×10^{-3} M) of the ring-open monobenzylated DTE **2.1** (5 mg, 0.006 mmol) in CD_2Cl_2 (5.0 mL) was prepared and a known volume (0.70 mL) of that solution was transferred into a quartz NMR tube *via* a graduated pipette. This solution was irradiated with 365-nm light until a 1:1 mixture of the ring-open isomer **2.1**:the ring-closed isomer **2.2** was generated. The 1:1 ratio was assessed by measuring the relative integrals of the corresponding pairs of signals for the two isomers. Part of an approximately weighed amount (2 mg) of the metalloporphyrin

Ru(TTP)(CO)(EtOH) was added in small increments to the NMR sample using a spatula and the complex formation was monitored by ^1H NMR spectroscopy. This slow addition of the ruthenium porphyrin was continued until 0.93 molar equivalent of the latter was present in the solution mixture as monitored by measuring the relative integrals of the peaks corresponding to the total free ligands (ring-open form **2.1** and ring-closed form **2.2**) and the total bound ligands (**2.1RuP** and **2.2RuP**). The difference in the coordination behaviour between the two DTE isomers was assessed by comparing the relative ratios of the peak integrals for the bound to free ligands, which were measured to be 52:48 for **2.1RuP:2.1** and 42:58 in the case of **2.2RuP:2.2**. The ^1H NMR spectra for this study are shown in the appendix.

Comparing the coordination ability of the ring-open isomer 2.1 and the ring-closed counterpart 2.2 of the monobenzylated DTE to the ruthenium porphyrin using the pyridylthiophene 2.3 as a competing ligand. In a next step, a portion of an approximately weighed amount of the pyridylthiophene **2.3** (2 mg) was added in small increments to the above NMR sample until measurements of the relative integrals of free (**2.1**, **2.2** and **2.3**) and bound (**2.1RuP**, **2.2RuP** and **2.3RuP**) ligands indicated that 0.79 molar equivalent of the competing ligand was present in the mixture. The latter was then irradiated using light of wavelength greater than 490 nm for 20 min leading to the complete disappearance of the peaks corresponding to the ring-open form of the monobenzylated DTE **2.2** and its corresponding DTE–porphyrin complex **2.2RuP**. The relative ratio of the peak integrals corresponding to the pyridylthiophene–porphyrin adduct **2.3RuP** and the free pyridylthiophene **2.3** was measured to be 0.33:0.67 in this

fully ring-open mixture. The next step involved the complete ring-cyclization of the monobenzylated DTE **2.1** and its respective DTE–porphyrin adduct **2.1RuP** by irradiating the solution mixture with 365-nm light for 10 min leading to a different distribution of bound **2.3RuP** to free **2.3**, which was measured to be 0.39:0.61. The ^1H NMR spectra for this study are shown in the appendix as well.

General procedure for the preparation of the KBr pellets for the IR study. The KBr reagent was added to a solution of the appropriate coordination complex (generated *in situ*) in CD_2Cl_2 (0.5 mL) maintaining the approximate ratio of 100:1 by weight of KBr reagent : porphyrin complex. The solvent was removed on the flash evaporator and the mixture was subsequently dried under high vacuum (1 mmHg) for 2 h. The latter was ground using a mortar and pestle until a fine powder was obtained. A weighed amount of that mixture (100 mg) was then cast in a pellet for the IR measurements.

Preparation of the KBr pellet for the ruthenium porphyrin RuTTP(CO)(EtOH). The KBr reagent (200 mg) was added to a solution of the metalloporphyrin RuTTP(CO)(EtOH) (2 mg) in CD_2Cl_2 (0.5 mL) and cast in a pellet as described in the general procedure. The IR spectrum showed a CO stretching frequency of 1946 cm^{-1} .

Preparation of the KBr pellet for the pyridylthiophene–porphyrin complex 2.3RuP. Small portions of the ruthenium porphyrin RuTTP(CO)(EtOH) (3.7 mg) were added to a solution of the pyridylthiophene **2.3** (1.1 mg) in CD_2Cl_2 (0.5 mL) until the formation of a 1:1 complex as monitored by ^1H NMR spectroscopy. The KBr reagent (480 mg) was

added to the resulting complex **2.3RuP** and the mixture was cast in a pellet as described in the general procedure. The IR spectrum showed a CO stretching frequency of 1951 cm^{-1} .

Preparation of the KBr pellet for the monomethylated bipyridinium–porphyrin complex 2.4RuP. Small portions of the ruthenium porphyrin RuTTP(CO)(EtOH) (2.9 mg) were added to a solution of the monomethylated bipyridinium **2.4** (1.1 mg) in CD_2Cl_2 (0.5 mL) until the formation of a 1:1 complex as monitored by ^1H NMR spectroscopy. The KBr reagent (400 mg) was added to the resulting complex **2.4RuP** and the mixture was cast in a pellet as described in the general procedure. The IR spectrum showed a CO stretching frequency of 1956 cm^{-1} .

Preparation of the KBr pellet for the ring-open DTE–porphyrin complex 2.1RuP. A stock solution ($3.6 \times 10^{-3}\text{ M}$) of the ring-open isomer **2.1** (3.6 mg, $4.3\text{ }\mu\text{mol}$) in CD_2Cl_2 (1.2 mL) was prepared. A known volume of that solution (0.50 mL) was transferred into an NMR tube and small portions of the ruthenium porphyrin RuTTP(CO)(EtOH) (1.5 mg) were added until the formation of a 1:1 complex as monitored by ^1H NMR spectroscopy. The KBr reagent (300 mg) was added to the resulting complex **2.1RuP** and the mixture was cast in a pellet as described in the general procedure. The IR spectrum showed a CO stretching frequency of 1949 cm^{-1} .

Preparation of the KBr pellet for the ring-closed DTE–porphyrin complex 2.2RuP.

The same volume (0.50 mL) of the stock solution (3.6×10^{-3} M) of the ring-open DTE **2.1** prepared above was transferred into a quartz NMR tube and irradiated with 365-nm light until complete ring-cyclization to **2.2** was achieved as monitored by ^1H NMR spectroscopy. Small portions of the ruthenium porphyrin RuTTP(CO)(EtOH) (1.5 mg) were added until the formation of a 1:1 complex was observed. The KBr reagent (300 mg) was added to the resulting complex **2.2RuP** and the mixture was cast in a pellet as described in the general procedure. The IR spectrum showed a CO stretching frequency of 1954 cm^{-1} .

Photochemical ring-closing reaction of the DTE–porphyrin complex 2.1RuP in the solid KBr matrix. The pellet prepared from the ring-open DTE–porphyrin complex **2.1RuP** was irradiated at 365 nm whereby a gradual shift in the CO stretching frequency to lower energy was observed but stopped at a stretching frequency of 1952 cm^{-1} upon irradiation for more than 2 h.

Photochemical ring-opening reaction of the DTE–porphyrin complex 2.2RuP in the solid KBr matrix. The pellet prepared from the ring-closed DTE–porphyrin complex **2.2RuP** was exposed to light of wavelengths greater than 490 nm whereby a gradual shift in the CO stretching frequency to lower energy was observed and irradiation of this pellet for 1 h generated the ring-open complex **2.1RuP** with a stretching frequency of 1949 cm^{-1} . Re-irradiation of this pellet using 365 nm light regenerated the ring-closed complex **2.2RuP** with the stretching frequency going back to 1954 cm^{-1} after 90 min.

3 Modulation of Chemical Reactivity using Photoresponsive DTEs

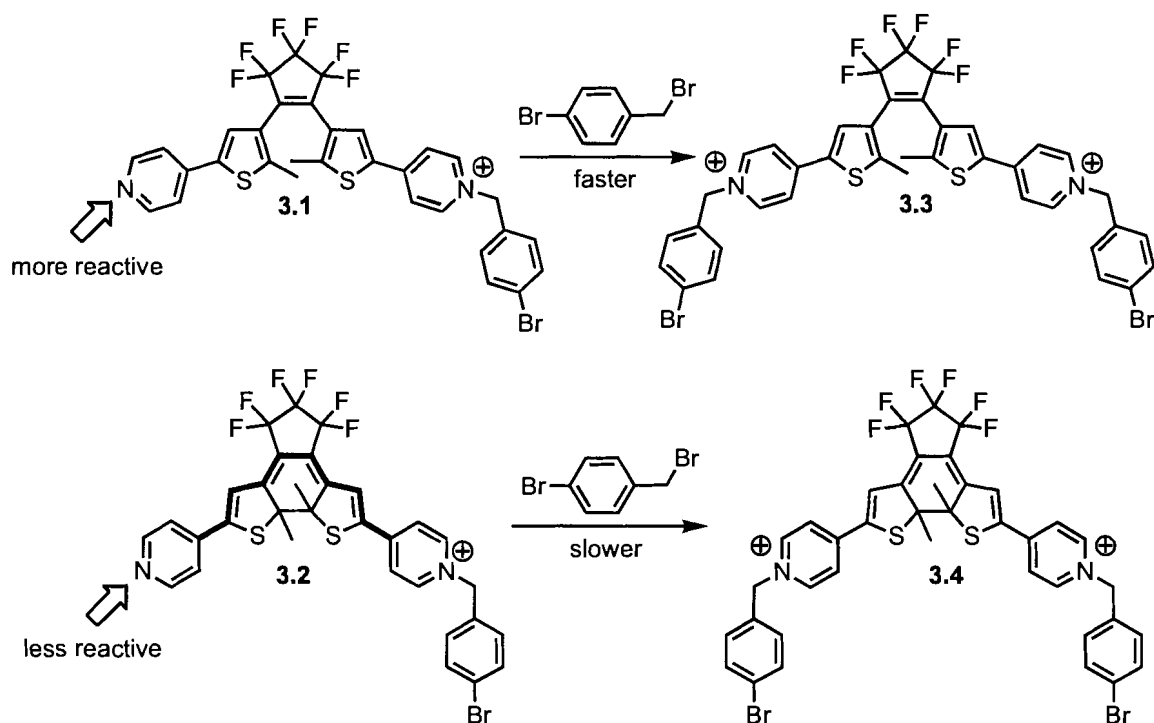
3.1 Introduction to Light-Induced Switching of Reaction Rates

Controlling the outcome of a chemical reaction is a well-established concept amongst chemists. The practical reasons for seeking such control range from suppressing unwanted side products to synthesizing new structures and new materials that can mimic biological systems. The ring-opening and ring-closing reaction of DTEs influences the potential polarization of electrons through the DTE backbone and provides a handle to photomodulate the nucleophilic strength of an appropriately functionalized DTE derivative. This has potential applications in the design of light-activated reagents and catalysts. The concept of photoregulating the Lewis basicity of a pyridine-functionalized DTE by comparing the stability of the ring-open and the ring-closed forms of a ruthenium porphyrin-DTE hybrid was presented in *Chapter 2* of this thesis. In this chapter, a kinetic approach is used to probe the effect of the electron-withdrawing pyridinium on the nucleophilicity of the pendant pyridine group in the ring-open form **3.1** and the ring-closed form **3.2** (previously synthesized and isolated as the nitrate salt **2.10** in *Chapter 2*) of the monobenzylated DTE.

3.1.1 Choice of Test Reaction

It is well documented that empirical measures of nucleophilicity can usually be obtained by comparing the relative rates of reaction of a standard reactant with various nucleophiles.^{105,106} It can thus be expected that any variations in the nucleophilic character of the pendant pyridine between the ring-open and the ring-closed isomers of

the monobenzylated DTE will be reflected in the relative rates of the reactions with a reagent such as 4-bromobenzyl bromide in an alkylation reaction.



Scheme 3.1.1. Monocationic DTEs **3.1** and **3.2** expected to show differing reactivity due to the changes in electronic communication between the two sides of the DTE backbone resulting in different rates of benzylation.

The two thiophenes in the ring-open isomer **3.1** are electronically insulated from each other (Scheme 3.1.1) such that the nucleophilic pyridine will not sense the electron-withdrawing behaviour of the pyridinium group. The photocyclization event creates the electronic communication between the pyridine and the electron-deficient pyridinium moiety (shown in bold in Scheme 3.1.1) and lowers its nucleophilic strength. Consequently, the ring-open isomer **3.1** is expected to react faster with 4-bromobenzyl bromide than its ring-closed counterpart **3.2**. The fact that optimal yields of the monobenzylated DTE are achieved when it is synthesized in the ring-closed form **3.2** (labelled **2.10** in *Chapter 2*), as already mentioned in *Section 2.6.5*, provides an indirect

proof that the ring-open isomer **3.1** reacts faster than its ring-closed isomer **3.2**. One approach to demonstrate this concept involves *pseudo*-first-order kinetics using the technique of *flooding*.¹⁰³

3.2 Technique of Flooding

It is known that the substitution reaction between pyridine and benzyl bromide proceeds via an S_N2 pathway.^{107,108} In general, nucleophilic substitution reactions that follow an S_N2 pathway exhibit an overall second-order kinetics.^{109,110} Assuming that the substitution reaction of the monobenzylated DTE with 4-bromobenzyl bromide proceeds by an S_N2 pathway, it can be expected to exhibit an overall second-order kinetics. Consider a reaction between reactants 'A' and 'B'. The reaction is said to exhibit second-order kinetics if one mole of each of the reactants 'A' and 'B' are consumed during the reaction and the reaction rate depends on the concentration of both reacting species. The rate law for the decrease in the concentration of 'A' with time is shown in Equation 3.2.1 where *k* is the proportionality constant of the equation and is called the rate constant.

$$-\frac{d[A]}{dt} = k[A][B]$$

Equation 3.2.1. Rate law for a system that follows second-order kinetics.

This reaction can be simplified by adding a sufficiently high concentration of one of the reagents such that its concentration remains effectively constant during the course of the reaction making it possible to treat the system as a *pseudo*-first-order reaction. Such an experimental design is termed as the method of *flooding* (also known as the method of *isolation*).¹¹¹ For instance, a very high concentration of reagent 'B' simplifies the rate

equation to a *pseudo*-first-order equation where the decrease in the concentration of 'A' with time depends only on the concentration of 'A' and k' is the *pseudo*-first-order rate constant as shown in Equation 3.2.2.

$$-\frac{d[A]}{dt} = k'[A] \text{ where } k' = k[B]$$

Equation 3.2.2. Simplified rate equation in the presence of a very high excess of reagent 'B'.

Integration of this equation between the limits (time = 0, $[A]_0$) and (time = t , $[A]_t$) shows that the concentration of 'A' decreases exponentially with time where $[A]_t$ corresponds to the concentration of 'A' at time t and $[A]_0$ refers to the initial concentration of 'A' as shown in Equation 3.2.3.

$$[A]_t = [A]_0 e^{-k't}$$

Equation 3.2.3. Equation showing the exponential decrease in the concentration of 'A' with time under *pseudo*-first-order conditions.

Taking the natural log on both sides affords a linear equation of the type $y = mx + c$ (Equation 3.2.4) and graphical treatment of the data by plotting the natural log of the concentration of 'A' at time 't' against time gives a straight line with a slope of $-k'$ where k' is the *pseudo*-first-order rate constant.

$$\ln[A]_t = -k't + \ln[A]_0$$

Equation 3.2.4. Linear equation relating the natural log of the concentration of 'A' with time.

However, one important assumption for Equation 3.2.4 to hold true is that there is no significant back reaction. The term apparent *pseudo*-first order rate constant will be

used throughout this chapter in order to take into account any back reaction where the apparent *pseudo*-first order rate constant refers to the sum of the forward *pseudo*-first order rate constant and the backward *pseudo*-first order rate constant.¹¹¹ Thus, the difference in the apparent rates of alkylation between the two isomers of the monobenzylated DTE can be assessed under *pseudo-first* order conditions using the method of *flooding*.

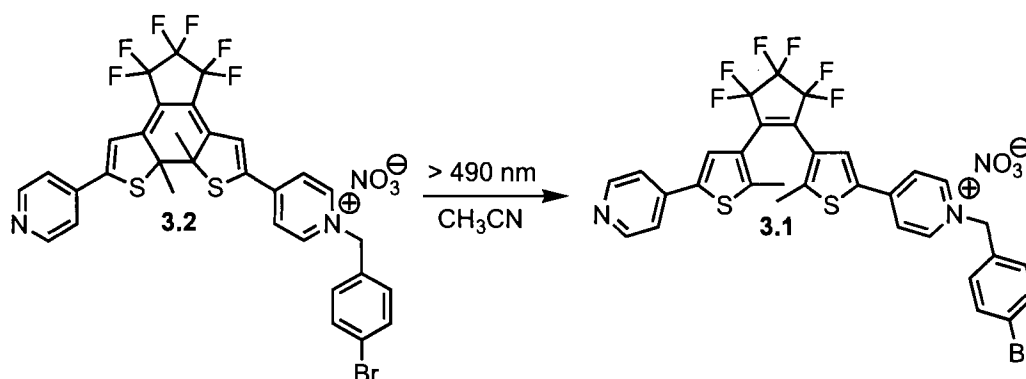
3.3 ¹H NMR Spectroscopy as a Diagnostic Tool

As already mentioned in *Chapter 2*, ¹H NMR spectroscopy is an elegant means to measure the relative amounts of different species present in a reaction. This technique can be very useful to assess the progress of the alkylation reaction of both the ring-open (**3.1**) and the ring-closed (**3.2**) isomers of the monobenzylated DTE. There are two types of “relaxation” processes by which the nuclei return to their initial state following the delivery of a radiofrequency pulse in NMR spectroscopy: (1) longitudinal relaxation denoted by the time T_1 which influences the peak intensity and (2) transverse relaxation designated by the time T_2 which affects the peak width (i.e. peak sharpness).¹¹² One important assumption that makes the use of ¹H NMR spectroscopy possible is that the peak intensities of the protons are proportional to the number of protons involved and allows the relative number of different protons to be determined by measuring the areas under the peaks. However, this assumption only holds true if the time delay between acquisitions is sufficient to allow complete relaxation of all the protons under investigation. In principle, the time delay needs to be at least 5 times the slowest T_1 value.¹¹³ To ensure that the appropriate time delay is used the relaxation times, T_1 , for each species (ring-open and ring-closed isomers of both the monobenzylated and the

dibenzylated compounds) need to be measured independently. The synthesis and the photochromic properties of the ring-open isomers (**3.1** and **3.3**) of the mono and the dibenzylated DTEs, respectively will be discussed in the next sections prior to determining the appropriate time delays used for monitoring the progress of the alkylation reaction.

3.4 Results and Discussion

3.4.1 Photochemical Synthesis of the Monobenzylated DTE **3.1**



Equation 3.4.1. Photochemical synthesis of the nitrate salt of the ring-open isomer **3.1** of the monobenzylated *bis*(pyridinium) by irradiating a solution (2.7×10^{-3} M) of the ring-closed isomer **3.2** in CH₃CN with light of wavelengths greater than 490 nm.

As already discussed in *Section 2.6.5*, the monobenzylated DTE was synthesized and isolated as its ring-closed isomer **3.2** (labelled **2.10** in *Chapter 2*). The ring-open isomer (**3.1**) of the monobenzylated *bis*(pyridinium) was prepared by irradiating a solution (2.7×10^{-3} M) of the ring-closed isomer **3.2** in CH₃CN with light of wavelengths greater than 490 nm and monitoring aliquots of the sample by ¹H NMR spectroscopy until no further change was observed. The progress of the ring-opening reaction was assessed by monitoring the methine peaks of the thiophene rings (7.30 and 7.06 ppm for the ring-closed isomer **3.2** as opposed to 8.00 and 7.62 ppm for the ring-open **3.1**), as

discussed earlier in *Section 2.3.3*, until complete disappearance of the peaks corresponding to the ring-closed isomer **3.2** was observed at the PSS. The ring-open monobenzylated DTE **3.1** was collected after evaporation of the solvent without any purification.

3.4.2 UV-Vis Absorption Spectra, Photochemical Cycling, and ¹H NMR Spectra of the Monobenzylated DTE 3.1

The photochemical interconversion between the ring-open (**3.1**) and the ring-closed (**3.2**) isomers of the monoalkylated DTE was accompanied by differences in the UV-Vis absorption profiles as illustrated in part (a) of Figure 3.4.1.

The UV-Vis absorption study of a CH₃CN solution (2.0×10^{-5} M) of the ring-open form **3.1** showed the appearance of an absorption band in the visible region of the spectrum (649 nm) corresponding to the coloured ring-closed form **3.2** when irradiated with 365 nm light for 5 sec. The solution was irradiated with 365 nm light until no further increase in the absorption band at 649 nm was observed at the PSS. Subsequent exposure of the solution to light of wavelengths greater than 490 nm was accompanied by the complete disappearance of the absorption band in the visible region of the spectrum (649 nm) and the regeneration of the original UV-Vis absorption trace corresponding to the ring-open isomer **3.1** as shown by the dashed trace shown in bold in part (a) of Figure 3.4.1. Furthermore, alternate irradiation with 365 nm light and wavelengths greater than 490 nm showed no apparent signs of photodegradation after 10 cycles as shown in part (b) of Figure 3.4.1.

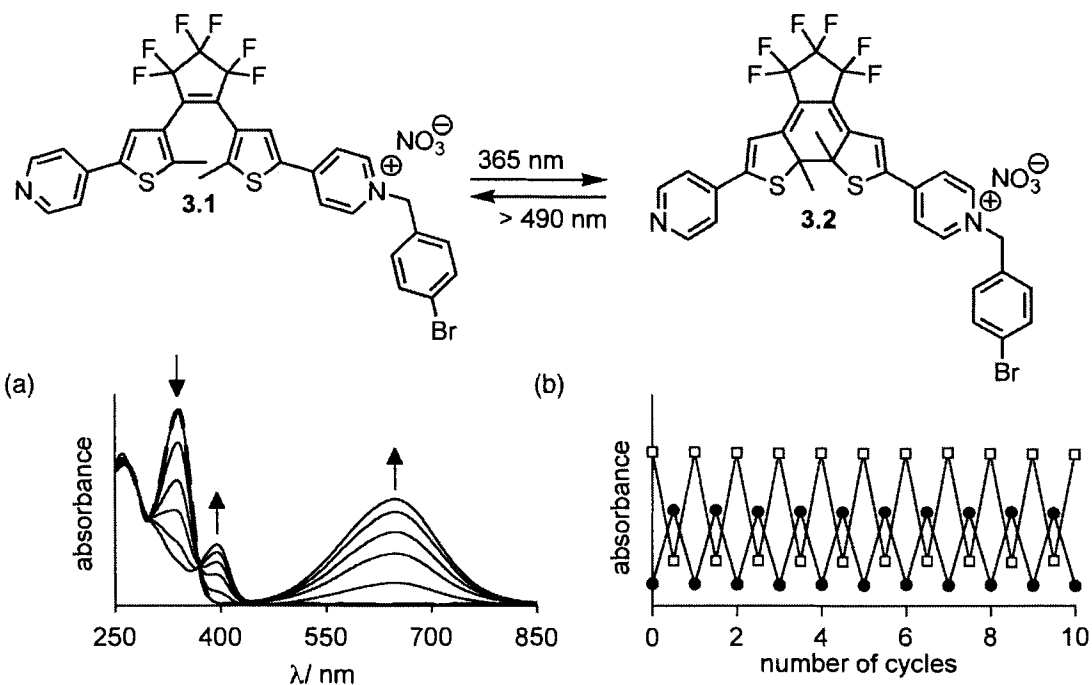


Figure 3.4.1. (a) Changes in the UV-Vis absorption spectra of a CH_3CN solution (2.0×10^{-5} M) of the ring-open form **3.1** of the monobenzylated *bis*(pyridinium) nitrate upon irradiation with 365 nm light until no further increase in the absorption band at 649 nm was observed at the PSS. Total irradiation periods are 0, 5, 10, 15, and 20 sec. The dashed trace (— —) shown in bold corresponds to the spectrum after irradiation of the solution of the ring-closed isomer **3.2** at the PSS with light of wavelengths greater than 490 nm for 5 min, regenerating the original UV-Vis trace corresponding to the ring-open isomer **3.1**. (b) Photochemical cycling of a CH_3CN solution (2.0×10^{-5} M) of the monoalkylated DTE between its ring-open form **3.1** and its ring-closed form **3.2**. The figure shows the changes in the absorptions at 356 nm (open squares) and 649 nm (black circles) during alternate irradiation at 365 nm for 20 s and light of wavelengths greater than 490 nm for 5 min.

The photochemical interconversion between the ring-open (**3.1**) and the ring-closed (**3.2**) isomers of the monoalkylated DTE was also analyzed using ^1H NMR spectroscopy. The signals in the ^1H NMR spectra of the ring-open isomer **3.1** and the ring-closed isomer **3.2** (shown in Figure 3.4.2) were assigned using ^1H - ^1H COSY and selective 1-D NOE experiments.

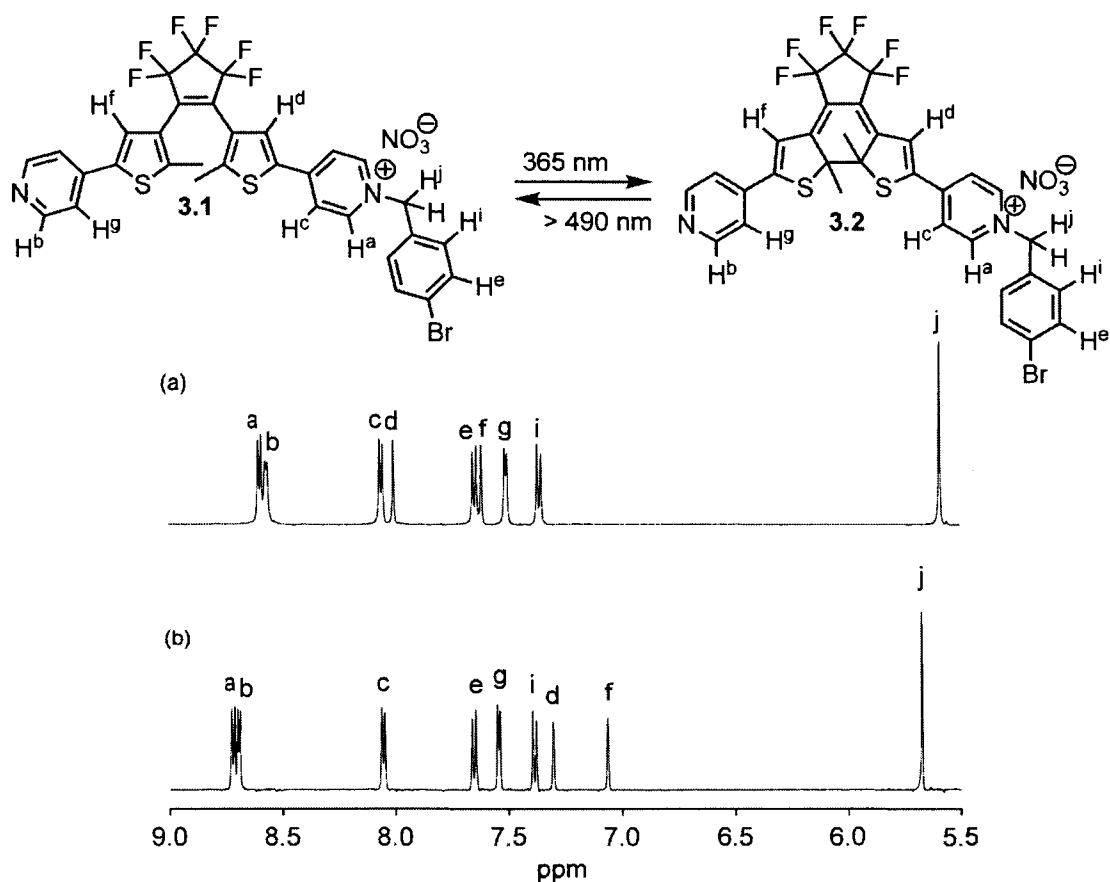


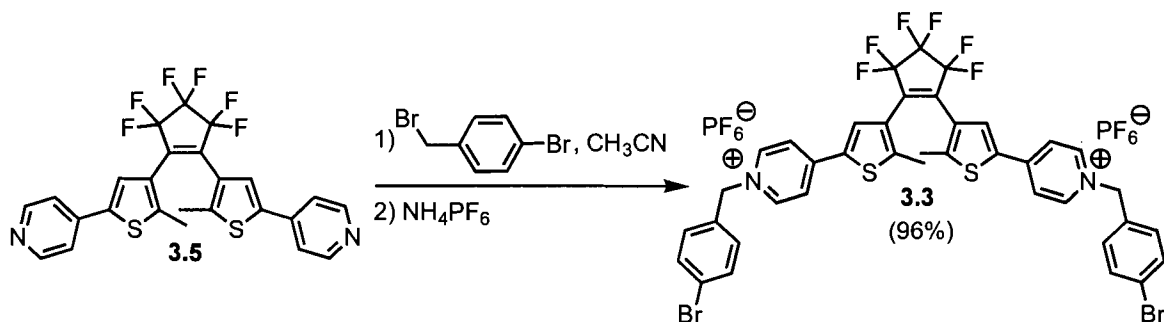
Figure 3.4.2. Selected ^1H NMR spectra (500 MHz) of a CD_3CN solution (2.4×10^{-3} M) of the ring-open isomer **3.1** (a) before irradiation and (b) after irradiation with 365 nm light for 10 min to produce the ring-closed isomer **3.2** at the PSS. The PSS was obtained by irradiating the solution of the ring-open isomer **3.1** with 365 nm light until the peaks corresponding to the ring-open form **3.1** were no longer observed.

The ring-closing event was carried out by irradiating a CD_3CN solution (2.4×10^{-3} M) of the ring-open isomer **3.1** with 365 nm light in a quartz NMR tube and similar observations to that previously described in *Section 2.6.6* were made: (1) the ring-closing reaction was accompanied by the appearance of a new set of signals corresponding to the ring-closed isomer **3.2** while the peaks corresponding to the ring-open form **3.1** gradually decreased in intensity and after 10 min, the peaks corresponding to the ring-open isomer **3.1** were no longer observed; (2) the solution of the generated ring-closed isomer **3.2** showed no apparent signs of degradation even after prolonged irradiation; (3) the

irradiation of the solution containing the ring-closed isomer **3.2** with light of wavelengths greater than 490 nm resulted in the complete regeneration of the peaks corresponding to the ring-open isomer **3.1** (peaks corresponding to the ring-closed isomer **3.2** were no longer observed) without the formation of photostable side-products.

These experiments show that the monoalkylated DTE can be toggled between its ring-open (**3.1**) and its ring-closed (**3.2**) isomers numerous times without observable degradation and that the ring-closing (ring-opening) reaction proceeds with a high PSS.

3.4.3 Synthesis of the Dibenzylated DTE **3.3**



Equation 3.4.2. Synthesis of the dibenzylated *bis*(pyridinium) *bis*(hexafluorophosphate) **3.3**.

The synthesis of the dibenzylated *bis*(pyridinium) **3.3** was achieved in one step by the alkylation reaction of the known *bis*(pyridine) **3.5** (prepared following literature procedure²⁹ in *Section 2.6.5* and labelled **2.8**) with 4-bromobenzyl bromide (3 molar equiv) and was isolated as the *bis*(hexafluorophosphate) salt in good yields (Equation 3.4.2).

3.4.4 UV-Vis Absorption Spectra, Photochemical Cycling, and ¹H NMR Spectra of the Dibenzylated DTE **3.3**

The UV-Vis absorption study of a CH₃CN solution (2.0×10^{-5} M) of the ring-open form **3.3** showed the appearance of an absorption band in the visible region of the

spectrum (670 nm) corresponding to the coloured ring-closed form **3.4** when irradiated with 365 nm light for 5 sec.

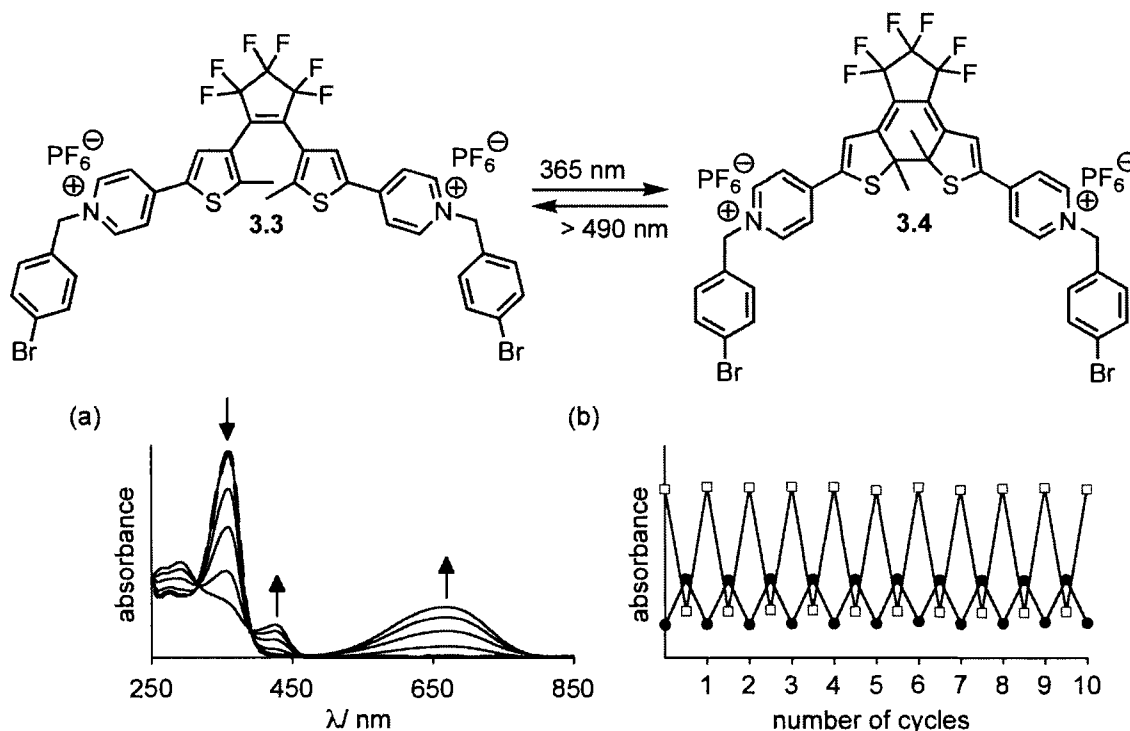


Figure 3.4.3. (a) Changes in the UV-Vis absorption spectra of a CH_3CN solution (2.0×10^{-5} M) of the ring-open form **3.3** of the dibenzylated *bis*(pyridinium) upon irradiation with 365 nm light until no further increase in the absorption band at 670 nm was observed at the PSS. Total irradiation periods are 0, 5, 10, 15, and 20 sec. The dashed trace (---) shown in bold corresponds to the spectrum after irradiation of the solution of the ring-closed isomer **3.4** at the PSS with light of wavelengths greater than 490 nm for 5 min, regenerating the original UV-Vis trace corresponding to the ring-open isomer **3.3**. (b) Photochemical cycling of a CH_3CN solution (2.0×10^{-5} M) of the dialkylated DTE between its ring-open form **3.3** and its ring-closed form **3.4**. The figure shows the changes in the absorptions at 360 nm (open squares) and 670 nm (black circles) during alternate irradiation at 365 nm for 20 s and light of wavelengths greater than 490 nm for 5 min.

The solution was irradiated with 365 nm light until no further increase in the absorption band at 670 nm was observed at the PSS. Subsequent exposure of the solution to visible light (light of wavelengths greater than 490 nm) was accompanied by the complete disappearance of the absorption band in the visible region of the spectrum (670 nm) and the regeneration of the original UV-Vis absorption trace corresponding to the

ring-open isomer **3.3** as shown by the dashed trace shown in bold in part (a) of Figure 3.4.3. Furthermore, alternate irradiation with 365 nm light and wavelengths greater than 490 nm showed no apparent signs of photodegradation after 10 cycles as shown in part (b) of Figure 3.4.3.

The photochemical interconversion between the ring-open (**3.3**) and the ring-closed (**3.4**) isomers of the dialkylated DTE was also analyzed using ^1H NMR spectroscopy.

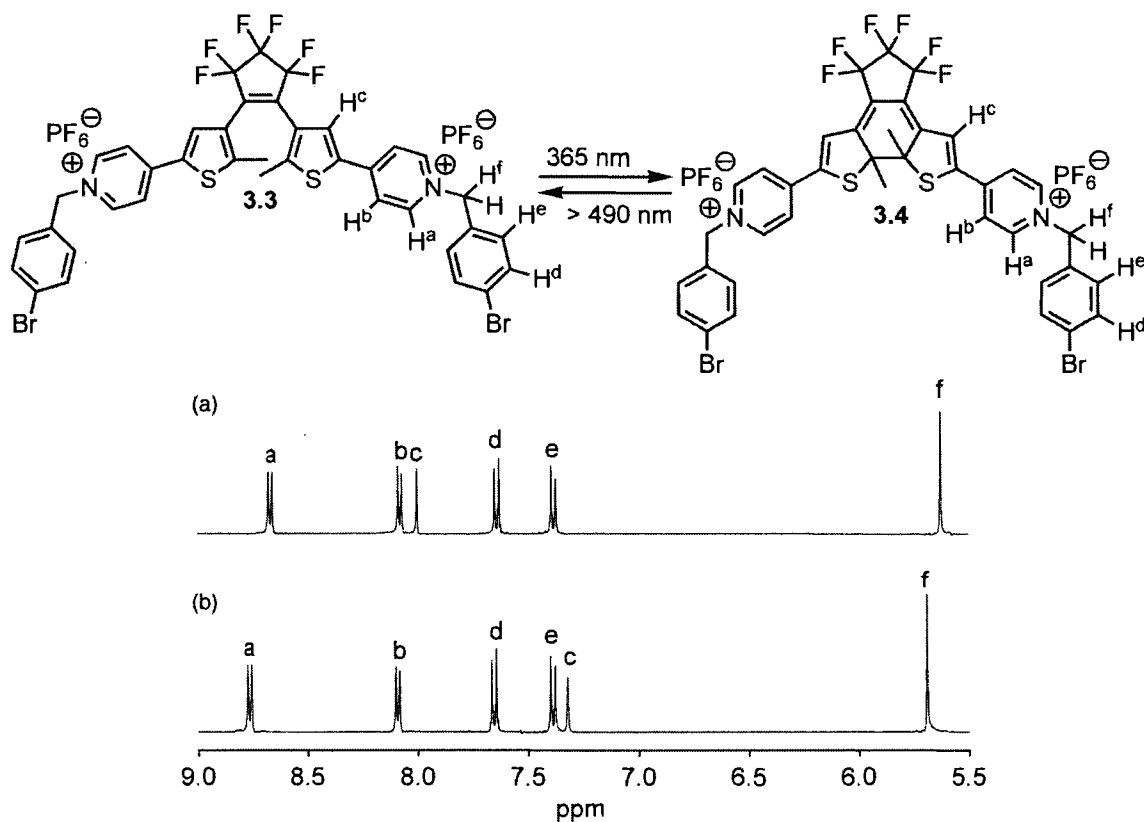


Figure 3.4.4. Selected ^1H NMR spectra (500 MHz) of a CD_3CN solution (2.0×10^{-3} M) of the ring-open isomer **3.3** (a) before irradiation and (b) after irradiation with 365 nm light for 10 min to produce the ring-closed isomer **3.4** at the PSS. The PSS was obtained by irradiating the solution of the ring-open isomer **3.3** with 365 nm light until the peaks corresponding to the ring-open form **3.3** were no longer observed.

The signals in the ^1H NMR spectra of the ring-open isomer **3.3** and the ring-closed isomer **3.4** are shown in Figure 3.4.4. The ring-closing event was carried out by

irradiating a CD₃CN solution (2.0×10^{-3} M) of the ring-open isomer **3.3** with 365 nm light in a quartz NMR tube until the peaks corresponding to the ring-open isomer **3.3** were no longer observed by ¹H NMR spectroscopy. The solution of the generated ring-closed isomer **3.4** showed no apparent signs of degradation, even after prolonged irradiation with 365 nm light. Moreover, irradiation of that solution with light of wavelengths greater than 490 nm resulted in the complete regeneration of the peaks corresponding to the ring-open isomer **3.3** (peaks corresponding to the ring-closed isomer **3.4** were no longer observed) without the formation of photostable side-products. These experiments show that the dialkylated DTE can be toggled between its ring-open (**3.3**) and its ring-closed (**3.4**) isomers numerous times without observable degradation and that the ring-closing (ring-opening) reaction proceeds with a high PSS.

The T_1 values for the protons of the ring-open (**3.1** and **3.3**) and the ring-closed (**3.2** and **3.4**) forms of the monobenzylated and the dibenzylated DTE isomers were measured using the inversion-recovery method¹¹⁴ and from these values, it was established that the slowest T_1 was 4.11 sec for the ring-open isomers (**3.1** and **3.3**) and 4.22 sec for the ring-closed isomers (**3.2** and **3.4**). Since the time delay needs to be at least 5 times the slowest T_1 , as already mentioned in *Section 3.3*, the appropriate time delay between acquisitions for monitoring the rate of reaction of the ring-open isomer **3.1** is 21 sec and that of the ring-closed isomer **3.2** is 22 sec. Consequently, a time delay of 25 sec was used for all the alkylation reactions. The graphs and the fitted parameters for the T_1 measurements are shown in the appendix. With the time delays between acquisitions in hand, the next step was to determine the conditions for the alkylation

reaction. The choice of the appropriate reaction condition will be addressed in the next section.

3.4.5 Choice of Reaction Conditions

Prior to comparing the apparent rates of reaction of the ring-open and the ring-closed DTE isomers, it was important to determine the appropriate concentration^{111,115,116} of 4-bromobenzyl bromide needed to ensure (1) that *pseudo-first-order* conditions prevail and (2) that the progress of the reaction by ¹H NMR spectroscopy is not made difficult by the use of a huge excess of the reagent. In this approach, three CD₃CN samples (0.70 mL) of the ring-open DTE **3.1** of different concentrations were independently treated with a known excess of the 4-bromobenzyl bromide (7.3×10^{-2} M) and the progress of the reaction of each sample at 22°C was assessed by ¹H NMR spectroscopy.

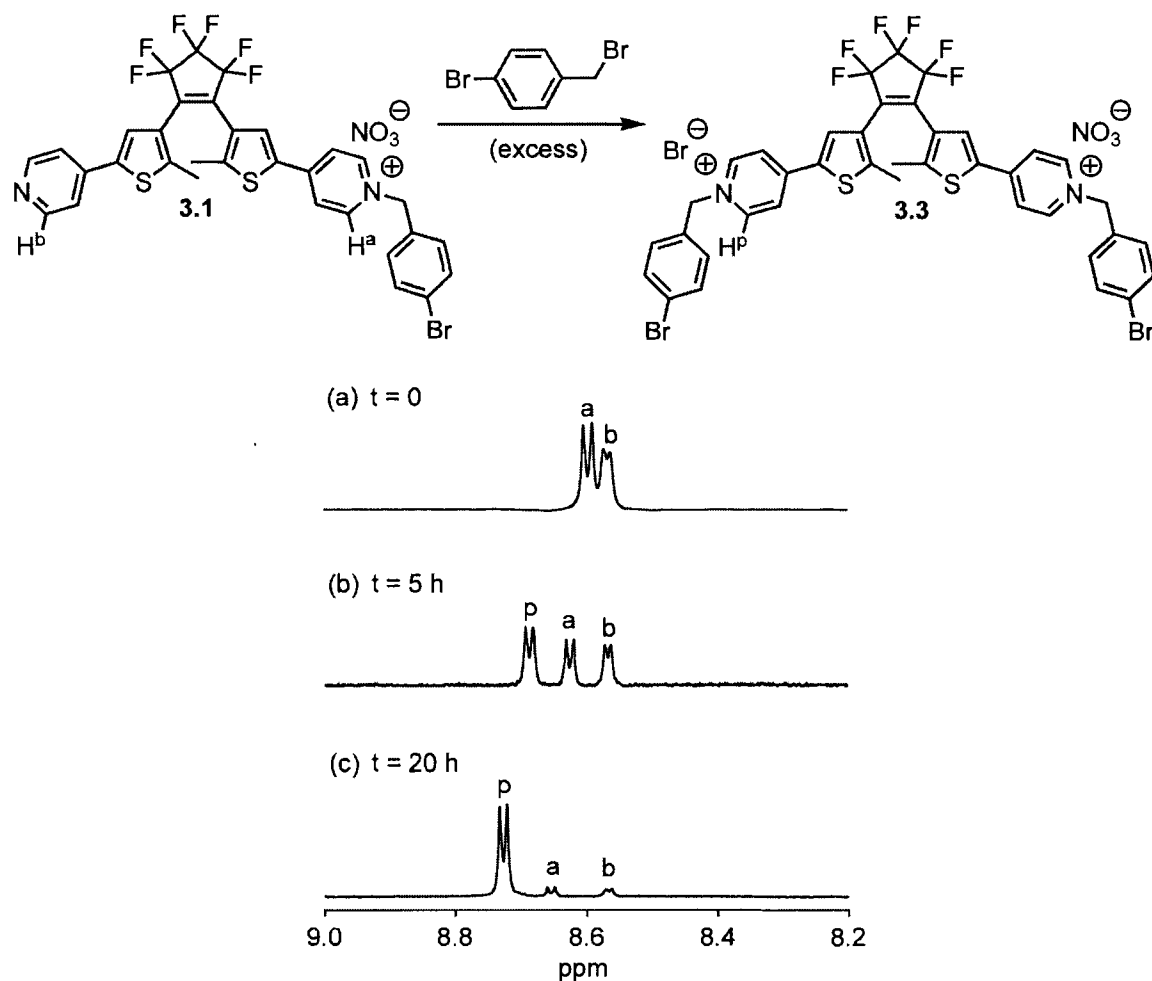


Figure 3.4.5 Representative example showing the use of ¹H NMR spectroscopy to monitor the progress of the reaction of the ring-open isomer **3.1** of the monobenzylated *bis*(pyridinium) with an excess of 4-bromobenzyl bromide to generate the dialkylated DTE **3.3**. Partial ¹H NMR spectra (600 MHz, CD₃CN) showing the aromatic region of a solution (1.9×10^{-3} M) of the ring-open isomer **3.1** in CD₃CN (a) before, (b) 5 h after and (c) 20 h after adding an excess of 4-bromobenzyl bromide (7.3×10^{-2} M). The mole fractions ($\chi_{3,1}$ and $\chi_{3,2}$) of the monoalkylated DTE **3.1** and the dialkylated DTE **3.3** can be obtained using the integral values for peaks 'a', 'b' and 'p'.

As shown in Figure 3.4.5, the aromatic region of the monobenzylated DTE **3.1** prior to the addition of the 4-bromobenzyl bromide contains a two-proton signal at 8.57 ppm (peak 'b') that can be attributed to the α -protons of the unreacted pyridine and a two-proton doublet further downfield at 8.73 ppm (peak 'a') corresponding to the α -protons of the pyridinium group. Reaction of the monocation **3.1** with 4-bromobenzyl

bromide generated the dibenzylated product **3.3** with a four-proton doublet further downfield (peak 'p') that corresponds to the α -protons of the pyridinium groups in **3.3**.

Thus, the mole fractions $\chi_{3.1}$ and $\chi_{3.3}$ (corresponding to the monobenzylated DTE **3.1** and the dibenzylated DTE **3.3** respectively) were obtained by measuring the integrals of the areas under the peaks corresponding to signals 'a', 'b' and 'p' as shown in Equations 3.4.3 and 3.4.4. These studies were carried out in the absence of an internal standard because the ^1H NMR spectra showed no apparent signs of degradation of either the mono or the dialkylated DTEs during the course of the reaction.¹¹⁷⁻¹¹⁹

$$\chi_{3.1} = \frac{(a + b)}{(a + b) + p}$$

Equation 3.4.3. Equation relating the mole fraction of the monobenzylated *bis*(pyridinium) **3.1** to the peak integrals 'a', 'b' and 'p'.

$$\chi_{3.3} = \frac{p}{(a + b) + p}$$

Equation 3.4.4. Equation relating the mole fraction of the dibenzylated *bis*(pyridinium) **3.3** to the peak integrals 'a', 'b' and 'p'.

With the mole fractions in hand, it was possible to monitor the decrease in the concentration of the monobenzylated DTE **3.1** as the reaction proceeded and a plot of the natural log of the concentration of **3.1** against time was obtained for each of the three samples of different concentrations. A linear least squares regression analysis of the data from each sample using the 'Excel Data Analysis Tool Package' revealed a linear relationship for all three samples. The calculated apparent *pseudo*-first-order rate constants, k' , for the three samples were found to be very similar and they are listed in Table 3.4.1. This result indicates that at constant high concentrations of the 4-

bromobenzyl bromide, the apparent *pseudo*-first-order rate constant, k' , shows minimal fluctuations regardless of the initial concentration of the monobenzylated DTE **3.1** and is consistent with *pseudo*-first-order kinetics. The plots of the natural log of the concentration of monobenzylated DTE **3.1** against time, the linear least squares regression analysis of the data and the residual plots for the three samples are shown in the appendix.

Table 3.4.1. Calculated apparent *pseudo*-first-order rate constants, k' , at 22°C for the reaction of three independent solutions (three different concentrations) of the ring-open isomer **3.1** of the monobenzylated *bis*(pyridinium) in CD₃CN with an excess of 4-bromobenzyl bromide.

Experiment	1	2	3
^a [3.1] ₀ (mM)	1.9	2.8	3.8
total volume (mL)	0.70	0.70	0.70
[4-bromobenzyl bromide] (mM)	73	73	73
k' ($\times 10^{-5} \text{ sec}^{-1}$) ^b	2.9 ± 0.1	2.9 ± 0.1	2.8 ± 0.1

^a [**3.1**]₀ refers to the initial concentration of the solution of the ring-open isomer **3.1** before the addition of the alkylating reagent. ^b The uncertainty in the calculated value of the apparent *pseudo*-first-order rate constant is the standard deviation from the regression analysis.

3.4.6 Reactivity of the Ring-Open Form of the Monocationic DTE 3.1

A stock solution (2.4×10^{-3} M) of the monobenzylated DTE 3.1 in CD_3CN was prepared and a known volume (0.70 mL) was transferred into an NMR tube. An excess of 4-bromobenzyl bromide (7.3×10^{-2} M, 30 molar equiv) was added and the progress of the reaction at 22°C was monitored by ^1H NMR spectroscopy over a 24-hour period. By measuring the integrals of the areas under the peaks corresponding to the signals 'a', 'b' and 'p' it was possible to determine the mole fractions of the starting DTE compound 3.1 and the dibenzylated product 3.3 following the procedure described in *Section 3.4.5*.

Graphical treatment of the data for the alkylation reaction by plotting the natural log of the concentration of monobenzylated DTE 3.1 against time followed by a linear least squares regression analysis of the data, as previously described in *Section 3.4.5*, indicated the expected linear relationship as illustrated in Figure 3.4.6. From the slope of the graph, an apparent *pseudo*-first-order rate constant of $(2.9 \pm 0.1) \times 10^{-5} \text{ sec}^{-1}$ was obtained.

Although the linear response was indicative of *pseudo*-first-order kinetics, graphical inspection of the data fit was desirable. The coefficient of determination, R^2 , is a measure of how closely the estimated values for the regression line correspond to the actual data and ranges from 0 to 1. In general, the closer R^2 is to unity, the better the fit. Unfortunately, R^2 is a very poor indicator of the quality of the regression since it does not account for systematic variations.^{120,121}

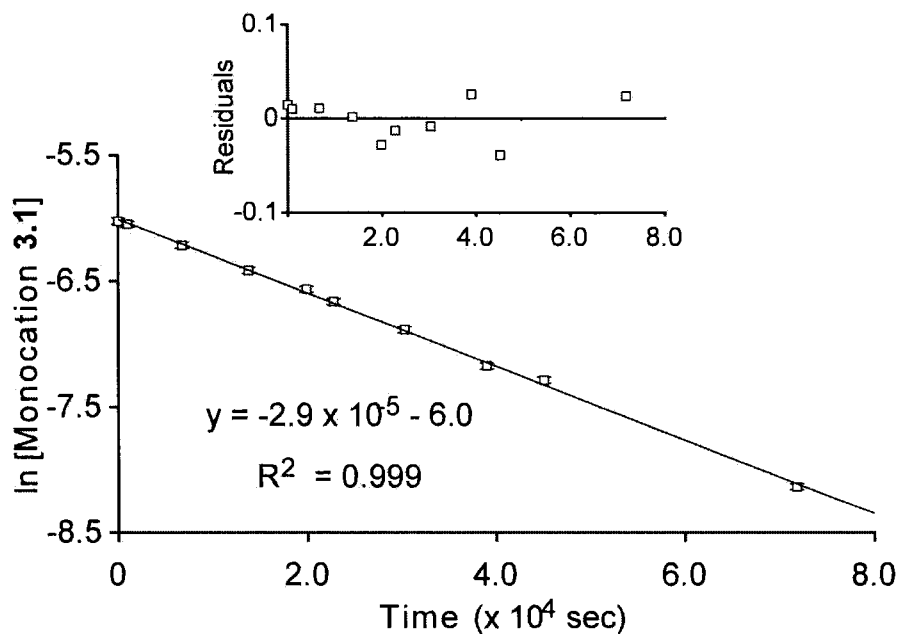


Figure 3.4.6. Representative example of the plot of the natural log of the concentration of the monocationic DTE **3.1** against time showing the progress of the reaction of a solution (2.4×10^{-3} M) of the ring-open isomer **3.1** in CD_3CN with an excess of 4-bromobenzyl bromide (7.3×10^{-2} M) at 22°C over a 24-hour period. The best-fit line obtained using least-squares-fit regression analysis shows a linear trend and is indicative of a *pseudo*-first-order pattern. The error bars represent the experimental error, which was based on a 2% integration error estimate from 9 repeated NMR integrations. The inset shows a plot of the residual values against time for the ring-open DTE **3.1** where the points in the plots seem to be fluctuating somewhat randomly around zero in an un-patterned fashion at the beginning of the reaction while showing more deviations from the linear model with the build-up of product.

The use of residual plots provides a more effective approach to assess the quality of the regression and to detect systematic deviations in regression diagnostics.¹²² A residual plot is a graph of the residuals, which corresponds to the difference between the observed response variable ‘y’ values and the values predicted by the regression line, against the ‘x’ values. Plots in which the residuals do not exhibit any systematic structure indicate that the model fits the data well. The residual plot for the substitution reaction of the ring-open DTE **3.1** shows no definite pattern at the beginning of the reaction, as illustrated in the inset in Figure 3.4.6, and is indicative of a good fit to the linear model. However, there is a noticeable deviation from linearity near the end of the experiment

indicating that the build-up of product is leading to a ‘side reaction’ (inset in Figure 3.4.6).

To test the reproducibility of the results, the alkylation reaction was repeated twice following the described procedure using samples prepared from the same stock solution and the apparent *pseudo*-first-order rate constants for the three individual runs are listed in Table 3.4.2. From these values, the average apparent *pseudo*-first-order rate constant, $\bar{k}'_{3,1}$, for the benzylation reaction of the ring-open DTE **3.1** was calculated to be $(2.9 \pm 0.1) \times 10^{-5} \text{ sec}^{-1}$. The plots of the natural log of the concentration of monobenzylated DTE **3.1** against time, the linear least squares regression analysis of the data, and the residual plots for the three samples are shown in the appendix.

Table 3.4.2. List of apparent *pseudo*-first-order rate constants, $k'_{3,1}$, obtained when three samples of the ring-open isomer **3.1** of the monobenzylated DTE in CD₃CN were independently treated with an excess of 4-bromobenzyl bromide ($7.3 \times 10^{-2} \text{ M}$) at 22°C.

Experiment	1	2	3
^a [3.1] ₀ (mM)	2.4	2.4	2.4
[4-bromobenzyl bromide] (mM)	73	73	73
$k'_{3,1} (\times 10^{-5} \text{ sec}^{-1})^b$	2.9 ± 0.1	2.8 ± 0.1	2.9 ± 0.1

^a [**3.1**]₀ refers to the initial concentration of the solution of the ring-open isomer **3.1** before the addition of the alkylating reagent. The three samples were prepared from the same stock solution ($2.4 \times 10^{-3} \text{ M}$) of the ring-open isomer **3.1** in CD₃CN. ^b The uncertainty in the calculated value of the apparent *pseudo*-first-order rate constant is based on the standard deviation from the regression analysis.

3.4.7 Reactivity of the Ring-Closed Form of the Monocationic DTE 3.2

Another sample (0.70 mL) prepared using the same stock solution (2.4×10^{-3} M) of the monocationic DTE 3.1 in CD_3CN was exposed to 365 nm light until complete ring-cyclization was achieved at the PSS as monitored by ^1H NMR spectroscopy.

An excess of 4-bromobenzyl bromide (7.3×10^{-2} M, 30 molar equiv) was added and the progress of the reaction at 22 °C was monitored by ^1H NMR spectroscopy over a 24-hour period. The aromatic region of the starting monobenzylated DTE 3.2 prior to the addition of the 4-bromobenzyl bromide contains a two-proton signal at 8.70 ppm (peak 'b') that can be attributed to the α -protons of the unreacted pyridine and a two-proton doublet at 8.73 ppm (peak 'a'), which partially overlaps with peak 'b' and which corresponds to the α -protons of the pyridinium group. Reaction of the monocation 3.2 with 4-bromobenzyl bromide generated the dibenzylated product 3.4 with a four-proton doublet further downfield (peak 'p') that corresponds to the α -protons of the pyridinium groups in 3.4 (Figure 3.4.7).

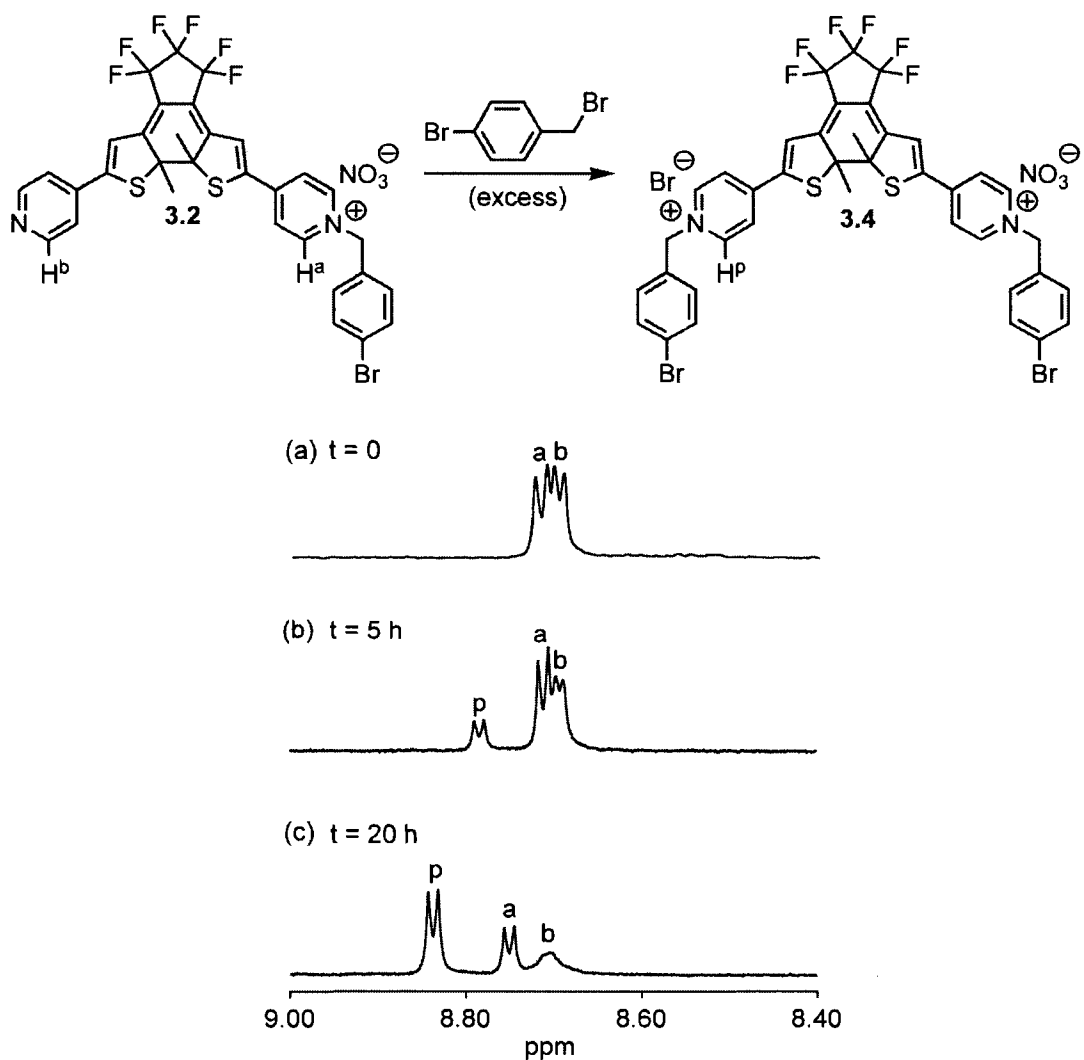


Figure 3.4.7. Representative example showing the use of ¹H NMR spectroscopy to monitor the progress of the reaction of the ring-closed isomer **3.2** of the monobenzylated *bis*(pyridinium) with an excess of 4-bromobenzyl bromide to generate the dialkylated DTE **3.4**. Partial ¹H NMR spectra (600 MHz, CD₃CN) showing the aromatic region of a solution (2.4×10^{-3} M) of the ring-closed isomer **3.2** in CD₃CN (a) before, (b) 5 h after, and (c) 20 h after adding an excess of 4-bromobenzyl bromide (7.3×10^{-2} M). The mole fractions ($\chi_{3,2}$ and $\chi_{3,4}$) of the monoalkylated DTE **3.2** and the dialkylated DTE **3.4** were obtained using the integral values for peaks 'a', 'b' and 'p'.

Thus, the mole fractions $\chi_{3.2}$ and $\chi_{3.4}$ (corresponding to the monobenzylated DTE **3.2** and the dibenzylated DTE **3.4**, respectively) were obtained using the integral values for 'a', 'b' and 'p' as shown in Equations 3.4.5 and 3.4.6.

$$\chi_{3.2} = \frac{(a + b)}{(a + b) + p}$$

Equation 3.4.5. Equation relating the mole fraction of the monobenzylated *bis*(pyridinium) **3.2** to the peak integrals 'a', 'b' and 'p'.

$$\chi_{3.4} = \frac{p}{(a + b) + p}$$

Equation 3.4.6. Equation relating the mole fraction of the dibenzylated *bis*(pyridinium) **3.4** to the peak integrals 'a', 'b' and 'p'.

Graphical treatment of the data by plotting the natural log of the concentration of monobenzylated DTE **3.2** against time followed by a linear least squares regression analysis of the data, as already described in *Section 3.4.5*, revealed a linear relationship as depicted in Figure 3.4.8. From the slope of the graph an apparent *pseudo*-first-order rate constant of $(9.0 \pm 0.5) \times 10^{-6} \text{ sec}^{-1}$ was obtained.

The residual plot for the alkylation reaction of the ring-closed DTE **3.2** shows the absence of any specific pattern at the beginning of the reaction and is suggestive of a good fit to the linear model, as illustrated in the inset in Figure 3.4.8.

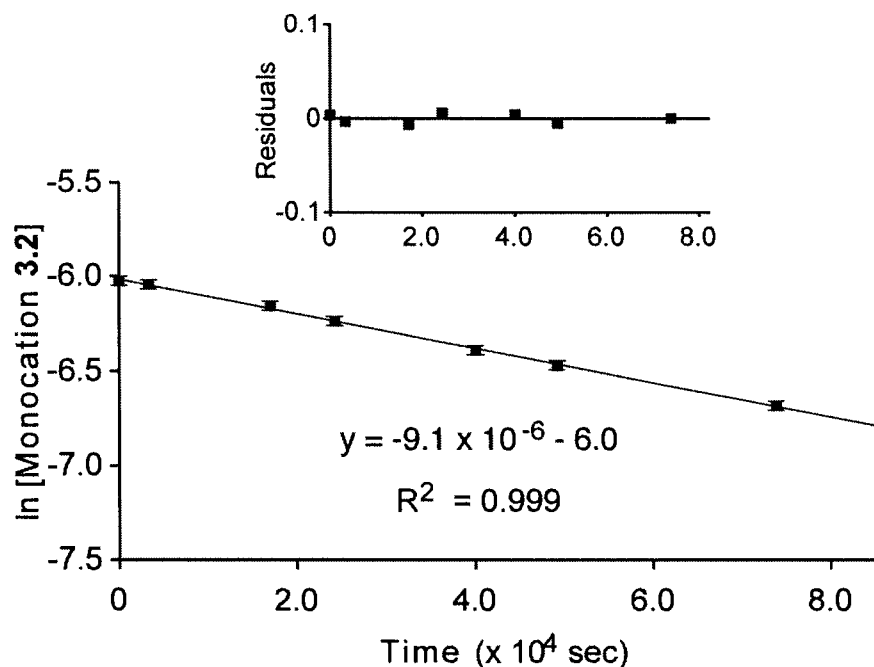


Figure 3.4.8. Representative example of the plot of the natural log of the concentration of the monocationic DTE 3.2 against time showing the progress of the reaction of a solution ($2.4 \times 10^{-3} \text{ M}$) of the ring-closed isomer 3.2 in CD_3CN with an excess of 4-bromobenzyl bromide ($7.3 \times 10^{-2} \text{ M}$) at 22°C over a 24-hour period. The best-fit line obtained using least-squares-fit regression analysis shows a linear trend and is indicative of a *pseudo*-first-order pattern. The error bars represent the experimental error, which was based on a 2% integration error estimate from 9 repeated NMR integrations. The inset shows a plot of the residual values against time for the ring-closed DTE 3.2 where the points in the plots seem to be fluctuating somewhat randomly around zero in an un-patterned fashion at the beginning of the reaction.

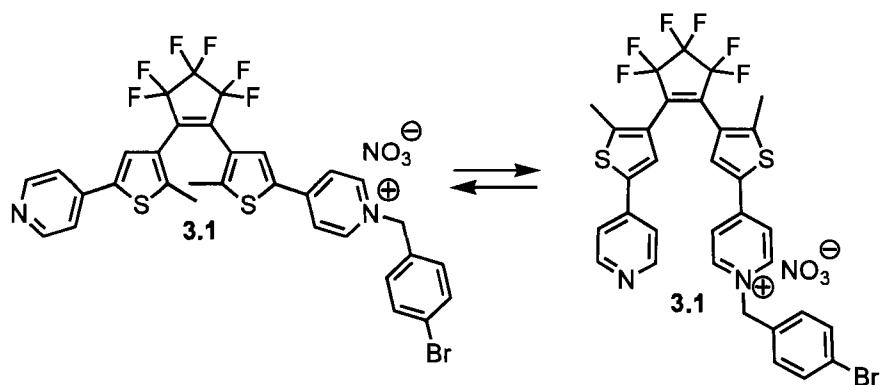
To test the reproducibility of the results, the alkylation reaction was repeated twice following the described procedure using samples prepared from the same stock solution and the apparent *pseudo*-first-order rate constants for the three individual runs are listed in Table 3.4.3. From these values the average apparent *pseudo*-first-order rate constant, $\overline{k}_{3,2}$, for the alkylation of the ring-closed DTE 3.2, was calculated to be $(9.0 \pm 0.1) \times 10^{-6} \text{ sec}^{-1}$. The plots of the natural log of the concentration of monobenzylated DTE 3.1 against time, the linear least squares regression analysis of the data, and the residual plots for each run are shown in the appendix.

Table 3.4.3. List of apparent *pseudo*-first-order rate constants, $k'_{3,2}$, obtained when three samples of the ring-closed isomer **3.2** of the monobenzylated DTE in CD₃CN were independently treated with an excess of 4-bromobenzyl bromide (7.3×10^{-2} M) at 22°C.

Experiment	1	2	3
^a [3.2] ₀ (mM)	2.4	2.4	2.4
[4-bromobenzyl bromide] (mM)	73	73	73
$k'_{3,2}$ ($\times 10^{-6}$ sec ⁻¹) ^b	9.0 \pm 0.2	9.1 \pm 0.2	8.9 \pm 0.1

^a [**3.2**]₀ refers to the initial concentration of the solution of the ring-closed isomer **3.2** before the addition of the alkylating reagent. The three samples were prepared from the same stock solution (2.4×10^{-3} M) of the ring-open isomer **3.1** in CD₃CN by irradiating each sample with 365 nm light until no peaks corresponding to the ring-open isomer **3.1** were observed by ¹H NMR spectroscopy. ^b The uncertainty in the calculated value of the apparent *pseudo*-first-order rate constant is based on the standard deviation from the regression analysis.

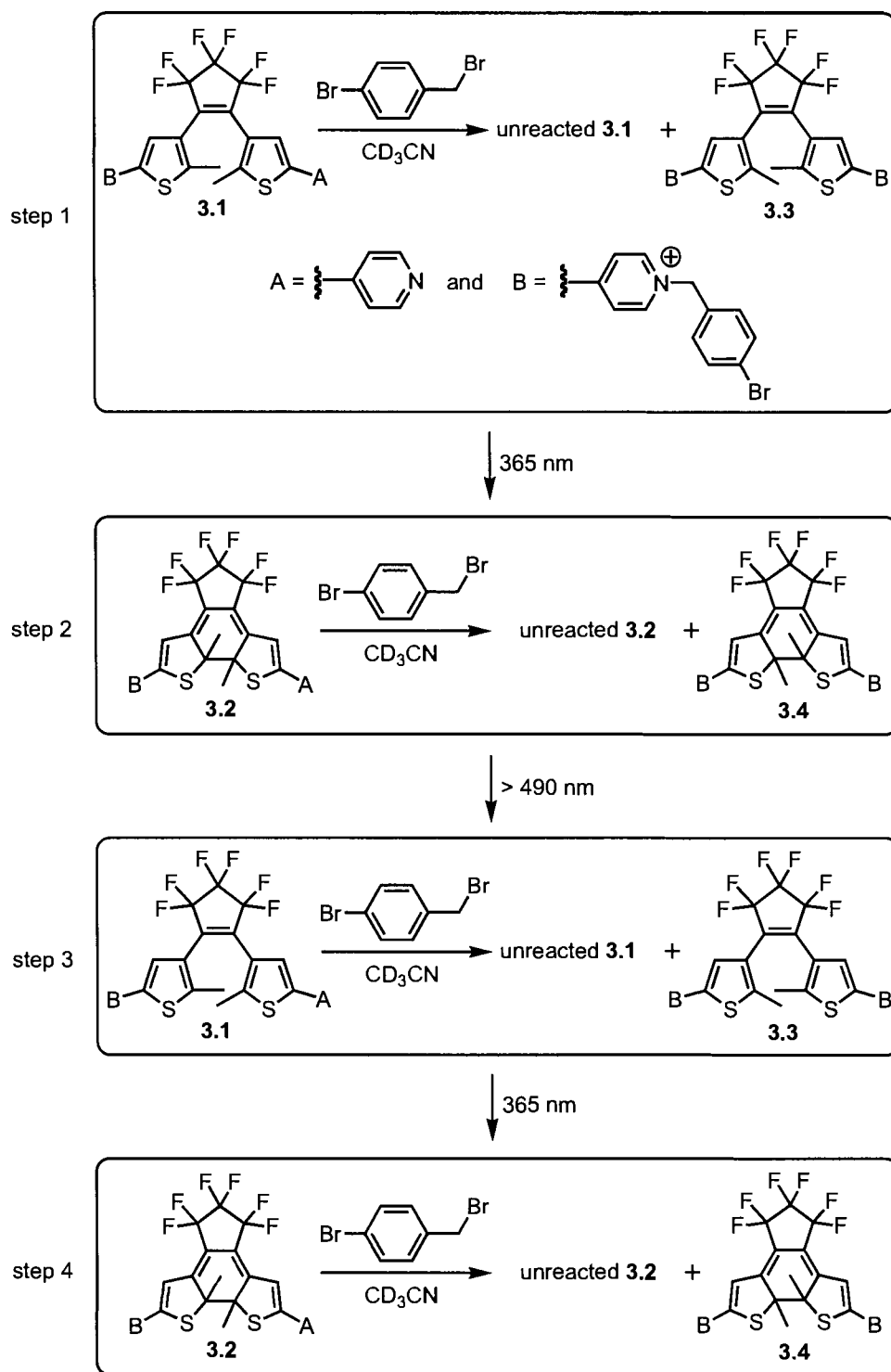
Comparison of the average values for the apparent *pseudo*-first-order rate constants, $\bar{k}'_{3,1}$ and $\bar{k}'_{3,2}$, reveals that the ring-open **3.1** reacts approximately 3.2 times faster than its ring-closed counterpart **3.2**. The small difference in reactivity can be ascribed in part to the fact that in the case of the ring-closed isomer **3.2**, the pendant pyridine is twisted 20-30° out of coplanarity from the π -conjugated backbone as discussed in *Section 2.6.9*. Another factor that can contribute to the small magnitude of the change is the fact that the structural flexibility of the ring-open isomer **3.1**, previously discussed in *Section 1.4.1* of the introductory chapter, allows the pendant pyridine and the positively charged pyridinium moiety to be in close proximity (Equation 3.4.7) leading to through-space effects such as (1) crowded reaction site, (2) attraction between the “relatively” electron rich pyridine and the electron-poor pyridinium, and (3) charge-charge repulsion in the transition state leading to the formation of the dicationic DTE **3.3**.



Equation 3.4.7. The structural flexibility of the ring-open isomer **3.1** allows the pendant pyridine and the positively charged pyridinium moiety to converge towards each other resulting in through-space effects such as (1) crowded reaction site, (2) attraction between the “relatively” electron rich pyridine and the electron-poor pyridinium, and (3) electrostatic repulsion in the transition state leading to the formation of the dicationic DTE **3.3**.

3.4.8 Phototuning the Alkylation Reaction of the Monobenzylated DTE *In Situ*

Even though the work done in the previous section has shown that the ring-open isomer (**3.1**) of the monobenzylated *bis*(pyridinium) reacts slightly more than three times faster than the ring-closed form **3.2**, there is still a need to demonstrate that this trend in reactivity will prevail if the same reaction solution is subjected to a series of ring-opening and ring-closing cycles. As already described in *Sections 3.4.2* and *3.4.3*, the photochemical cycling studies on the independent solutions of the monobenzylated DTE (**3.1**) and the dibenzylated DTE (**3.3**) indicate that both DTE compounds can be toggled between their ring-open (**3.1** and **3.3**) and their ring-closed (**3.2** and **3.4**) isomers numerous times without observable degradation and that the ring-closing (ring-opening) reaction proceeds with a high PSS. Consequently, it can be expected that the same trend in reactivity will be observed if the reaction solution is subjected to a series of ring-opening and ring-closing cycles.



Scheme 3.4.1. Ring-opening and ring-closing reaction steps used to photoregulate reactivity *in situ*.

To test the trend in reactivity *in situ*, a solution (2.4×10^{-3} M) of the ring-open isomer **3.1** in CD₃CN was treated with an excess of 4-bromobenzyl bromide (7.3×10^{-2} M, 30 molar equiv) and the progress of the reaction at 22 °C was measured by ¹H NMR spectroscopy. After about 3 hours, the solution was irradiated with 365 nm light until both the ring-open reactant **3.1** and the ring-open product **3.3** were completely converted to their respective ring-closed forms. After another 3 hours, all the ring-open species were regenerated using light of wavelengths greater than 490 nm. Such *in situ* switching by alternating irradiation at 365 nm and > 490 nm over 3-hour intervals was repeated (Scheme 3.4.1).

Graphical treatment of the data, in a similar fashion to the method described in *Section 3.4.6*, for the reaction of the ring-open isomer **3.1** and *Section 3.4.7* for the reaction of the ring-closed isomer **3.2**, revealed a linear relationship and gave rise to the graph shown in Figure 3.4.9.

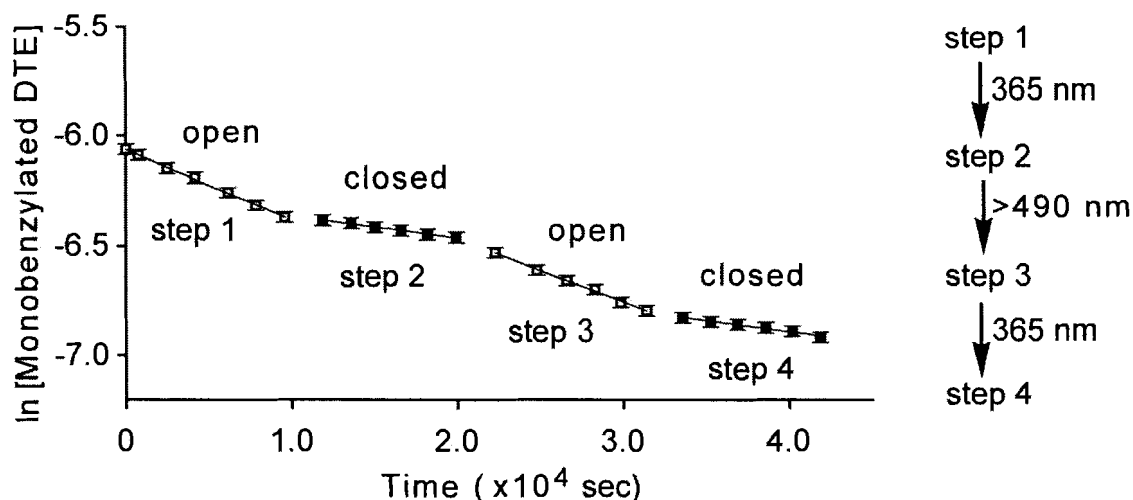


Figure 3.4.9. Graph showing the *in situ* photoregulation of the rate of reaction of a solution (2.4×10^{-3} M) of the ring-open isomer **3.1** of the monobenzylated *bis*(pyridinium) in CD_3CN with an excess of 4-bromobenzyl bromide (7.3×10^{-2} M, 30 molar equiv) at 22°C by alternating irradiation at 365 nm and wavelengths greater than 490 nm over 3-hour intervals. The step-like feature of the graph is indicative of a change in the apparent rate of alkylation reaction on changing from the ring-open isomer **3.1** to the ring-closed isomer **3.2**. The error bars represent the experimental error, which was based on a 2% integration error estimate from 9 repeated NMR integrations.

The step-like feature of the graph attests to a change in the apparent rate of reaction on changing from the ring-open isomer to the ring-closed isomer. Determination of the slope of the graph for each step of the reaction confirmed that the apparent *pseudo*-first-order rate constants for the two ring-open steps (step 1 and step 3 in Scheme 3.4.1) were very close in value ($k'_{(\text{step } 1)} = (3.0 \pm 0.1) \times 10^{-5} \text{ sec}^{-1}$ and $k'_{(\text{step } 3)} = (3.0 \pm 0.1) \times 10^{-5} \text{ sec}^{-1}$) and that of the two ring-closed steps (step 2 and step 4 in Scheme 3.4.1) were also similar ($k'_{(\text{step } 2)} = (1.0 \pm 0.1) \times 10^{-5} \text{ sec}^{-1}$ and $k'_{(\text{step } 4)} = (9.9 \pm 0.1) \times 10^{-6} \text{ sec}^{-1}$) and these values are listed in Table 3.4.4. These values indicate the success in phototuning the reactivity of the monoalkylated DTE in solution without any observable degradation.

Table 3.4.4 The observed in situ changes in the apparent *pseudo*-first-order rate constants at 22°C by alternating irradiation at 365 nm and > 490 nm over 3-hour intervals.

	ring-open (3.1)	ring-closed (3.2)
$k'_{(\text{step } 1)} (\text{sec}^{-1})^{\text{a}}$	$(3.0 \pm 0.1) \times 10^{-5}$	–
$k'_{(\text{step } 2)} (\text{sec}^{-1})^{\text{b}}$	–	$(1.0 \pm 0.1) \times 10^{-5}$
$k'_{(\text{step } 3)} (\text{sec}^{-1})^{\text{c}}$	$(3.0 \pm 0.1) \times 10^{-5}$	–
$k'_{(\text{step } 4)} (\text{sec}^{-1})^{\text{d}}$	–	$(9.9 \pm 0.1) \times 10^{-6}$
$\bar{k}'_{3.1} (\text{sec}^{-1})^{\text{e}}$	$(2.9 \pm 0.1) \times 10^{-5}$	–
$\bar{k}'_{3.2} (\text{sec}^{-1})^{\text{f}}$	–	$(9.0 \pm 0.1) \times 10^{-6}$

^a The apparent *pseudo*-first-order rate constant, $k'_{(\text{step } 1)}$, corresponds to the trend in reactivity when a solution (2.3×10^{-3} M) of the ring-open isomer **3.1** in CD_3CN was treated with an excess of 4-bromobenzyl bromide (7.3×10^{-2} M, 30 molar equiv) and the progress of the reaction was monitored for 3 hours. ^b The apparent *pseudo*-first-order rate constant, $k'_{(\text{step } 2)}$, corresponds to the trend in reactivity when the solution was irradiated with 365 nm light until both the ring-open reactant **3.1** and the ring-open product **3.3** were completely converted to their respective ring-closed forms and the progress of the reaction was monitored for another 3 hours. ^c The apparent *pseudo*-first-order rate constant, $k'_{(\text{step } 3)}$, corresponds to the trend in reactivity when the solution was irradiated with light of wavelengths greater than 490 nm until both the ring-closed reactant **3.2** and the ring-closed product **3.4** were completely converted to their respective ring-open forms and the progress of the reaction was monitored for an additional 3 hours. ^d The apparent *pseudo*-first-order rate constant, $k'_{(\text{step } 4)}$, corresponds to the trend in reactivity when the solution was irradiated with 365 nm light until both the ring-open reactant **3.1** and the ring-open product **3.3** were completely converted to their respective ring-closed forms and the progress of the reaction was monitored for an another 3 hours. ^e The apparent *pseudo*-first-order rate constant, $\bar{k}'_{3.1}$, corresponds to the average value obtained in Section 3.4.6 when three samples (2.4×10^{-3} M) of the ring-open isomer **3.1** in CD_3CN , were independently treated with an excess of 4-bromobenzyl bromide (7.3×10^{-2} M) and the progress of each reaction was monitored for 24 hours. ^f The apparent *pseudo*-first-order rate constant, $\bar{k}'_{3.2}$, corresponds to the average value obtained in Section 3.4.7 when three samples (2.4×10^{-3} M) of the ring-closed isomer **3.2** in CD_3CN were independently treated with an excess of 4-bromobenzyl bromide (7.3×10^{-2} M) and the progress of each reaction was monitored for 24 hours.

3.5 Reactivity of the Ring-Open and the Ring-Closed *Bis*(pyridine)

As already mentioned in *Section 2.6.5*, optimal yields of the monobenzylated DTE were achieved when it was synthesized as its ring-closed isomer **3.2** (labelled **2.10** in Chapter 2). The fact that the reaction of the ring-closed isomer **3.6** (labelled **2.9** in Chapter 2) with 4-bromobenzyl bromide gives mainly the monoalkylated product while the ring-open isomer **3.5** (labelled **2.8** in Chapter 2) of the *bis*(pyridine) gives mainly the dialkylated product suggests that (1) the pyridine 'A' in the ring-closed isomer **3.6** is more reactive than the pyridine 'A' in the generated monocation **3.2** and (2) the pyridine 'A' in the ring-open isomer **3.5** is not necessarily more reactive than the pyridine 'A' in the generated monobenzylated DTE **3.1** (Figure 3.5.1). The work done in the first part of this chapter has shown that the pyridine 'A' of the ring-open isomer (**3.1**) of the monoalkylated DTE reacts faster than the pyridine 'A' of the ring-closed isomer **3.2**. The second part of this work focuses on analyzing whether (1) the rates of reaction of the two pyridines (**3.5** and **3.1**) in the ring-open form are different, (2) whether the two pyridines in the ring-open form (**3.5** and **3.1**) react faster than the two pyridines (**3.6** and **3.2**) of the ring-closed form, and (3) the pyridine 'A' of the ring-open *bis*(pyridine) **3.5** reacts faster than the pyridine 'A' of the ring-closed isomer **3.6** to generate their respective monoalkylated products **3.1** and **3.2**. One approach to analyze and compare the rates of reaction of the ring-open (**3.5** and **3.1**) and the ring-closed (**3.6** and **3.2**) isomers of the *bis*(pyridine) and the monobenzylated *bis*(pyridinium) involves the use of consecutive first-order kinetics.

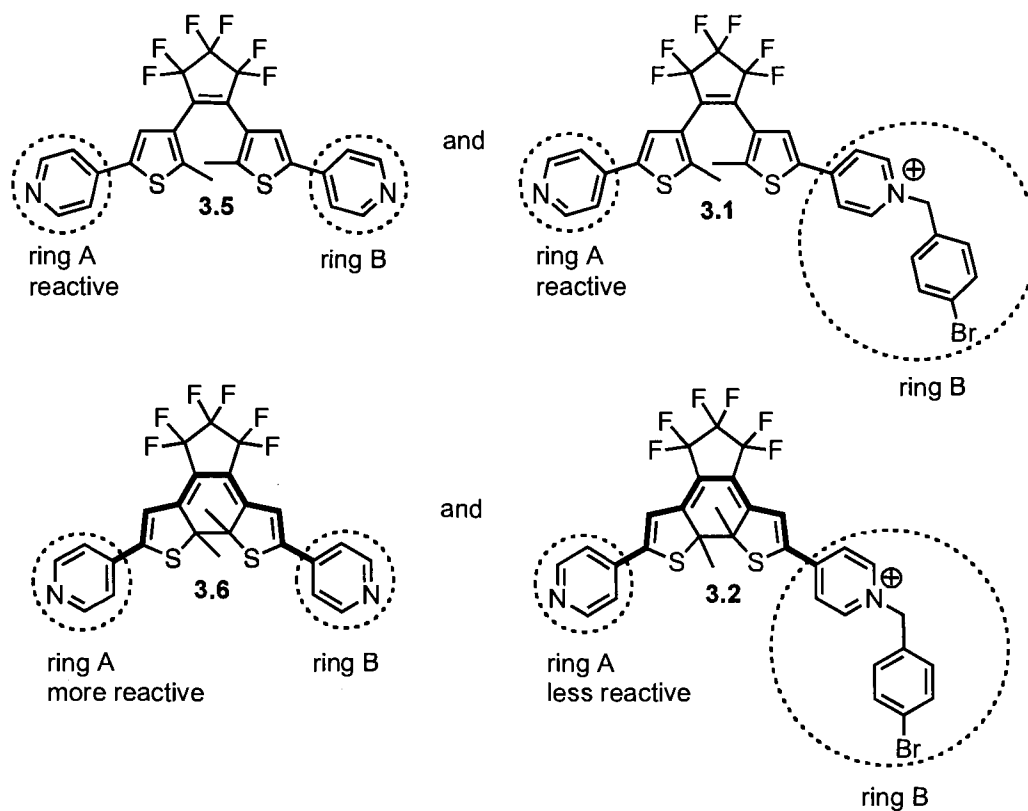
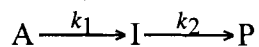


Figure 3.5.1. The reaction of the ring-closed isomer (3.6) of the *bis*(pyridine) with 4-bromobenzyl bromide gives mainly the monoalkylated product 3.2 indicating that the pyridine 'A' in the ring-closed isomer 3.6 is more reactive than the pyridine 'A' in the generated monocation 3.2. The reaction of the ring-open isomer (3.5) of the *bis*(pyridine) gives mainly dialkylated products suggests that both pyridines are reactive and that the pyridine 'A' in the ring-open isomer 3.5 is not necessarily more reactive than the pyridine 'A' in the generated monobenzylated DTE 3.1.

3.5.1 Consecutive First-Order Reactions

A system is said to undergo a consecutive reaction when the product of one reaction becomes the reactant in the next reaction. Consider a general example consisting of a sequence of two first-order reactions in which a reagent 'A' forms a product 'I', which, in turn, generates another product 'P' as shown in Scheme 3.5.1.



Scheme 3.5.1. General example of a reaction showing two consecutive first-order reaction steps.

The rate equations for the decrease in the concentration of 'A', the increase in the concentration of 'I', and the increase in the concentration of 'P' with time for such a system are given in Equations 3.5.1, 3.5.2 and 3.5.3, respectively, where k_1 refers to the first-order rate constant for the reaction of 'A' to 'I' while k_2 represents the first-order rate constant for the reaction of 'I' to 'P'.

$$-\frac{d[A]}{dt} = k_1[A]$$

Equation 3.5.1. Rate expression for the change in the concentration of 'A' with time.

$$\frac{d[I]}{dt} = k_1[A] - k_2[I]$$

Equation 3.5.2. Rate expression for the change in the concentration of 'I' with time.

$$\frac{d[P]}{dt} = k_2[I]$$

Equation 3.5.3. Rate expressions for the change in the concentration of 'P' with time.

Mathematical treatment of the above differential equations^{123,124} gives rise to the expressions shown in Equations 3.5.4, 3.5.5 and 3.5.6 where $[A]_t$, $[I]_t$, and $[P]_t$ refer to the respective concentrations of 'A', 'I' and 'P' at time t while $[A]_0$ refers to the initial concentration of 'A'.

$$[A]_t = [A]_0 e^{-k_1 t}$$

Equation 3.5.4. Integrated rate expression for the exponential decrease in the concentration of 'A' with time.

$$[I]_t = \frac{k_1[A]_0}{k_2 - k_1} [e^{-k_1 t} - e^{-k_2 t}]$$

Equation 3.5.5. Integrated rate expression showing that the concentration of ‘I’ with time is the difference of two exponentials.

$$[P]_t = [A]_0 \left\{ 1 - \frac{1}{k_2 - k_1} [k_2 e^{-k_1 t} - k_1 e^{-k_2 t}] \right\}$$

Equation 3.5.6. Integrated rate expression for the increase in the concentration of ‘P’ with time.

Graphical treatment of the data by plotting the relative concentrations of ‘A’, ‘I’ and ‘P’ against time followed by non-linear least-squares regression analysis of the exponential expression for [A] and the biexponential expressions for [I] and [P] can be used to solve for the rate constants k_1 and k_2 . However, as already mentioned in *Section 3.2*, one important assumption is that there is no significant back reaction and the term apparent rate constant will be used in order to take into account any back reaction.¹¹¹

Assuming that the reaction of the *bis*(pyridine)s **3.5** and **3.6** with 4-bromobenzyl bromide consists of a sequence of two second-order steps, it can be expected that the *bis*(pyridine)s will react leading first to the formation of the monobenzylated DTEs **3.1** and **3.2** as the intermediates, which will in turn be consumed as they react with more 4-bromobenzyl bromide to generate the dibenzylated products **3.3** and **3.4**. This reaction sequence can be simplified using the technique of *flooding* as discussed earlier in this chapter making it possible to treat the system as a sequence of two consecutive *pseudo*-first-order reactions.¹¹¹

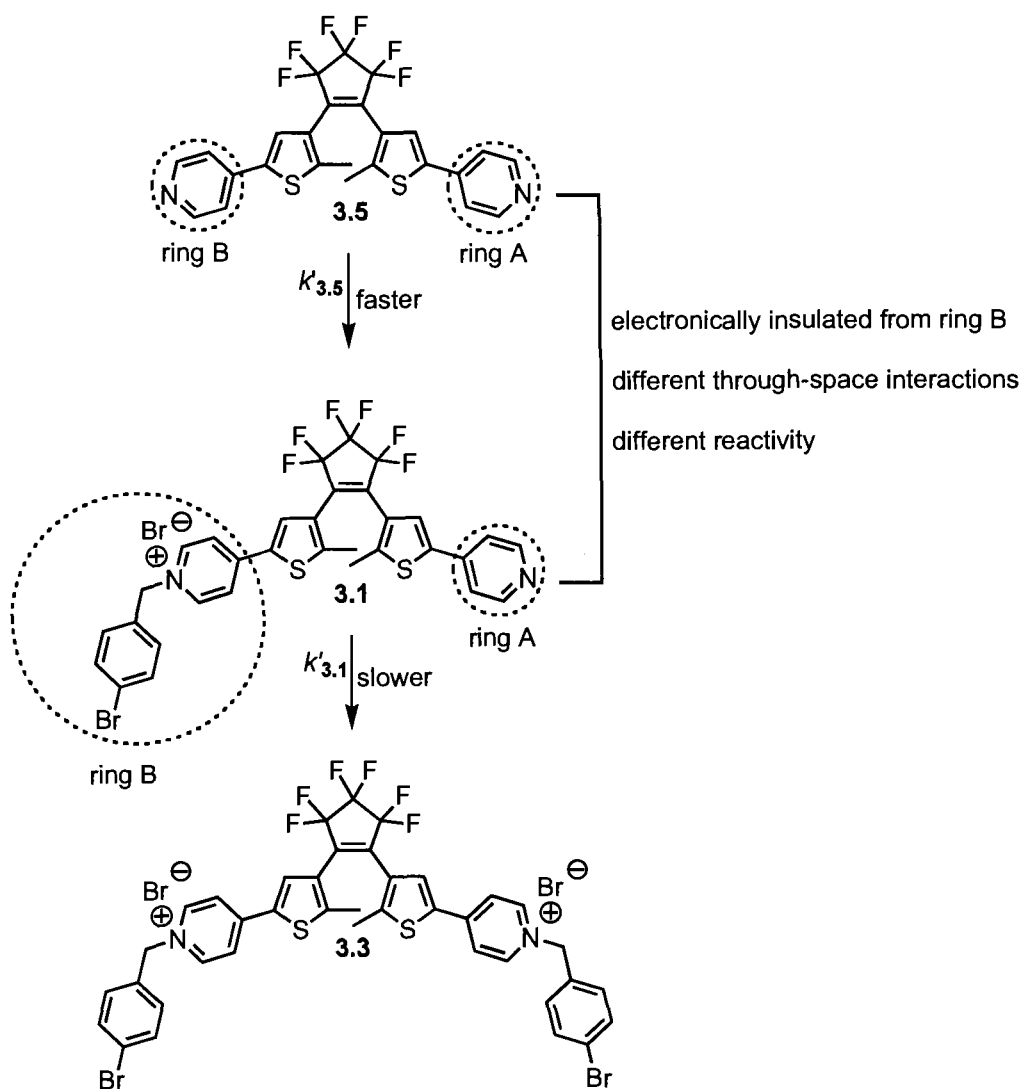
3.6 Results and Discussion

3.6.1 Choice of Reaction Conditions

As already discussed in the first part of this chapter, ^1H NMR spectroscopy can be very useful to assess the progress of the alkylation reaction of both the ring-open (**3.5**) and the ring-closed (**3.6**) isomers of the *bis*(pyridine). The T_1 values for the protons of the ring-open (**3.5**) and the ring-closed (**3.6**) isomers of the *bis*(pyridine) were also measured using the inversion-recovery method¹¹⁴ and from these values, it was established that the same time delay (25 s) used for monitoring the rate of reaction of the ring-open isomer (**3.1**) and of the ring-closed (**3.2**) isomers of the monobenzylated DTE (*Section 3.4.4*) can be used. The graphs and the fitted parameters for the T_1 measurements are shown in the appendix.

3.6.2 Reactivity of the Ring-Open Form of the *Bis*(pyridine) **3.5**

In the case of the ring-open forms, the two thiophene heterocycles (in both the *bis*(pyridine) **3.5** and the monocation **3.1**) are electronically insulated from each other such that ring 'A' and ring 'B' can be expected to be electronically independent as shown in Scheme 3.6.1. However, as already discussed in *Section 3.4.7*, the structural flexibility of the ring-open isomer **3.1** allows the pyridine 'A' and the pyridinium 'B' to be in close proximity leading to through-space effects that can be expected to slow down the reaction of the monobenzylated DTE **3.1** compared to that of the *bis*(pyridine) **3.5**. Thus, the apparent *pseudo*-first-order rate constant $k'_{3,5}$ is expected to be higher than $k'_{3,1}$.



Scheme 3.6.1. Consecutive *pseudo*-first-order sequence for the ring-open isomer **3.5** leading to the formation of the monoalkylated product **3.1** and subsequent dialkylated product **3.3**. The two thiophene heterocycles are electronically insulated from each other such that ring 'A' and ring 'B' can be expected to be electronically independent while the through-space effects, arising from the structural flexibility of the isomers, can be expected to slow down the reaction of the monobenzylated DTE **3.1** compared to that of the *bis*(pyridine) **3.5**.

A sample of the ring-open form (**3.5**) of the *bis*(pyridine), prepared by transferring a known volume (0.70 mL) of a stock solution (4.6×10^{-3} M) of the *bis*(pyridine) in CD_3CN into an NMR tube, was treated with an excess of 4-bromobenzyl bromide (1.2×10^{-1} M, 27 molar equiv) and the progress of the reaction at 22 °C was monitored by ^1H

NMR spectroscopy. As shown in Figure 3.6.1, the aromatic region of the *bis*(pyridine) **3.5** contains a four-proton signal at 8.56 ppm (peak 'a') that can be attributed to the α -protons of the pyridine and formation of the monobenzylated DTE **3.1** was accompanied by the appearance of a two-proton doublet further downfield (peak 'b') which corresponds to the α -protons of the pyridinium group. The two-proton signal corresponding to the α -protons of the unreacted pyridine in **3.1** overlaps with the peak for the α -protons of the *bis*(pyridine) **3.5** (peak 'a'). Reaction of the monocation **3.1** with 4-bromobenzyl bromide generated the dibenzylated product **3.3** with a four-proton doublet further downfield (peak 'c') that corresponds to the α -protons of the pyridinium groups in **3.3**.

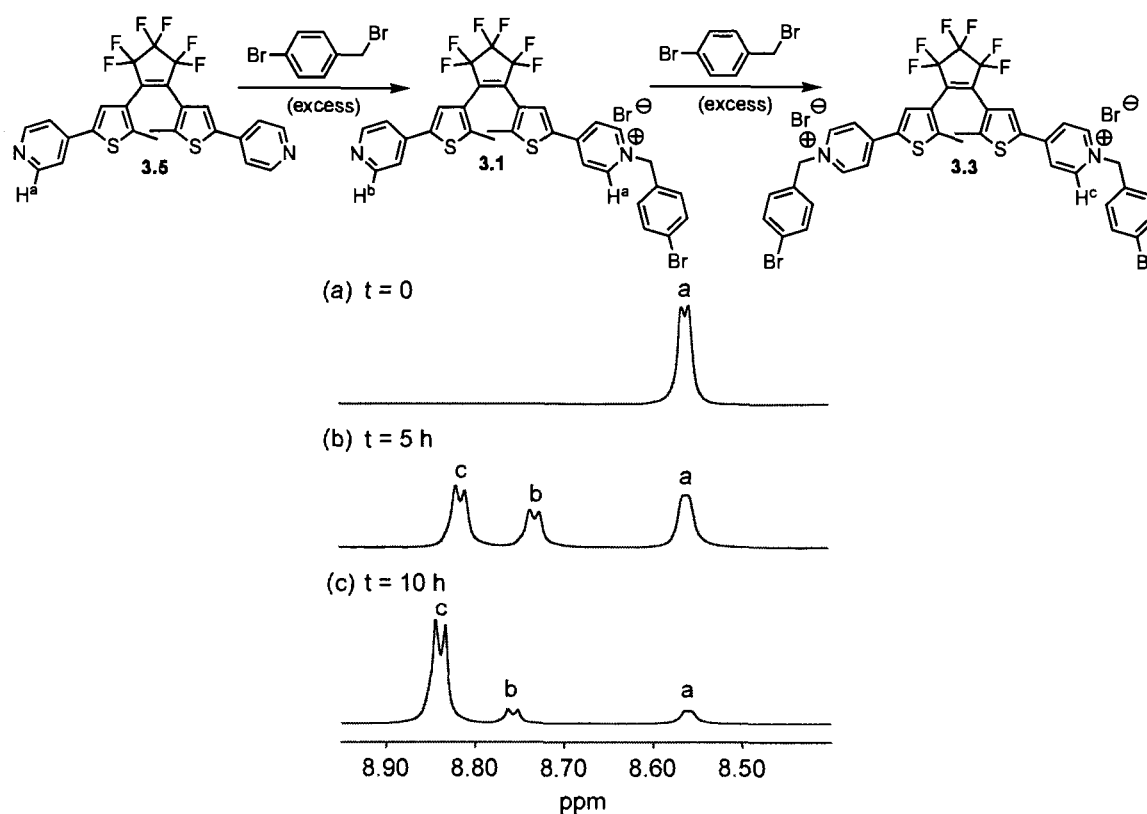


Figure 3.6.1. Partial ¹H NMR spectra (600 MHz, CD₃CN) showing the aromatic region of a solution (4.6×10^{-3} M) of the ring-closed isomer **3.5** in CD₃CN (a) before, (b) 5 hours after, and (c) 10 hours after adding an excess of 4-bromobenzyl bromide (1.2×10^{-1} M). The mole fractions ($\chi_{3.5}$, $\chi_{3.1}$ and $\chi_{3.3}$) of the *bis*(pyridine) **3.5**, the monoalkylated DTE **3.1** and the dialkylated DTE **3.3** were obtained using the integral values for peaks 'a', 'b' and 'c'.

Thus, the mole fractions $\chi_{3.5}$, $\chi_{3.1}$ and $\chi_{3.3}$ (corresponding to the *bis*(pyridine) **3.5**, the monobenzylated DTE **3.1** and the dibenzylated DTE **3.3**, respectively) were obtained using the integral values for 'a', 'b' and 'c' as shown in Equations 3.6.1, 3.6.2 and 3.6.3.

$$\chi_{3.5} = \frac{a - b}{(a + b) + c}$$

Equation 3.6.1. Relating the mole fraction of the *bis*(pyridine) **3.5** to the peak integrals 'a', 'b' and 'c'.

$$\chi_{3.1} = \frac{2b}{(a + b) + c}$$

Equation 3.6.2. Relating the mole fraction of the monobenzylated *bis*(pyridinium) **3.1** to the peak integrals 'a', 'b' and 'c'.

$$\chi_{3.3} = \frac{c}{(a + b) + c}$$

Equation 3.6.3. Relating the mole fraction the dibenzylated *bis*(pyridinium) **3.3** to the peak integrals 'a', 'b' and 'c'.

These studies were carried out in the absence of an internal standard because the ¹H NMR spectra of the *bis*(pyridine) **3.5**, the monoalkylated DTE **3.1** and the dialkylated DTE **3.3** showed no apparent signs of degradation during the course of the reaction.

With the mole fractions in hand, it was possible to monitor the decrease in the concentration of the *bis*(pyridine) **3.5**, the formation and disappearance of the monobenzylated DTE **3.1**, and the formation of the dibenzylated DTE **3.3** as the reaction proceeded. The plots of the relative concentrations of **3.5**, **3.1**, and **3.3** against time (Figure 3.6.2) are consistent with consecutive *pseudo*-first-order kinetics.

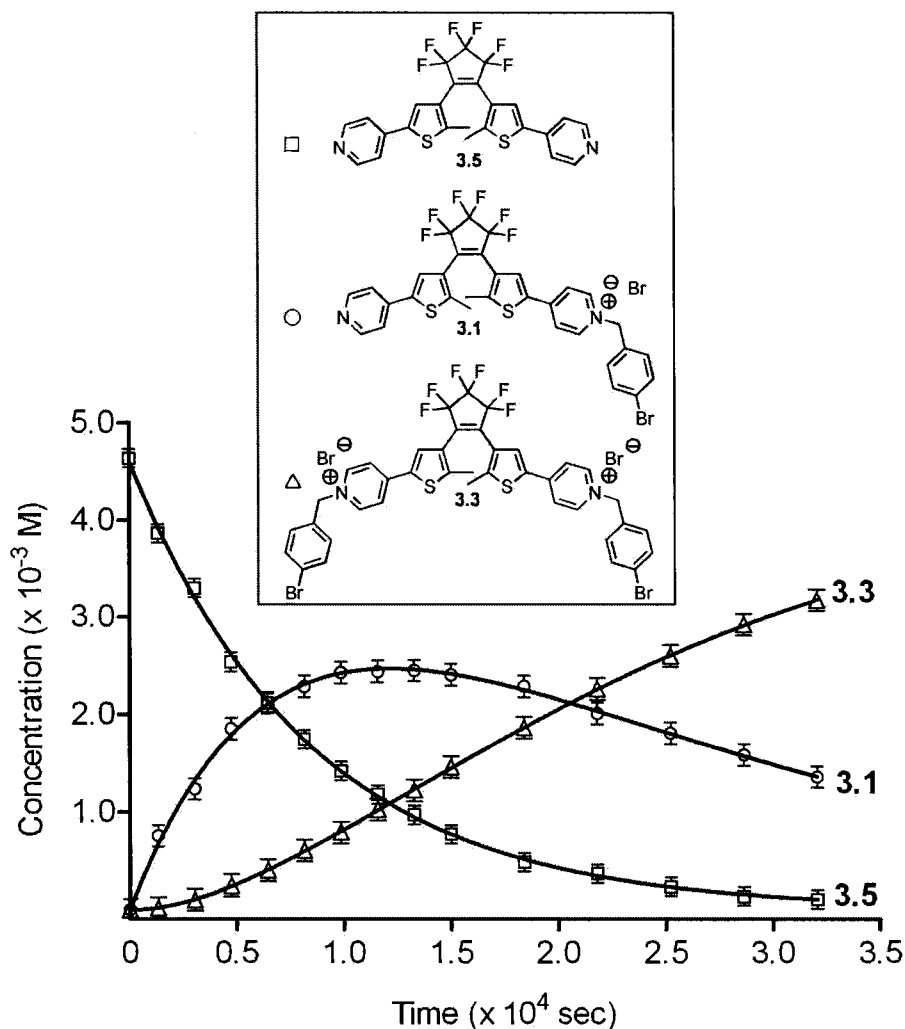


Figure 3.6.2. Plots of the concentration of the *bis*(pyridine) **3.5**, the monocation **3.1**, and the dication **3.3** against time consistent with a consecutive *pseudo*-first-order trend. The concentration of the *bis*(pyridine) **3.5** shows the predicted exponential decay with time indicative of a *pseudo*-first-order trend. The shape of the graph for the monobenzylated DTE **3.1** is consistent with a system in which the concentration builds up to a maximum and then decays with time because the concentration of the monobenzylated DTE **3.1** is dependent on both the rate of reaction of the *bis*(pyridine) **3.5** and the rate of conversion to the dibenzylated DTE **3.3**. The shape of the graph for the dibenzylated DTE **3.3** shows the characteristic initial delay in the formation of the latter, which is governed by the time required for the monocationic DTE **3.1** to be generated. The error bars represent the experimental error, which was based on a 2% integration error estimate from 9 repeated NMR integrations.

Indeed, the concentration of the *bis*(pyridine) **3.5** shows the predicted exponential decay with time (Equation 3.6.4), indicative of a *pseudo*-first-order trend. The shape of the graph for the monobenzylated DTE **3.1** is consistent with a system in which the concentration builds up to a maximum and then decays with time (i.e. the concentration of the monobenzylated DTE **3.1** is dependent on both the rate of reaction of the *bis*(pyridine) **3.5** and the rate of conversion to the dibenzylated DTE **3.3**) and is obtained by taking the difference of two exponentials as shown in Equation 3.6.5. The shape of the graph for the dibenzylated DTE **3.3** shows the characteristic initial delay in the formation of the latter, which is governed by the time required for the monocationic DTE **3.1** to be generated.

Using the equations described in *Section 3.5.1* for consecutive first-order reactions, the exponential expression for the concentration of the *bis*(pyridine) **3.5** and the biexponential expressions for the concentration of the monocation **3.1** and the dication **3.3** are shown in Equations 3.6.4, 3.6.5 and 3.6.6 where $[bis(\text{pyridine}) \text{ 3.5}]_t$, $[\text{monobenzylated DTE } \text{3.1}]_t$ and $[\text{dibenzylated DTE } \text{3.3}]_t$ refer to the respective concentrations at time t while $[bis(\text{pyridine}) \text{ 3.5}]_0$ refers to the initial concentration of the *bis*(pyridine) **3.5** before the addition of the 4-bromobenzyl bromide.

$$[bis(\text{pyridine}) \text{ 3.5}]_t = [bis(\text{pyridine}) \text{ 3.5}]_0 e^{-k'_{3.5}t}$$

Equation 3.6.4. Integrated rate expressions for the exponential decrease in the concentration of the *bis*(pyridine) **3.5** with time in the presence of an excess of 4-bromobenzyl bromide.

$$[\text{monobenzylated DTE } \text{3.1}]_t = \frac{k'_{3.5}[bis(\text{pyridine}) \text{ 3.5}]_0}{k'_{3.1} - k'_{3.5}} [e^{-k'_{3.5}t} - e^{-k'_{3.1}t}]$$

Equation 3.6.5. Integrated rate expression showing that the concentration of the generated monobenzylated DTE **3.1** with time is the difference of two exponentials.

$$[\text{dibenzylated DTE } \mathbf{3.3}]_t = [\text{bis(pyridine) } \mathbf{3.5}]_0 \left\{ 1 - \frac{1}{k'_{3.1} - k'_{3.5}} \left[k'_{3.1} e^{-k'_{3.5}t} - k'_{3.5} e^{-k'_{3.1}t} \right] \right\}$$

Equation 3.6.6. Integrated rate expression for the concentration of the dibenzylated DTE **3.3** with time.

Treatment of the data using a non-linear least squares regression analysis (GraphPad Prism Software) of the three integrated expressions, shown in Equations 3.6.4, 3.6.5 and 3.6.6, made it possible to determine the apparent *pseudo*-first-order rate constants $k'_{3.5}$ and $k'_{3.1}$. The values for $k'_{3.5}$ are listed in Table 3.6.1 while the values for $k'_{3.1}$ are listed in Table 3.6.2.

Table 3.6.1. Apparent *pseudo*-first-order rate constant, $k'_{3.5}$, for the reaction of *bis*(pyridine) **3.5** with an excess of bromobenzyl bromide at 22 °C.

Apparent <i>pseudo</i> -first-order rate constant $k'_{3.5}$ ($\times 10^{-4} \text{ sec}^{-1}$) ^a			
(1)	(2)	(3)	mean ($\bar{k}'_{3.5}$) ^b
1.2 ± 0.1	1.2 ± 0.1	1.1 ± 0.1	1.2 ± 0.1

^a The apparent *pseudo*-first-order rate constants in columns (1), (2) and (3) were obtained from the non-linear least-squares fit to the integrated rate expressions in Equations 3.6.4, 3.6.5 and 3.6.6 using GraphPad Prism software. The uncertainty shown in columns (1), (2) and (3) is based on the standard deviation from the regression analysis. ^b The uncertainty in the average apparent *pseudo*-first-order rate constant, $\bar{k}'_{3.5}$, corresponds to the standard deviation of the values in columns (1), (2) and (3) from the mean value.

Comparison of the average value of the apparent *pseudo*-first-order rate constants $\bar{k}'_{3.5}$ and $\bar{k}'_{3.1}$ (corresponding to the rates of reaction of the *bis*(pyridine) **3.5** and the monobenzylated DTE **3.1**, respectively) revealed that the pyridine in the *bis*(pyridine) **3.5** reacted about 2.1 times faster than the pyridine in the monobenzylated DTE **3.1**. This result supports the initial arguments that through-space interactions between the pyridine

'A' and the pyridinium 'B' in the generated monobenzylated DTE **3.1** contribute to slowing down its reaction to form the dibenzylated product **3.3**.

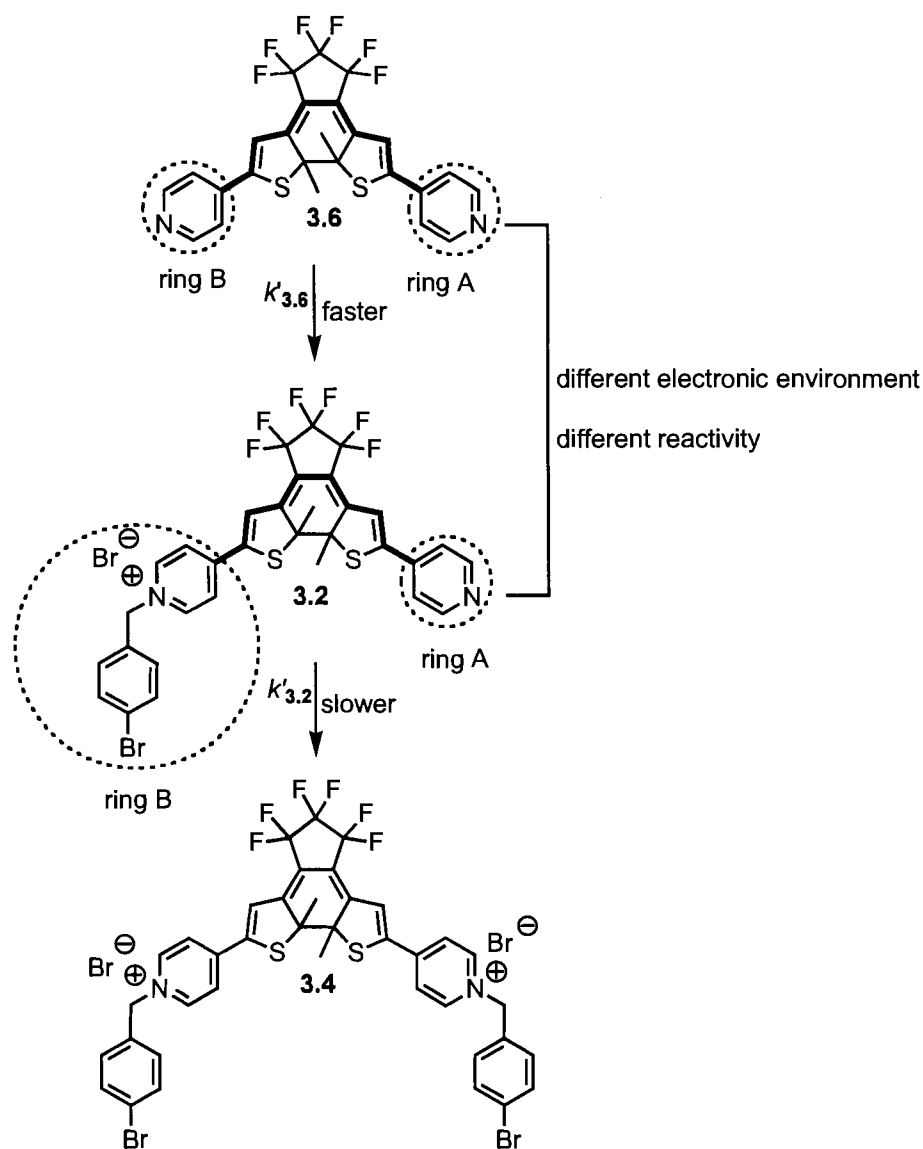
Table 3.6.2. Apparent *pseudo*-first-order rate constant, $k'_{3.1}$, corresponding to the rate of reaction of the monobenzylated DTE **3.1** with an excess of 4-bromobenzyl bromide at 22 °C.

Apparent <i>pseudo</i> -first-order rate constant $k'_{3.1}$ ($\times 10^{-5} \text{ sec}^{-1}$) ^a		
(1)	(2)	mean ($\bar{k}'_{3.1}$) ^b
5.2 \pm 0.1	5.6 \pm 0.1	5.4 \pm 0.3

^a The apparent *pseudo*-first-order rate constants in columns (1) and (2) were obtained from the non-linear least-squares fit to the corresponding integrated rate expressions in Equations 3.6.5 and 3.6.6 using GraphPad Prism software. The uncertainty shown in columns (1) and (2) is based on the standard deviation from the regression analysis. ^b The uncertainty in the average apparent *pseudo*-first-order rate constant, $\bar{k}'_{3.1}$, corresponds to the standard deviation of the values in columns (1) and (2) from the mean value.

3.6.3 Reactivity of the Ring-Closed Isomer of the *Bis*(pyridine) **3.6**

In the case of the ring-closed forms, the two thiophene rings in both the *bis*(pyridine) **3.6** and the monocation **3.2** are in electronic communication owing to the linear π -conjugated pathway running along the backbone of the DTE (shown in bold in Scheme 3.6.2). This allows through-bond communication between ring 'A' and ring 'B' such that the electronic environment and the nucleophilicity of the pyridine 'A' can be expected to be different when the ring 'B' is a pyridine [*bis*(pyridine) **3.6**] and when the ring 'B' is an electron-deficient pyridinium group (monocation **3.2**). Thus, the *bis*(pyridine) **3.6** is expected to react faster than the monobenzylated cation **3.2** giving rise to different apparent *pseudo*-first-order rate constants for $k'_{3.6}$ and $k'_{3.2}$.



Scheme 3.6.2. Consecutive *pseudo*-first-order sequence for the ring-closed isomer **3.6** leading to the formation of the monoalkylated product **3.2** and the dialkylated product **3.4**. The electronic environment and the nucleophilicity of the pyridine 'A' can be expected to be different when the ring 'B' is a pyridine (*bis*(pyridine) **3.6**) and when the ring 'B' is an electron-deficient pyridinium group (monobenzylated DTE **3.2**) due to the electronic communication along the DTE backbone. Thus, the *bis*(pyridine) **3.6** is expected to react faster than the monobenzylated cation **3.2**.

A sample of the ring-closed form (**3.6**) of the *bis*(pyridine) was prepared by transferring a known volume (0.70 mL) of a stock solution (4.6×10^{-3} M) of the *bis*(pyridine) **3.5** in CD_3CN into an NMR tube and irradiating the sample with 313 nm light until 98 % of the ring-closed form was observed by ^1H NMR spectroscopy at the

PSS, as already discussed in *Section 2.6.5*. Without attempting to isolate the pure ring-closed form **3.6**, the solution was subjected to an excess of 4-bromobenzyl bromide (1.2×10^{-1} M, 27 molar equiv). The progress of the reaction at 22 °C was assessed by ^1H NMR spectroscopy.

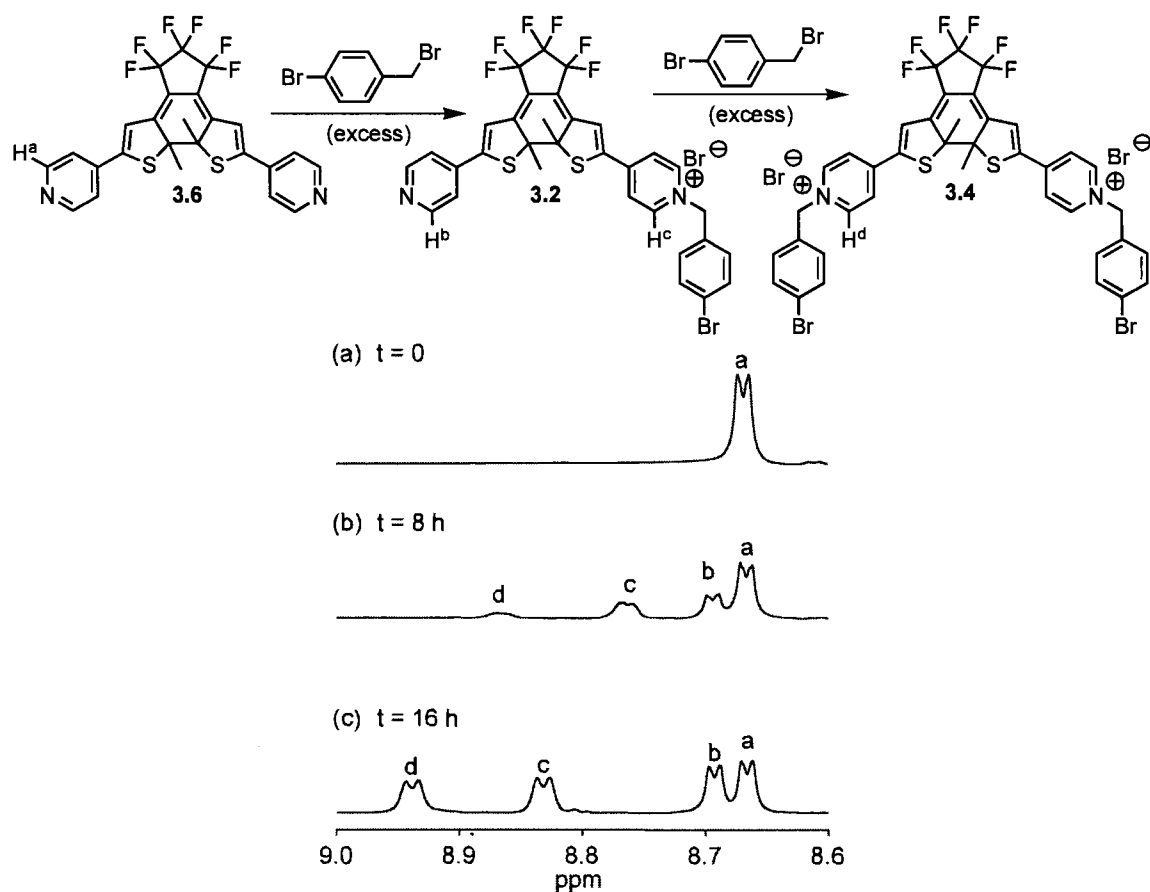


Figure 3.6.3. Partial ^1H NMR spectra (600 MHz, CD_3CN) showing the aromatic region of a solution (4.6×10^{-3} M) of the ring-closed isomer **3.6** in CD_3CN (a) before, (b) 8 h after, and (c) 16 h after adding an excess of 4-bromobenzyl bromide (1.2×10^{-1} M). The mole fractions ($\chi_{3.6}$, $\chi_{3.2}$ and $\chi_{3.4}$) of the *bis*(pyridine) **3.6**, the monoalkylated DTE **3.2** and the dialkylated DTE **3.4** were obtained using the integral values for peaks 'a', 'b', 'c' and 'd'.

The aromatic region of the *bis*(pyridine) **3.6** has a four-proton doublet at 8.67 ppm (peak 'a') that corresponds to the α -protons of the two pyridines. Formation of the monobenzylated DTE **3.2** was accompanied by the appearance of a two-proton doublet

(peak 'c'), which can be attributed to the α -protons of the pyridinium group, while the two-proton signal corresponding to the α -protons of the unreacted pyridine (peak 'b') is shifted slightly downfield compared to the α -protons of the *bis*(pyridine) **3.6**. Reaction of the monocation **3.2** with 4-bromobenzyl bromide generated the dibenzylated product **3.4** with a four-proton signal (peak 'd') that can be attributed to the α -protons of the pyridinium groups (Figure 3.6.3). Thus, the mole fractions $\chi_{3.6}$, $\chi_{3.2}$ and $\chi_{3.4}$ (corresponding to the *bis*(pyridine) **3.6**, the monocation **3.2**, and the dibenzylated DTE **3.4** respectively) were obtained using the integral values for 'a', 'b', 'c' and 'd' as shown in Equations 3.6.7, 3.6.8, and 3.6.9.

$$\chi_{3.6} = \frac{(a + b) - c}{(a + b) + c + d}$$

Equation 3.6.7. Relating the mole fraction of *bis*(pyridine) **3.6** to the peak integrals 'a', 'b', 'c' and 'd'.

$$\chi_{3.2} = \frac{2c}{(a + b) + c + d}$$

Equation 3.6.8. Relating the mole fraction of the monocation **3.2** to the peak integrals 'a', 'b', 'c' and 'd'.

$$\chi_{3.4} = \frac{d}{(a + b) + c + d}$$

Equation 3.6.9. Relating the mole fraction of the dibenzylated *bis*(pyridinium) **3.4** to the peak integrals 'a', 'b', 'c' and 'd'.

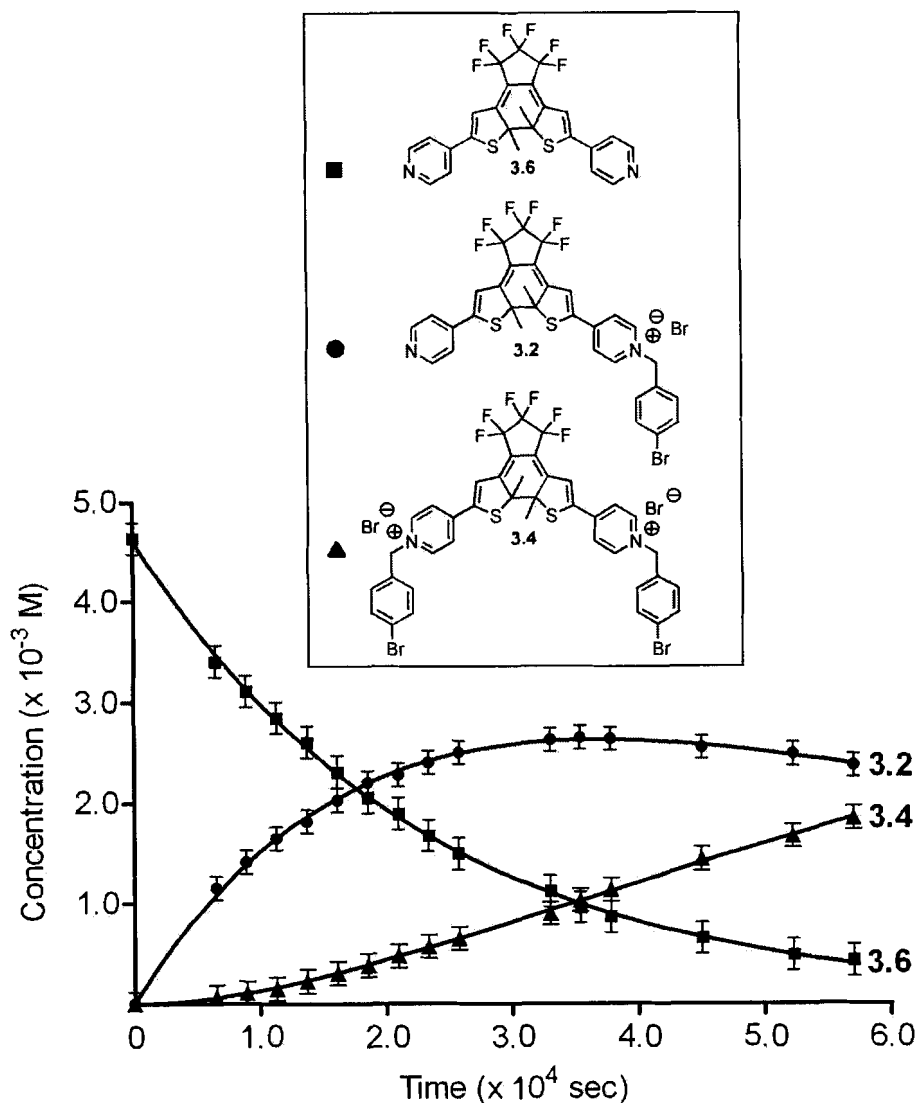


Figure 3.6.4. Plots of the concentration of the *bis*(pyridine) **3.6**, the monocation **3.2**, and the dication **3.4** against time consistent with a consecutive *pseudo*-first-order trend. The concentration of the *bis*(pyridine) **3.6** shows the predicted exponential decay with time indicative of a *pseudo*-first-order trend. The shape of the graph for the monobenzylated DTE **3.2** is consistent with a system in which the concentration builds up to a maximum and then decays with time because the concentration of the monobenzylated DTE **3.2** is dependent on both the rate of reaction of the *bis*(pyridine) **3.6** and the rate of conversion to the dibenzylated DTE **3.4**. The shape of the graph for the dibenzylated DTE **3.4** shows the characteristic initial delay in the formation of the latter, which is governed by the time required for the monocationic DTE **3.2** to be generated. The error bars represent the experimental error, which was based on a 2% integration error estimate from 9 repeated NMR integrations.

These studies were carried out in the absence of an internal standard because the ^1H NMR spectra of the *bis*(pyridine) **3.6**, the monoalkylated DTE **3.2** and the dialkylated

DTE 3.4 showed no apparent signs of degradation during the course of the reaction. With the mole fractions in hand, it was possible to monitor the decrease in the concentration of the *bis*(pyridine) 3.6, the formation and disappearance of the monobenzylated DTE 3.2, and the formation of the dibenzylated DTE 3.4 as the reaction proceeded. The plots of the relative concentrations of 3.6, 3.2, and 3.4 against time, shown in Figure 3.6.4, are consistent with a consecutive *pseudo*-first-order type of system.

Using the equations described in Section 3.5.1 for consecutive first-order reactions, the exponential expression for the concentration of the *bis*(pyridine) 3.6 and the biexponential expressions for the concentration of the monocation 3.2 and the dication 3.4 are shown in Equations 3.6.10, 3.6.11 and 3.6.12 where $[bis(\text{pyridine})\ 3.6]_t$, $[\text{monobenzylated DTE } 3.2]_t$ and $[\text{dibenzylated DTE } 3.4]_t$ refer to the respective concentrations at time t while $[bis(\text{pyridine})\ 3.6]_0$ refers to the initial concentration of the *bis*(pyridine) 3.6 before the addition of the 4-bromobenzyl bromide.

$$[bis(\text{pyridine})\ 3.6]_t = [bis(\text{pyridine})\ 3.6]_0 e^{-k'_{3.6}t}$$

Equation 3.6.10. Integrated rate expressions for the exponential decrease in the concentration of the *bis*(pyridine) 3.6 with time in the presence of an excess of 4-bromobenzyl bromide.

$$[\text{monobenzylated DTE } 3.2]_t = \frac{k'_{3.6}[bis(\text{pyridine})\ 3.6]_0}{k'_{3.2} - k'_{3.6}} [e^{-k'_{3.6}t} - e^{-k'_{3.2}t}]$$

Equation 3.6.11. Integrated rate expression showing that the concentration of the generated monobenzylated DTE 3.2 with time is the difference of two exponentials.

$$[\text{dibenzylated DTE } 3.4]_t = [bis(\text{pyridine})\ 3.6]_0 \left\{ 1 - \frac{1}{k'_{3.2} - k'_{3.6}} [k'_{3.2}e^{-k'_{3.6}t} - k'_{3.6}e^{-k'_{3.2}t}] \right\}$$

Equation 3.6.12. Integrated rate expression for the concentration of the dibenzylated DTE 3.4 with time.

Treatment of the data using a non-linear least squares regression analysis (GraphPad Prism Software) of the three integrated expressions, shown in Equation 3.6.10, 3.6.11 and 3.6.12, made it possible to determine the apparent *pseudo*-first-order rate constants $k'_{3,6}$ and $k'_{3,2}$. The values for $k'_{3,6}$ are listed in Table 3.6.3 while the values for $k'_{3,2}$ are listed in Table 3.6.4.

Table 3.6.3. Apparent *pseudo*-first-order rate constant, $k'_{3,6}$, for the reaction of the *bis*(pyridine) 3.6 with an excess of bromobenzylbromide at 22 °C.

Apparent <i>pseudo</i> -first-order rate constant $k'_{3,6}$ ($\times 10^{-5} \text{ sec}^{-1}$) ^a			
(1)	(2)	(3)	mean ($\bar{k}'_{3,6}$) ^b
4.4 ± 0.1	4.4 ± 0.1	5.0 ± 0.3	4.6 ± 0.3

^a The apparent *pseudo*-first-order rate constants in columns (1), (2) and (3) were obtained from the non-linear least-squares fit to the corresponding integrated rate expressions in Equations 3.6.10, 3.6.11 and 3.6.12 using GraphPad Prism software. The uncertainty shown in columns (1), (2) and (3) is based on the standard deviation from the regression analysis. ^b The uncertainty in the average apparent *pseudo*-first-order rate constant, $\bar{k}'_{3,6}$, corresponds to the standard deviation of the values from columns (1), (2) and (3) from the mean value.

Table 3.6.4. Apparent *pseudo*-first-order rate constant, $k'_{3,2}$, corresponding to the rate of reaction of the monobenzylated DTE **3.2** with an excess of 4-bromobenzyl bromide at 22 °C.

Apparent <i>pseudo</i> -first-order rate constant $k'_{3,2}$ ($\times 10^{-5} \text{ sec}^{-1}$) ^a		
(1)	(2)	Mean ($\bar{k}'_{3,2}$) ^b
1.6 \pm 0.1	1.4 \pm 0.1	1.5 \pm 0.1

^a The apparent *pseudo*-first-order rate constants in columns (1) and (2) were obtained from the non-linear least-squares fit to the corresponding integrated rate expressions in Equations 3.6.11 and 3.6.12, respectively using GraphPad Prism software. The uncertainty shown in columns (1) and (2) is based on the standard deviation from the regression analysis. ^b The uncertainty in the average apparent *pseudo*-first-order rate constant, $\bar{k}'_{3,2}$, corresponds to the standard deviation of the values in columns (1) and (2) from the mean value.

Comparison of the average value of the apparent *pseudo*-first-order rate constants $\bar{k}'_{3,6}$ and $\bar{k}'_{3,2}$ (corresponding to the rates of reaction of the *bis*(pyridine) **3.6** and the monobenzylated DTE **3.2**, respectively) revealed that the pyridine in the *bis*(pyridine) **3.6** reacted about 3.1 times faster than the pyridine in the monobenzylated DTE **3.2**. This result supports the initial arguments that the electronic communication between the thiophene heterocycles leads to a lowering in the nucleophilic character of the pyridine 'A' when ring 'B' is an electron-deficient group instead of a pyridine.

Comparison of the average apparent *pseudo*-first-order rate constants, listed in Table 3.6.5, of the ring-open (**3.5** and **3.1**) and the ring-closed (**3.6** and **3.2**) isomers of the *bis*(pyridine) and the monobenzylated DTE indicates that (1) both ring-open isomers (**3.5** and **3.1**) react faster with the 4-bromobenzyl bromide than both ring-closed isomers (**3.1** and **3.2**); (2) the ring-open isomer (**3.1**) of the monobenzylated DTE reacts only slightly faster than the ring-closed isomer (**3.6**) of the *bis*(pyridine) suggesting that the through-bond communication (electronic communication) between the pyridine 'A' and

the pyridine 'B' in the ring-closed isomer (3.6) of the *bis*(pyridine) lowers the reactivity of the pyridine 'A' to a greater extent than the through-space communication between the relatively electron-rich pyridine 'A' and the electron-deficient pyridinium 'B' in the ring-open isomer (3.1); and (3) the monobenzylated DTE reacts about 3.5 times faster than the ring-closed isomer (3.2) of the monobenzylated DTE and is consistent with the trend observed in *Section 3.4.7*.

Table 3.6.5. Average apparent *pseudo*-first-order rate constants corresponding to the rates of reaction of the ring-open (3.5 and 3.1) and the ring-closed (3.6 and 3.2) isomers of the *bis*(pyridine) and the monobenzylated DTE with an excess of 4-bromobenzyl bromide at 22 °C.

Apparent <i>pseudo</i> -first-order rate constant (sec ⁻¹)		
<i>bis</i> (pyridine) 3.5	$\bar{k}'_{3.5}$	$(1.2 \pm 0.1) \times 10^{-4}$
monobenzylated DTE 3.1	$\bar{k}'_{3.1}$	$(5.4 \pm 0.3) \times 10^{-5}$
<i>bis</i> (pyridine) 3.6	$\bar{k}'_{3.6}$	$(4.6 \pm 0.3) \times 10^{-5}$
monobenzylated DTE 3.2	$\bar{k}'_{3.2}$	$(1.5 \pm 0.1) \times 10^{-5}$

3.7 Conclusions

This first part of this work has demonstrated the use of the kinetic aspects of a chemical reaction (alkylation) as a probe for studying the photoinduced changes in nucleophilicity in a monobenzylated DTE. The results indicate that the free pyridine in the ring-open form 3.1 reacts about three times faster than the ring-closed form 3.2 under *pseudo*-first-order conditions. This difference in reactivity, albeit small, is attributed to

the fact that the ring-cyclization reaction creates the communication between the free pyridine and the electron-deficient pyridinium moiety and reduces its nucleophilic character. The small magnitude of the change can be ascribed to: (1) the fact that the pyridine is twisted out of coplanarity from DTE backbone in the ring-closed form **3.2**, preventing the pyridine from experiencing the full electronic effect of the pyridinium group and (2) the structural flexibility of the ring-open form **3.1**, which allows the pyridine to feel the effect of the pyridinium group through-space. This research has also shown that the same trend in reactivity prevails if a solution of the ring-open isomer **3.1** is subjected to a series of ring-opening and ring-closing cycles under *pseudo*-first-order conditions. The possibility of turning reactions “on” and “off” using light has potential applications in catalysis and although this work has clearly shown that this level of control has not been achieved by this DTE system, the fact there is still a “higher” and “lower” type of control over the alkylation reaction makes it noteworthy to investigate whether there is a measurable difference in the extent to which the ring-open and the ring-closed isomers can influence an actual reaction when used as potential nucleophilic catalysts. This research will be discussed in *Chapter 4*.

The second part of this work has demonstrated the use of consecutive *pseudo*-first-order kinetics to probe the differences in reactivity between the ring-open (**3.5** and **3.1**) and the ring-closed (**3.6** and **3.2**) isomers of the *bis*(pyridine) and the monobenzylated DTE to better understand the through-bond and the through-space effects of having (1) two pyridines and (2) a pyridine and an electron-deficient pyridinium at the external positions of the DTE backbone. The results suggest that the through-bond communication between (1) the pyridine and the pyridinium of the

monobenzylated DTE **3.2** and (2) the two pyridine groups of the *bis*(pyridine) **3.6** lowers the reactivity of the pyridine nitrogen to a higher extent than the through-space interaction between the pyridine and the pyridinium in the monobenzylated DTE **3.1**.

3.8 Future Work

The development of a photoresponsive DTE system capable of turning reactions ‘on’ and ‘off’ is still at a stage of basic research. The presented research shows that the chosen DTE system can only achieve a “higher” and “lower” type of control over the alkylation reaction, which is consistent with the small magnitude of the change observed when the same system was used to photomodulate coordination chemistry in *Chapter 2*. Some examples on ways to re-design the DTE system so as to achieve a more pronounced difference in nucleophilicity between the two isomers were addressed in *Section 2.8*.

The structural flexibility of the ring-open isomer is another factor that contributes to the small magnitude of the change between the two DTEs of the chosen system. One approach to minimize the structural flexibility of the ring-open form involves the introduction of bulky substituents at the internal positions of the thiophene rings. However, this approach may have a detrimental effect on the photochromic behaviour of the system. Irie and coworkers³⁵ have shown that replacing the methyl substituents at the internal positions of the thiophene rings with bulky isopropyl groups leads to the thermal ring-opening reaction of the ring-closed form.

3.9 Experimental

Materials. All solvents for synthesis were dried and degassed by passing them through steel columns containing activated alumina under nitrogen using a solvent purification system (MBraun). All other solvents were used as received. Solvents for NMR analysis (Cambridge Isotope Laboratories) were used as received. Column chromatography was performed using silica gel 60 (230-400 mesh) from Silicycle Inc. The 4-bromobenzyl bromide used in the ^1H NMR spectroscopic studies was purchased from Aldrich. The *bis*(pyridine) **3.5** (labelled **2.8** in *Chapter 2*) was prepared following literature procedure²⁹ as described in *Chapter 2*, while the nitrate salt of the ring-closed isomer (**3.2**) of the monobenzylated DTE (labelled **2.10** in *Chapter 2*) was prepared and characterized as described in *Chapter 2*.

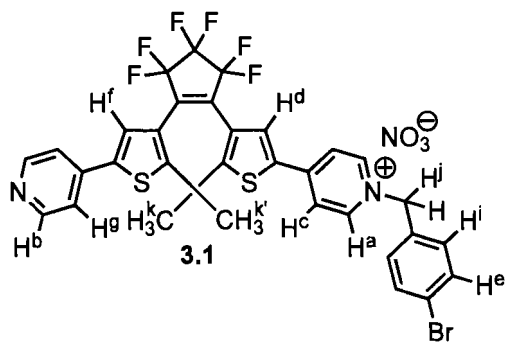
Techniques. Melting points (Mp) were measured on a Gallenkamp capillary melting point apparatus. ^1H and ^{13}C NMR characterizations were performed on a Varian Mercury 400 instrument working at 400.1 MHz for ^1H NMR and 100.6 MHz for ^{13}C NMR or a Bruker TCI 600 instrument working at 600.3 MHz for ^1H NMR and 150.5 MHz for ^{13}C NMR. The ^{13}C NMR spectra are ^1H -decoupled but ^{19}F -coupled. Assignments were confirmed using ^1H - ^1H COSY and selective 1-D NOE experiments when necessary. Chemical shifts (δ) are reported in parts per million relative to tetramethylsilane using the residual solvent peak as an internal reference. Coupling constants (J) are reported in Hertz. Relaxation measurements (T_1) were performed on the Bruker TCI 600 instrument, with the temperature set to 22°C and the values are reported in seconds. FT-IR measurements were performed using a Perkin Elmer 599B IR spectrophotometer. UV-

Vis measurements were performed using a Varian Cary 300 Bio spectrophotometer. Low resolution mass spectrometry (LRMS) measurements were performed using a matrix assisted laser desorption/ionization source (MALDI) using a PerSeptive Biosystems Voyager-DE instrument and the MALDI-TOF mass spectra were obtained using 2,5-hydroxybenzoic acid as the matrix. Microanalyses (Anal.) were performed on a Carlo Erba Model 1106 CHN analyzer.

Fitting of data. Linear least squares regression analysis of the data for (1) the independent reaction of the ring-open and the ring-closed isomers of the monobenzylated DTE (3.1 and 3.2) with an excess of the 4-bromobenzyl bromide and (2) the *in situ* reaction of both the ring-open and the ring-closed isomers of the monobenzylated DTE (3.1 and 3.2) with an excess of the 4-bromobenzyl bromide were completed using the commercially available Excel Data Analysis Tool Package. Non-linear least squares regression analysis of the data for the reaction of both the ring-open (3.5) and the ring-closed (3.6) isomers of the *bis*(pyridine) with an excess of the 4-bromobenzyl bromide were completed using a free trial version of GraphPad Prism Software.

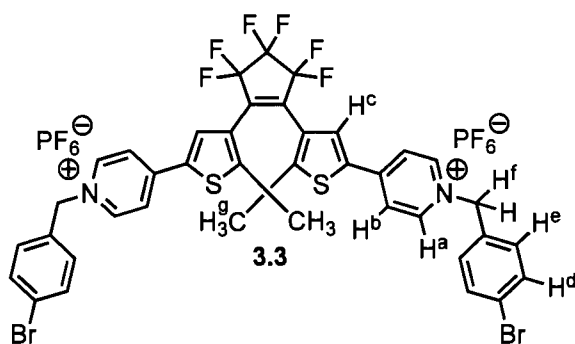
Photochemistry. Standard hand-held lamps used for visualizing TLC plates (Spectroline E-series, $470 \mu\text{W cm}^{-2}$) were used to carry out the ring-closing reactions. A 313 nm light source was used for the *bis*(pyridine) 3.5 and a 365 nm light source was used for the monobenzylated *bis*(pyridinium) 3.1 and the dibenzylated *bis*(pyridinium) 3.3. The ring-opening reactions of the *bis*(pyridine) 3.6, the monobenzylated *bis*(pyridinium) 3.2 and

the dibenzylated *bis*(pyridinium) **3.4** were carried out using the light of a 150 W tungsten source that was passed through a 490 nm cut-off filter to eliminate higher energy light.



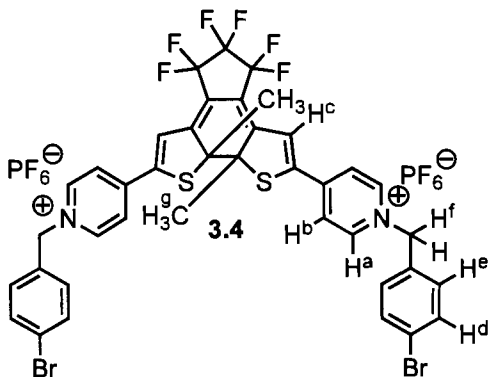
Photochemical synthesis of the nitrate salt of the ring-open isomer (3.1) of the monobenzylated DTE. The nitrate salt (previously synthesized, characterized and labelled **2.10** in *Chapter 2*) of the ring-closed isomer (**3.2**) of the monobenzylated DTE (29 mg, 38 μmol) was dissolved in anhydrous CH_3CN (15 mL) and the greenish blue solution was irradiated with light of wavelengths greater than 490 nm until a colourless solution was observed. Aliquots (2 mL) of the reaction mixture were removed via a pipette, concentrated to dryness *in vacuo*, and redissolved in CD_3CN and monitored by ^1H NMR spectroscopy until complete disappearance of the peaks corresponding to the ring-closed isomer **3.2** (methine peaks of the thiophene rings at 7.30 and 7.06 ppm) was observed at the PSS. The solvent was evaporated to dryness yielding the nitrate salt of the ring-open monobenzylated DTE **3.1** (28 mg, 97%) as an off-white solid. ^1H NMR (CD_3CN , 500 MHz): δ 8.60 (H^a , d, 2H, $J = 7.0$ Hz), 8.57 (H^b , d, 2H, $J = 6.0$ Hz), 8.06 (H^c , d, 2H, $J = 7.0$ Hz), 8.00 (H^d , s, 1H), 7.65 (H^e , d, 2H, $J = 8.5$ Hz), 7.62 (H^f , s, 1H), 7.51 (H^g , d, 2H, $J = 6.0$ Hz), 7.36 (H^i , d, 2H, $J = 8.5$ Hz), 5.69 (H^j , s, 2H), 2.11 (H^k , s, 3H), 2.04 ($\text{H}^{k'}$, s, 3H). ^{13}C NMR (CD_3CN , 150 MHz): δ 151.2, 150.7, 148.9, 145.7, 145.3,

145.2, 140.7, 140.3, 136.1, 134.0, 133.1, 132.7, 132.2, 127.9, 126.6, 126.5, 126.4, 126.3, 124.2, 123.7, 62.8, 15.3, 15.0 (23 of 26 carbons found). UV/Vis (CH₃CN): λ_{max} / nm (log $\epsilon/M^{-1} \text{ cm}^{-1}$) 356 (4.37).



Synthesis of the *bis*(hexafluorophosphate) salt of 1,2-*bis*(2'-methyl-5'-[N-(4'''-bromobenzyl)-pyrid-4''-yl]thien-3'-yl)perfluorocyclopentene 3.3. The ring-open isomer (3.5) of the *bis*(pyridine) (25 mg, 48 μmol) was dissolved in anhydrous CH₃CN (15 mL), treated with 4-bromobenzyl bromide (13 mg, 96 μmol) and the reaction mixture was heated under reflux for 18 h under an N₂ atmosphere. The heating source was removed and the mixture was allowed to slowly cool down to room temperature. The solvent was removed *in vacuo* and the reaction mixture was sonicated with Et₂O (3 \times 10 mL) to remove any unreacted 4-bromobenzyl bromide. The product was collected by vacuum filtration, washed with Et₂O (3 \times 5 mL), and left to dry yielding the dibenzylated DTE as the bromide salt. The green solid was dissolved in the minimum amount of EtOH (1 mL) and a saturated solution of NH₄PF₆ was added. The resultant pale green precipitate was collected by vacuum filtration, washed with copious amounts of water and left to dry yielding the *bis*(hexafluorophosphate) salt of the dibenzylated DTE 3.3 (52

mg, 96%) as a very pale green solid. Mp: 230-232 °C. ^1H NMR (CD_3CN , 400 MHz): δ 8.67 (H^a , d, 4H, $J = 6.8$ Hz), 8.08 (H^b , d, 4H, $J = 6.8$ Hz), 8.00 (H^c , s, 2H), 7.64 (H^d , d, 4H, $J = 8.4$ Hz), 7.38 (H^e , d, 4H, $J = 8.4$ Hz), 5.63 (H^f , s, 4H), 2.11 (H^g , s, 6H). ^{13}C NMR (CD_3CN , 100 MHz): δ 151.7, 149.3, 145.5, 136.3, 133.3, 133.4, 132.5, 132.0, 127.7, 124.4, 123.9, 63.5, 15.4 (13 of 16 carbons found). UV/Vis (CH_3CN): λ_{max} / nm ($\log \epsilon/\text{M}^{-1}\text{cm}^{-1}$) 360 (4.59). FT-IR (KBr-cast): 3139, 1638, 1553, 1518, 1470, 1441, 1407, 1339, 1276, 1227, 1193, 1149, 1115, 1056, 988, 964, 844, 815, 748 cm^{-1} . LRMS (MALDI-TOF): m/z 691, 693 [$\mathbf{3.1}\text{-PF}_6$] $^+$ (could not find peaks corresponding to the dibenzylated DTE $\mathbf{3.3}$, but found fragmentation peaks corresponding to the monobenzylated DTE $\mathbf{3.1}$). Anal. Calcd for $\text{C}_{39}\text{H}_{28}\text{Br}_2\text{F}_6\text{N}_2\text{S}_2(\text{PF}_6)_2$: C, 40.64; H, 2.45; N, 2.43. Found: C, 40.74; H, 2.42; N, 2.23.



Photochemical synthesis of the ring-closed isomer ($\mathbf{3.4}$) of the dibenzylated DTE.

The ring-open isomer ($\mathbf{3.3}$) of the dibenzylated DTE (2 mg) was dissolved in CD_3CN (0.7 mL) and transferred into an NMR tube. The solution was irradiated with 365 nm light and monitored by ^1H NMR spectroscopy. The progress of the photocyclization was assessed by monitoring the methine peaks of the thiophene rings (8.00 ppm for the ring-open isomer $\mathbf{3.3}$ as opposed to 7.35 ppm for the ring-closed form $\mathbf{3.4}$) until the peak

corresponding to the ring-open isomer **3.3** was no longer observed at the PSS. ^1H NMR (CD_3CN , 400 MHz): δ 8.80 (H^{a} , d, 4H, $J = 6.4$ Hz), 8.12 (H^{b} , d, 4H, $J = 6.4$ Hz), 7.67 (H^{d} , d, 4H, $J = 8.0$ Hz), 7.41 (H^{e} , d, 4H, $J = 8.0$ Hz), 7.35 (H^{c} , s, 2H), 5.72 (H^{f} , s, 4H), 2.28 (H^{g} , s, 6H). UV/Vis (CH_3CN): $\lambda_{\text{max}}/\text{nm}$ ($\log \epsilon/\text{M}^{-1}\text{cm}^{-1}$) 670(4.03).

General procedure for T_1 relaxation measurements using the inversion-recovery pulse sequence.¹¹⁴

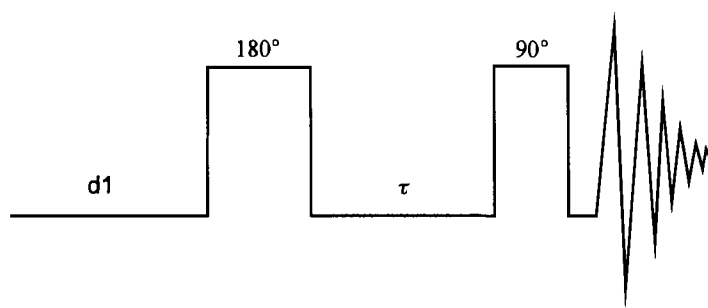


Figure 3.9.1. The inversion-recovery pulse sequence.

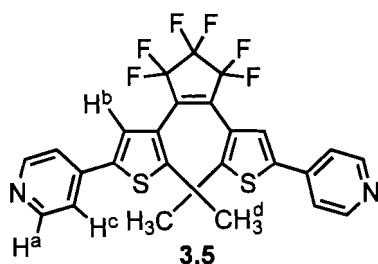
In a typical experiment (Figure 3.9.1), the pulse sequence began with a recycle delay time $d1$ that was sufficiently long to ensure that all magnetization returned to equilibrium i.e the pure z -magnetization. A 180° pulse was applied leading to the inversion of the magnetization, which was then allowed to recover to a certain amount as governed by the recovery delay time, τ . The 90° pulse then converted the residual z -magnetization into an observable transverse magnetization, which was detected during the acquisition period. In general for a very short τ , the pulse sequence is still in the $-z$ -axis (no time for relaxation back to the pure z -magnetization) when the 90° pulse is applied such that the pulse sequence is equivalent to a 270° pulse and the detected signal has full, negative intensity. If τ is very long, full T_1 relaxation occurs between the 180° and the 90° pulses and the

detected signal has full positive intensity. The T_1 value for each proton was determined by repeating the experiment with different recovery delay values for τ . Graphical treatment of the data by plotting the intensity against time (τ) gave an exponential curve indicating that the intensity I of a peak in the spectrum depends on the delay recovery time, τ , and the relaxation time, T_1 , as shown in Equation 3.9.1, where I_0 is the signal intensity as τ tends to infinity.

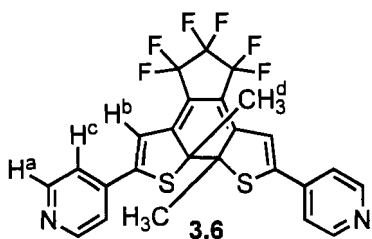
$$\frac{I}{I_0} = 1 - 2e^{-\left(\frac{\tau}{T_1}\right)}$$

Equation 3.9.1. Equation relating the intensity I of a peak to the relaxation time T_1 .

Fitting of the experimental data allowed the relaxation time, T_1 , for various protons of the ring-open (**3.1**, **3.3** and **3.5**) and the ring-closed (**3.2**, **3.4** and **3.6**) isomers of the monobenzylated DTE, the dibenzylated DTE and the *bis*(pyridine) to be determined. The plots of intensity against time and the relaxation time, T_1 , for these protons are shown in the appendix.

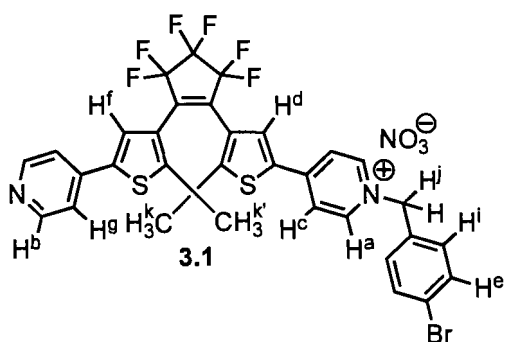


Relaxation measurements (T_1) for the ring-open isomer (3.5**) of the *bis*(pyridine).** A solution of the *bis*(pyridine) **3.5** (2 mg, 0.004 mmol) in CD_3CN (0.6 mL) was used for the relaxation measurements. T_1 : 1.43 (H^a); 2.54 (H^b); 2.52 (H^c); 1.56 (H^d).



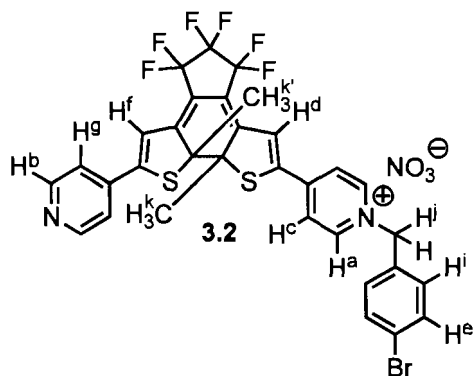
Relaxation measurements (T_1) for the ring-closed isomer (3.6) of the *bis*(pyridine).

The same sample of the *bis*(pyridine) 3.5 (2 mg, 0.004 mmol) in CD_3CN (0.6 mL) used in the previous T_1 experiment was irradiated with 313 nm light and monitored by ^1H NMR spectroscopy. The progress of the ring-closing reaction was assessed by monitoring the methine peaks of the thiophene rings (7.63 ppm for the ring-open isomer 3.5 as opposed to 7.02 ppm for the ring-closed form 3.6) until a solution containing 98% of the ring-closed form 3.6 was observed at the PSS. The T_1 measurements were carried out on that solution without any attempts to isolate the pure ring-closed isomer 3.6. T_1 : 0.98 (H^a); 2.11 (H^b); 2.18 (H^c); 0.66 (H^d).

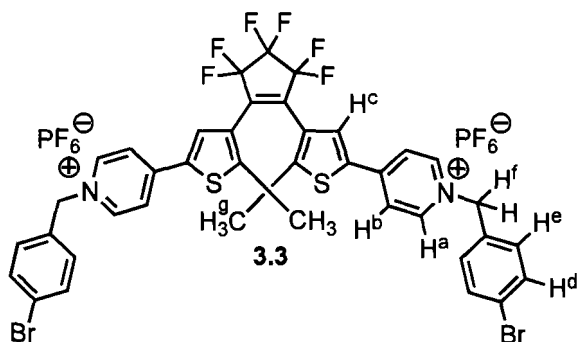


Relaxation measurements (T_1) for the ring-open isomer (3.1) of the monobenzylated

DTE. A solution of the monobenzylated DTE 3.1 (2 mg, 0.003 mmol) in CD_3CN (0.7 mL) was used for the relaxation measurements. T_1 : 1.15 (H^a); 1.15 (H^b); 1.58 (H^c); 1.47 (H^d); 2.89 (H^i); 0.82 (H^j); 1.06 (H^k); 1.39 (H^k).

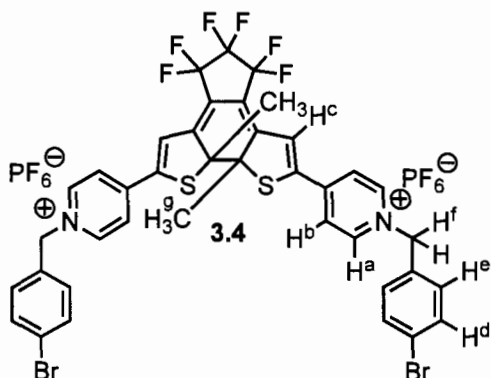


Relaxation measurements (T_1) for the ring-closed isomer (3.2) of the monobenzylated DTE. The same sample of the monobenzylated DTE **3.1** (2 mg, 0.003 mmol) in CD_3CN (0.7 mL) used in the previous T_1 experiment was irradiated with 365 nm light and monitored by ^1H NMR spectroscopy. The progress of the ring-closing reaction was assessed by monitoring the methine peaks of the thiophene rings (8.00 and 7.62 ppm for the ring-open isomer **3.1** as opposed to 7.30 and 7.06 ppm for the ring-closed form **3.2**) until the peaks corresponding to the ring-open isomer **3.1** were no longer observed at the PSS. T_1 : 1.01 (H^a); 1.01 (H^b); 1.31 (H^c); 2.71 (H^i); 1.39 (H^d); 0.99 (H^f); 0.71 (H^j); 0.50 (H^k); 0.50 ($\text{H}^{k'}$).



Relaxation measurements (T_1) for the ring-open isomer (3.3) of the dibenzylated DTE. A solution of the dibenzylated DTE **3.3** (2 mg, 0.002 mmol) in CD_3CN (0.7 mL)

was used for the relaxation measurements. T_1 : 1.59 (H^a); 1.80 (H^b); 1.59 (H^c); 4.11 (H^d); 3.40 (H^e); 0.81 (H^f); 1.06 (H^g).



Relaxation measurement (T_1) for the ring-closed isomer (3.4) of the dibenzylated DTE. The same sample of the dibenzylated DTE **3.3** (2 mg, 0.002 mmol) in CD_3CN (0.7 mL) used in the previous T_1 experiment was irradiated with 365 nm light and monitored by 1H NMR spectroscopy. The progress of the ring-closing reaction was assessed by monitoring the methine peaks of the thiophene rings (8.00 ppm for the ring-open isomer **3.3** as opposed to 7.35 ppm for the ring-closed form **3.4**) until the peak corresponding to the ring-closed isomer **3.4** was no longer observed at the PSS. T_1 : 1.60 (H^a); 1.78 (H^b); 4.22 (H^d); 3.35 (H^e); 1.56 (H^c); 0.80 (H^f); 0.77 (H^g).

Choice of appropriate reaction conditions to ensure *pseudo*-first-order conditions. A solution of the ring-open isomer (**3.1**) of the monoalkylated DTE (1.0 mg, 1.3 μ mol) in CD_3CN (0.70 mL) was prepared and transferred into an NMR tube (via a pipette). The solution was treated with an excess of 4-bromobenzyl bromide (13 mg, 52 μ mol), making note of the time, and the sample was immediately placed in the NMR instrument, which

was already set to 22°C. The sample was kept in the probe throughout the reaction and the progress of the reaction was monitored by ^1H NMR spectroscopy over a period of 24 h. By measuring the relative integrals of the areas under the peaks corresponding to the starting monobenzylated DTE **3.1** and the dibenzylated DTE **3.3** generated, the mole fractions $\chi_{3,1}$ and $\chi_{3,3}$ (corresponding to the monobenzylated DTE **3.1** and the dibenzylated DTE **3.3** respectively) were obtained. From these values, a plot of the natural log of the concentration of **3.1** against time was obtained allowing the apparent *pseudo*-first-order rate constant, k' , to be determined using linear least squares regression analysis of the data. The alkylation reaction was repeated twice following the described procedure using (1) a solution of the ring-open isomer (**3.1**) of the monoalkylated DTE (1.5 mg, 2.0 μmol) in CD_3CN (0.70 mL) and (2) a solution of the ring-open isomer (**3.1**) of the monoalkylated DTE (2.0 mg, 2.7 μmol) in CD_3CN (0.70 mL), all the while keeping the concentration of the 4-bromobenzyl bromide (13 mg, 52 μmol , 7.3×10^{-2} M) constant. The calculated apparent *pseudo*-first-order rate constants were very similar for all three samples regardless of the initial concentration of the monobenzylated DTE **3.1** consistent with a *pseudo*-first-order pattern. The plots of the natural log of the different concentrations of the monobenzylated DTE **3.1** against time, the linear least squares regression analysis of the data, and the residual plots for the three samples are shown in the appendix.

Assessment of the alkylation reaction of the ring-open isomer (3.1) of the monobenzylated DTE under *pseudo*-first-order conditions. A stock solution (2.4×10^{-3} M) of the ring-open isomer (3.1) of the monoalkylated DTE (12 mg, 16 μmol) in CD_3CN (6.5 mL) was prepared and a known volume of that solution (0.70 mL, 1.71 μmol) was transferred into an NMR tube (via a pipette). The solution was treated with an excess of 4-bromobenzyl bromide (13 mg, 52 μmol) making note of the time, and the sample was immediately placed in the NMR instrument, which was already set to 22°C. The sample was kept in the probe throughout the reaction and the progress of the reaction was monitored by ^1H NMR spectroscopy over a period of 24 h. By measuring the relative integrals of the areas under the peaks corresponding to the starting monobenzylated DTE 3.1 and the dibenzylated DTE 3.3 generated, the mole fractions $\chi_{3.1}$ and $\chi_{3.3}$ (corresponding to the monobenzylated DTE 3.1 and the dibenzylated DTE 3.3, respectively) were obtained. From these values, a plot of the natural log of the concentration of 3.1 against time was obtained allowing the apparent *pseudo*-first-order rate constant, $k'_{3.1}$, to be determined using linear least squares regression analysis of the data. To test the reproducibility of the results, the alkylation reaction was repeated twice following the described procedure using samples prepared from the same stock solution (2.4×10^{-3} M) of the ring-open isomer 3.1 in CD_3CN . From these values, the average apparent *pseudo*-first-order rate constant, $\overline{k'_{3.1}}$, for the alkylation reaction of the ring-open isomer (3.1) of the monobenzylated DTE was calculated to be $(2.9 \pm 0.1) \times 10^{-5} \text{ sec}^{-1}$. The plots of the natural log of the concentration of monobenzylated DTE 3.1 against time, the linear least squares regression analysis of the data, and the residual plots for the two other samples are shown in the appendix.

Assessment of the alkylation reaction of the ring-closed isomer (3.2) of the monobenzylated DTE under *pseudo*-first-order conditions. The same volume (0.70 mL, 1.71 μmol) of the stock solution (2.4×10^{-3} M) of the ring-open isomer (3.1) of the monoalkylated DTE (12 mg, 16 μmol) in CD_3CN (6.5 mL), used for the previous experiment, was transferred into an NMR tube (via a pipette). The solution was irradiated with 365 nm light until the methine peaks of the thiophene rings corresponding to the ring-open isomer 3.1 (8.00 and 7.62 ppm for the ring-open isomer 3.1 as opposed to 7.30 and 7.06 ppm for the ring-closed form 3.2) were no longer observed at the PSS, as monitored by ^1H NMR spectroscopy. The resultant dark bluish solution was treated with an excess of 4-bromobenzyl bromide (13 mg, 52 μmol) following the same procedure used for the ring-open isomer 3.1 (previous experiment) and the progress of the reaction was monitored under the same conditions for 24 h. Graphical treatment of the data by plotting the natural log of the concentration of monobenzylated DTE 3.2 against time followed by a linear least squares regression analysis of the data gave the apparent *pseudo*-first-order rate constant, $k'_{3.2}$. To test the reproducibility of the results the alkylation reaction was repeated twice following the described procedure using samples prepared from the same stock solution (2.4×10^{-3} M) of the ring-open isomer (3.1) in CD_3CN . From these values, the average apparent *pseudo*-first-order rate constant, $\overline{k'_{3.2}}$, for the alkylation reaction of the ring-closed isomer (3.2) of the monobenzylated DTE was calculated to be $(9.0 \pm 0.1) \times 10^{-6} \text{ sec}^{-1}$. The plots of the natural log of the concentration of monobenzylated DTE 3.2 against time, the linear least squares regression analysis of the data, and the residual plots for the two other samples are shown in the appendix.

***In situ* photomodulation of the alkylation reaction of the ring-open (3.1) and the ring-closed (3.2) isomers of the monobenzylated DTE under pseudo-first-order conditions.** A stock solution (2.4×10^{-3} M) of the ring-open isomer (3.1) of the monoalkylated DTE (1.8 mg, 2.4 μ mol) in CD₃CN (1.0 mL) was prepared and a known volume of that solution (0.70 mL, 1.67 μ mol) was transferred into a quartz NMR tube (via a pipette). The solution was treated with an excess of 4-bromobenzyl bromide (13 mg, 52 μ mol) following the same procedure used for the ring-open isomer 3.1 and the ring-closed isomer 3.2 (previous experiments) and the progress of the reaction was monitored under the same conditions at regular intervals of time by ¹H NMR spectroscopy. After about 3 h, the NMR tube was ejected from the NMR probe and the solution was irradiated with 365 nm light until the peaks corresponding to the ring-open reactant 3.1 (monobenzylated DTE) and the ring-open product 3.3 (dibenzylated DTE) were no longer observed at the PSS. The sample was quickly placed in the NMR probe and the progress of the reaction was monitored under the same conditions at regular intervals of time. After another 3 h, the sample was irradiated with light of wavelengths greater than 490 nm until the peaks corresponding to the ring-closed species were no longer observed at the PSS. Such *in situ* switching by alternating irradiation at 365 nm and > 490 nm over 3-hour intervals were repeated. Graphical treatment of the data in a similar fashion to the method already described for the reaction of independent solutions of the ring-open (3.1) and the ring-closed (3.2) isomers showed that the apparent rate constants for the two ring-open steps are very close in value ($k'_{(\text{step } 1)} = (3.0 \pm 0.1) \times 10^{-5}$ sec⁻¹ and $k'_{(\text{step } 2)} = (3.0 \pm 0.1) \times 10^{-5}$ sec⁻¹) and that of the two ring-closed steps are also similar ($k'_{(\text{step } 3)} = (1.0 \pm 0.1) \times 10^{-5}$ sec⁻¹ and $k'_{(\text{step } 4)} = (9.9 \pm 0.1) \times 10^{-6}$ sec⁻¹).

Assessment of the alkylation reaction of the ring-open isomer (3.5) of the bis(pyridine) under consecutive pseudo-first-order conditions. A stock solution (4.6×10^{-3} M) of the ring-open isomer (3.5) of the bis(pyridine) (5.1 mg, 9.7 μmol) in CD_3CN (2.1 mL) was prepared and a known volume of that solution (0.70 mL, 3.3 μmol) was transferred into an NMR tube (via a pipette). The solution was treated with an excess of 4-bromobenzyl bromide (22 mg, 87 μmol) following the same procedure used for the alkylation reactions of the ring-open (3.1) and the ring-closed (3.2) isomers of the monobenzylated DTE and the progress of the reaction was monitored under the same conditions for 10 h. By measuring the relative integrals of the areas under the peaks corresponding to the starting bis(pyridine) 3.5, the generated monobenzylated DTE 3.1 (as an intermediate) and the generated dibenzylated DTE 3.3, the mole fractions $\chi_{3.5}$, $\chi_{3.1}$, and $\chi_{3.3}$ (corresponding to the bis(pyridine) 3.5, the monobenzylated DTE 3.1 and the dibenzylated DTE 3.3, respectively) were obtained. From these values, a plot of the relative concentrations for all three species (3.5, 3.1 and 3.3) against time was obtained. The average apparent pseudo-first-order rate constants, $\bar{k}'_{3.5}$ ($(1.2 \pm 0.1) \times 10^{-4} \text{ sec}^{-1}$) and $\bar{k}'_{3.1}$ ($(5.4 \pm 0.2) \times 10^{-5} \text{ sec}^{-1}$), corresponding to the two consecutive pseudo-first-order alkylation steps, were obtained after non-linear regression analysis of the data.

Assessment of the alkylation reaction of the ring-closed isomer (3.6) of the bis(pyridine) under consecutive pseudo-first-order conditions. The same volume (0.70 mL, 3.3 μmol) of the stock solution (4.6×10^{-3} M) of the ring-open isomer (3.5) of the bis(pyridine) (5.1 mg, 9.7 μmol) in CD_3CN (2.1 mL), used for the previous experiment, was transferred into an NMR tube (via a pipette). The solution was irradiated with 313

nm light by monitoring the methine peaks of the thiophene rings (7.63 ppm for the ring-open isomer **3.5** as opposed to 7.02 ppm for the ring-closed form **3.6**) until a solution containing 98% of the ring-closed isomer **3.6** was observed at the PSS. Without attempting to isolate the pure ring-closed isomer **3.6**, the solution was treated with an excess of 4-bromobenzyl bromide (22 mg, 87 μmol) following the same procedure used for the ring-open isomer **3.5** (previous experiment) and the progress of the reaction was monitored under the same conditions for 17 h. Graphical treatment of the data by plotting the relative concentrations of the *bis*(pyridine) **3.6**, the monobenzylated DTE **3.2**, and the dibenzylated DTE **3.4** against time, followed by non-linear least squares regression analysis of the data, gave the average apparent *pseudo*-first-order rate constants, $\bar{k}'_{3,6}$ ($(4.6 \pm 0.3) \times 10^{-5} \text{ sec}^{-1}$) and $\bar{k}'_{3,2}$ ($(1.5 \pm 0.1) \times 10^{-5} \text{ sec}^{-1}$), corresponding to the two consecutive *pseudo*-first-order alkylation steps.

4 PHOTOMODULATION OF CATALYSIS USING DTEs

4.1 Introduction to Photoregulation of Catalysis

The possibility to photomodulate nucleophilic strength has potential applications in the design of light-activated reagents and catalysts. The ring-opening and the ring-closing reactions of DTEs influence the movement of electrons through the DTE backbone and provide a handle to photomodulate the nucleophilicity of an appropriately functionalized DTE derivative. In fact, the concept of photoregulating the nucleophilicity of a pyridine-functionalized DTE by comparing (1) the stability of the ring-open and the ring-closed forms of a monobenzylated DTE–porphyrin hybrid and (2) the rate of alkylation of the two isomers of the monobenzylated DTE was presented in *Chapter 2* and *Chapter 3*, respectively. The research discussed in this chapter shows an attempt to take advantage of this difference, although disappointingly small, in nucleophilic behaviour to demonstrate the concept of photoregulation of nucleophilic catalysis. Nucleophilic catalysis is a popular approach to accelerate a chemical reaction and has widespread applications ranging from organic chemistry to pharmaceutical industries and biochemistry.⁶³⁻⁶⁵ One of the most popular and efficient nucleophilic catalysts, that has widespread use in all the aforementioned applications, is DMAP and many research groups focus on (1) developing more efficient derivatives of DMAP and (2) finding alternative catalysts that are as effective as DMAP.^{64,67} The goal of the work presented in this chapter is merely to show the concept of controlling nucleophilic catalysis using light.

The work from the previous chapters has shown that the ring-open isomer **4.1** (labelled **3.1** in *Chapter 3*) is more nucleophilic than the ring-closed isomer **4.2** (labelled

3.2 in Chapter 3) and that the small magnitude of the difference can be ascribed to (1) the pyridine being twisted out of coplanarity from the DTE backbone in the ring-closed form **4.2** preventing the pyridine from experiencing the full electronic effect of the electron-poor pyridinium and (2) the structural flexibility of the ring-open form **4.1** preventing the pyridine from being completely insulated from the electron-deficient pyridinium. It can thus be expected that the more nucleophilic ring-open isomer **4.1** will be a better nucleophilic catalyst than the ring-closed isomer **4.2** (Figure 4.1.1).

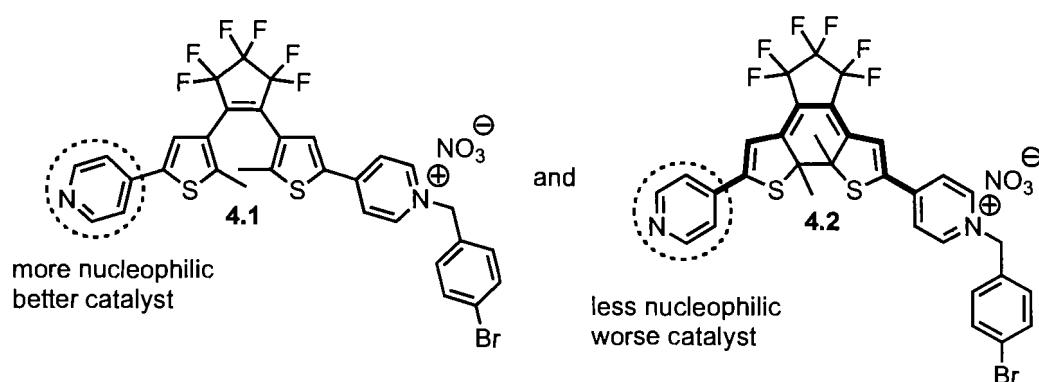
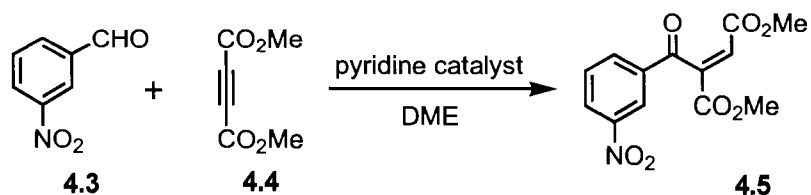


Figure 4.1.1. The more nucleophilic ring-open isomer **4.1** can be expected to act as a better catalyst than its ring-closed counterpart **4.2**.

4.2 Choice of Reaction

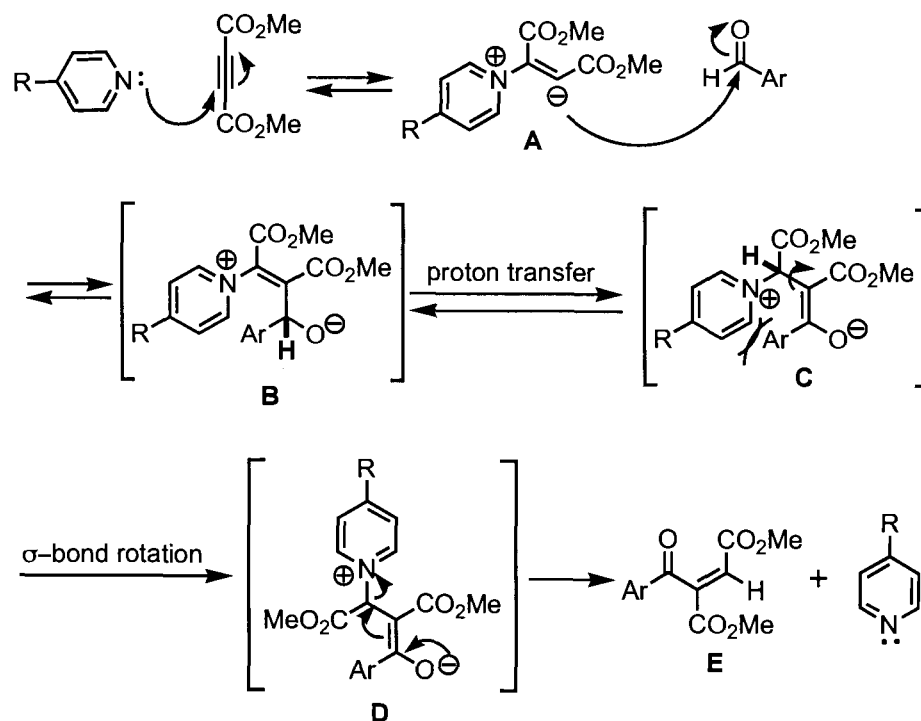
One reaction involving pyridine as a nucleophilic catalyst is the reaction of 3-nitrobenzaldehyde **4.3** with dimethylacetylene dicarboxylate (DMAD) **4.4**. This is a good reaction to illustrate the concept of photomodulation of nucleophilic catalysis using DTEs because it provides a simple model reaction and the product can be easily analyzed by ^1H NMR spectroscopy and has already been characterized in literature.^{125,126}



Equation 4.2.1. Pyridine-catalyzed addition of aldehyde **4.3** to DMAD **4.4**.

The main focus of this chapter is to (1) verify whether the ring-open isomer **4.1** and the ring-closed isomer **4.2** of the monobenzylated DTE can behave as nucleophilic catalysts in the reaction of the aldehyde **4.3** with the acetylene derivative **4.4** and (2) determine whether there is the expected difference in their ability to catalyze the reaction.

The suggested mechanism¹²⁵ for the reaction of aldehydes with DMAD, shown in Scheme 4.2.1, begins with the coordination of the ‘pyridine catalyst’ to the dimethylacetylene dicarboxylate **4.4** generating the zwitterionic species **A**. The next step involves the nucleophilic addition of species **A** to the aldehyde forming the tetrahedral intermediate **B** that undergoes a proton transfer (the hydrogen is shown in bold in species **B** and **C** in Scheme 4.2.1) to form species **C**. The steric interaction between the pyridinium moiety and the aryl group in **C** is the driving force for the σ -bond rotation to form species **D** leading to the regeneration of the ‘pyridine catalyst’ and the product **E**.



Scheme 4.2.1. Mechanism for the pyridine-catalyzed reaction of aldehydes with DMAD. Adapted from reference 125.

4.3 Results and Discussion

One approach to test whether the two DTE isomers act as nucleophilic catalysts involves (1) carrying out the reaction in the absence of any pyridine-containing compound as a background test, (2) setting up one experiment using equimolar amounts of the ‘pyridine catalyst’, the 3-nitrobenzaldehyde **4.3** and DMAD **4.4** (condition A), and (3) setting up another experiment using a smaller amount (0.2 molar equiv) of the ‘pyridine catalyst’, with respect to the 3-nitrobenzaldehyde **4.3** and DMAD **4.4** (condition B). It can be expected that in the absence of the DTE isomers **4.1** and **4.2**, no reaction will take place.

4.3.1 Assessment of the Effect of the Ring-Open (4.1) and the Ring-Closed (4.2) Isomers of the Monoalkylated DTE on the Reaction of the Aldehyde 4.3 and the Acetylenyl Derivative 4.4

The background reaction of equimolar amounts of the 3-nitrobenzaldehyde **4.3** and DMAD **4.4** in anhydrous DME in the absence of the monobenzylated DTE ligands **4.1** and **4.2** did not lead to any product formation after 2 days. This is very convenient since any changes in the extent of product formation can be directly linked to the nucleophilic character of the pyridine-containing catalyst used. The effects of adding one molar equivalent and 0.2 molar equivalents of the appropriate DTE isomer (ring-open isomer **4.1** and ring-closed isomer **4.2**) to one molar equivalent of the aldehyde **4.3** and one molar equivalent of DMAD **4.4** in anhydrous DME were evaluated under similar conditions. The extent of product formation for each reaction was assessed after 2 days by running the reaction mixture through a short plug of silica (hexanes/EtOAc = 2:1) to remove any unreacted DMAD before analyzing the ratios of the integrals of the product **4.5** to the starting aldehyde **4.3** by ^1H NMR spectroscopy. The 3-nitrobenzaldehyde **4.3** has a characteristic one-proton singlet (peak 'a') corresponding to the aldehydic proton. Reaction with the acetylenyl derivative **4.4** led to the appearance of a one-proton singlet more upfield (peak 'j') corresponding to the olefinic proton of the 'keto-fumarate' group in product **4.5**.

Analysis of the areas under the peaks corresponding to the unreacted aldehyde **4.3** and the product **4.5** indicated that 20% of the product **4.5** was observed in the presence of one molar equivalent of the ring-open form of the monobenzylated DTE **4.1**. Lowering the amount of the compound to 0.2 molar equivalent (Figure 4.3.1) led to a marked

decrease in the yield of the product **4.5** to 11%. This result indicates that the monobenzylated DTE **4.1** is acting as a nucleophilic catalyst.

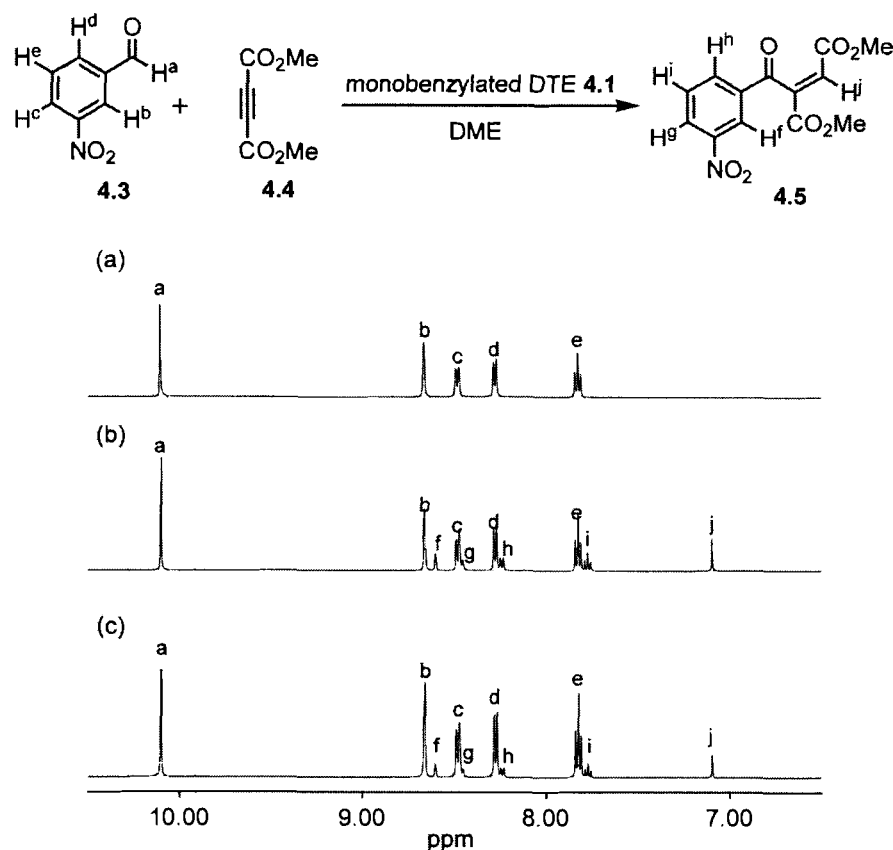


Figure 4.3.1. Partial ¹H NMR (500 MHz, CD₃CN) spectra showing the peaks corresponding to the starting 3-nitrobenzaldehyde **4.3** (a) before, (b) after the reaction with DMAD **4.4** and the ring-open isomer **4.1** under condition A, and (c) after the reaction with DMAD **4.4** and the ring-open isomer **4.1** under condition B for 2 days. The spectra were obtained after running the reaction mixture through a short plug of silica (hexanes/EtOAc = 2:1) to remove any unreacted DMAD **4.4** and the ring-open DTE **4.1**. The ratio of the product **4.5** to the unreacted aldehyde **4.3** was determined from the peak integrals 'j' and 'a'.

In the case of the ring-closed isomer (**4.2**) of the monobenzylated DTE, the extent of product formation was only 4% when one molar equivalent of the latter was used. Changing the amount of the ligand **4.2** to 0.2 molar equivalent showed no observable peaks corresponding to the product **4.5** (Figure 4.3.2). The results show that the ring-open isomer **4.1** is more effective than the ring-closed isomer **4.2** as predicted from the trend observed in the previous chapters of this thesis. However, the fact that the extent of

product formation is low in the presence of an equimolar amount of the ring-open DTE isomer **4.1** coupled with the considerable decrease observed in the yield on changing to 0.2 molar equivalent of the compound unfortunately indicates that the latter is not an appropriate nucleophilic catalyst for this particular reaction under the conditions used.

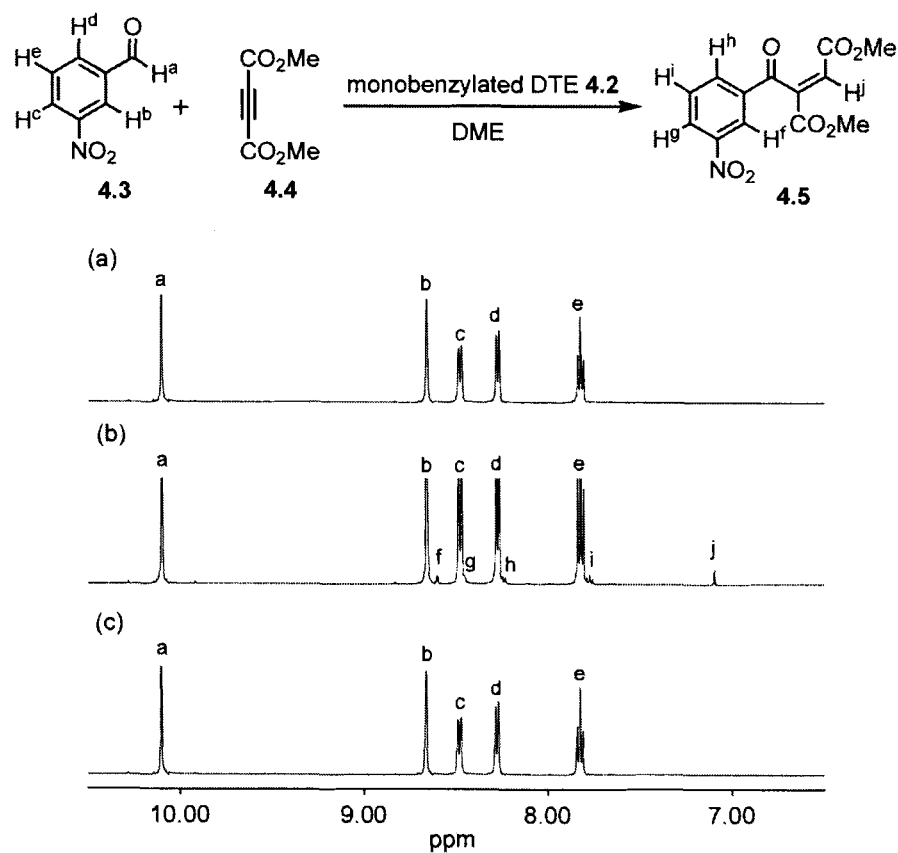


Figure 4.3.2. Partial ^1H NMR (500 MHz, CD_3CN) spectra showing the peaks corresponding to the starting 3-nitrobenzaldehyde **4.3** (a) before, (b) after the reaction with DMAD **4.4** and the ring-closed isomer **4.2** under condition A, and (c) after the reaction with DMAD **4.4** and the ring-closed isomer **4.2** under condition B for 2 days. The spectrum (c) shows that no reaction has taken place after 2 days in the presence of the ring-closed isomer **4.2**. The spectra were obtained after running the reaction mixture through a short plug of silica (hexanes/EtOAc = 2:1) to remove any unreacted DMAD **4.4** and the ring-closed DTE **4.2**. The ratio of the product **4.5** to the unreacted aldehyde **4.3** was determined from the peak integrals 'j' and 'a'.

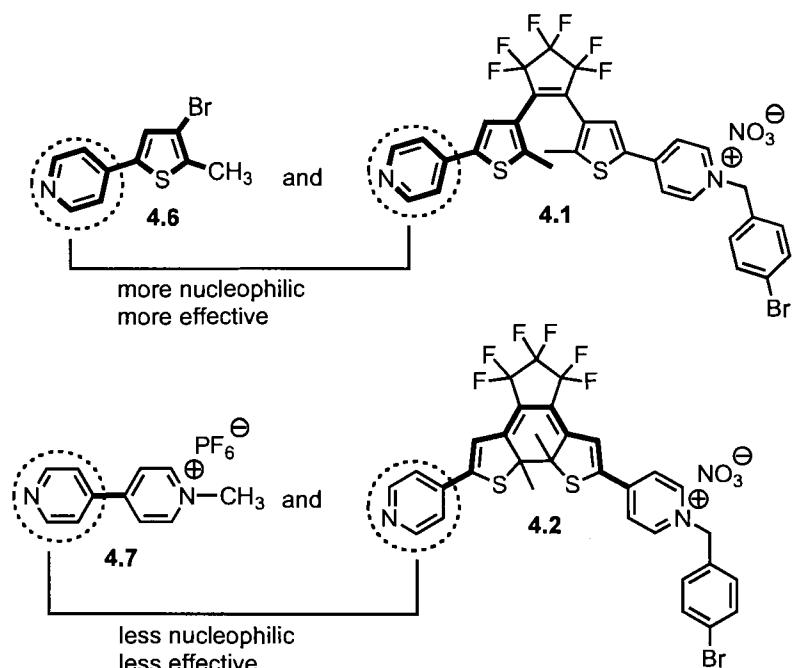


Figure 4.3.3. The pyridylthiophene **4.6**, which is a close representative of the ring-open isomer **4.1**, is expected to be more effective as a catalyst than the monomethylated bipyridinium **4.7**, which is a close analogue of the ring-closed isomer **4.2**.

In order to find out whether the low reactivity of the ring-open isomer **4.1** is due in part to the electronic effect of the perfluorinatedcyclopentenyl substituent, it seemed appropriate to repeat the same set of experiments using simpler pyridyl compounds that can act as model compounds for the DTE isomers. It has already been discussed in *Chapter 2* that the pyridylthiophene **4.6** (labelled as **2.3** in that chapter) acts as a close representative of the ring-open isomer **4.1** and that the monomethylated bipyridinium **4.7** (labelled as **2.4** in *Chapter 2*) can be used as a model compound for the ring-closed isomer **4.2** (Figure 4.3.3). The results indicated that 55% of the compound **4.5** was observed in the presence of one molar equivalent of the pyridylthiophene **4.6**. Changing the amount of compound to 0.2 molar equivalent (Figure 4.3.4) led to a significant decrease in the yield to 27%.

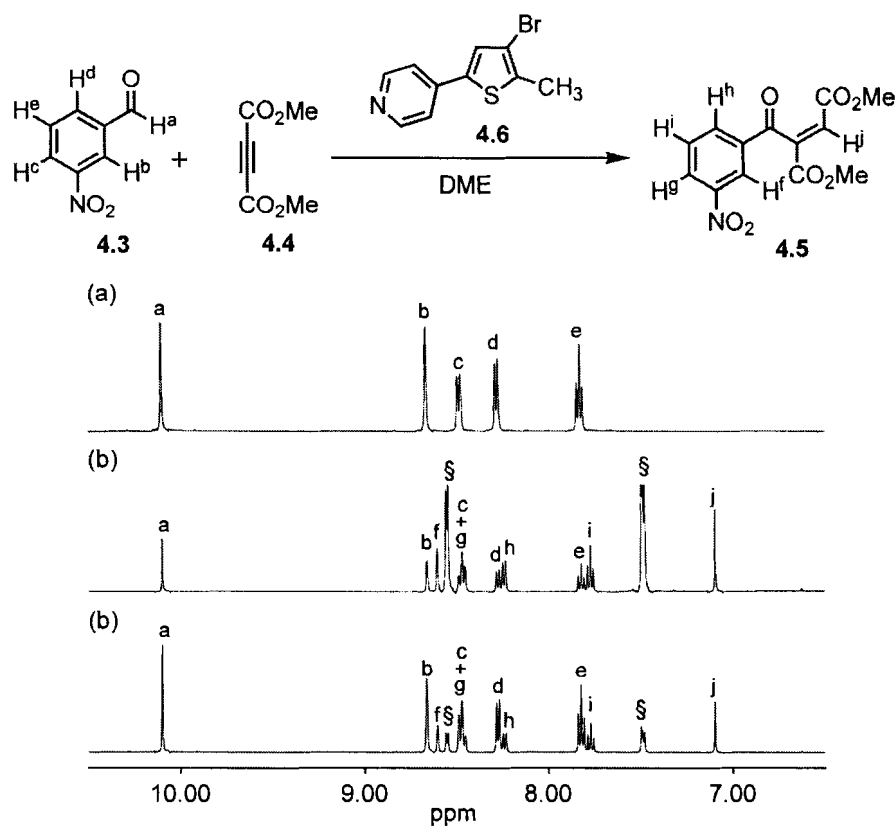


Figure 4.3.4. Partial ^1H NMR (500 MHz, CD_3CN) spectra showing the peaks corresponding to the starting 3-nitrobenzaldehyde **4.3** (a) before, (b) after the reaction with DMAD **4.4** and the pyridylthiophene **4.6** under condition A, and (c) after the reaction with DMAD **4.4** and the pyridylthiophene **4.6** under condition B for 2 days. The spectra were obtained after running the reaction mixture through a short plug of silica (hexanes/EtOAc = 2:1) to remove any unreacted DMAD **4.4**. The ratio of the product **4.5** to the unreacted aldehyde **4.3** was determined from the peak integrals 'j' and 'a'. The (§) denotes peaks corresponding to the pyridylthiophene **4.6**.

In the case of the monomethylated bipyridinium **4.7**, there was no product formation when either one molar equivalent or 0.2 molar equivalent of the pyridine was present (Figure 4.3.5). Although the results show the expected trend, where the pyridylthiophene **4.6** acts as a more effective catalyst than the monomethylated bipyridinium **4.7**, the decrease in the yield of the compound **4.5** on going from one molar equivalent to 0.2 molar equivalent of the pyridylthiophene **4.7** suggests that the model compound is not an appropriate nucleophilic catalyst for this particular reaction under the conditions used.

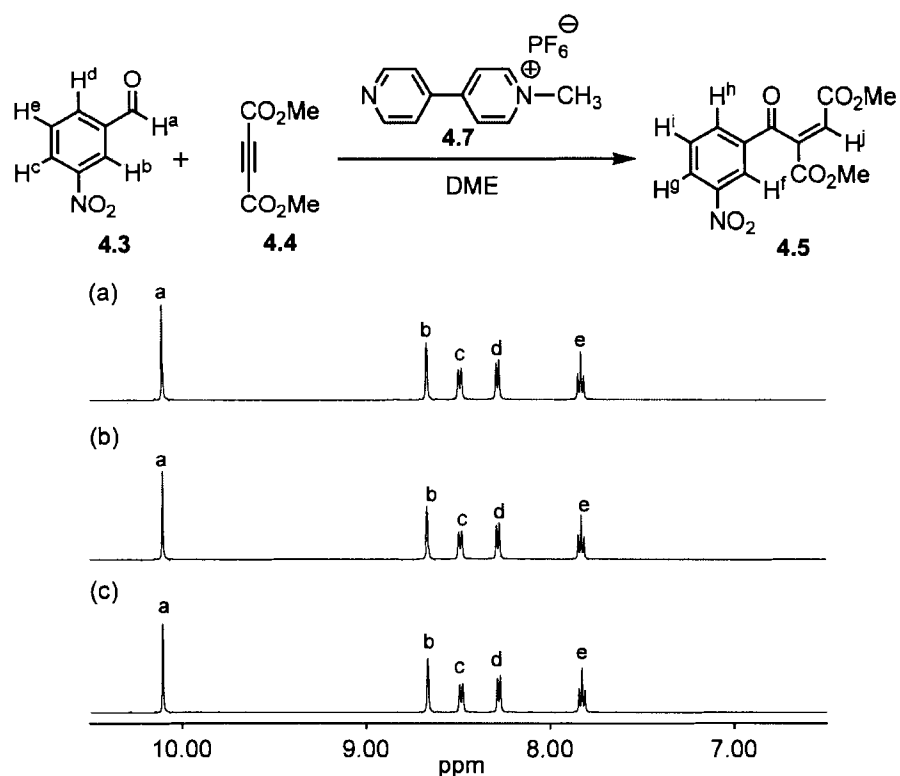
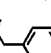
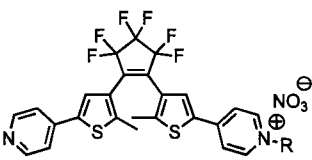
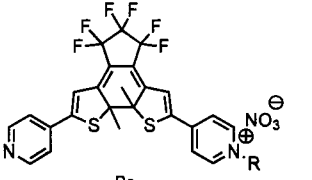
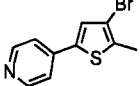
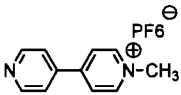


Figure 4.3.5. Partial ^1H NMR (500 MHz, CD_3CN) spectra showing the peaks corresponding to the starting 3-nitrobenzaldehyde **4.3** (a) before, (b) after the reaction with DMAD **4.4** and the monomethylated bipyridinium **4.7** under condition A, and (c) after the reaction with DMAD **4.4** and the monomethylated bipyridinium **4.7** under condition B for 2 days. The spectrum (c) shows that no reaction had taken place after 2 days in the presence of the monomethylated bipyridinium **4.7**. The spectra were obtained after running the reaction mixture through a short plug of silica (hexanes/EtOAc = 2:1) to remove any unreacted DMAD **4.4** and the monomethylated bipyridinium **4.7**.

The results suggest that the conditions of the reaction have to be changed or that an alternate reaction has to be chosen to be able to demonstrate the concept of photoregulating nucleophilic catalysis. However, the results also show that there is about 2.5 times more of the product **4.5** generated when the pyridylthiophene **4.6** is used compared to the ring-open DTE isomer **4.1**. This difference in reactivity suggests that the presence of the perfluorinated cyclopentenyl substituent plays a role in lowering the ability of the ring-open form of the monobenzylated DTE to catalyze the chosen reaction.

The yields and conditions for the reaction of the DTE isomers and their respective model compounds are listed in Table 4.3.1.

Table 4.3.1. Results of the reaction of 3-nitrobenzaldehyde **4.3** with DMAD **4.4** in the presence of the ring-open isomer **4.1** and the ring-closed isomer **4.2** of the monobenzylated DTE and their respective model compounds (pyridylthiophene **4.6** and monomethylated bipyridinium **4.7**).^a

	Catalyst (R = )	condition A ^b % yield 4.5 *	condition B ^c % yield 4.5 *
	none ^d	0	—
4.1 ^e		20	11
4.2 ^f		4	0
4.6 ^g		55	27
4.7 ^h		0	0

^a All reactions were carried out using the appropriate volumes of a stock solution (8.6×10^{-2} M) of the 3-nitrobenzaldehyde **4.3** in anhydrous DME and a stock solution (4.1×10^{-1} M) of DMAD **4.4** in anhydrous DME. The reactions were carried out in anhydrous DME at -10°C and allowed to warm up to room temperature after which the reaction mixtures were left to stir at room temperature for 2 days. ^b condition A refers to reactions performed in the presence of one molar equivalent of the appropriate pyridine-containing ligand. ^c condition B refers to reactions performed in the presence of 0.2 molar equivalent of the appropriate pyridine-containing ligand. ^d Background reaction carried out in the absence of any pyridine-containing ligands. ^e The appropriate volume (0.63 mL for condition A and 0.13 mL for condition B) of a stock solution (8.3×10^{-3} M) of the ring-open isomer **4.1** in CD_3CN was evaporated to dryness *in vacuo* and dried under high vacuum (1 mmHg) for 3 hours prior to setting up the experiment. ^f The appropriate volume (0.63 mL for condition A and 0.13 mL for condition B) of a stock solution (8.3×10^{-3} M) of the ring-open isomer **4.1** in CD_3CN was transferred into a quartz NMR tube (an additional 0.5 mL of CD_3CN was added when 0.14 mL of the stock solution was used) and the solution was irradiated with 365 nm light until complete conversion to the ring-closed isomer **4.2** was observed by ^1H NMR spectroscopy. The solvent was evaporated to dryness *in vacuo* and dried under high vacuum (1 mmHg) for 3 hours prior to setting up the experiment. ^g The appropriate volume (0.80 mL for condition A and 0.16 mL for condition B) of a stock solution (6.6×10^{-3} M) of the pyridylthiophene **4.6** in anhydrous DME was used. ^h The appropriate volume (0.75 mL for condition A and 0.15 mL for condition B) of a stock solution (7.1×10^{-3} M) of the monomethylated bipyridinium **4.7** in anhydrous DME was used. *The yield was calculated from the ratios of the integrals of the peaks corresponding to the unreacted 3-nitrobenzaldehyde **4.3** and the product **4.5** by ^1H NMR spectroscopy.

4.4 Conclusion

In this work, the use of the ring-open and the ring-closed DTE isomers as nucleophilic catalysts was attempted by looking at the reaction of 3-nitrobenzaldehyde with dimethylacetylene dicarboxylate. The results show the concept of photomodulating reactivity with the ring-open monobenzylated DTE **4.1** acting as the more efficient catalyst for the formation of product **4.5**.

4.5 Future Work

Since the work done in this chapter has shown that the presence of the perfluorinated cyclopentene substituent affects the nucleophilicity of the monobenzylated DTE, the next step is to investigate the reactivity of the non-fluorinated version **4.8** of the DTE (shown in Figure 4.5.1). Preliminary results on the ring-open isomer **4.8** and its ring-closed counterpart **4.9** indicate that there is a slight increase in the yields of the compound **4.5** as would be expected with the removal of the electron-withdrawing fluorine groups. However, this system exhibits poor fatigue resistance characteristics in solution and seems to give rise to the same photochemical side-product previously reported by Branda and Peters⁹⁹ and by other groups^{127,128} upon prolonged irradiation with 365 nm light (Figure 4.5.1).

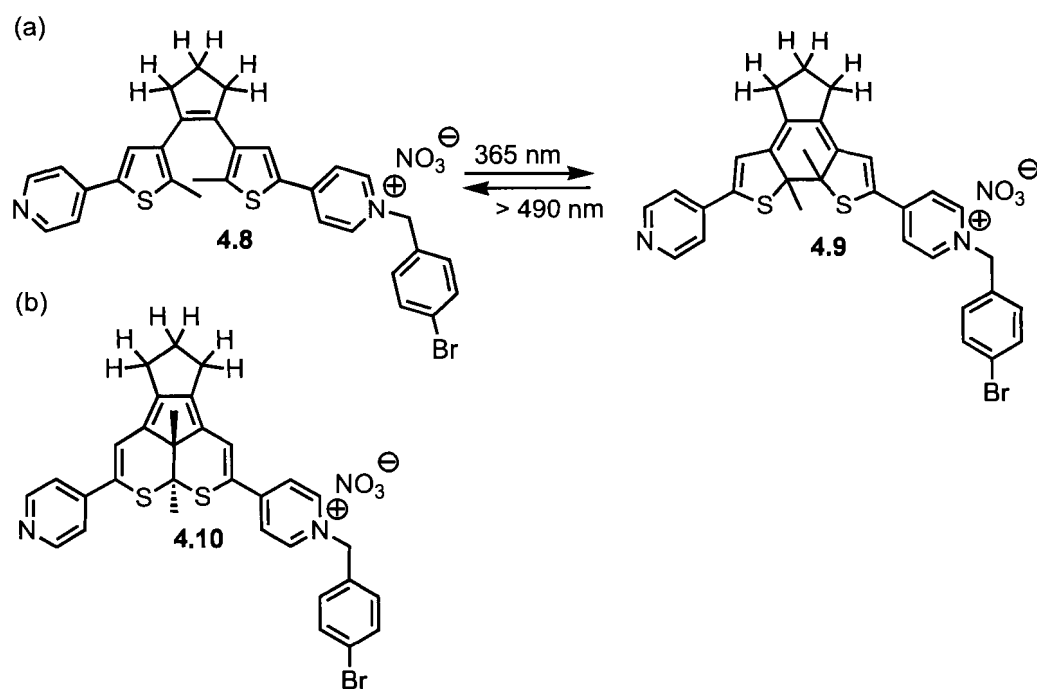


Figure 4.5.1. (a) Ring-open and ring-closed isomers of the non-fluorinated version of the monobenzylated DTE. (b) Possible structure of the photochemical side-product **4.10**.

There is much still to be done to fully exploit the ability of photoresponsive DTEs to act as nucleophilic catalysts let alone to achieve complete photoswitchable “on/off” activity. Further synthetic modifications of the DTE framework are required to achieve better differences in reactivity between the two isomers all the while making sure that the photochromic behaviour of the resulting system is maintained, as already mentioned in *Sections 2.8* and *3.8*.

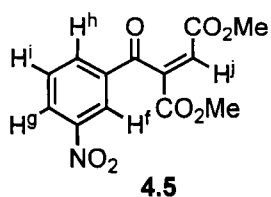
4.6 Experimental

Materials. The anhydrous DME needed for the catalysis reactions was purchased from Aldrich and used as received. All other solvents were used as received. The solvent (CD_3CN) used for the NMR analysis (Cambridge Isotope Laboratories) was used as received. Flash chromatography was performed using silica gel 60 (230-400 mesh) from

Silicycle Inc. 3-Nitrobenzaldehyde **4.3** (purchased by a previous member of the lab) and dimethylacetylene dicarboxylate (DMAD) **4.4** were purchased from Aldrich. The nitrate salt of the ring-closed isomer (**4.2**) of the monobenzylated *bis*(pyridinium) (labelled **2.10** in *Chapter 2* and **3.1** in *Chapter 3*) was prepared and characterized as described in *Chapter 2*. The 3-bromo-2-methyl-5-pyridylthiophene **4.6** (labelled **2.3** in *Chapter 2*) and the 4-monomethylated bipyridinium **4.7** (labelled **2.4** in *Chapter 2*) were prepared according to literature procedure^{29,97} as described in *Chapter 2*.

Techniques. The melting point (Mp) of the compound **4.5** was measured on a Gallenkamp capillary melting point apparatus. ¹H and ¹³C NMR characterizations were performed on a Varian Inova 500 instrument working at 499.8 MHz for ¹H NMR and 125.7 MHz for ¹³C NMR. The ¹³C NMR spectrum is ¹H-decoupled. Chemical shifts (δ) are reported in parts per million relative to tetramethylsilane using the residual solvent peak as an internal reference. Coupling constants (*J*) are reported in Hertz.

Photochemistry. Standard hand-held lamps used for visualizing TLC plates (Spectroline E-series, 470 $\mu\text{W cm}^{-2}$) were used to carry out the ring-closing reaction with a 365 nm light source being used for the monobenzylated DTE **4.1**. The ring-opening reaction of the monobenzylated DTE **4.2** was carried out using the light of a 150 W tungsten source that was passed through a 490 nm cut-off filter to eliminate higher energy light.



Synthesis of dimethyl(2*E*)-2-(3-nitrobenzoyl)but-2-enedioate 4.5.^{129,130} A solution of the dimethyl acetylenedicarboxylate **4.4** (43 μ L, 0.35 mmol) and the 3-nitrobenzaldehyde **4.3** (53 mg, 0.35 mmol) in anhydrous DME (20 mL) was cooled to -10°C under an N_2 atmosphere. Pyridine (5.7 μ L, 0.070 mmol) was added via a Hamilton syringe and after stirring at this temperature for 30 min, the cooling bath was removed and the reaction was allowed to warm to room temperature and left to stir at that temperature for 3 h. The solvent was removed *in vacuo* and the crude product was purified by flash chromatography (silica, hexanes/EtOAc = 8:1) affording the compound **4.5** (80 mg, 78%) as a shiny white solid. Mp: $96\text{--}98^{\circ}\text{C}$ (lit. $97\text{--}99^{\circ}\text{C}$). ^1H NMR (CDCl_3 , 500 MHz): δ 8.63 (H^f , s, 1H), 8.44 (H^g , d, 1H, $J = 8.0$ Hz), 8.21 (H^h , d, 1H, $J = 8.0$ Hz), 7.69 (H^i , dd, 1H, $J = 8.0$ Hz, 8.0 Hz), 7.14 (H^j , s, 1H), 3.79 (s, 3H), 3.66 (s, 3H). ^{13}C NMR (CDCl_3 , 125 MHz): δ 190.4, 164.4, 163.1, 148.7, 144.4, 137.0, 134.1, 131.7, 130.3, 128.1, 123.6, 53.7, 52.9.

General procedure for the catalysis reactions. In a typical reaction, stock solutions of the 3-nitrobenzaldehyde **4.3** (26 mg, 0.17 mmol) in anhydrous DME (2.0 mL) and dimethyl acetylenedicarboxylate **4.4** (0.10 mL, 0.81 mmol) in anhydrous DME (2.0 mL) were prepared and kept under an N_2 atmosphere. The appropriate volume of anhydrous DME was added to a reaction flask containing the appropriate ‘pyridine catalyst’ (condition A: 1 molar equiv of the ‘pyridine catalyst’ and condition B: 0.2 molar equiv of

the 'pyridine catalyst') so as to maintain a constant total volume of solvent in each reaction flask. The solution was cooled to -10°C under an N_2 atmosphere and known volumes of the stock solutions of the aldehyde **4.3** (62 μL , 5.3 μmol) and the DMAD **4.4** (13 μL , 5.3 μmol) were added (*via* Hamilton syringes). After stirring at this temperature for 30 min, the cooling bath was removed and the reaction was allowed to warm to room temperature and left to stir at that temperature for 2 days. The crude reaction mixture was allowed to run through a short plug (silica, hexanes/EtOAc = 2:1), evaporated to dryness *in vacuo* and dried under high vacuum (1 mmHg) for 1 hour. The resulting mixture was dissolved in CD_3CN (0.7 mL) and the yield of the product **4.5** was calculated by measuring the relative integrals of the areas under the peaks corresponding to the unreacted 3-nitrobenzaldehyde **4.3** and the compound **4.5** by ^1H NMR spectroscopy.

Background reaction. A mixture of the aldehyde **4.3** and DMAD **4.4** (prepared as described in the general procedure) was left to stir at room temperature in the absence of any catalyst. Analysis of the reaction mixture by ^1H NMR spectroscopy indicated that no background reaction had taken place in the absence of a 'pyridine catalyst' as anticipated.

Assessment of the effect of the ring-open isomer (4.1) of the monobenzylated DTE on the reaction of the aldehyde 4.3 and the acetylenyl derivative 4.4 (condition A). A stock solution (8.3×10^{-3} M) of the ring-open isomer **4.1** (16 mg, 21 μmol) in CD_3CN (2.5 mL) was prepared. An appropriate volume (0.63 mL) of the stock solution was transferred into a reaction flask (*via* a graduated pipette) and the solvent was evaporated to dryness *in vacuo* and left to dry under high vacuum (1 mmHg) for 3 h before being

redissolved in anhydrous DME (3.0 mL). The solution was cooled to -10°C followed by the addition of the aldehyde **4.3** and the DMAD **4.4** and the reaction was left to proceed as described in the general procedure. Analysis of the reaction mixture by ¹H NMR spectroscopy showed that 20% of the product **4.5** was formed.

Assessment of the effect of the ring-open isomer (4.1) of the monobenzylated DTE on the reaction of the aldehyde 4.3 and the acetylenyl derivative 4.4 (condition B).

Another portion (0.13 mL) of the stock solution (8.3×10^{-3} M) was transferred into a reaction flask (*via* a graduated pipette) and the solvent was evaporated to dryness *in vacuo* and left to dry under high vacuum (1 mmHg) for 3 h before being redissolved in anhydrous DME (3.0 mL). The solution was cooled to -10°C followed by the addition of the aldehyde **4.3** and the DMAD **4.4** and the reaction was left to proceed as described in the general procedure. Analysis of the reaction mixture by ¹H NMR spectroscopy showed that 11% of the product **4.5** was formed.

Assessment of the effect of the ring-closed isomer (4.2) of the monobenzylated DTE on the reaction of the aldehyde 4.3 and the acetylenyl derivative 4.4 (condition A).

An appropriate volume (0.63 mL) of the stock solution (8.3×10^{-3} M) of the ring-open isomer **4.1** in CD₃CN was transferred into a quartz NMR tube (*via* a graduated pipette) and the solution was irradiated with 365 nm light until the methine peaks of the thiophene rings (8.00 and 7.62 ppm for the ring-open isomer **3.1** as opposed to 7.30 and 7.06 ppm for the ring-closed form **3.2**) corresponding to the ring-open isomer **4.1** were no longer observed at the PSS, as monitored by ¹H NMR spectroscopy. The resulting solution was

transferred into a reaction flask and the solvent was evaporated to dryness *in vacuo* and left to dry under high vacuum (1 mmHg) for 3 h before being redissolved in anhydrous DME (3.0 mL). The solution was cooled to -10°C followed by the addition of the aldehyde **4.3** and the DMAD **4.4** and the reaction was left to proceed as described in the general procedure. Analysis of the reaction mixture by ¹H NMR spectroscopy showed that 4% of the product **4.5** was formed.

Assessment of the effect of the ring-closed isomer (4.2) of the monobenzylated DTE on the reaction of the aldehyde 4.3 and the acetylenyl derivative 4.4 (condition B).

Another portion (0.13 mL) of the stock solution (8.3×10^{-3} M) of the ring-open isomer **4.1** in CD₃CN was transferred into a quartz NMR tube (*via* a graduated pipette) and more CD₃CN (0.5 mL) was added to the solution. The sample was irradiated with 365 nm light until the peaks corresponding to the ring-open isomer **4.1** were no longer observed at the PSS, as monitored by ¹H NMR spectroscopy. The resulting solution was transferred into a reaction flask and the solvent was evaporated to dryness *in vacuo* and left to dry under high vacuum (1 mmHg) for 3 h before being redissolved in anhydrous DME (3.0 mL). The solution was cooled to -10°C followed by the addition of the aldehyde **4.3** and the DMAD **4.4** and the reaction was left to proceed as described in the general procedure. Analysis of the reaction mixture by ¹H NMR spectroscopy showed no observable peaks corresponding to the product **4.5**.

Assessment of the effect of the pyridylthiophene 4.6 on the reaction of the aldehyde 4.3 and the acetylenyl derivative 4.4 (condition A). A stock solution (6.6×10^{-3} M) of the pyridylthiophene 4.6 (5.0 mg, 0.020 mmol) in DME (3.0 mL) was prepared. An appropriate volume (0.80 mL) of the prepared stock solution (6.6×10^{-3} M) was transferred into a flame-dried reaction flask and more anhydrous DME (2.2 mL) was added. The solution was cooled to -10°C followed by the addition of the aldehyde 4.3 and the DMAD 4.4 and the reaction was left to proceed as described in the general procedure. Analysis of the reaction mixture by ^1H NMR spectroscopy showed that 55% of the product 4.5 was formed.

Assessment of the effect of the pyridylthiophene 4.6 on the reaction of the aldehyde 4.3 and the acetylenyl derivative 4.4 (condition B). Another portion (0.16 mL) of the prepared stock solution (6.6×10^{-3} M) was transferred into a flame-dried reaction flask (*via* a graduated pipette) and more anhydrous DME (2.8 mL) was added. More anhydrous DME (40 μL) was added to ensure that the total volume of solvent in the reaction flask was similar to the total volume used under condition A. The solution was cooled to -10°C followed by the addition of the aldehyde 4.3 and the DMAD 4.4 and the reaction was left to proceed as described in the general procedure. Analysis of the reaction mixture by ^1H NMR spectroscopy showed that 27% of the product 4.5 was formed.

Assessment of the effect of the monomethylated bipyridinium 4.7 on the reaction of the aldehyde 4.3 and the acetylenyl derivative 4.4 (condition A). A stock solution (7.1×10^{-3} M) of the pyridylthiophene 4.6 (5.6 mg, 18 μmol) in DME (2.5 mL) was prepared. An appropriate volume (0.75 mL) of the prepared stock solution (7.1×10^{-3} M) was transferred into a flame-dried reaction flask (*via* a graduated pipette) and more anhydrous DME (2.2 mL) was added. More anhydrous DME (50 μL) was added to ensure that the total volume of solvent in the reaction flask was similar to the total volume used in the previous experiment. The solution was cooled to -10°C followed by the addition of the aldehyde 4.3 and the DMAD 4.4 and the reaction was left to proceed as described in the general procedure. Analysis of the reaction mixture by ^1H NMR spectroscopy showed no observable peaks corresponding to the product 4.5.

Assessment of the effect of the monomethylated bipyridinium 4.7 on the reaction of the aldehyde 4.3 and the acetylenyl derivative 4.4 (condition B). Another portion (0.15 mL) of the prepared stock solution (7.1×10^{-3} M) was transferred into a flame-dried reaction flask (*via* a graduated pipette) and more anhydrous DME (2.8 mL) was added. More anhydrous DME (50 μL) was added to ensure that the total volume of solvent in the reaction flask was similar to the total volume used under condition A. The solution was cooled to -10°C followed by the addition of the aldehyde 4.3 and the DMAD 4.4 and the reaction was left to proceed as described in the general procedure. Analysis of the reaction mixture by ^1H NMR spectroscopy showed no observable peaks corresponding to the product 4.5.

5 CONCLUSIONS

The DTE backbone is well-suited to modulate chemical reactivity since the electronic differences between the ring-open and the ring-closed isomers can be used as the “on” and “off” functions to “start” and stop reactions using light and has potential applications in the design of light-activated reagents, catalysts, and biochemical reagents. These applications require systems that show measurable differences in chemical reactivity. It is well documented that the nucleophilicity of a nitrogen-containing compound is very sensitive to its electronic environment and the research presented in this thesis has focused on using the electronic differences between the ring-open and the ring-closed isomers of a pyridine-functionalized DTE to demonstrate the concept of photomodulation of nucleophilicity. The novel contribution to science lies in the fact that the work done in this thesis has shown that even though the small magnitude of the change between the two isomers does not provide the desired ‘on’ and ‘off’ level of control for this DTE system to be used in a practical setting, the nucleophilic character of a pyridine-functionalized DTE can be photomodulated. This work has helped gain further insight into the possible ways to fine-tune the electronic properties of future DTE systems to achieve more pronounced differences in nucleophilicity, the dramatic effects of structural modification on the photochromic behaviour of DTEs, and the ways to probe and measure the differences in reactivity in future systems.

The initial approach took advantage of the fact that the axial coordination to a metalloporphyrin involves a Lewis acidic–Lewis basic interaction to probe the differences in Lewis basicity between the two DTE isomers using both ^1H NMR and IR spectroscopy as diagnostic tools. The results show that the ring-open isomer is about 1.3

times more effective as a ligand than the ring-closed form. This difference in coordination ability can be attributed to a decrease in the Lewis basicity of the nitrogen of the pyridine owing to the electronic communication between the pyridine and the electron-withdrawing pyridinium, found at the external positions of the DTE backbone in the ring-closed isomer. The low selectivity can be ascribed to the fact that the pyridine is twisted out of coplanarity from the DTE backbone in the ring-closed form preventing the pyridine from experiencing the full electronic effect of the electron-withdrawing pyridinium.

The same concept was then evaluated in chemical synthesis using *pseudo*-first-order kinetics to probe the differences in the apparent rates of alkylation between the two isomers of the pyridine-functionalized DTE. The results indicate that the ring-open form reacts three times faster than the ring-closed form and is consistent with the results obtained in the axial coordination studies. This difference in reactivity is attributed to the fact that the ring-cyclization reaction creates the communication between the pyridine and the electron-deficient pyridinium at the other end of the DTE backbone and lowers its nucleophilic character. The small magnitude of the change can be ascribed to the fact that the pyridine is twisted out of coplanarity from DTE backbone in the ring-closed form and the fact the structural flexibility of the ring-open form allows the pyridine to feel the effect of the electron-withdrawing pyridinium through-space. The same trend in reactivity prevails if the ring-open isomer is subjected to a series of ring-opening and ring-closing cycles under *pseudo*-first-order conditions. Although, this work shows that the chosen DTE system only provides a “higher” and “lower” type of control over the

alkylation reaction, it represents a starting point for the development of better photoresponsive DTE systems capable of turning reactions “on” and “off”.

The effect of the ring-open and the ring-closed DTE isomers on the reaction of an aromatic aldehyde with an acetylene derivative, which is generally catalyzed by pyridine, was also investigated in an attempt to demonstrate the concept of photoregulating nucleophilic catalysis. The results show the concept of phototuning reactivity with the ring-open isomer acting as the more efficient catalyst for the formation of the product.

The research presented in this thesis has shown that the major hurdle with the chosen pyridine-functionalized DTE system is the small magnitude of the change in nucleophilicity between the two isomers. Preliminary studies have shown that replacing the perfluorinated cyclopentene ring of the DTE system with the perhydrocyclopentene ring leads to a slightly more pronounced difference in nucleophilicity between the two isomers. However, these studies also indicate that the perhydrocyclopentene version of the DTE system exhibits poor fatigue resistance properties. Thus, alternate ways to fine-tune the electronic properties of the DTE system that do not interfere with the photochromic performance or behaviour of the system need to be addressed.

6 APPENDIX

6.1 Supplementary ^1H NMR Spectra

6.1.1 Selective NOE Experiments for *Chapter 2*

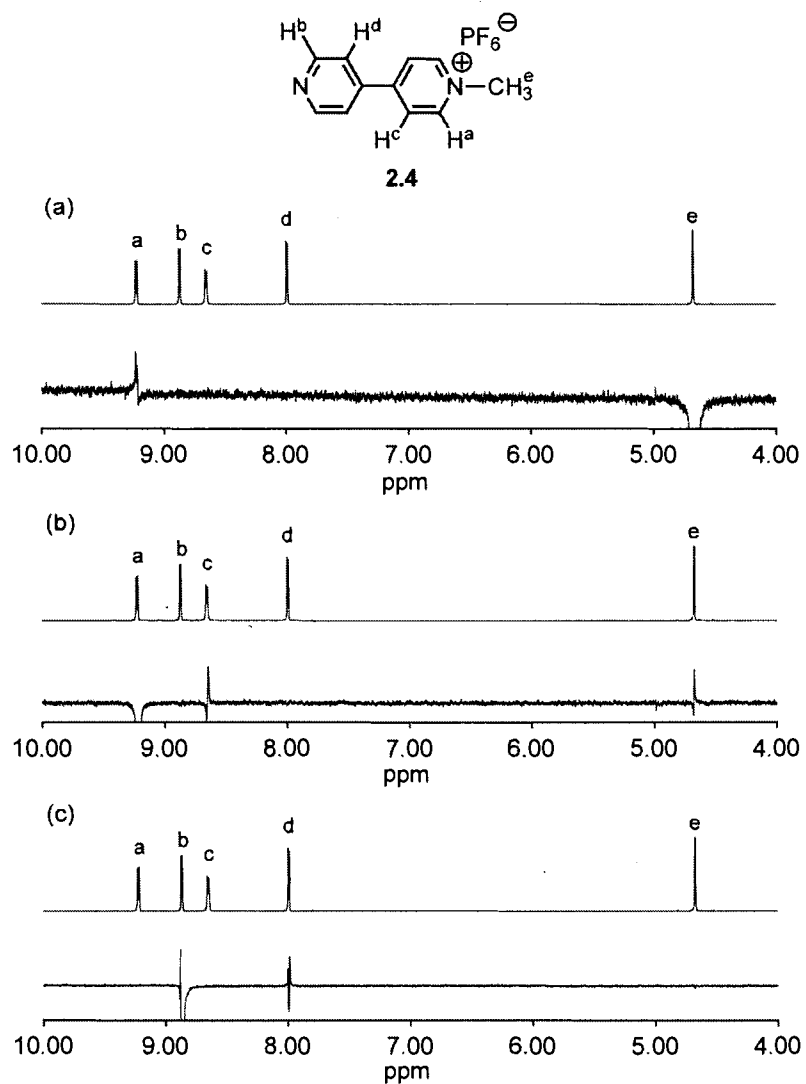


Figure 6.1.1. Partial ^1H NMR (500 MHz, CD_3COCD_3) spectra of the 1-D NOE experiments on the monomethylated bipyridinium **2.4** showing the selective irradiation of (a) peak 'e', (b) peak 'a' and (c) peak 'b'.

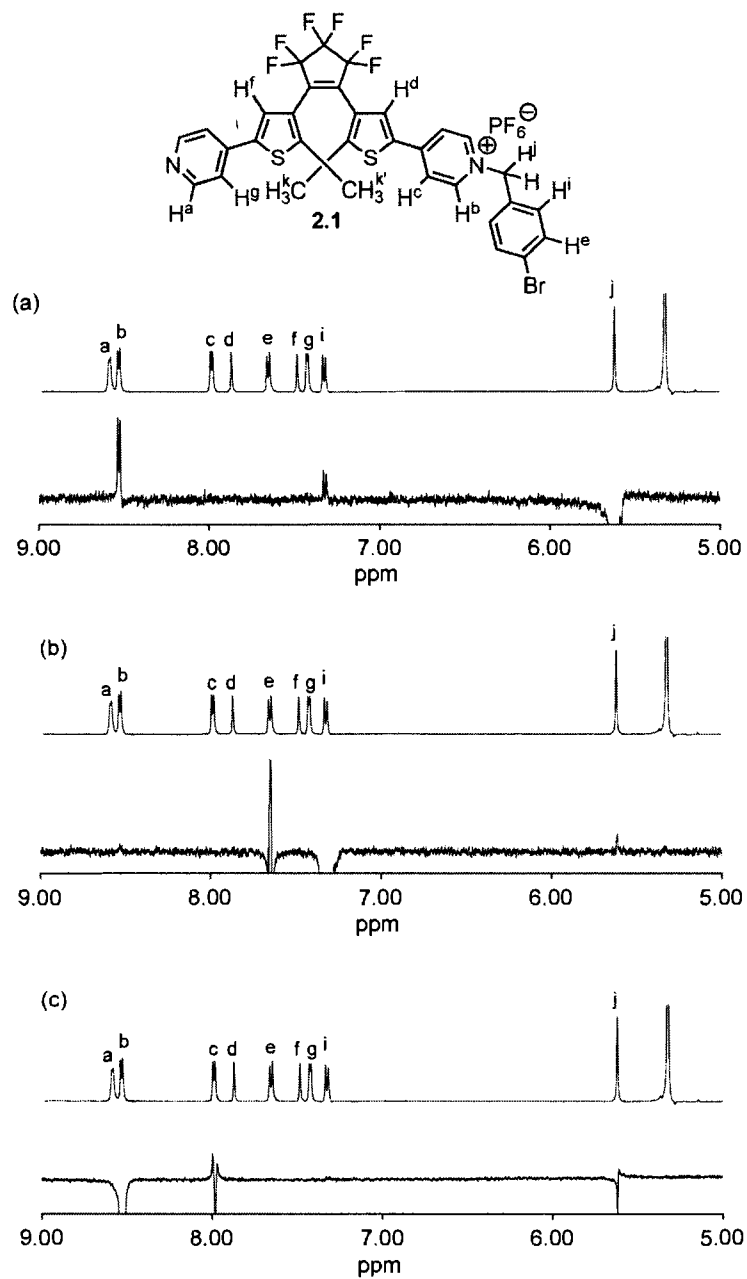


Figure 6.1.2. Partial ¹H NMR (500 MHz, CD₂Cl₂) spectra of the 1-D NOE experiments on the ring-open isomer (2.1) of the monobenzylated *bis*(pyridinium) hexafluorophosphate showing the selective irradiation of (a) peak 'j', (b) peak 'i' and (c) peak 'b'.

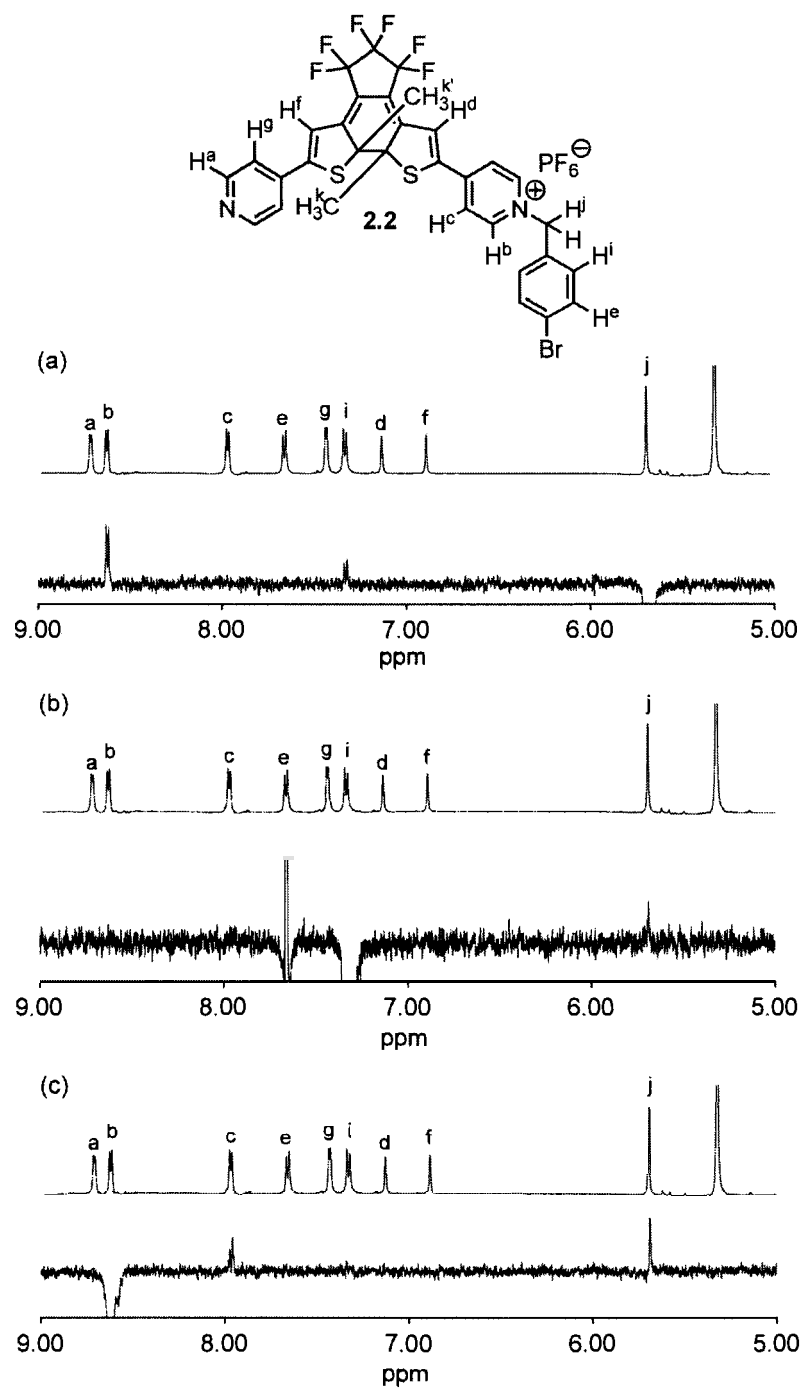


Figure 6.1.3. Partial 1H NMR (500 MHz, CD_2Cl_2) spectra of the 1-D NOE experiments on the ring-closed isomer (2.2) of the monobenzylated *bis*(pyridinium) hexafluorophosphate showing the selective irradiation of (a) peak 'j', (b) peak 'i' and (c) peak 'b'.

6.1.2 Selective NOE experiments for Chapter 3

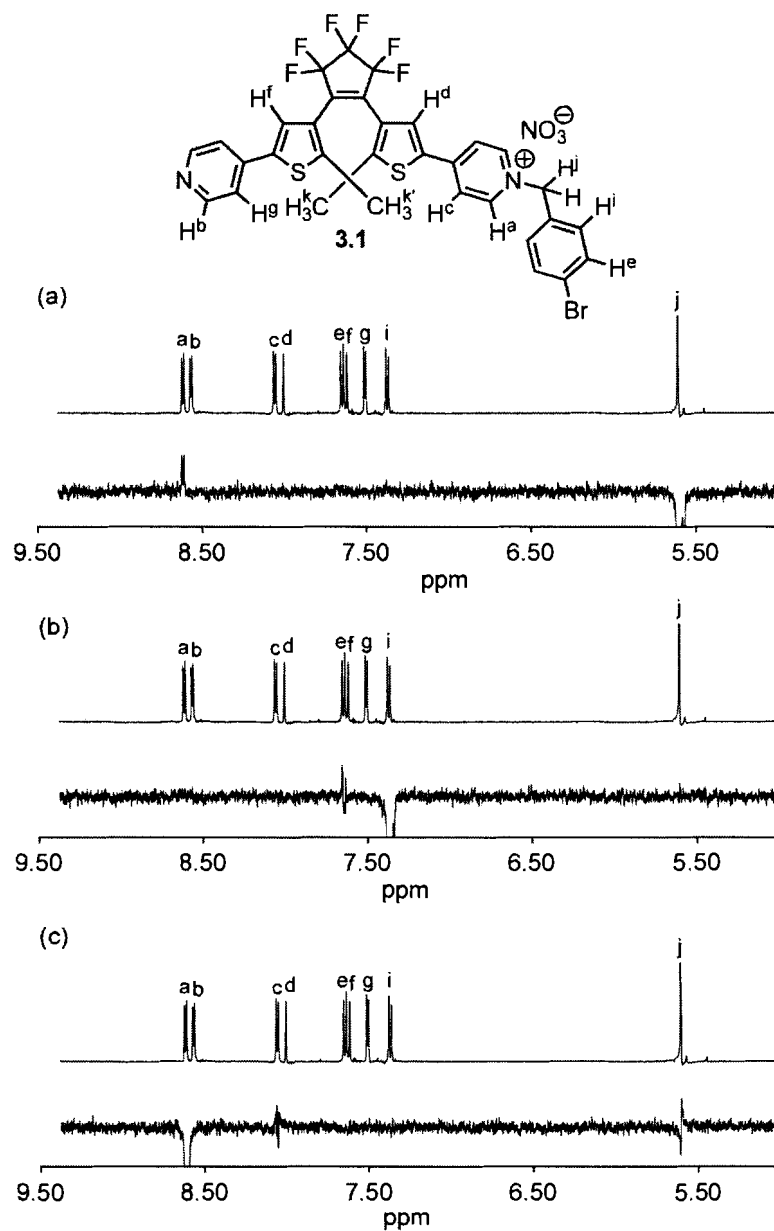


Figure 6.1.4. Partial ¹H NMR (500 MHz, CD₃CN) spectra of the 1-D NOE experiments on the ring-open isomer (3.1) of the monobenzylated bis(pyridinium) nitrate showing the selective irradiation of (a) peak 'j', (b) peak 'i' and (c) peak 'a'.

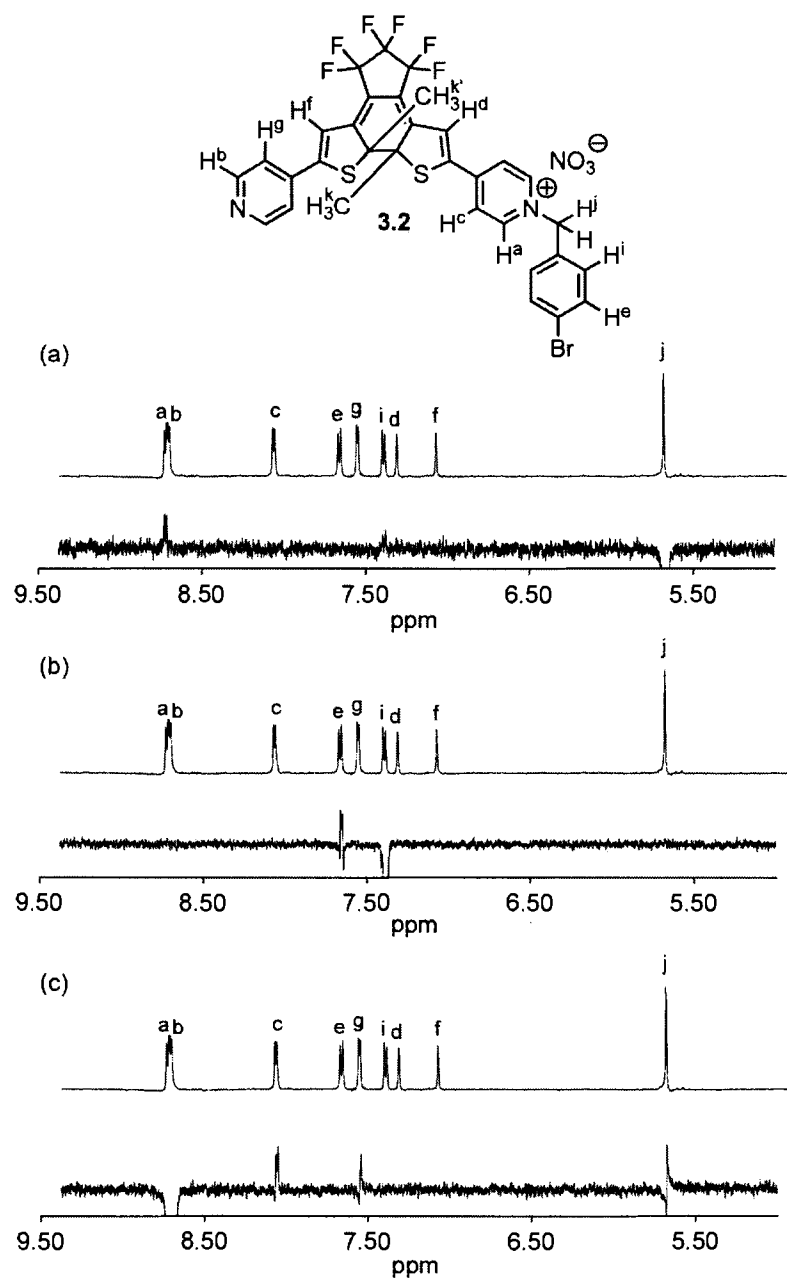


Figure 6.1.5. Partial ¹H NMR (500 MHz, CD₃CN) spectra of the 1-D NOE experiments on the ring-closed isomer (3.2) of the monobenzylated bis(pyridinium) nitrate showing the selective irradiation of (a) peak 'j', (b) peak 'i' and (c) peaks 'a' and 'b'.

6.1.3 Axial Coordination Experiments for Chapter 2

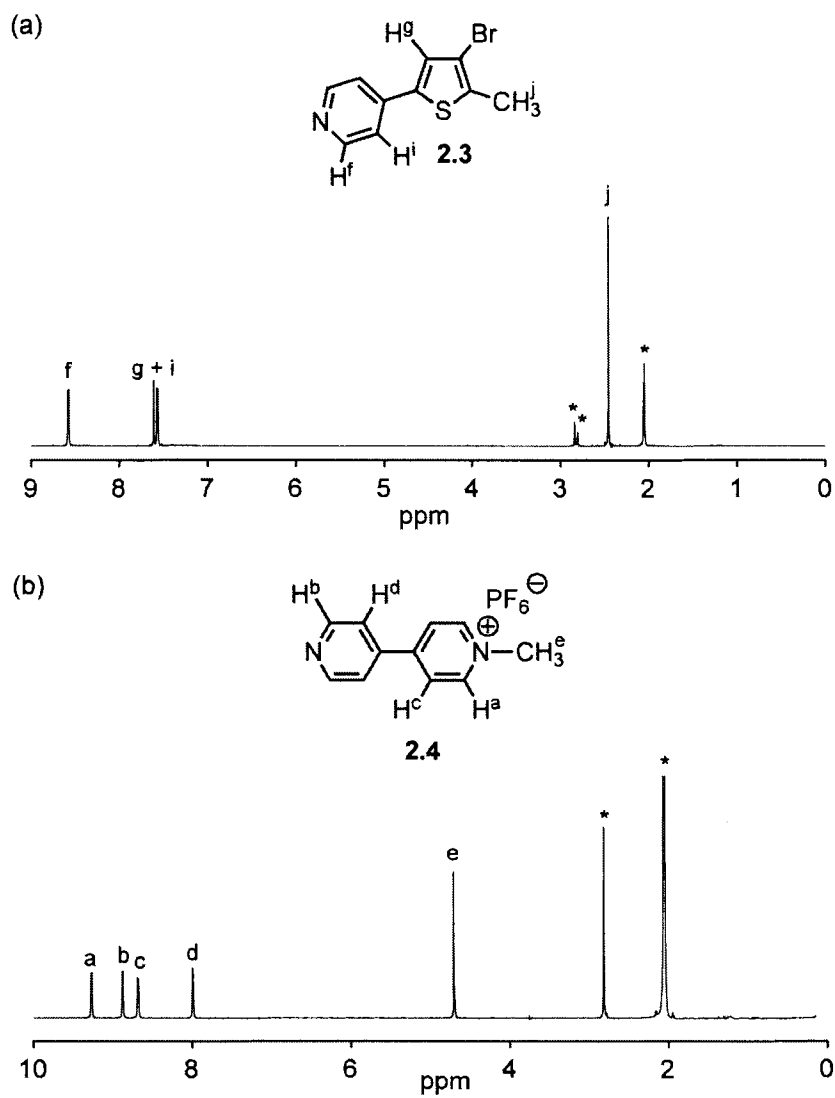


Figure 6.1.6. ^1H NMR (600 MHz, CD_3COCD_3) spectra showing the peaks corresponding to (a) the pyridylthiophene **2.3** and (b) the monomethylated bipyridinium **2.4**. The (*) denotes signals corresponding to the residual solvent peak (2.05 ppm) and the dissolved water peak (2.75 ppm).

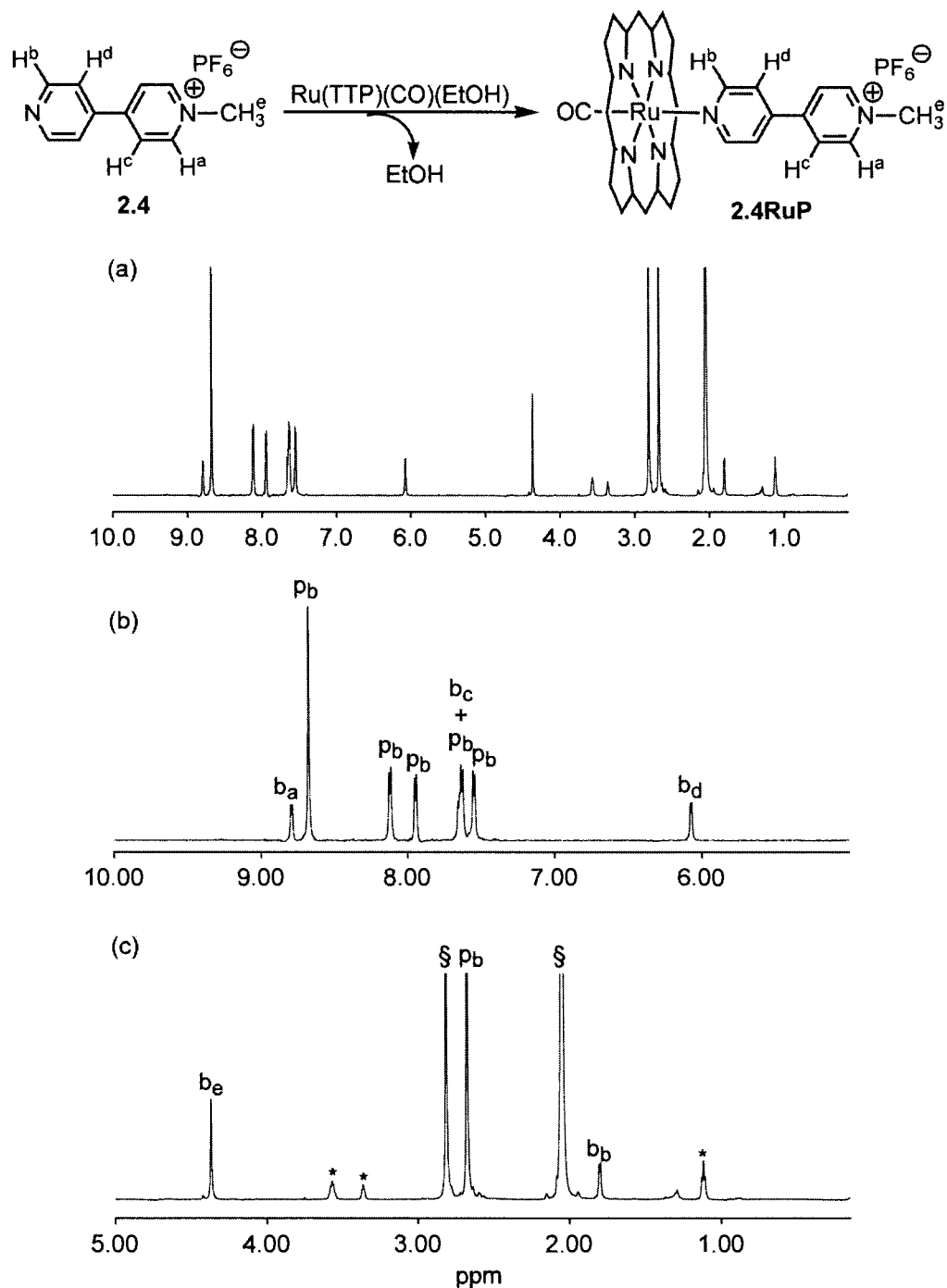


Figure 6.17. ¹H NMR (600 MHz, CD₃COCD₃) spectra showing the peaks corresponding to the complex formed when 1 molar equiv of RuTTP(CO)(EtOH) is added to a solution (5.3 × 10⁻³ M) of the monomethylated bipyridinium 2.4. The (§) denotes signals corresponding to the residual solvent peak (2.05 ppm) and the dissolved water peak (2.75 ppm). The (*) denotes signals corresponding to the EtOH (3.57 and 3.39 ppm) displaced upon axial coordination of the pyridyl ligand 2.4 to RuTTP(CO).

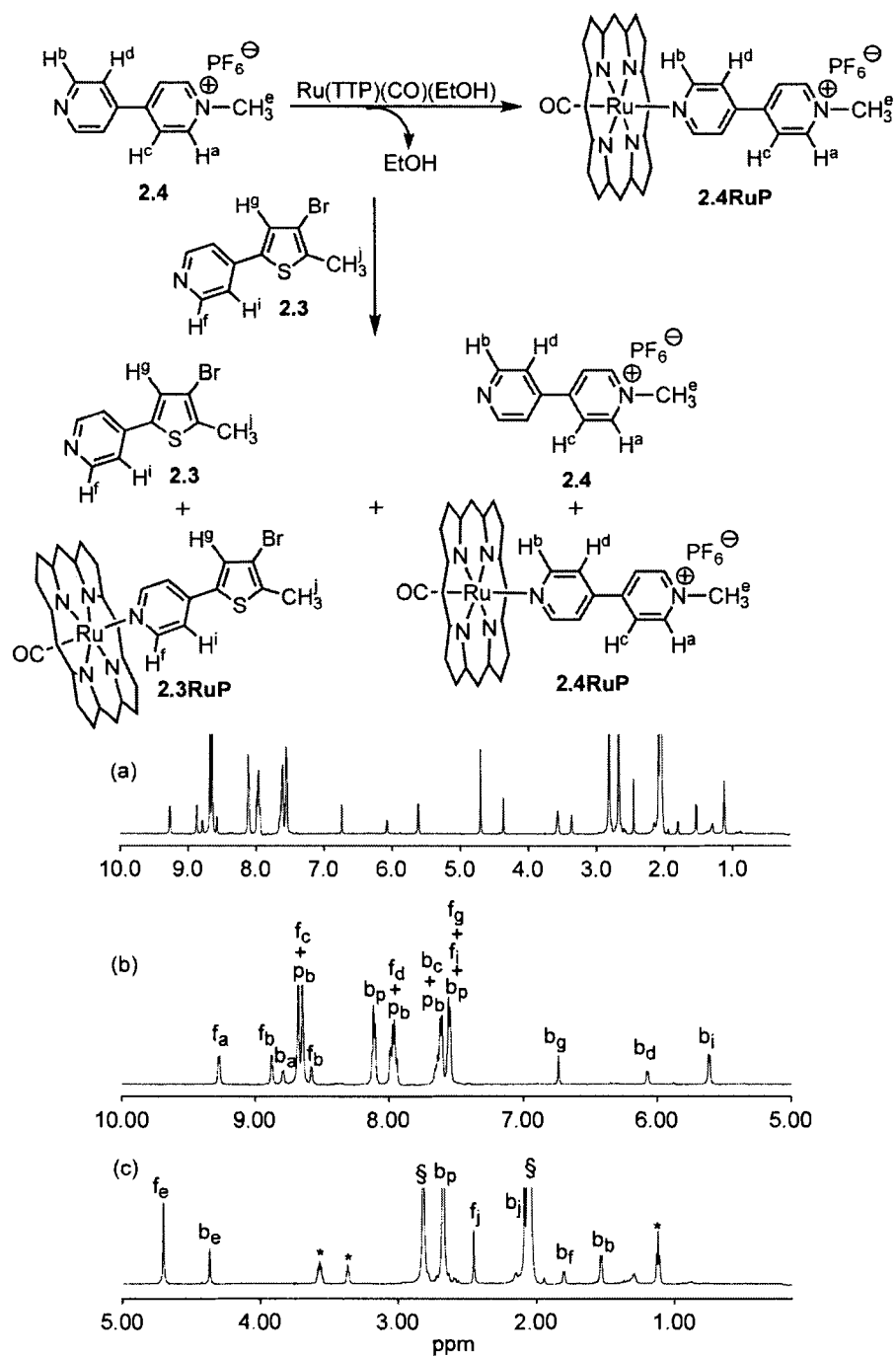


Figure 6.1.8. 1H NMR (600 MHz, CD_3COCD_3) spectra when 1 molar equiv of the stronger Lewis basic pyridylthiophene **2.3** is added to the porphyrin complex **2.4RuP** leading to a redistribution of free (**2.3** and **2.4**) and bound (**2.3RuP** and **2.4RuP**) ligands. The letters 'f' and 'b' denote signals corresponding to the free and bound ligands, respectively. The (§) denotes signals corresponding to the residual solvent peak (2.05 ppm) and the dissolved water peak (2.75 ppm). The (*) denotes signals corresponding to the EtOH (3.57 and 3.39 ppm) displaced upon axial coordination of the pyridyl ligand **2.4** to $RuTTP(CO)$.

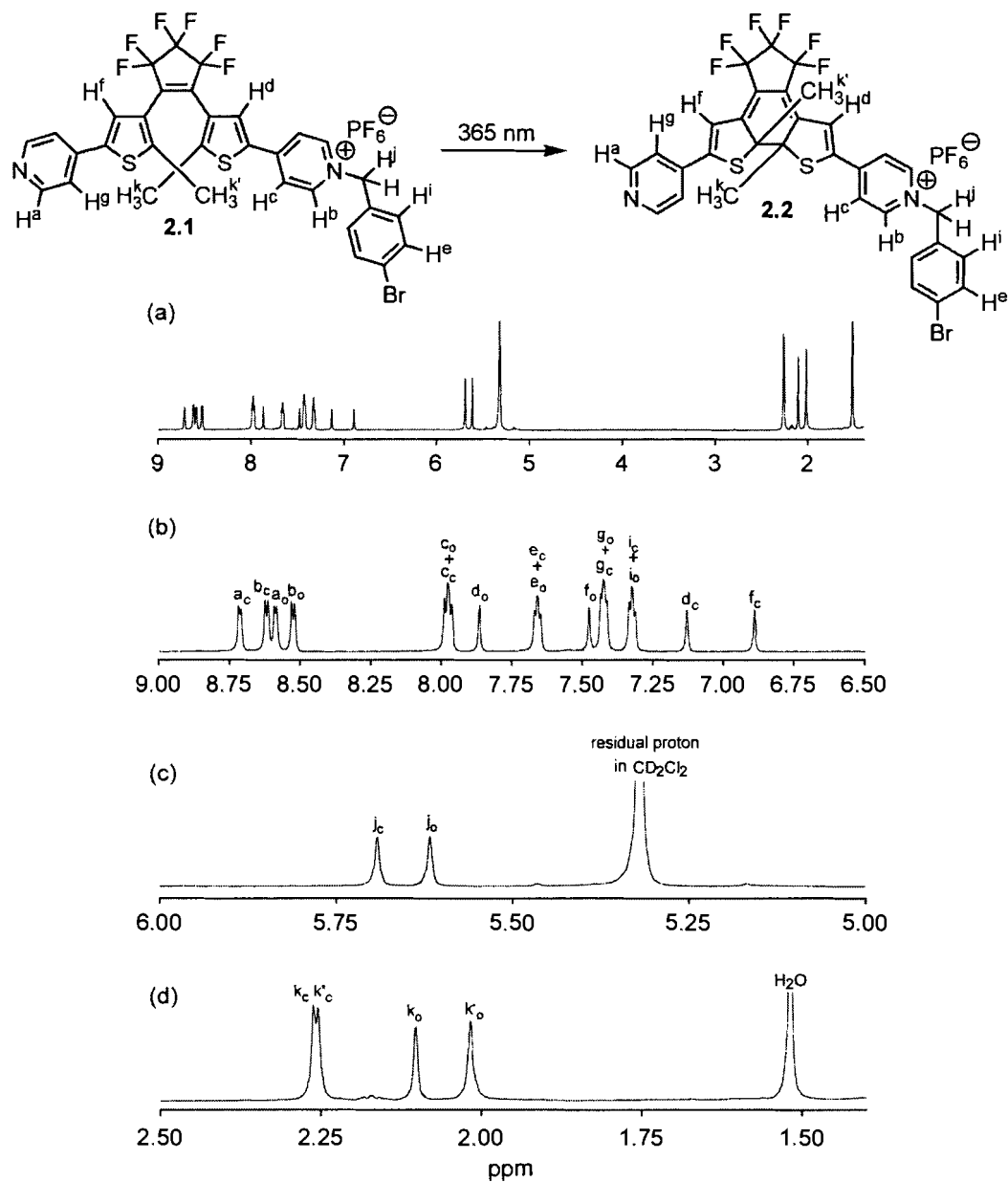


Figure 6.1.9. ^1H NMR (600 MHz, CD_2Cl_2) spectra showing the peaks corresponding to an equimolar mixture of the ring-open isomer **2.1** (labelled with the subscript 'o') and the ring-closed isomer **2.2** (labelled with the subscript 'c'). The 1:1 mixture is obtained by irradiating a solution (1.1×10^{-3} M) of the ring-open isomer **2.1** with 365 nm light until the appropriate ratio is achieved by measuring the relative integrals of the areas under the peaks for the corresponding pairs of signals for the two isomers.

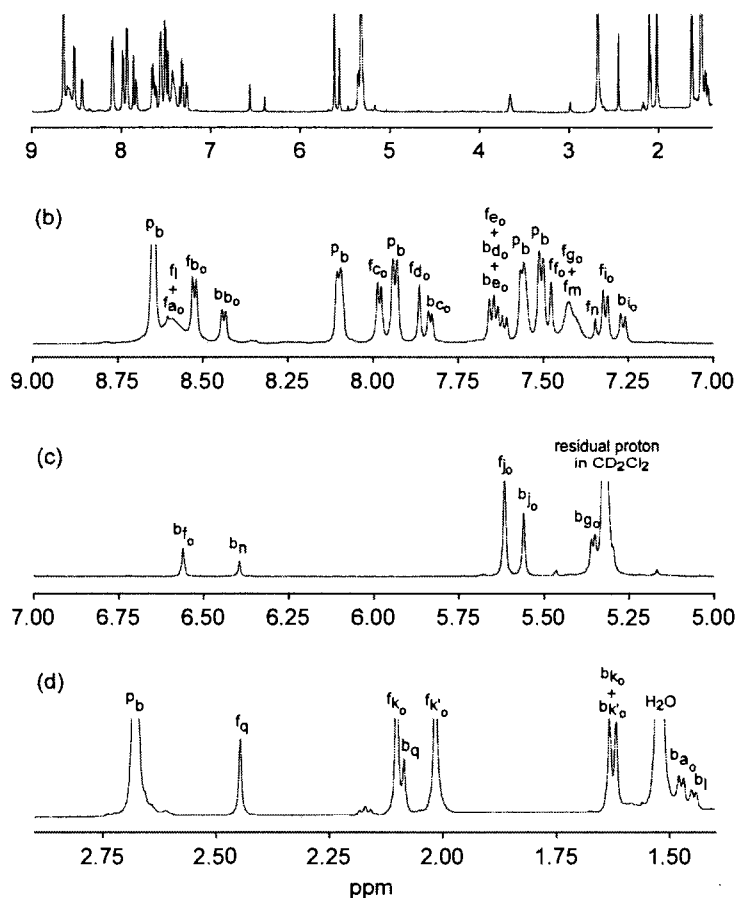
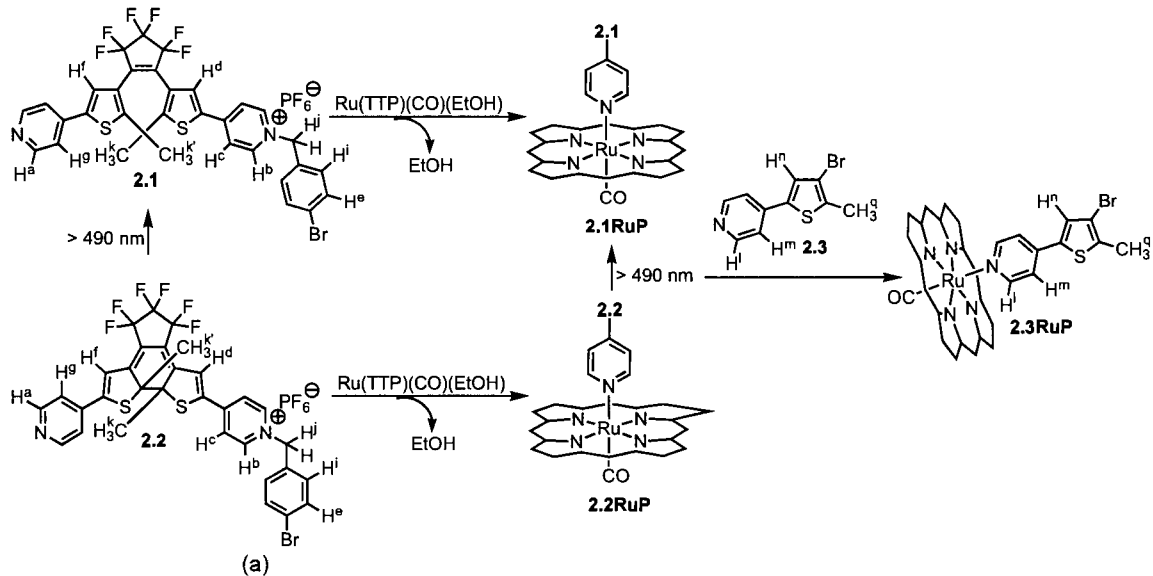


Figure 6.1.11. ^1H NMR (600 MHz, CD_2Cl_2) spectra when 0.79 molar equiv of the competing Lewis basic pyridylthiophene **2.3** is added to the mixture (1:1:0.93) consisting of the ring-open isomer **2.1**, the ring-closed isomer **2.2** and the $\text{RuTTP}(\text{CO})$ and the mixture is irradiated with light of wavelengths greater than 490 nm for 20 min.

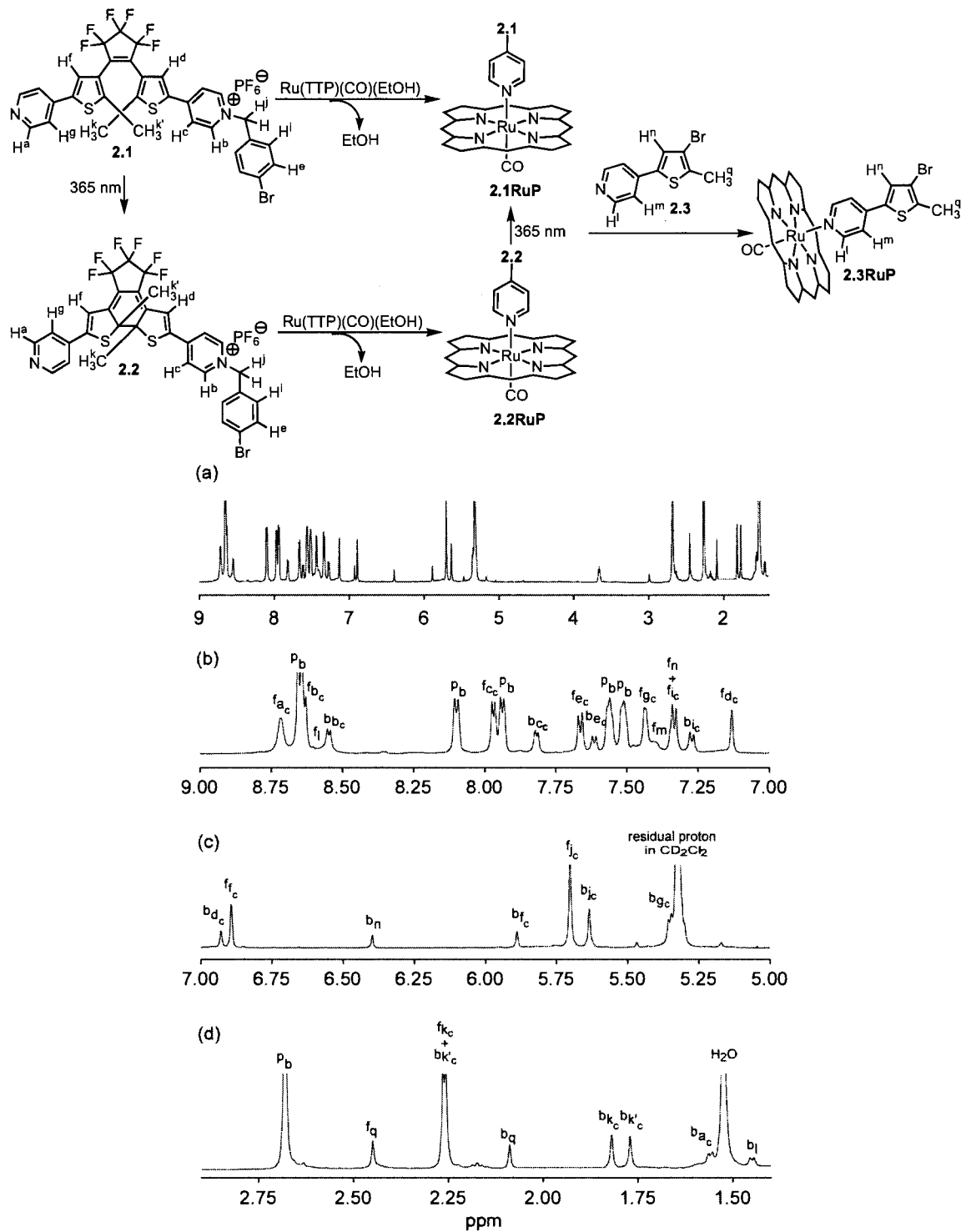


Figure 6.1.12. ^1H NMR (600 MHz, CD_2Cl_2) spectra when the mixture (1:1:0.93:0.79) consisting of the ring-open isomer **2.1**, the ring-closed isomer **2.2**, the RuTTP(CO) and the pyridylthiophene **2.3** is irradiated with 365 nm light for 10 min.

6.1.4 Pseudo-First-Order Experiments for Chapter 3

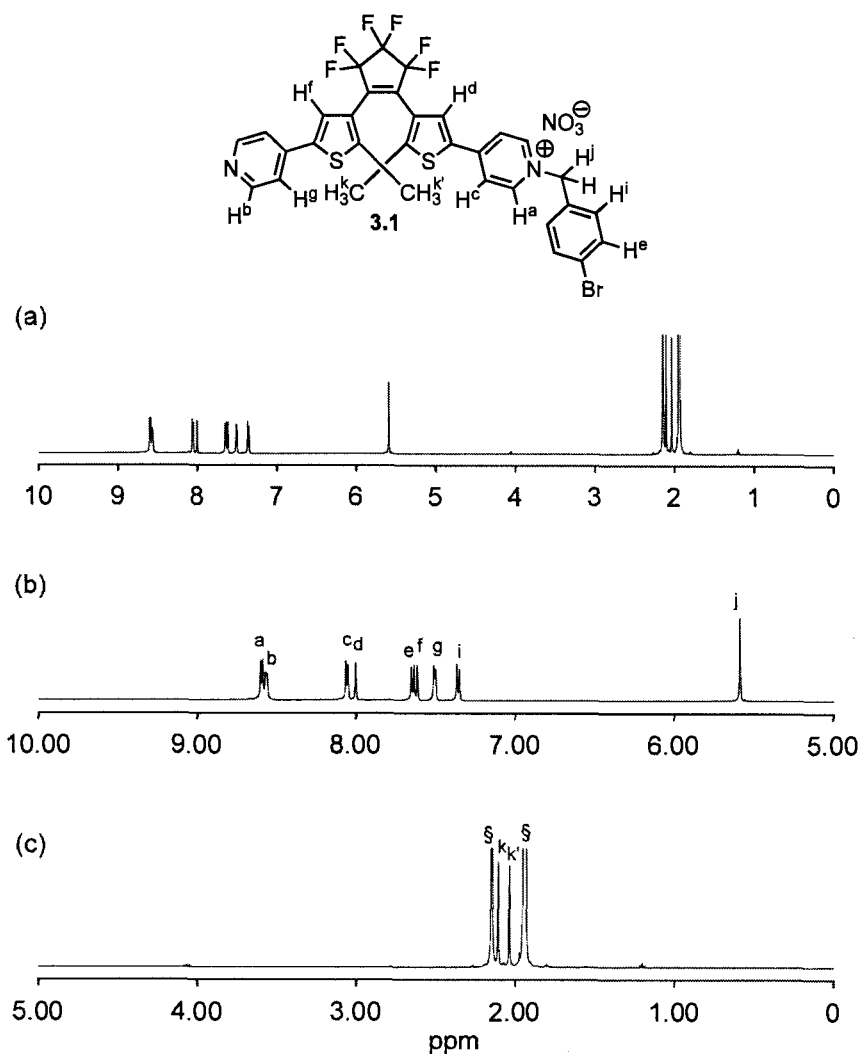


Figure 6.1.13. ^1H NMR (600 MHz, CD_3CN) spectra showing the peaks corresponding to a solution ($2.4 \times 10^{-3}\text{M}$) of the ring-open isomer (3.1) of the monobenzylated DTE in CD_3CN before the addition of an excess of the 4-bromobenzyl bromide. The (s) denotes the peaks corresponding to the residual solvent peak (1.94 ppm) and the dissolved water peak (2.13 ppm).

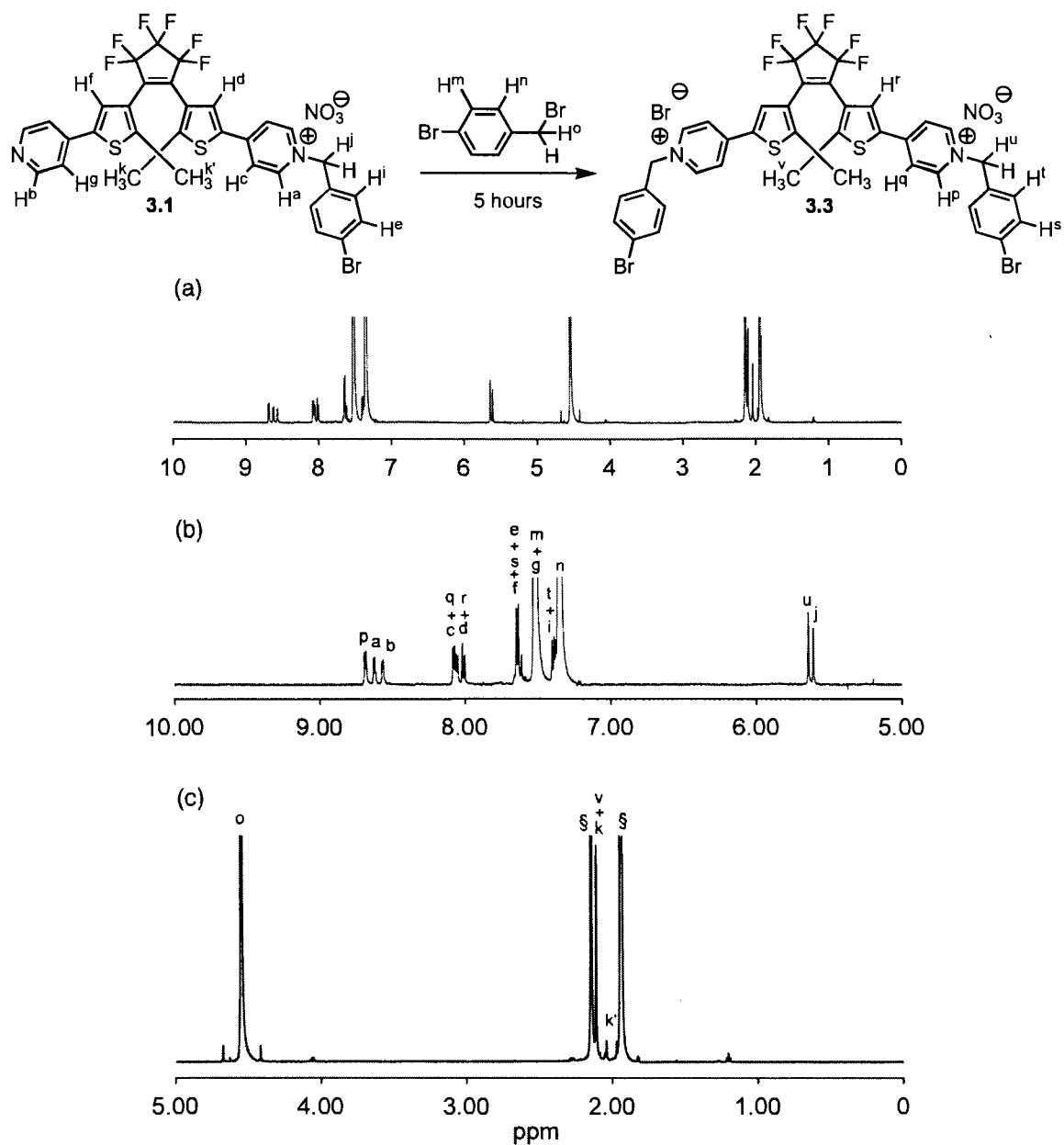


Figure 6.114. ^1H NMR (600 MHz, CD_3CN) spectra showing the progress of the reaction of a solution ($2.4 \times 10^{-3}\text{M}$) of the ring-open isomer **3.1** in CD_3CN with an excess of 4-bromobenzyl bromide ($7.3 \times 10^{-2}\text{M}$) after 5 h. The (§) denotes the peaks corresponding to the residual solvent peak (1.94 ppm) and the dissolved water peak (2.13 ppm).

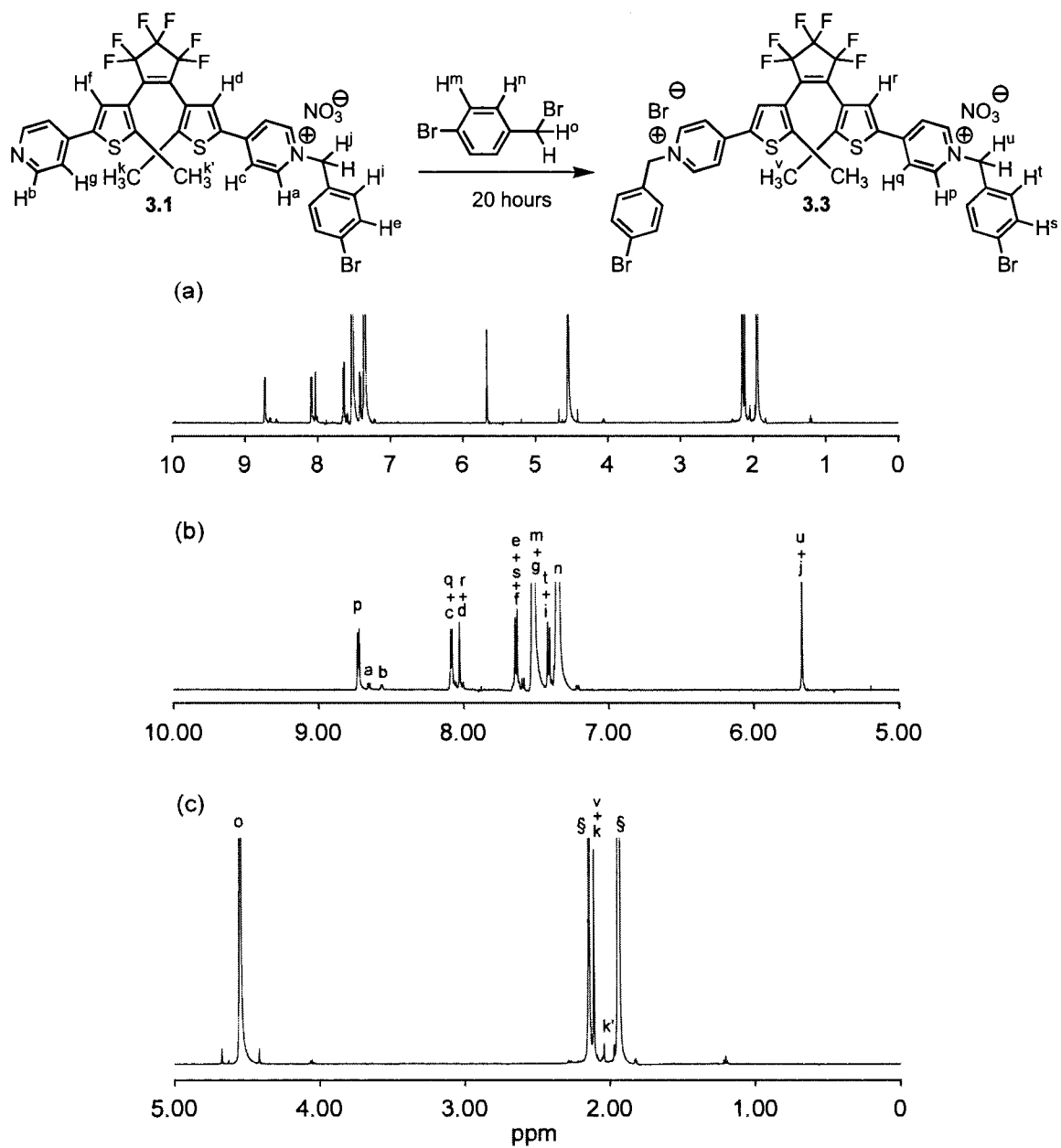


Figure 6.15. ¹H NMR (600 MHz, CD₃CN) spectra showing the progress of the reaction of a solution (2.4×10^{-3} M) of the ring-open isomer **3.1** in CD₃CN with an excess of 4-bromobenzyl bromide (7.3×10^{-2} M) after 20 h. The (§) denotes the peaks corresponding to the residual solvent peak (1.94 ppm) and the dissolved water peak (2.13 ppm).

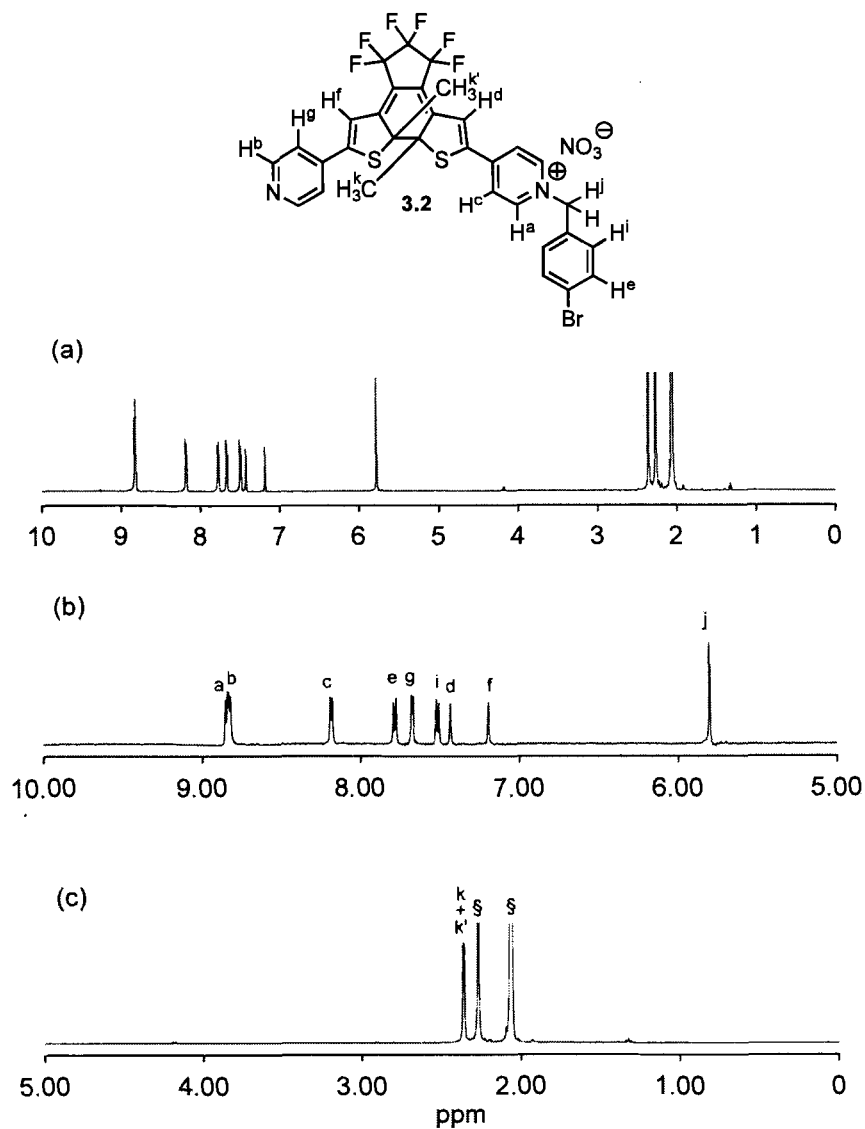
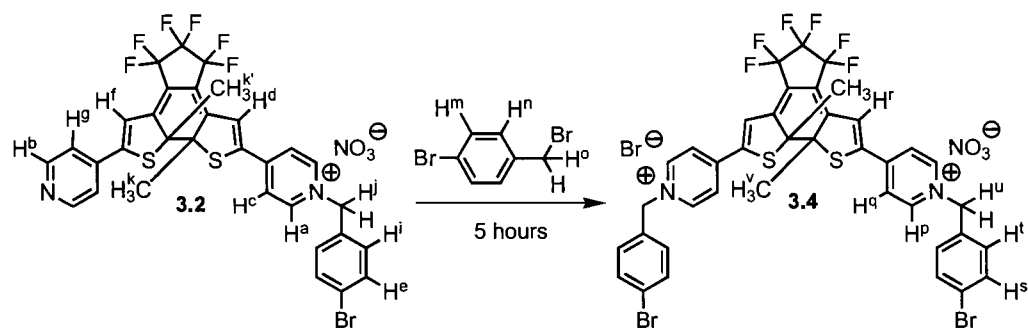
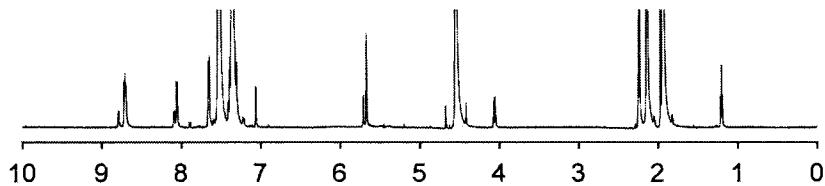


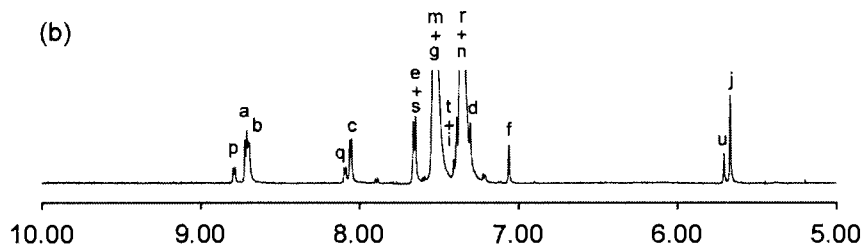
Figure 6.1.16. ¹H NMR (600 MHz, CD₃CN) spectra showing the peaks corresponding to a solution (2.4×10^{-3} M) of the ring-closed isomer (3.2) of the monobenzylated DTE in CD₃CN before the addition of an excess of the 4-bromobenzyl bromide. The ring-closing reaction is achieved by irradiating a solution (2.4×10^{-3} M) of the ring-open isomer 3.1 with 365 nm light until the peaks corresponding to the ring-open isomer 3.1 are no longer observed by ¹H NMR spectroscopy. The (§) denotes the peaks corresponding to the residual solvent peak (1.94 ppm) and the dissolved water peak (2.13 ppm).



(a)



(b)



(c)

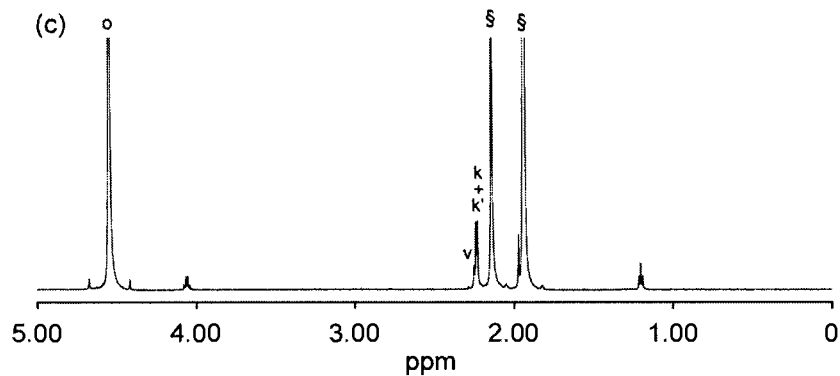


Figure 6.1.17. ^1H NMR (600 MHz, CD_3CN) spectra showing the progress of the reaction of a solution ($2.4 \times 10^{-3}\text{M}$) of the ring-closed isomer **3.2** in CD_3CN with an excess of 4-bromobenzyl bromide ($7.3 \times 10^{-2}\text{M}$) after 5 h. The (s) denotes the peaks corresponding to the residual solvent peak (1.94 ppm) and the dissolved water peak (2.13 ppm).

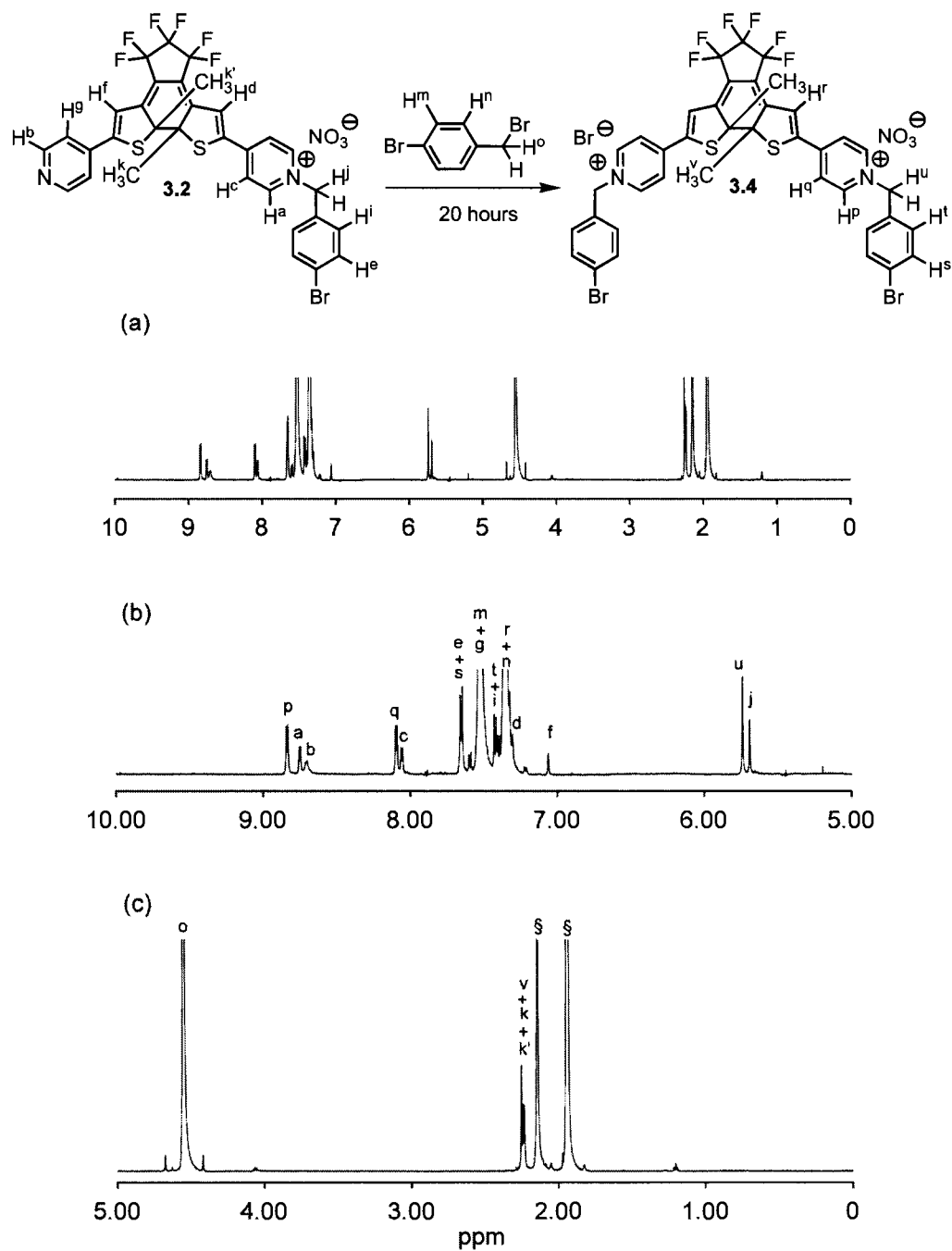


Figure 6.1.18. ^1H NMR (600 MHz, CD_3CN) spectra showing the progress of the reaction of a solution ($2.4 \times 10^{-3}\text{M}$) of the ring-closed isomer **3.2** in CD_3CN with an excess of 4-bromobenzyl bromide ($7.3 \times 10^{-3}\text{M}$) after 20 h. The (§) denotes the peaks corresponding to the residual solvent peak (1.94 ppm) and the dissolved water peak (2.13 ppm).

6.1.5 Consecutive *Pseudo-First-Order* Experiments for Chapter 3

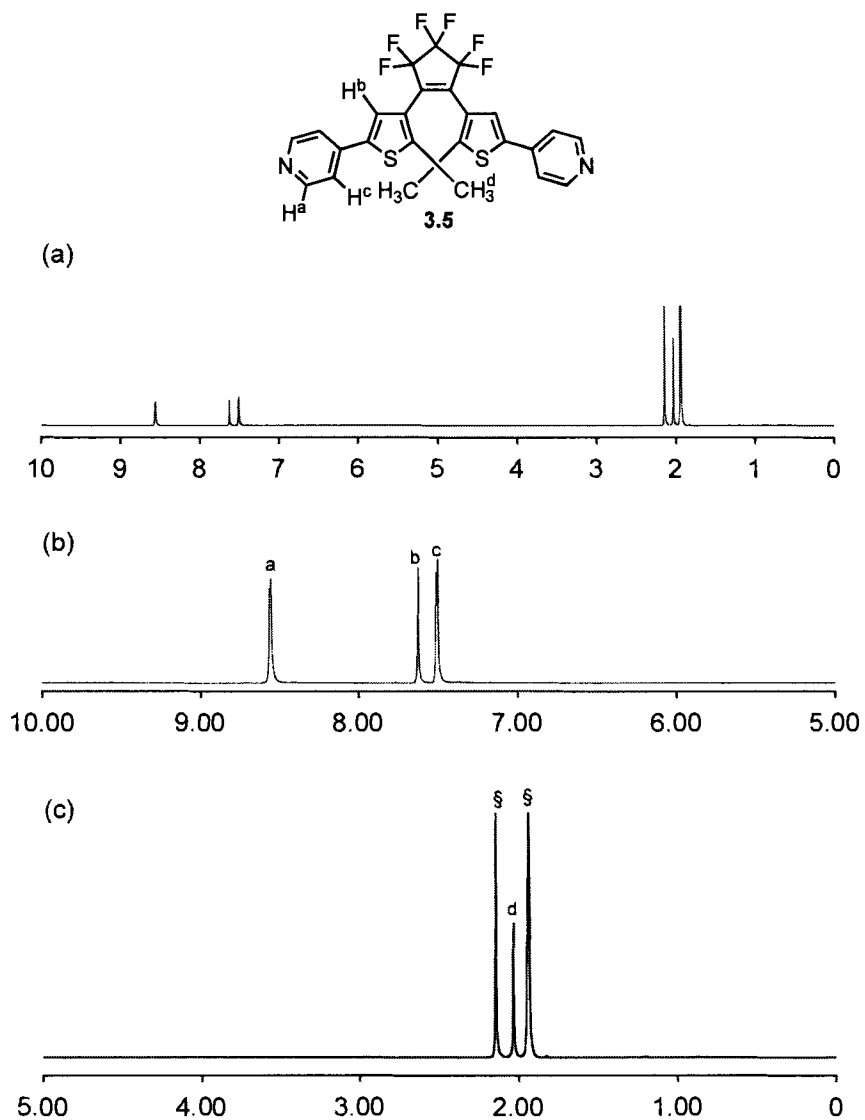


Figure 6.1.19. ¹H NMR spectra (600 MHz, CD₃CN) showing the peaks corresponding to a solution (4.6×10^{-3} M) of the ring-open isomer (3.5) of the *bis*(pyridine) in CD₃CN before adding an excess of 4-bromobenzyl bromide (1.2×10^{-1} M). The (§) denotes the peaks corresponding to the residual solvent peak (1.94 ppm) and the dissolved water peak (2.13 ppm).

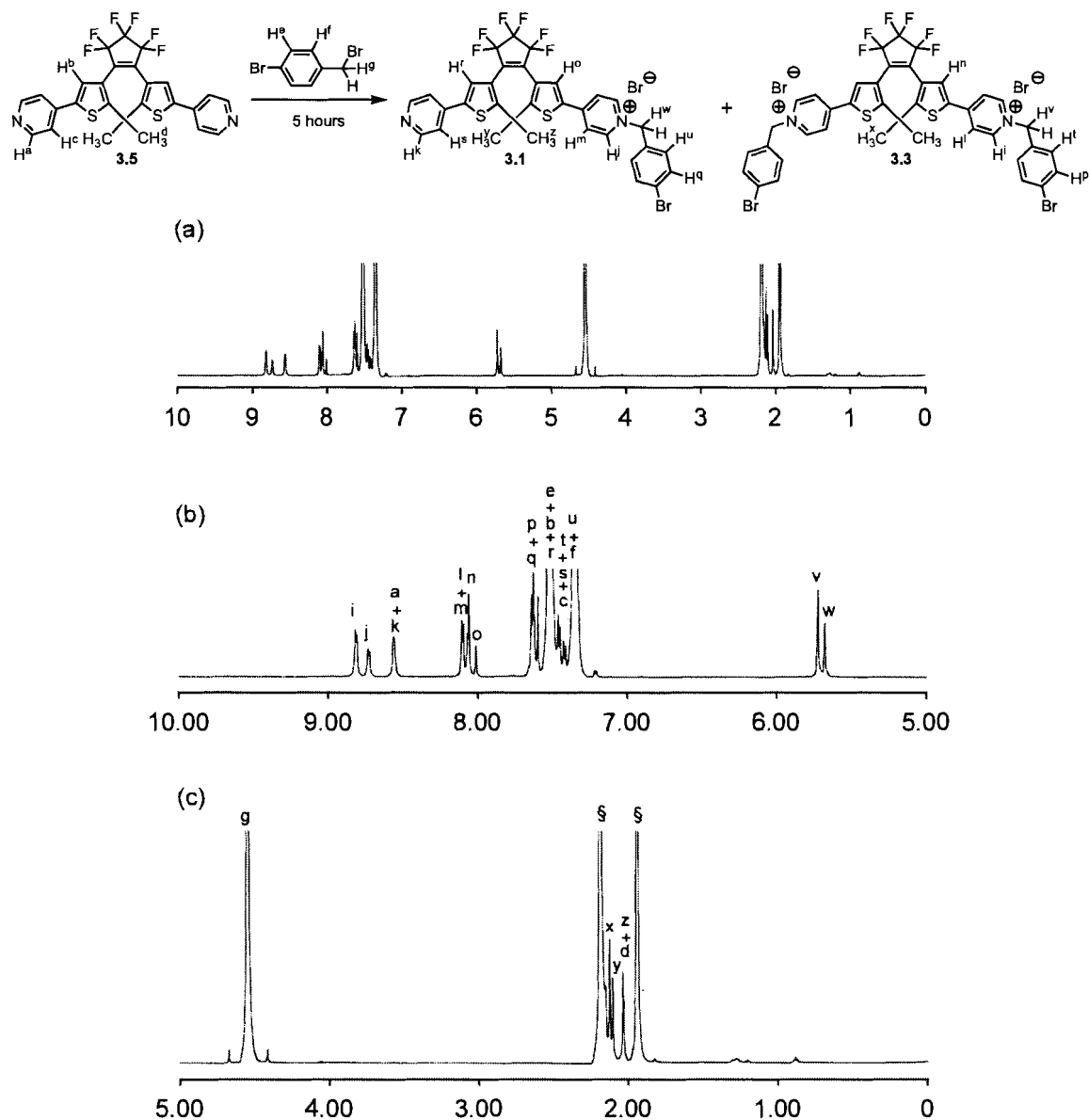


Figure 6.1.20. ¹H NMR spectra (600 MHz, CD₃CN) showing the progress of the reaction of a solution (4.6×10^{-3} M) of the ring-open isomer **3.5** in CD₃CN with an excess of 4-bromobenzyl bromide (1.2×10^{-1} M) after 5 h. The (§) denotes the peaks corresponding to the residual solvent peak (1.94 ppm) and the dissolved water peak (2.13 ppm).

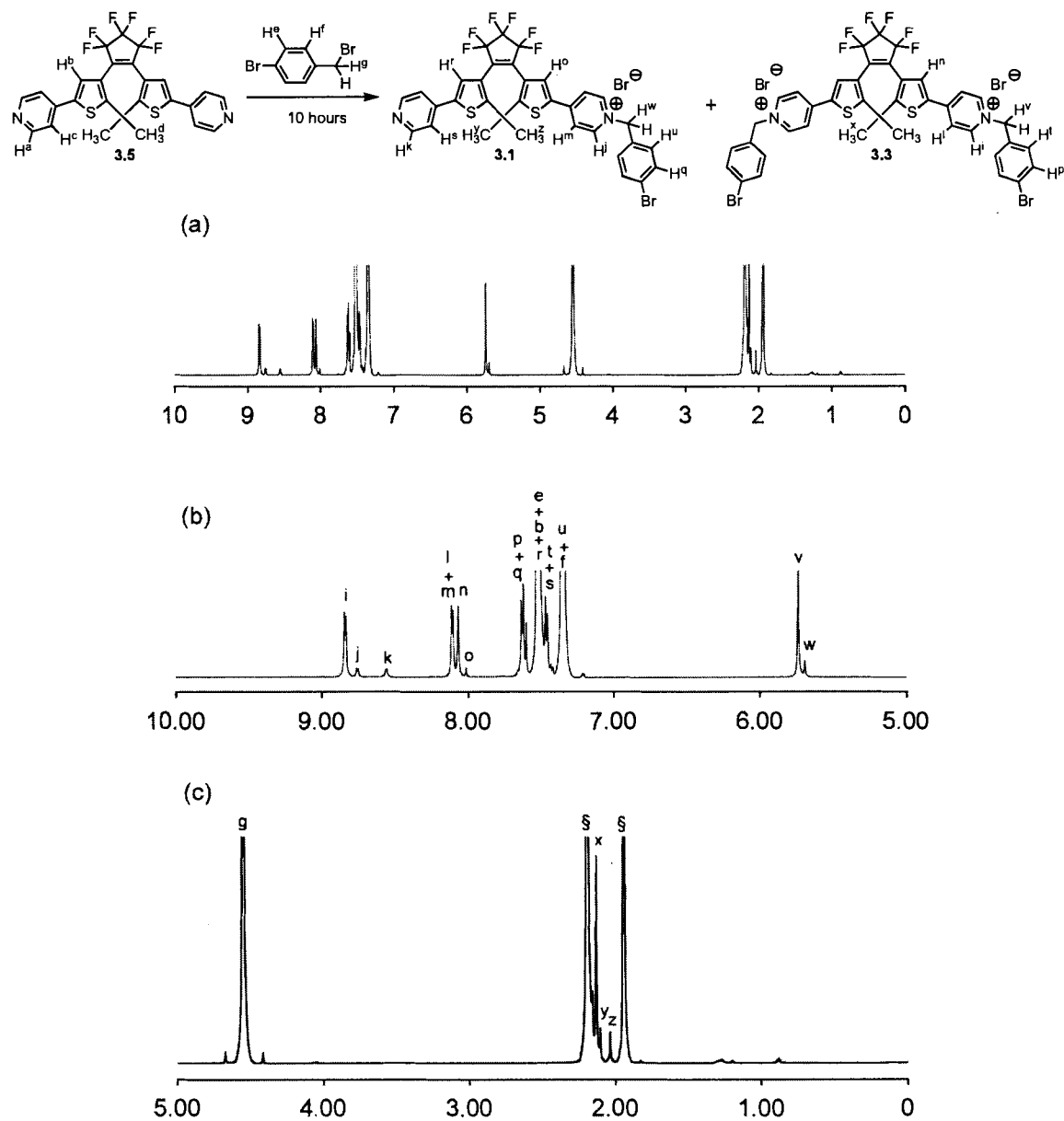


Figure 6.1.21. ^1H NMR spectra (600 MHz, CD_3CN) showing the progress of the reaction of a solution (4.6×10^{-3} M) of the ring-open isomer **3.5** in CD_3CN with an excess of 4-bromobenzyl bromide (1.2×10^{-1} M) after 10 h. The (§) denotes the peaks corresponding to the residual solvent peak (1.94 ppm) and the dissolved water peak (2.13 ppm).

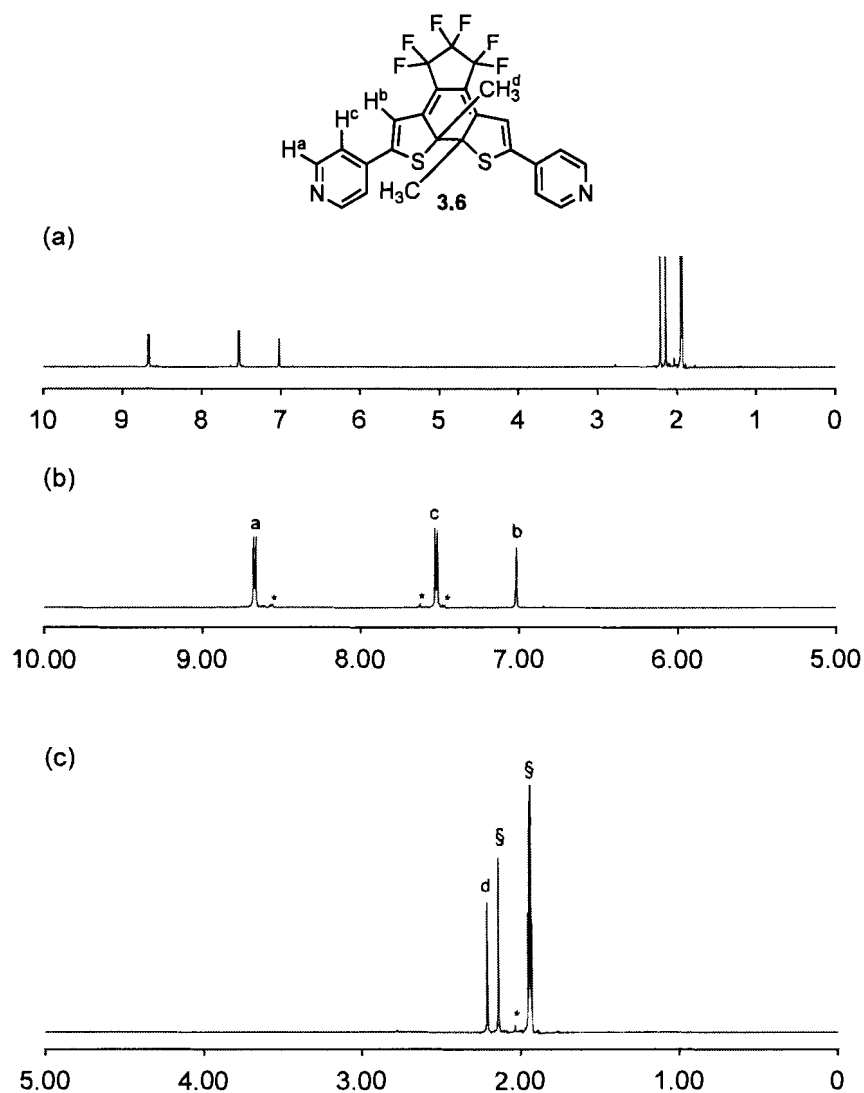


Figure 6.1.22. ^1H NMR (600 MHz, CD_3CN) spectra showing the peaks corresponding to a solution (4.6×10^{-3} M) of the ring-closed isomer **3.6** in CD_3CN before the addition of an excess of the 4-bromobenzyl bromide. The ring-closing reaction is achieved by irradiating a solution (4.6×10^{-3} M) of the ring-open isomer **3.5** with 313 nm light until a solution containing 98 % of the ring-closed isomer **3.6** is observed at the PSS as monitored by ^1H NMR spectroscopy. The (*) denotes the residual ring-open form **3.5** in the solution. The (§) denotes the peaks corresponding to the residual solvent peak (1.94 ppm) and the dissolved water peak (2.13 ppm).

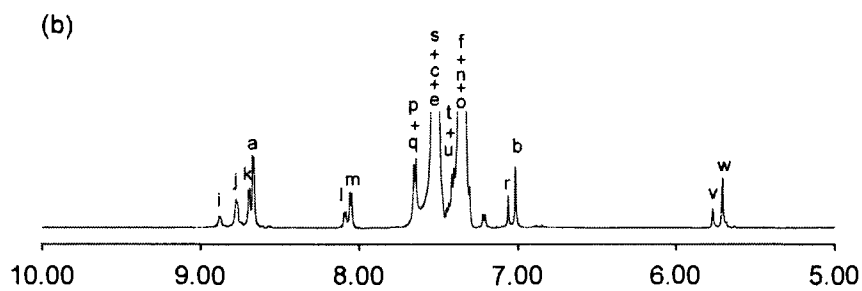
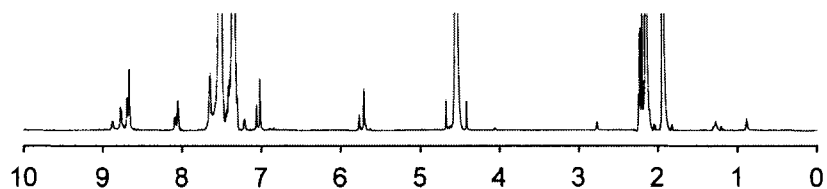
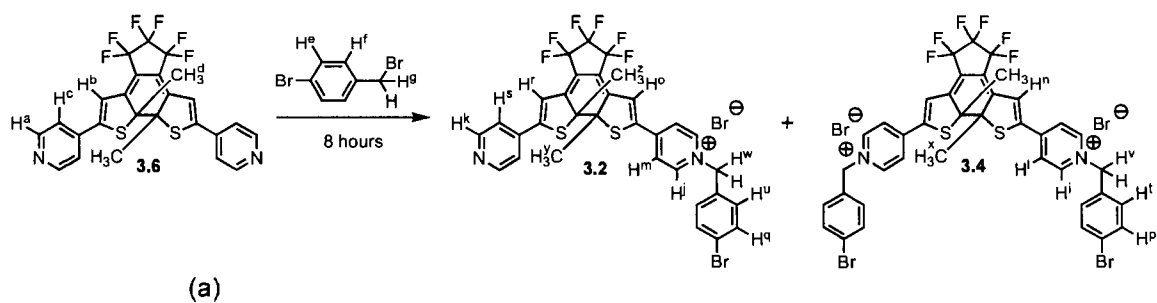
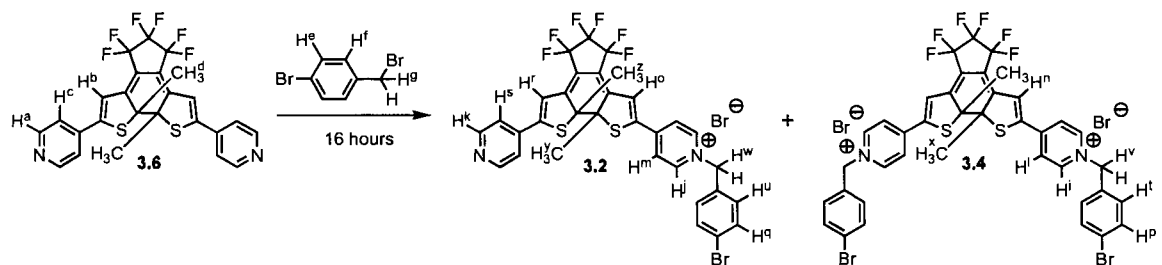
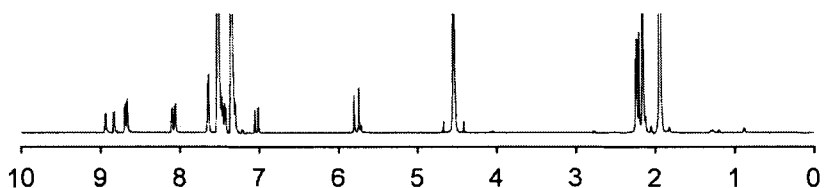


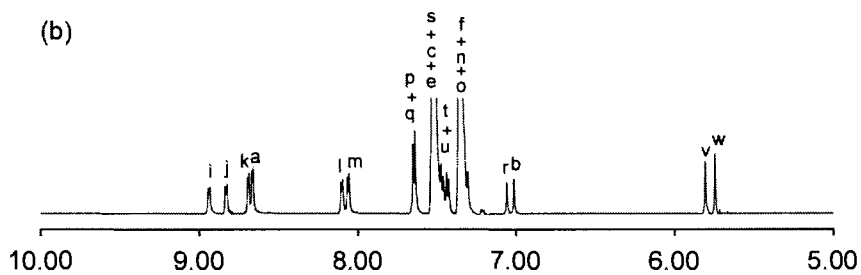
Figure 6.1.23. ¹H NMR spectra (600 MHz, CD₃CN) showing the progress of the reaction of a solution (4.6×10^{-3} M) of the ring-closed isomer **3.6** in CD₃CN with an excess of 4-bromobenzyl bromide (1.2×10^{-1} M) after 8 h. The (s) denotes the peaks corresponding to the residual solvent peak (1.94 ppm) and the dissolved water peak (2.13 ppm).



(a)



(b)



(c)

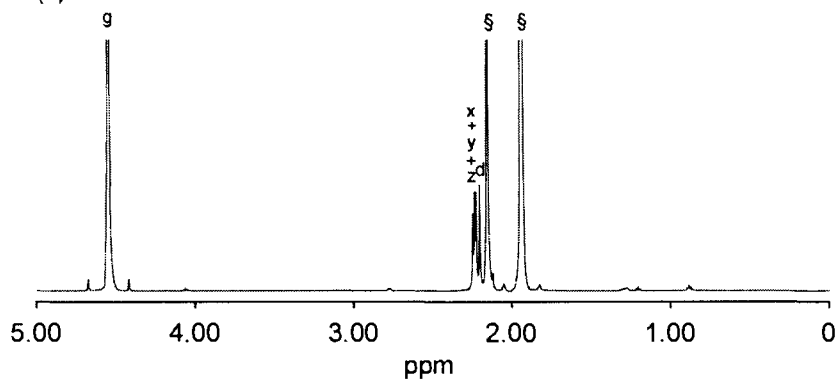


Figure 6.1.24. ^1H NMR spectra (600 MHz, CD_3CN) showing the progress of the reaction of a solution (4.6×10^{-3} M) of the ring-closed isomer **3.6** in CD_3CN with an excess of 4-bromobenzyl bromide (1.2×10^{-1} M) after 16 h. The (§) denotes the peaks corresponding to the residual solvent peak (1.94 ppm) and the dissolved water peak (2.13 ppm).

6.2 Supplementary T_1 Relaxation Measurements for Chapter 3

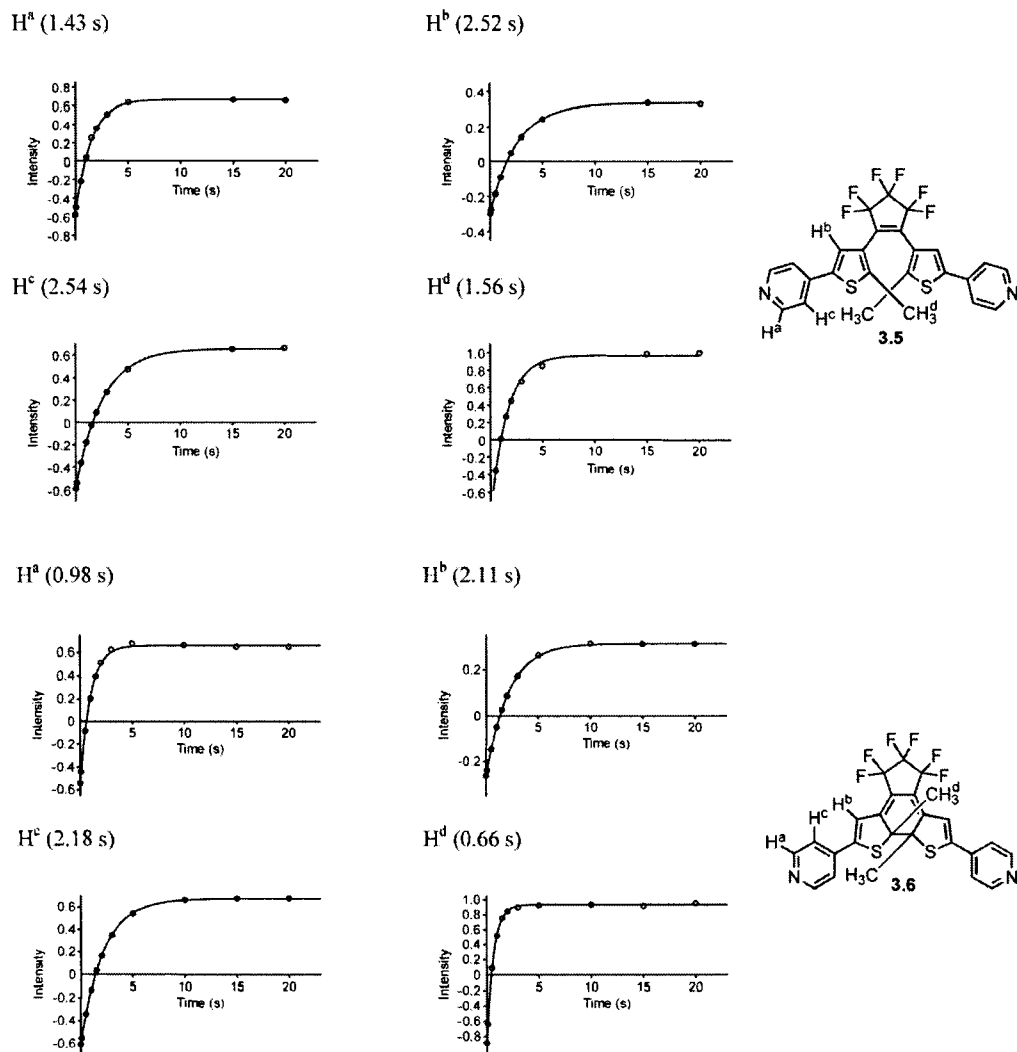


Figure 6.2.1. Relaxation measurements (T_1) for the ring-open (3.5) and the ring-closed (3.6) isomers of the bis(pyridine). The T_1 values can be obtained from the fitted parameters and are shown above each graph.

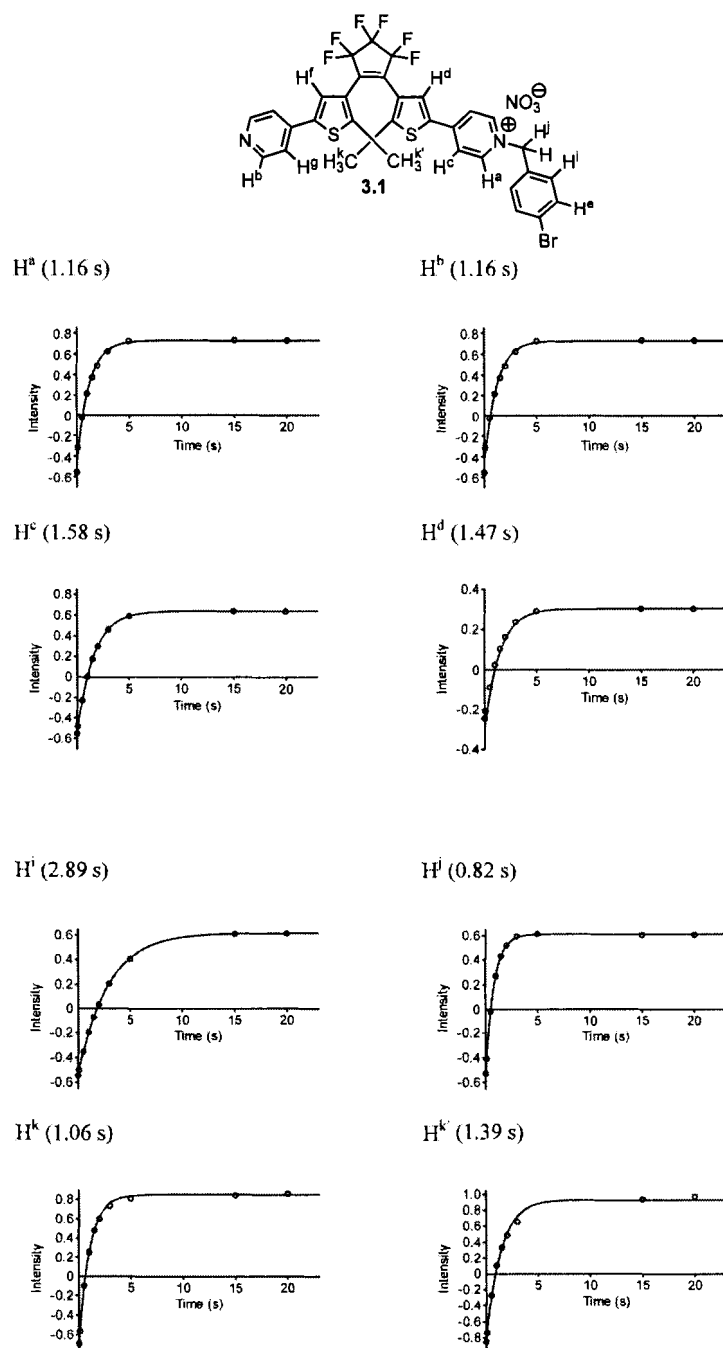


Figure 6.2.2. T_1 relaxation measurements for the ring-open isomer (**3.1**) of the monobenzylated DTE. The T_1 values can be obtained from the fitted parameters and are shown above each graph.

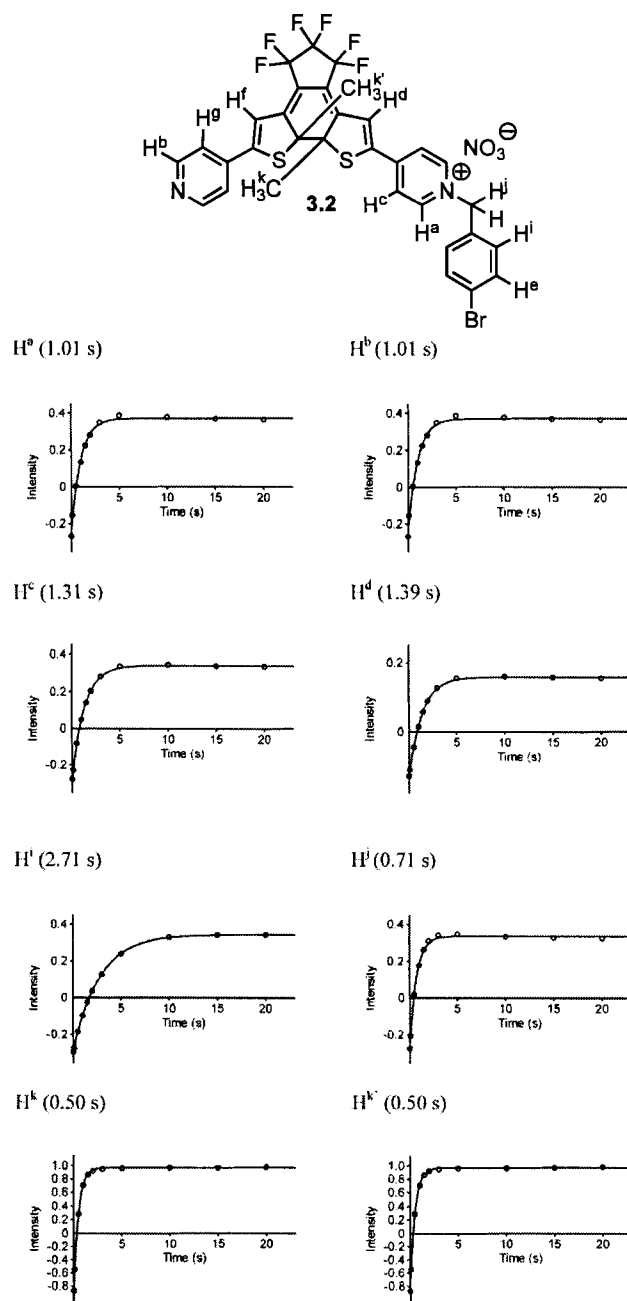


Figure 6.2.3. T_1 relaxation measurements for the ring-closed isomer (3.2) of the monobenzylated DTE. The T_1 values can be obtained from the fitted parameters and are shown above each graph.

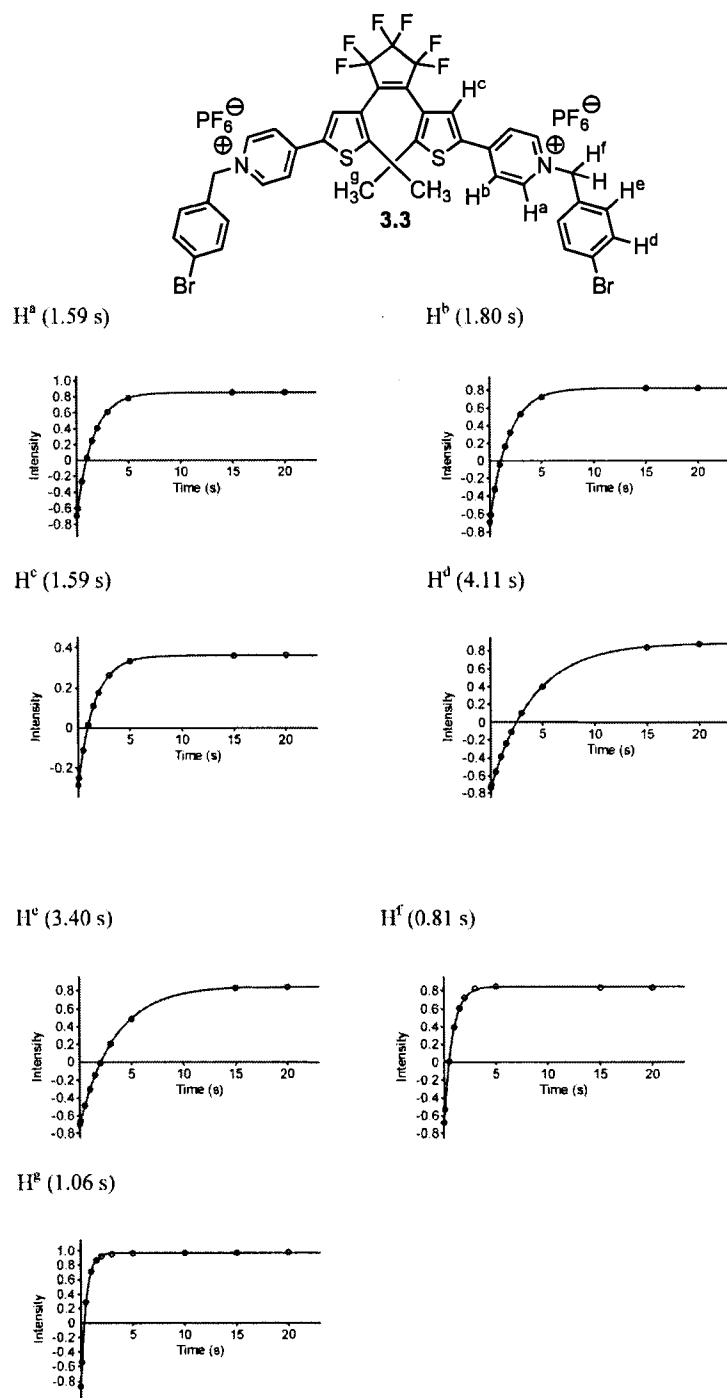


Figure 6.2.4. T_1 relaxation measurements for the ring-open isomer (**3.3**) of the dibenzylated DTE. The T_1 values can be obtained from the fitted parameters and are shown above each graph.

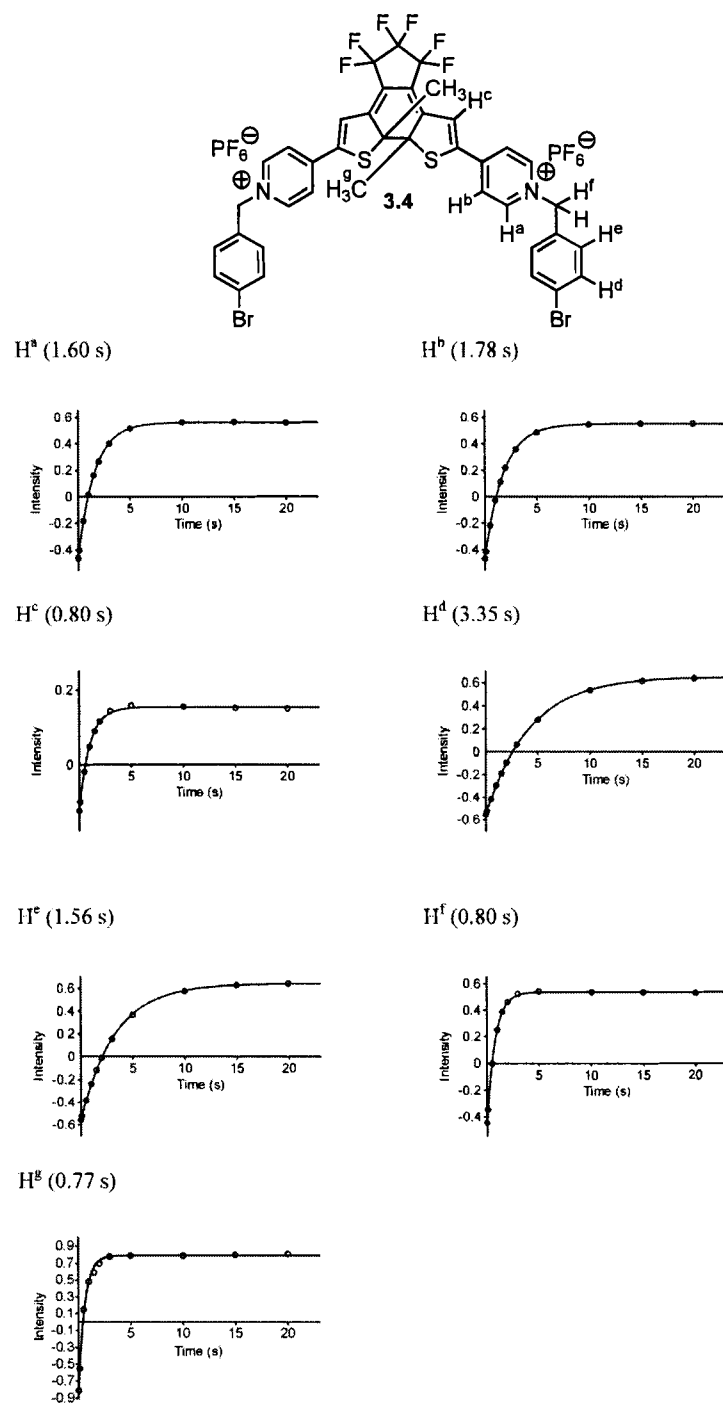


Figure 6.2.5. T_1 relaxation measurements for the ring-closed isomer (**3.4**) of the dibenzylated DTE. The T_1 values can be obtained from the fitted parameters and are shown above each graph.

6.3 Supplementary Pseudo-First-Order Plots for Chapter 3

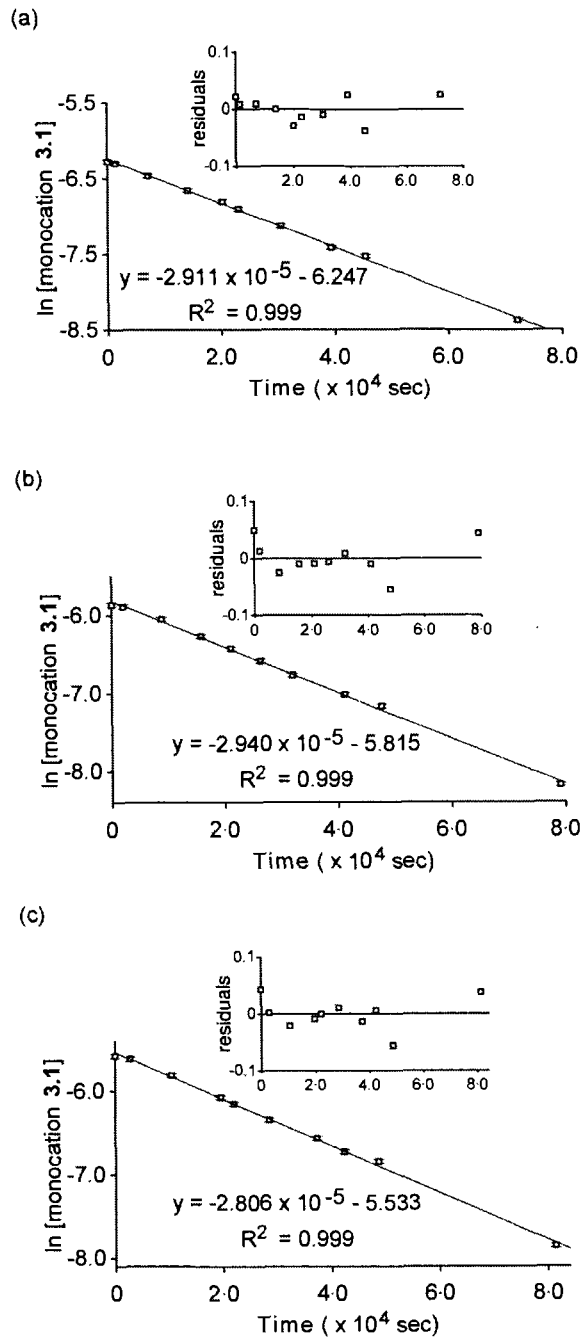


Figure 6.3.1. Plots of the natural log of the concentration of the ring-open isomer **3.1** against time showing the progress of the reaction when (a) a 1.9×10^{-3} M solution, (b) a 3.8×10^{-3} M solution, and (c) a 2.8×10^{-3} M solution of the ring-open isomer **3.1** in CD_3CN is treated with an excess of 4-bromobenzyl bromide (7.3×10^{-2} M) at 22°C over 24 h. The error bars represent the experimental error, which was based on a 2% integration error estimate from 9 repeated NMR integrations. The plots of the residuals against time are shown as insets.

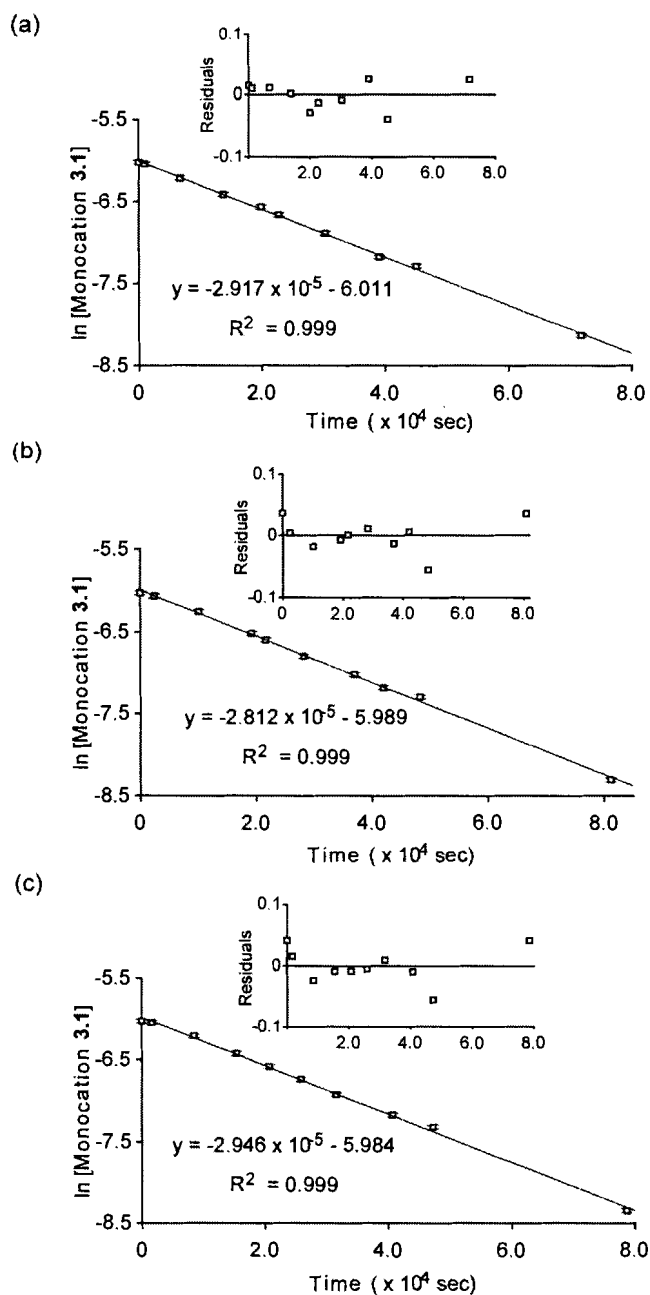


Figure 6.3.2. Plots of the natural log of the concentration of the ring-open isomer **3.1** against time showing the progress of the reaction of a solution (2.4×10^{-3} M) of the ring-open isomer **3.1** in CD_3CN with an excess of 4-bromobenzyl bromide (7.3×10^{-2} M) at 22°C over 24 h. The plots (a), (b), and (c) correspond to the data collected for 3 individual reactions using samples prepared from the same stock solution (2.4×10^{-3} M) in order to test the reproducibility of the results. The error bars represent the experimental error, which was based on a 2% integration error estimate from 9 repeated NMR integrations. The plots of the residuals against time are shown as insets.

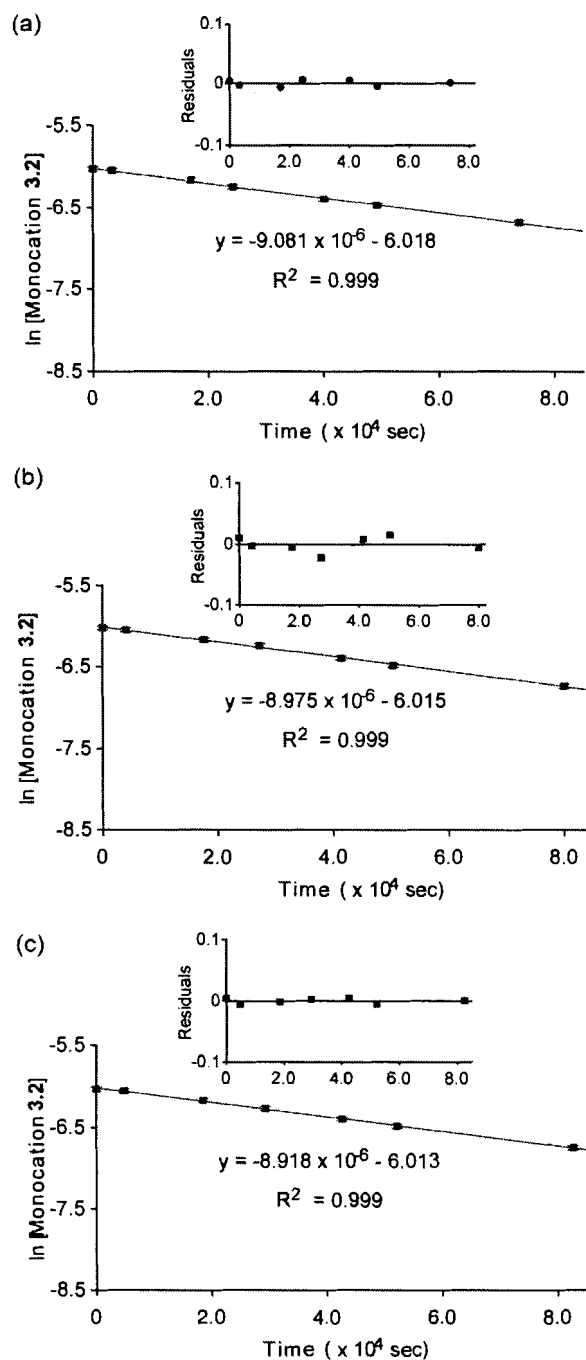


Figure 6.3.3. Plots of the natural log of the concentration of the ring-closed **3.2** against time showing the progress of the reaction of a solution ($2.4 \times 10^{-3} \text{ M}$) of the ring-closed isomer **3.2** in CD_3CN with an excess of 4-bromobenzyl bromide ($7.3 \times 10^{-2} \text{ M}$) at 22°C over 24 h. The plots (a), (b), and (c) correspond to the data collected for 3 individual reactions using samples prepared from the same stock solution ($2.4 \times 10^{-3} \text{ M}$) in order to test the reproducibility of the results. The error bars represent the experimental error, which was based on a 2% integration error estimate from 9 repeated NMR integrations. The plots of the residuals against time are shown as insets.

6.4 Supplementary IR Studies for Chapter 2

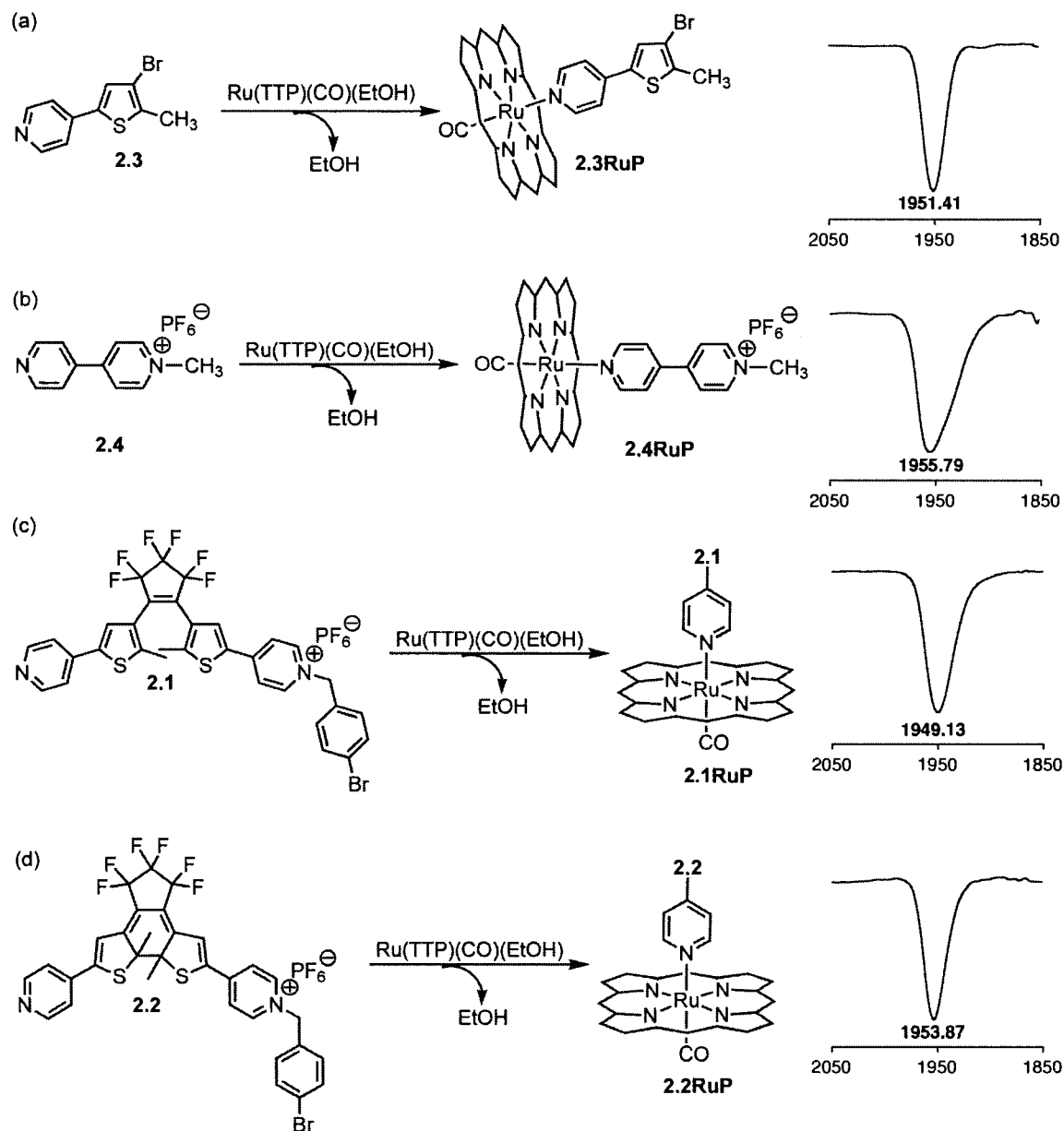


Figure 6.4.1. Selected IR (cast in KBr pellet) spectra showing the CO stretching frequencies when RuTTP(CO) is axially coordinated to (a) the pyridylthiophene **2.3**, (b) the monomethylated bipyridinium **2.4**, (c) the ring-open isomer (**2.1**) of the monobenzylated DTE, and (d) the ring-closed isomer (**2.2**) of the monobenzylated DTE. The CO stretching frequency for the metalloporphyrin appears at 1946 cm^{-1} in the IR spectrum.

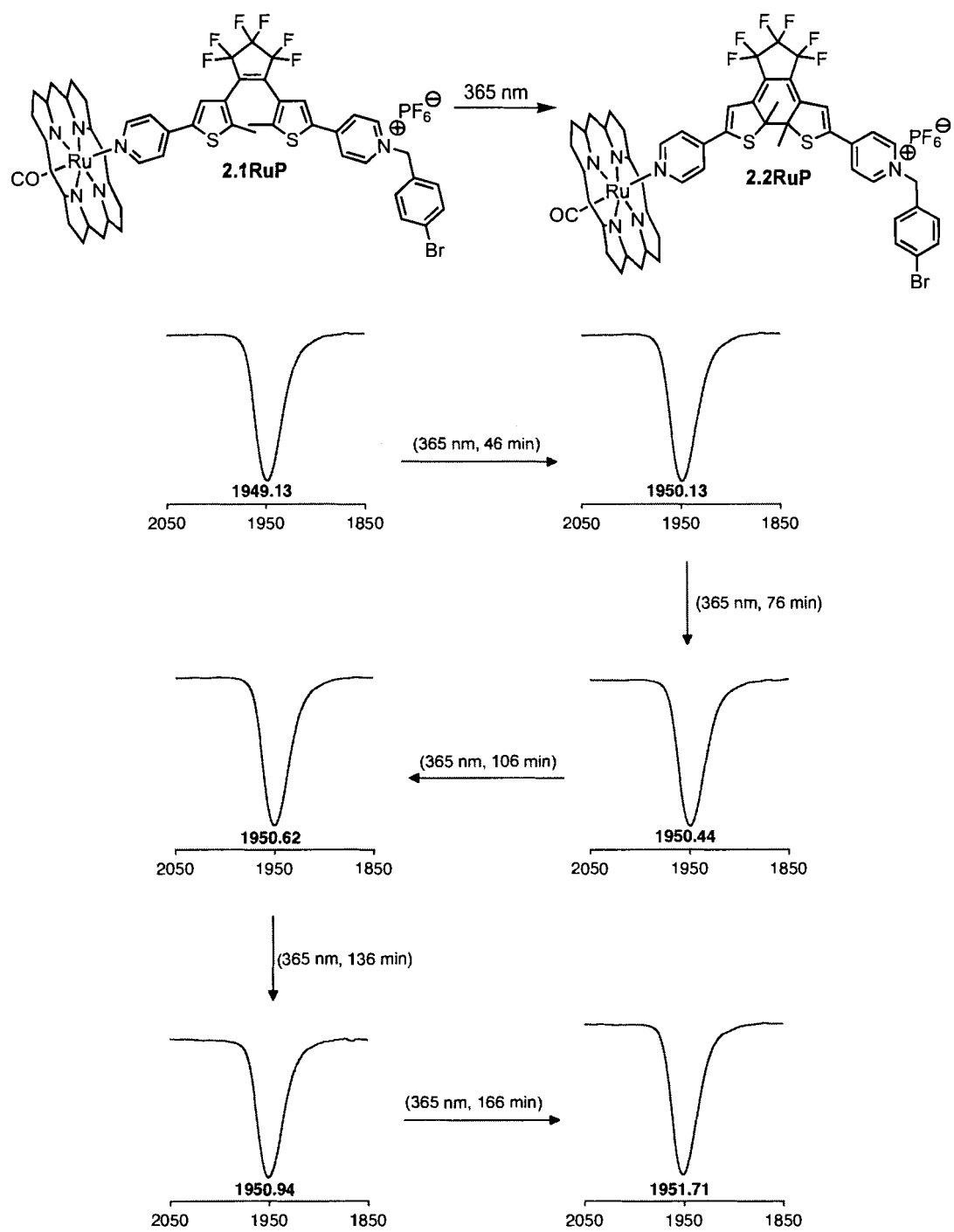


Figure 6.4.2. Selected IR (cast in KBr pellet) spectra of the porphyrin-DTE complex **2.1RuP** showing the gradual shift in the CO stretching frequency to higher energy when the pellet is irradiated with 365 nm light for more than 2 hours. The close packing in the solid KBr pellet prevents the free rotation and does not allow conformational interconversion between the photoinactive *parallel* and the photoactive *anti-parallel* conformer such that the frequency stays at 1952 cm⁻¹ even upon prolonged irradiation.

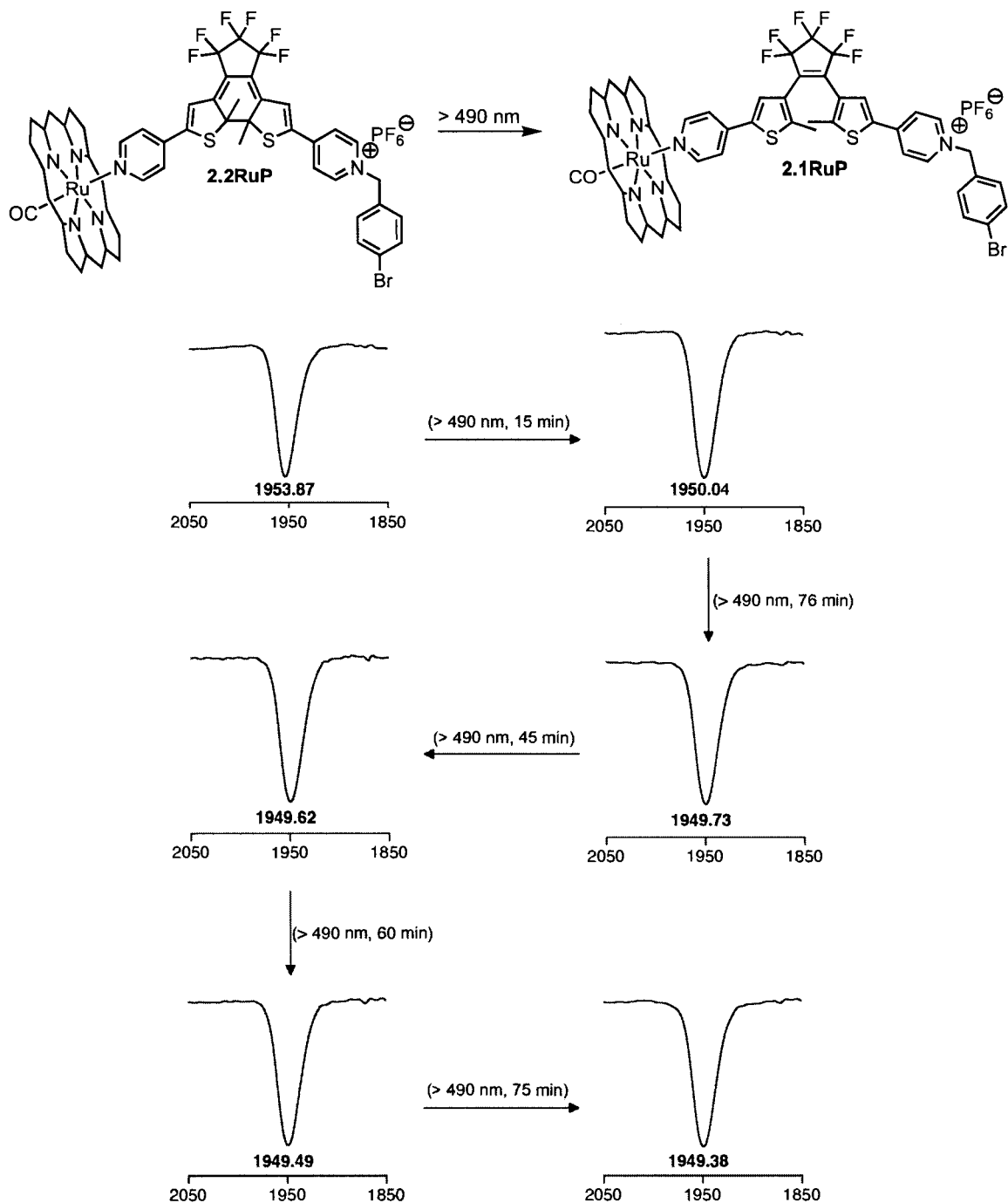


Figure 6.4.3. Selected IR (cast in KBr pellet) spectra of the porphyrin-DTE complex **2.2RuP** showing the complete ring-opening reaction of the complex upon exposure of the pellet to light of wavelengths greater than 490 nm for 75 min.

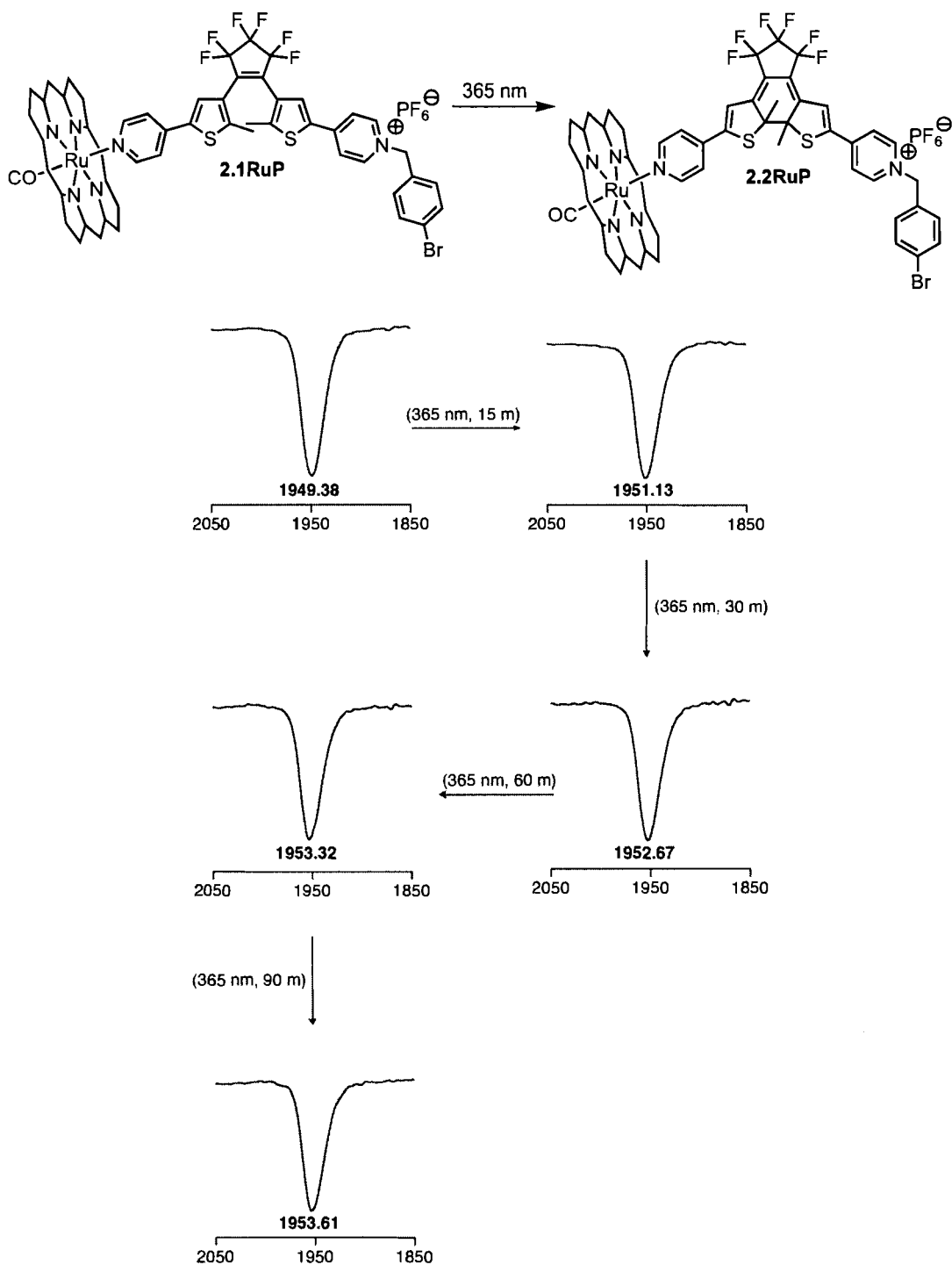


Figure 6.4.4. Selected IR (cast in KBr pellet) spectra of the porphyrin-DTE complex **2.1RuP** showing the gradual shift in the CO stretching frequency to higher energy, corresponding to the stretching frequency of the ring-closed complex **2.2RuP** upon re-irradiation of the pellet with 365 nm light for 90 min.

7 REFERENCES

1. Ballardini, R.; Balzani, V.; Credi, A.; Gandolfi, M. T.; Venturi, M. *Acc. Chem. Res.* **2001**, *34*, 445-455.
2. *Molecular Switches*. Feringa, B. L. ed.; Wiley-VCH: Weinheim, Germany, 2001.
3. *Organic Photochromic and Thermochromic Compounds*. Crano, J. C.; Guglielmetti, R. J. ed.; Plenum Press: New York, 1999; Vol. 1 and 2.
4. Irie, M.; Mohri, M. *J. Org. Chem.* **1988**, *53*, 803-808.
5. Jiang, G.; Wang, S.; Yuan, W.; Jiang, L.; Tian, H.; Zhu, D. *Chem. Mater.* **2006**, *18*, 235-237.
6. Golovkova, T. A.; Kozlov, D. V.; Neckers, D. C. *J. Org. Chem.* **2005**, *70*, 5545-5549.
7. Matsuda, K.; Irie, M. *J. Photochem. Photobiol. C: Photochem. Rev.* **2004**, *5*, 169-182.
8. Norsten, T. B.; Branda, N. R. *J. Am. Chem. Soc.* **2001**, *123*, 1784-1785.
9. Norsten, T. B.; Branda, N. R. *Adv. Mater.* **2001**, *13*, 347-349.
10. Bertarelli, C.; Bianco, A.; D'amore, F.; Gallazi, M. C.; Zerbi, G. *Adv. Funct. Mater.* **2004**, *14*, 357-363.
11. Kim, M. S.; Maruyama, H.; Kawai, T.; Irie, M. *Chem. Mater.* **2003**, *15*, 4539-4543.
12. Kim, E.; Choi, Y.-K.; Lee, M.-H. *Macromolecules* **1999**, *32*, 4855-4860.
13. Wigglesworth, T. J.; Sud, D.; Lehki, V. S.; Norsten, T. B.; Branda, N. R. *J. Am. Chem. Soc.* **2005**, *127*, 7272-7273.
14. Kose, M.; Shinoura, M.; Yokoyama, Y. *J. Org. Chem.* **2004**, *69*, 8403-8406.
15. De Jong, J. J. D.; Lucas, L. N.; Kellogg, R. M.; Van Esch, J. H.; Feringa, B. L. *Science* **2004**, *304*, 278-281.
16. Yamamoto, S.; Matsuda, K.; Irie, M. *Org. Lett.* **2003**, *5*, 1769-1772.
17. Pieraccini, S.; Masiero, S.; Spada, G. P.; Gotarelli, G. *Chem. Commun.* **2003**, 598-599.
18. Murguly, E.; Norsten, T. B.; Branda, N. R. *Angew. Chem. Int. Ed.* **2001**, *40*, 1752-1755.
19. Tanifuji, N.; Irie, M.; Matsuda, K. *J. Am. Chem. Soc.* **2005**, *127*, 13344-13353.
20. Katsonis, N.; Kudernac, T.; Walko, M.; Van der Molen, S. J.; Van Wees, B. J.; Feringa, B. L. *Adv. Mater.* **2006**, *18*, 1397-1400.
21. Li, J.; Speyer, G.; Sankey, O. *Phys. Rev. Lett.* **2004**, *93*, 248301-248304.
22. Guo, X.; Zhang, D.; Yu, G.; Wan, M.; Li, J.; Liu, Y.; Zhu, D. *Adv. Mater.* **2004**, *16*, 636-640.

23. Tsujioka, T.; Hamada, Y.; Shibata, K. *Appl. Phys. Lett.* **2001**, *78*, 2282-2284.
24. Guirado, G.; Coudret, C.; Hliwa, M.; Launay, J.-P. *J. Phys. Chem. B* **2005**, *109*, 17445-17459.
25. Gorodetsky, B.; Samachetty, H. D.; Donkers, R. L.; Workentin, M. S.; Branda, N. R. *Angew. Chem. Int. Ed.* **2004**, *43*, 2812-2815.
26. Peters, A.; Branda, N. R. *J. Am. Chem. Soc.* **2003**, *125*, 3404-3405.
27. Peters, A.; Branda, N. R. *Chem. Commun.* **2003**, 954-955.
28. Fraysse, S.; Coudret, C.; Launay, J.-P. *Eur. J. Inorg. Chem.* **2000**, 1581-1590.
29. Gilat, S. L.; Kawai, T.; Lehn, J.-M. *Chem. Eur. J.* **1995**, *1*, 275-284.
30. Koshido, T.; Kawai, T.; Yoshino, K. *J. Phys. Chem.* **1995**, *99*, 6110-6114.
31. Irie, M. In *Molecular Switches*, Feringa, B. L. ed.; Wiley-VCH: Weinheim, Germany, 2001; pp 37-60.
32. Irie, M. *Chem. Rev.* **2000**, *100*, 1685-1716.
33. Irie, M. In *Organic Photochromic and Thermochromic Compounds*, Crano, J. C.; Guglielmetti, R. J. ed.; Plenum Press: New York, 1999; Vol. 1 and 2, pp 207-221.
34. *Mechanism and Theory in Organic Chemistry*. Lowry, T. H.; Richardson, K. S. ed.; Harper Collins Publishers: New York, 1987.
35. Uchida, K.; Tsuchida, E.; Aoi, Y.; Nakamura, S.; Irie, M. *Chem. Lett.* **1999**, *28*, 63-64.
36. Takeshita, M.; Kato, N.; Kawauchi, S.; Imase, T.; Watanabe, J.; Irie, M. *J. Org. Chem.* **1998**, *63*, 9306-9313.
37. Irie, M.; Miyatake, O.; Uchida, K.; Eriguchi, T. *J. Am. Chem. Soc.* **1994**, *116*, 9894-9900.
38. Nakamura, S.; Irie, M. *J. Org. Chem.* **1988**, *53*, 6136-6138.
39. Yokoyama, Y. In *Molecular Switches*, Feringa, B. L., Ed. Wiley-VCH: Weinheim, Germany, 2001; pp 107-121.
40. Tian, H.; Yang, S. *Chem. Soc. Rev.* **2004**, *33*, 85-97.
41. Sud, D.; Norsten, T. B.; Branda, N. R. *Angew. Chem. Int. Ed.* **2005**, *44*, 2019-2021.
42. Kawai, S. H.; Gilat, S. L.; Lehn, J.-M. *Eur. J. Org. Chem.* **1999**, 2359-2366.
43. Odo, Y.; Matsuda, K.; Irie, M. *Chem. Eur. J.* **2006**, *12*, 4283-4288.
44. Taft, R. W. In *Steric Effects in Organic Chemistry*, Newman, M. S. ed.; Wiley: New York, 1956; pp 556-675.
45. Dewar, M. J. S.; Grisdale, P. J. *J. Am. Chem. Soc.* **1962**, *84*, 3548-3553.
46. Remick, A. E. *Electronic Interpretations of Organic Chemistry*. John Wiley & Sons: New York, 1949.

47. Charton, M. *J. Am. Chem. Soc.* **1975**, *97*, 3694-3697.
48. Conant, J. B.; Hüssey, R. E. *J. Am. Chem. Soc.* **1925**, *47*, 476-488.
49. Sands, R. D. *J. Org. Chem.* **1994**, *59*, 468-471.
50. Stirling, C. J. M. *Tetrahedron* **1985**, *41*, 1613-1666.
51. Brown, H. C.; Fletcher, R. S. *J. Am. Chem. Soc.* **1949**, *71*, 1845-1854.
52. Oki, M. *Acc. Chem. Res.* **1984**, *17*, 154-159.
53. Seeman, J. I. *Chem. Rev.* **1983**, *83*, 83-134.
54. Topsom, R. D. *J. Am. Chem. Soc.* **1981**, *103*, 39-44.
55. Acevedo, S.; Bowden, K. *J. Chem. Soc., Chem. Commun.* **1977**, 608-609.
56. Roberts, J. D.; Moreland, W. T. J. *J. Am. Chem. Soc.* **1953**, *75*, 2167-2173.
57. Wheland, G. W. *Resonance in Organic Chemistry*. Wiley: New York, 1955.
58. Valkenberg, M. H.; Holderich, W. F. *Catal. Rev.* **2002**, *44*, 321-374.
59. Lai, C.-Y.; Trewyn, B. G.; Jeftinija, D. M.; Jeftinija, K.; Xu, S.; Jeftinija, S.; Lin, V. S.-Y. *J. Am. Chem. Soc.* **2003**, *125*, 4451-4459.
60. Albert, A. *Nature* **1958**, *182*, 421-423.
61. McCoy, C. P.; Rooney, C.; Jones, D. S.; Gorman, S. P.; Nieuwenhuyzen, M. *Pharm. Res.* **2007**, *24*, 194-200.
62. Denny, W. A. *Eur. J. Med. Chem.* **2001**, *36*, 577-595.
63. Vaidya, R. A.; Mathias, L. J. *J. Am. Chem. Soc.* **1986**, *108*, 5514-5520.
64. Scriven, E. F. V. *Chem. Soc. Rev.* **1983**, *12*, 129-161.
65. Bender, M. L.; Turnquest, B. W. *J. Am. Chem. Soc.* **1957**, *79*, 1652-1655.
66. Bender, M. L.; Bergeron, R. J.; Komiyama, M. In *The Bioorganic Chemistry of Enzymatic Catalysts*, John Wiley & Sons: New York, 1984; pp 121-123.
67. Höfle, G.; Steglich, W.; Vorbruggen, H. *Angew. Chem. Int. Ed.* **1978**, *17*, 569-583.
68. Mayr, H.; Patz, M. *Angew. Chem. Int. Ed.* **1994**, *33*, 938-957.
69. Campodónico, P. R.; Aizman, A.; Contreras, R. *Chem. Phys. Lett.* **2006**, *422*, 204-209.
70. Niyazymbetov, M. E.; Rongfeng, Z.; Evans, D. H. *J. Chem. Soc., Perkin Trans. 2* **1996**, 1957-1961.
71. Pearson, R. G.; Songstad, J. *J. Am. Chem. Soc.* **1967**, *89*, 1827-1836.
72. Kalyanasundaram, K. *Photochemistry of Polypyridine and Porphyrin Complexes*. Academic Press San Diego, 1992.
73. *The Porphyrins*. Dolphin, D. ed.; Academic Press: New York, 1978; Vol. 1-5.

74. *Comprehensive Supramolecular Chemistry*. Atwood, J. L.; Davies, J. E.; MacNicol, D. D.; Vogtle, F. ed.; Pergamon: Oxford, 1996.
75. Lehn, J.-M. *Supramolecular Chemistry: Concepts and Perspectives*. Wiley-VCH: Weinheim, Germany, 1995.
76. Alessio, E.; Macchi, M.; Heath, S.; Marzilli, L. G. *Chem. Commun.* **1996**, 1411-1412.
77. Funatsu, K.; Imamura, T.; Ichimura, A.; Sasaki, Y. *Inorg. Chem.* **1998**, *37*, 4986-4995.
78. Kim, H.-J.; Bampos, N.; Sanders, J. K. M. *J. Am. Chem. Soc.* **1999**, *121*, 8120-8121.
79. Bonnet, J. J.; Eaton, S. S.; Eaton, G. R.; Holm, R. H.; Ibers, J. A. *J. Am. Chem. Soc.* **1973**, *95*, 2141-2149.
80. Chichak, K.; Branda, N. R. *Chem. Commun.* **2000**, 1211-1212.
81. Chichak, K.; Branda, N. R. *Chem. Commun.* **1999**, 523-524.
82. Chichak, K.; Walsh, M. C.; Branda, N. R. *Chem. Commun.* **2000**, 847-848.
83. Sanders, J. K. M.; Bampos, N.; Clyde-Watson, Z.; Darling, G. D.; Hawley, J. C.; Kim, H.-J.; Mak, C. C.; Webb, S. J. In *The Porphyrin Handbook*, Kadish, K. M., Smith, K. M. and Guilard, R., Ed. Academic Press: New York, 2000; Vol. 3, p 1.
84. Connors, K. A. *Chemical Kinetics: The Study of Reaction Rates in Solution*. VCH Publishers, Inc.: New York, 1990; p 166-169.
85. *The Porphyrin Handbook*. Kadish, K. M.; Smith, K. M.; Guilard, R. ed.; Academic Press: New York, 2000; Vol. 3 and 5.
86. Faller, J. W.; Chen, C. C.; Malerich, C. J. *J. Inorg. Biochem.* **1979**, *11*, 151-170.
87. Tsutsui, M.; Ostfeld, D.; Hoffman, L. M. *J. Am. Chem. Soc.* **1971**, *93*, 1820-1823.
88. Abraham, R. J. *Molec. Phys.* **1961**, 145-152.
89. Gutmann, V. *Coord. Chem. Rev.* **1976**, *18*, 225-255.
90. Kadish, K. M.; Chang, D. *Inorg. Chem.* **1982**, *21*, 3614-3618.
91. Jones, C. J. *d- and f-Block Chemistry*. Royal Society of Chemistry: Cambridge, UK, 2001; p 97-129.
92. Jean, Y. *Molecular Orbitals of Transition Metal Complexes*. Oxford, 2005; p 97-140.
93. Chichak, K. Metal-Directed Self-Assembly Synthesis: Supramolecular Chemistry Using Axial Coordination and Metal Chelation. Ph.D., University of Alberta, 2002.
94. Smith, B. *Infrared Spectral Interpretation*. CRC: New York, 1999; p 1-29.
95. Eaton, S. S.; Eaton, G. R. *Inorg. Chem.* **1977**, *16*, 72-75.
96. Lantz, R.; Hörnfeldt, A. B. *Chem. Scripta* **1972**, *2*, 9.

97. Feng, D.-J.; Li, X.-Q.; Wang, X.-Z.; Jiang, X.-K.; Li, Z.-T. *Tetrahedron* **2004**, *60*, 6137-6144.
98. Irie, M.; Lifka, T.; Uchida, K.; Kobatake, S.; Shindo, Y. *Chem. Commun.* **1999**, 747-748.
99. Peters, A.; Branda, N. R. *Adv. Mater. Opt. Electron.* **2000**, *10*, 245-249.
100. Takata, A.; Saito, M.; Murakami, A.; Nakamura, S.; Irie, M.; Uchida, K. *Adv. Funct. Mater.* **2003**, *13*, 755-762.
101. Wigglesworth, T. J.; Myles, A. J.; Branda, N. R. *Eur. J. Org. Chem.* **2005**, 1233-1238.
102. Wüstenberg, B.; Branda, N. R. *Adv. Mater.* **2005**, *17*, 2134-2138.
103. Myles, A. J.; Branda, N. R. *Tetrahedron Lett.* **2000**, *41*, 3785-3788.
104. Adler, A. D.; Longo, F. R.; Finarelli, J. D.; Goldmacher, J.; Assour, J.; Korsakoff, L. *J. Org. Chem.* **1967**, *32*, 476-476.
105. *Nucleophilicity, Advances in Chemistry Series*. Harris, J. M.; McManus, S. P. ed.; American Chemical Society: Washington, D.C., 1987.
106. Hudson, R. F. In *Chemical Reactivity and Reaction Paths*, Klopman, G. ed.; John Wiley & Sons: New York, 1974.
107. Haberfield, P.; Nudelman, A.; Bloom, A.; Romm, R.; Ginsberg, H. *J. Org. Chem.* **1971**, *36*, 1792-1795.
108. Ko, E. C. F.; Parker, A. J. *J. Am. Chem. Soc.* **1968**, *90*, 6447-6453.
109. Ingold, C. K. *Structure and Mechanism in Organic Chemistry*. 2d ed.; Cornell University Press: Ithaca, New York, 1969.
110. Ballistreri, F. P.; Maccarone, E.; Mamo, A. *J. Org. Chem.* **1976**, *41*, 3364-3367.
111. Espenson, J. H. *Chemical Kinetics and Reaction Mechanisms*. 2nd ed.; McGraw-Hill: New York, 1995; p 15-100.
112. Silverstein, R. M.; Webster, F. X. *Spectrometric Identification of Organic Compounds*. Sixth ed.; John Wiley & Sons: New York, 1998; p 144-148.
113. Evilia, R. F. *Anal. Lett.* **2001**, *34*, 2227-2236.
114. Abraham, R. J.; Fisher, J.; Loftus, P. *Introduction to NMR Spectroscopy*. John Wiley & Sons: New York, 1988; p 101-143.
115. Corbett, J. F. *J. Chem. Educ.* **1972**, *49*, 663.
116. Sicilio, F.; Peterson, M. D. *J. Chem. Educ.* **1961**, *38*, 576.
117. Deady, L. W.; Finlayson, W. L.; Korytsky, O. L. *Aust. J. Chem.* **1979**, *32*, 1735-1742.
118. Deady, L. W. *Aust. J. Chem.* **1973**, *26*, 1949-1953.
119. Deady, L. W.; Zoltewicz, J. A. *J. Am. Chem. Soc.* **1971**, *93*, 5475-5477.

120. Miller, J. N. *Analyst* **1991**, *116*, 3-14.
121. Hibbert, D. B.; Gooding, J. J. *Data Analysis for Chemistry*. Oxford University Press: New York, 2006.
122. Miller, J. N.; Miller, J. C. *Statistics and Chemometrics for Analytical Chemistry*. Pearson Education Limited: Harlow, England, 2005.
123. Benson, S. W. *The Foundations Of Chemical Kinetics*. McGraw-Hill: New York, 1960; p 33.
124. Lewis, F. S.; Johnson, M. D. *J. Am. Chem. Soc.* **1960**, *82*, 5408-5410.
125. Nair, V.; Pillai, A. N.; Menon, R. S.; Suresh, E. *Org. Lett.* **2005**, *7*, 1189-1191.
126. Nair, V.; Shreekanth, A. R.; Abhilash, N.; Biju, A. T.; Remadevi, B.; Menon, R. S.; Rath, N. P.; Srinivas, R. *Synthesis* **2003**, 1895-1902.
127. Higashiguchi, K.; Matsuda, K.; Kobatake, S.; Yamada, T.; Kawai, T.; Irie, M. *Bull. Chem. Soc. Jpn.* **2000**, *73*, 2389-2394.
128. Irie, M.; Lifka, T.; Uchida, K.; Kobatake, S.; Shindo, Y. *Chem. Commun.* **1999**, 747-750.
129. Nair, V.; Sreekanth, A. R.; Vinod, A. U. *Org. Lett.* **2001**, *3*, 3495-3497.
130. Nair, V.; Sreekanth, A. R.; Vinod, A. U. *Org. Lett.* **2002**, *4*, 2807.